UNIVERSITE DE LIEGE
FACULTE DE MEDECINE VETERINAIRE
DEPARTEMENT DES SCIENCES FONCTIONNELLES
LABORATOIRE D'IMMUNOPHYSIOLOGIE

Investigation du rôle de la signalisation TGFβ médiée par l'endothélium dans le développement et la fonction des macrophages interstitiels pulmonaires

Investigation of endothelial-driven TGFβ signaling in the development and function of lung interstitial macrophages

Wen PENG

THESE PRESENTEE EN VUE DE L'OBTENTION DU GRADE DE
DOCTORAT EN SCIENCES VETERINAIRES

ANNEE ACADEMIQUE 2024-2025

TABLE OF CONTENTS

ACKNOWLEDGEMENTS

Time flies—before I knew it, this has become my fifth year studying in Liège, Belgium. It feels just like yesterday that I had my interview with Thomas and Qiang. Back then, I didn't even know where Belgium was, nor the city of Liège. I began my "newbie" life in Liège feeling completely lost. At first, I couldn't even speak a complete sentence in English or French, but now I can express myself boldly. I've moved four times, caught COVID four times, and thanks to Belgium's great location, I've been able to travel to many countries. Like a true Liège local, I show up whenever the sun comes out, sometimes beer in hand. I no longer need Google Maps to explore the city easily—though by the end of April, even the bus lines are changing. My PhD journey has gone smoothly thanks to all the kind people around me who have taken care of this foreigner. So here, I want to express my heartfelt thanks to everyone who has helped me along the way.

First, I would like to thank my promoter, **Thomas**. From our first meeting, I had the impression that you were highly efficient—the interview was swift, and the decision came quickly. Throughout our time working together, you have maintained this style. Even when you were bedridden after surgery, I will never forget the image of you lying in bed while still attending our meetings. That level of dedication is something I deeply admire—only someone truly passionate about their work can be so committed. You are always positive and encouraging. Whenever I was frustrated or made mistakes, you would tell me, "Wen, this is inevitable, this is normal." Thomas, you are a truly charismatic and inspiring supervisor, and I am very lucky to have studied under your guidance.

I also want to thank my co-promoter, **Qiang**. It was thanks to your help that I received this PhD opportunity. In the early stages of my doctoral journey, you offered me so much guidance and support—not just academically, but in life as well. I wish you all the best in your career in France and hope to visit Montpellier someday to experience the sunshine of southern France.

Next is my colleague **Domien**. Your drive and passion for research are truly inspiring. Thank you for patiently teaching me so many lab techniques and for reminding me not to stop

even when I felt lost—to keep experimenting and thinking. This PhD thesis project went so smoothly in large part because of your help. I hope someone as outstanding as you will find a postdoc position that satisfies you and helps you realize your professional goals.

Joan, you are professional in your work. Whenever I had questions about bioinformatics, you provided answers quickly. You were also always willing to help with other things—for example, constantly fixing that color printer for me, just a joke. You were always thoughtful, too, often translating for me and supporting me, knowing that my French wasn't very strong.

Margot, you're such a high-energy person—full of enthusiasm. Because of your vibrant personality, our lab never had a dull moment. Whenever I was in trouble, you'd drop what you were doing to help me. I truly admire your resilience—no matter how big the challenge, you always seem to overcome it. Just like with your project, your "mountain"—I believe you'll conquer it, it's just a matter of time.

Cecilia, you're always gentle yet strong. It seems like you always have the answer to every question. I often came to you with all sorts of strange inquiries, and you always eased my anxiety with your calm and kind demeanor. I really admire how well you balance work and life—you have such a successful career and so many interests outside of it. I believe your postdoctoral journey will be even better.

Val, you consider everyone's opinions and organize everything so well. I remember that you gave me a ride home after every late lab gatherings and looked after me in the sea off Corsica. I hope your project goes well and rewards all the effort you've put in. **Pierre**, you are warm, friendly, and full of passion for sports and life. It's amazing how fast and high quality your work is. **Cora**, you are truly smart and kind. Thank you for guiding me. I'm so glad to have witnessed your wedding and your professional success. I wish you an even more wonderful journey ahead, both in your career and in life. **Monica**, you're like a kind of older sister, always taking care of everything in the lab. Thank you for all you've done for our lab, and for your effort in learning English just to communicate with me. Even though we couldn't speak so often, thank you, **Pauline**, for always quietly helping me with so many experiments. I'm so happy to

see you now pursuing your dream career with your dogs. **Alice**, you are the most emotionally intelligent person I've ever met. Being around you is always a joy. You always respond with positivity and warmth. Your serious work ethic is also something I really admire. I hope you complete your PhD smoothly and I wish you all the best in the future.

Thanks to my thesis committee members, **Benjamin** and **Francesca** for the insightful feedback and constructive discussions every committee meeting. Thanks to everyone at the GIGA platform and to the staff in the animal facility. Even though we didn't interact much, your professionalism made it possible for me to carry out my project smoothly.

Thank you to all my friends and family. Especially **my mom** and my best friend **Lili**, you have supported me emotionally, or accompanied me through one journey after another. There are too many words to express it all, but I carry the gratitude in my heart. Thanks to my cat **Umi**, every time I see your round little face, the stress from studying melts away.

Lastly, I want to thank my husband, **Jeff**. Because of you, my life became more colorful. Thank you for always encouraging me, supporting me, and making my life in Belgium not a memory of the past, but a story that's still unfolding.

LIST OF ABBREVIATIONS

A

AM: Alveolar Macrophage

AT1: Type 1 Alveolar Epithelial Cells

AT2: Type 2 Alveolar Epithelial Cells

B

BAM: Brain-Associated Macrophage

BAL: Bronchoalveolar Lavage

BDNF: Brain-Derived Neurotrophic Factor

BM: Bone Marrow

BMDM: Bone Marrow-Derived Macrophage

BMP: Bone Morphogenetic Protein

C

CCL2/MCP-1: Monocyte Chemoattractant Protein-1

cDC: Conventional Dendritic Cell

cMo: Ly6C^{+} Classical Monocytes

CMP: Common Myeloid Progenitor

CNS: Central Nervous System

COPD: Chronic Obstructive Pulmonary Disease

Co-SMAD: Common-Mediator SMAD

CSF1/M-CSF: Macrophage Colony-Stimulating Factor

CSF2/GM-CSF: Granulocyte-Macrophage Colony-Stimulating Factor

CSF3/G-CSF: Granulocyte Colony Stimulating Factor

D

DC: Dendritic Cell

Dll1: Delta-Like 1

DT: Diphtheria Toxin

DTR: Diphtheria Toxin Receptor

E

ECM: Extracellular Matrix

EMP: Erythro-Myeloid Progenitor

EMT: Epithelial-Mesenchymal Transition

ENS: Enteric Nervous System

F

G

GATA6: GATA Binding Protein 6

GARP: Glycoprotein-A Repetitions Predominant Protein

GDF: Growth Differentiation Factor

GMP: Granulocyte-Monocyte Progenitor

GTPase: Guanosine Triphosphatase

H

12-HETE: 12-Hydroxyeicosatetraenoic Acid

HDAC3: Histone Deacetylase 3

HDM: House Dust Mite

HSC: Hematopoietic Stem Cell

I

IBD: Inflammatory Bowel Disease

ID3: Inducing DNA3

IFN: Interferon

IL: Interleukin

IPF: Idiopathic Pulmonary Fibrosis

I-SMAD: Inhibitory SMAD

J

K

KC: Kupffer Cell

LXR: Liver X Receptor

L

LAP: Latency-Associated Peptide

LC: Langerhans Cell

LLC: Large Latent Complex

LP: Lamina Propria

LPM: Large Peritoneal Macrophage

LPS: Lipopolysaccharides

LRRC: Leucine-Rich Repeat-Containing Protein

LTBP: Latent TGFβ Binding Protein

M

MAPK: Mitogen-Activated Protein Kinase

MDP: Monocyte-Dendritic Cell Progenitor

MHC I: Major Histocompatibility Complex Class I

MHC II: Major Histocompatibility Complex Class II

MMP: Matrix Metalloproteinase

MNP: Mononuclear Phagocyte

MSC: Mesenchymal Stem Cell

MsIn: Mesothelin

Muc16: Mucin 16

N

NAM: Nerve-Associated Macrophage

NF-κB: Nuclear Factor-κB

NK: Natural Killer Cell

O

P

PAP: Pulmonary Alveolar Proteinosis

pDC: Plasmacytoid Dendritic Cell

PDGF: Platelet-Derived Growth Factor

pMo: Ly6C$^-$ Patrolling Monocytes

PPAR: Peroxisome Proliferator-Activated Receptor

PPR: Pattern Recognition Receptor

Q

R

RAE: Retinoic Acid Early Inducible

RGD: Arginylglycylaspartic Acid

RNS: Reactive Nitrogen Species

ROS: Reactive Oxygen Species

RPM: Red Pulp Macrophage

R-SMAD: Receptor-Regulated SMAD Protein

RTM: Resident Tissue Macrophage

S

SBE: SMAD-Binding Element

scRNA-seq: Single Cell RNA-sequencing

SLC: Small Latent Complex

S/M: Submucosal/Muscularis

SMAD: Suppressors of Mothers Against Decapentaplegic

SP: Surfactant Protein

SPM: Small Peritoneal Macrophage

SPP1: Secreted Phosphoprotein 1

T

TAM: Tumor-Associated Macrophage

TGFβ: Transforming Growth Factor β

Th1: Type 1 T helper Cell

Th2: Type 2 T helper Cell

TLO: Tertiary Lymphoid Organ

TLR: Toll-Like Receptor

TNF: Tumor Necrosis Factor

Treg: Regulatory T Cell

TSL: Tertiary Lymphoid Structure

TSP-1: Thrombospondin-1

U

V

vWF: von Willebrand factor

W

WT: Wild-type

X

Y

YS: Yolk Sac

Z

SUMMARY

SUMMARY

The mechanisms underlying lung homeostasis are fundamental importance and have critical implications for the prevention of chronic inflammatory disorders. Two main lung-resident tissue macrophage (RTM) populations participate to a sophisticated surveillance system to sustain homeostasis and host protection: alveolar macrophages (AMs) located in the alveolar lumen and interstitial macrophages (IMs) residing in the lung parenchyma. While AMs are well-studied and rely on type 2 alveolar epithelial cell (AT2)-derived GM-CSF (CSF2) and autocrine transforming growth factor β (TGF β) for their development and maintenance, IM biology remains more enigmatic. IMs can be primarily categorized into two main subsets, namely $CD206^+$ IMs and $CD206^-$ IMs occupying distinct niches. Studies using parabiosis, bone marrow chimeras, and fate mapping indicate that both IM subsets are slowly replenished by classical monocytes in adults. IM differentiation from monocytes follows a common pathway requiring MafB transcription factor and Csf1 receptor signaling. However, the lung microenvironment signals shaping IMs under normal conditions remain unclear. Functionally, IMs are thought to exert immunoregulatory functions in the context of allergic asthma, to dampen inflammatory responses and to organize tertiary lymphoid tissues in disease context. Yet, the potential tissue-supportive and homeostatic functions of IMs at steady-state are still unclear.

Here, we employed multiple approaches including single-cell RNA sequencing, CODEX imaging, multiplex flow cytometry and microscopy, combined with unique transgenic mouse models of IM targeting and bone marrow chimeras to investigate niche cell-IM interactions in the steady-state lung. We found that Tgfβ1, produced by lung vWF^+ blood vessel endothelial cells, shaped IM differentiation and imprinted a core IM identity, acting in concert with CSF1. In the absence of Tgfβ receptor in myeloid cells and of Tgfβ1 in endothelial cells, monocytes accumulate in the tissue and could not fully differentiate into functional IMs, regardless of the IM subset. Moreover, disruption of IM-intrinsic Tgfβ receptor signaling triggered development of age-related mechanical abnormalities, hyperinflation and collagen deposition. Our findings underscore an endothelial-IM axis that contributes to IM development and identity and prevents the premature development of age-related defects, demonstrating an as-yet-unknown Tgfβ receptor-dependent homeostatic function of resident IMs.

RESUME

Les mécanismes sous-tendant l'homéostasie pulmonaire sont d'une importance fondamentale et ont des implications cruciales pour la prévention des maladies inflammatoires chroniques. Deux principales populations de macrophages résidents tissulaires (RTM) du poumon participent à un système de surveillance sophistiqué afin de maintenir l'homéostasie et d'assurer la protection de l'hôte : les macrophages alvéolaires (AMs), situés dans la lumière alvéolaire, et les macrophages interstitiels (IMs), résidant dans le parenchyme pulmonaire.

Alors que les AMs sont bien étudiés et dépendent du GM-CSF (CSF2) dérivé des cellules épithéliales alvéolaires de type 2 (AT2) ainsi que du TGFβ autocrine pour leur développement et leur maintien, les IMs restent moins bien compris. On distingue principalement deux sous-populations d'IMs : les IMs CD206^{+} et les IMs CD206^{-}, qui occupent des niches distinctes. Des études utilisant la parabiose, des chimères de moelle osseuse et le traçage du devenir cellulaire indiquent que les deux sous-populations d'IMs sont lentement renouvelées par les monocytes classiques chez la souris adulte. La différenciation des IMs à partir des monocytes suit une trajectoire commune nécessitant le facteur de transcription MafB et une signalisation via le récepteur au CSF1. Cependant, les signaux du microenvironnement pulmonaire régulant les IMs en conditions physiologiques restent mal définis.

Sur le plan fonctionnel, les IMs exercent un rôle immunorégulateur dans le contexte de l'asthme allergique, atténuent les réponses inflammatoires et organisent les tissus lymphoïdes tertiaires en situation pathologique. Toutefois, leurs fonctions potentielles de soutien tissulaire et leur rôle homéostatique en conditions normales restent encore flous.

Dans cette étude, nous avons employé plusieurs approches, incluant le séquençage d'ARN à cellule unique, l'imagerie CODEX, la cytométrie en flux et la microscopie, combinées à des modèles murins transgéniques uniques ciblant les IMs ainsi qu'à des chimères de moelle osseuse, afin d'explorer les interactions entre les cellules de la niche et les IMs dans le poumon en état basal.

Nous avons découvert que le Tgfβ1, produit par les cellules endothéliales vasculaires vWF^{+} du poumon, joue un rôle clé dans la différenciation des IMs et leur confère une identité propre, en synergie avec CSF1. En l'absence du récepteur du Tgfβ dans les cellules myéloïdes et du Tgfβ1 dans les cellules endothéliales, les monocytes s'accumulent dans le tissu sans parvenir à se différencier pleinement en IMs fonctionnels, quel que soit le sous-type d'IM. De plus, l'altération du signal intrinsèque du récepteur Tgfβ dans les IMs entraîne l'apparition d'anomalies liées à l'âge, notamment une hyperinflation pulmonaire et un dépôt de collagène.

Nos résultats mettent en évidence un nouvel axe endothélium-IMs contribuant au développement et à l'identité des IMs, tout en prévenant l'apparition précoce de

dysfonctionnements liés à l'âge. Cette étude révèle ainsi une fonction homéostatique jusqu'ici inconnue des IMs, dépendante du récepteur du Tgfβ.

INTRODUCTION

GENERAL INTRODUCTION

1. Macrophage biology

The story of macrophages began in 1883 when Elie Metchnikoff first identified these cells as “phagocytes” during his study on primitive organisms lacking adaptive immunity [1]. Over the past century, massive research has revealed the origins, the functional diversity, and the complex regulatory mechanisms controlling the behavior of macrophages. These highly plastic immune cells exhibit a strong adaptability, allowing them to respond to distinct tissue environments and signals by differentiating into specialized subsets with specific functions. Today, it is clear that macrophages are integral to organ development, metabolism, tissue homeostasis and repair, as well as the coordination of both innate and adaptive immune responses [2].

1.1. Macrophage ontogeny

Early studies by van Furth and Cohn found macrophage precursor cells in the bone marrow (BM) [3], leading to the paradigm that circulating monocytes derived from hematopoietic stem cells (HSCs) in the BM migrate to tissues and differentiate into resident tissue macrophages (RTMs) [4]. However, subsequent research using sophisticated fate-mapping models has revealed that most adult RTMs originate during embryonic development rather than from postnatal monocyte recruitment [5]. Embryonic macrophages arise from progenitors in the yolk sac (YS), the fetal liver and regions near the embryonic dorsal aorta. These cells colonize their respective tissues during embryogenesis and can maintain their populations through self-renewal, independently of BM-derived monocytes [6-10]. For example, microglia in the central nervous system (CNS) [11, 12], Langerhans cells (LCs) in the epidermis layer of the skin [13], Kupffer cells (KCs) in the liver [14], and alveolar macrophages (AMs) in the lung [15], are established prenatally and can persist throughout life, demonstrating an exceptional self-maintenance capacity within their respective tissues [16]. In contrast, BM-derived monocytes can primarily contribute to other pools of macrophage populations in specific tissues, such as the intestinal mucosa and dermis [16, 17].

Throughout adulthood, the replenishment of RTMs by circulating monocytes varies significantly across tissues and is influenced by factors such as tissue accessibility, the extent of RTM depletion, and the nature of the perturbations involved [18-22]. While at steady-state, many RTMs maintain their populations through self-renewal, in response to injury or inflammation, BM-derived monocytes are rapidly recruited to tissues, where they differentiate into recruited BM-derived macrophages that can exert a wide range of beneficial or deleterious functions in disease and can also contribute to the restoration of perturbed RTMs [20, 23]. The distinct origins of macrophages are thought to contribute to their heterogeneity and specialized functions in different tissue microenvironments [24].

1.2. Macrophage function

Despite their diverse origins and their tissue specificity, macrophages share several core identity and functions. CD64 (encoded by *Fcgr1*) and MerTK have been identified as key markers to distinguish macrophages from dendritic cells (DCs) across various tissues and are universally associated with mature tissue macrophages in different mouse organs [25, 26]. Additional markers, such as F4/80, CD206, and major histocompatibility complex class II (MHC II), can further distinguish between macrophage subtypes [27].

Functionally, macrophages form a dynamic three-dimensional network within tissues and continuously survey the environment for signs of damage or infection, ensuring rapid responses when needed. They can engage in **phagocytosis** to clear cellular debris, apoptotic cells, and pathogens [28, 29]. This process includes several stages: detection, internalization, phagosome formation, and phagolysosome maturation [30, 31]. To recognize and internalize target particles, macrophages utilize a variety of receptors, including pattern recognition receptors (PRRs), complement, and Fc receptors [29]. MerTK play a vital role in efferocytosis by binding to phosphatidylserine on apoptotic cells through bridging ligands like Gas6 and Protein S [32]. Its kinase activity is essential for efferocytosis in both mouse and human macrophages [33]. MerTK also activates β2 integrins through a complex signaling pathway, forming a synapse for efferocytosis [34]. Another phosphatidylserine receptor, Tim4, also

enhances efferocytosis in tumor-associated macrophages (TAMs) [35]. Once internalized, apoptotic cells undergo an immunologically silent clearance, regulated by nuclear receptors such as liver X receptor (LXR) and peroxisome proliferator-activated receptor (PPAR) [36]. In contrast, necrotic debris at sites of injury and inflammation triggers a more robust inflammatory response because macrophages detect distinct "find-me" and "eat-me" signals, such as phosphatidylserine for apoptosis and HMGB1 for necrosis. Impaired debris clearance can lead to autoimmunity, so efficient phagocytosis is of utmost physiological importance [37].

Macrophages can exert their **microbicidal activity** by generating reactive oxygen species (ROS) and reactive nitrogen species (RNS) to kill engulfed pathogens while employing lysosomal enzymes to degrade microbial proteins, nucleic acids, and cell walls [38, 39]. Reciprocally, redox signaling, involving ROS and RNS, can regulate macrophage function [38].

Phagocytosis also serves as a critical bridge between **innate and adaptive immunity**. Macrophages, like DCs, can present antigens via major histocompatibility complex class I (MHC I) and MHC II, initiating both $CD4^+$ and $CD8^+$ T cell responses [40-44]. While DCs are more effective in initiating adaptive immune responses, macrophages and DCs collaborate in antigen presentation to activate T cells. Macrophages can transfer antigens to DCs through exosomes, enhancing $CD4^+$ T cell responses [45]. Various RTMs can cross-present antigens via similar pathways as type 1 conventional DCs, potentially contributing to $CD8^+$ T cell activation [46].The link between innate and adaptive immunity involves PRRs (Toll-like receptors, TLRs) and the Notch signaling pathway [47, 48]. TLRs recognize microbial components and activate innate immune responses, while also initiating adaptive immunity [49]. TLR stimulation in macrophages upregulates ligands for the NKG2D receptor, particularly the retinoic acid early inducible 1 (RAE-1) family, facilitating macrophage's communication with NK cells and activated T cells [50]. The Notch signaling regulates macrophage function during inflammation and infection, interacting with TLR signaling and inflammatory cytokines, like macrophages upregulate Notch ligands (Delta-like 1, Dll1) expression on macrophages specifically regulates IFN-γ levels from $CD4^+$ and $CD8^+$ T cells [47, 51].

In vitro, macrophage can **polarize** into distinct phenotypes: “M1” macrophages, which are pro-inflammatory and activated by the type 1 cytokine interferon (IFN)-γ and lipopolysaccharides (LPS), and “M2” macrophages, which are anti-inflammatory and activated by type 2 cytokines interleukin (IL)-4 and IL-13. These polarized macrophages produce and secrete a variety of cytokines that are essential for initiating, maintaining, and resolving inflammation [52, 53]. Pro-inflammatory cytokines like IL-1, IL-6, tumor necrosis factor (TNF)-α, and IL-12 coordinate the acute inflammatory response, while anti-inflammatory cytokines such as IL-10 and transforming growth factor β (TGFβ) help resolve inflammation and promote tissue repair [54]. Macrophages also regulate other immune cells through costimulatory signals and cytokines. “M1” macrophages exhibit potent microbicidal properties and promote type 1 T helper cell (Th1) immune responses, while “M2” macrophages support type 2 T helper cell (Th2) responses and contribute to inflammation resolution [52, 55]. However, recent studies have challenged the traditional M1/M2 macrophage classification, showing that macrophages can display mixed phenotypes, expressing both M1 and M2 markers simultaneously [56, 57]. Their activation states are continuously regulated by complex signals from the tissue microenvironment, resulting in a wide range of phenotypes between the M1 and M2 “extremes” [57, 58]. These findings suggest that the simple pro-inflammatory M1 and anti-inflammatory M2 dichotomy is an oversimplification. Instead, macrophages should be viewed as a heterogeneous population with high plasticity, dynamically shaped by microenvironmental signals [59, 60].

In addition to their immune functions, macrophages importantly contribute to **tissue development**. These versatile cells can help to various developmental processes, including branching morphogenesis, neuronal patterning, angiogenesis, bone morphogenesis, and adipose tissue formation [29, 61]. For example, colony-stimulating factor 1 (CSF1)-regulated macrophages are required throughout early mammary gland development for normal branching morphogenesis [62]. During organ development and remodeling, macrophages support angiogenesis by secreting growth factors, remodeling the extracellular matrix (ECM),

and physically interacting with sprouting vasculature [63]. Additionally, macrophages can modulate angiogenesis during the remodeling of the adipose tissue [64].

During wound healing, macrophages orchestrate several processes: clearing debris, activating and resolving inflammation, and promoting fibrosis [65]. They also support stem/progenitor cells, remodel the ECM, and stimulate angiogenesis [65, 66]. Constant ECM remodeling is vital for tissue restructuring, cell differentiation, and wound repair [67]. Macrophage-derived matrix metalloproteinases (MMPs) are key enzymes involved in degradation and remodeling of ECM during wound healing. These enzymes facilitate cell migration, angiogenesis, and granulation tissue formation [68] However, an imbalance between ECM production and degradation can result in chronic ulcers or excessive scarring [68], highlighting the crucial regulatory role of macrophages for proper **tissue remodeling and repair**.

In conclusion, macrophages are essential immune cells with diverse and dynamic functions. They play a central role in tissue homeostasis by continuously surveying the environment, clearing cellular debris through phagocytosis, and regulating immune responses [28, 29]. Their ability to bridge innate and adaptive immunity is crucial for pathogen defense, antigen presentation, and immune modulation [40, 41]. Macrophages also contribute to wound healing, angiogenesis, and tissue remodeling, while maintaining iron homeostasis and supporting erythropoiesis [29, 61, 71, 72]. Additionally, their phenotypic plasticity allows them to adapt to different microenvironments, exhibiting a spectrum of activation states beyond the traditional M1/M2 classification [56-58]. Macrophages also perform unique, tissue-specific roles that are critical for organ development and maintenance. Recent research continues to uncover novel macrophage functions across various tissues, particularly focusing on their remarkable adaptability and the complexity of their regulatory networks.

1.3. Mechanisms of macrophage differentiation and development

1.3.1. Stem cells and progenitor cells

In mice, macrophages arise from at least three distinct lineages during development. The first wave of macrophage development arises in the YS during early embryogenesis. YS-derived erythro-myeloid progenitors (EMPs) give rise to primitive macrophages, like microglia and some LCs, which seed various tissues before the establishment of definitive hematopoiesis [9, 14]. These YS-derived macrophages develop independently of HSCs and the transcription factor Myb [14]. By mid-gestation, YS-derived EMPs colonize the fetal liver, where they expand and differentiate into fetal monocytes. These monocytes contribute significantly to RTM pools in most organs, replacing YS-derived macrophages in some tissues [74], like AMs, some KCs and LCs. Finally, the third lineage stems from adult HSCs in the BM, which also generates circulating monocytes and replenish certain macrophage populations throughout adult life [75], such as IMs, heart macrophages and intestinal macrophages [76]. The differentiation of HSCs into macrophages involves a complex process of lineage commitment. Common myeloid progenitors (CMPs) give rise to granulocyte-monocyte progenitors (GMPs), which further differentiate into granulocytes and monocytes/macrophages [77-79]. However, recent research has shown that monocyte-dendritic cell progenitors (MDPs) can also produce monocytes independently of GMPs [21, 80]. The *Ms4a3* gene has been identified as a specific marker for GMPs, allowing for precise tracking of monocyte-derived cells [21]. This discovery has enabled accurate quantification of monocyte contribution to RTM populations during homeostasis and inflammation.

1.3.2. Signals guiding macrophage lineage commitment

Macrophages rely on trophic factors for their development and maintenance. Key factors include IL-34, CSF1, also known as macrophage colony-stimulating factor (M-CSF), and CSF2, also known as granulocyte-macrophage colony-stimulating factor (GM-CSF). Among these, CSF1 and IL-34 are often referred to as "twin cytokines" due to their shared signaling pathway through the CSF1 receptor (CSF1R) to regulate macrophage differentiation and homeostasis [81]. IL-34 is a secreted homodimeric glycoprotein that is not detectable in the circulation in mice but is produced locally by keratinocytes in the epidermis, neurons in the brain and hepatic stellate cells in the liver. It is primarily involved in the development of LCs, microglia and KCs

[82-85]. CSF1 exists in two distinct isoforms: a secreted glycoprotein (soluble isoform), which constitutes the circulating pool of CSF1, and a cell surface glycoprotein (membrane-bound isoform associated with the ECM), which serves as a local source of CSF1 [86-89]. This dual-isoform system ensures that CSF1 can effectively regulate macrophage populations in both systemic and tissue-specific contexts, contributing to its broader biological effects compared to IL-34. At steady-state, CSF1R blockade rapidly reduces mature monocyte and RTM numbers, while also triggering inflammatory macrophage accumulation [90]. *Csf1*-deficient mice lack most RTMs expect LCs and microglia, While *Il34*-deficient mice is only partial defective with LCs and brain microglia [82, 84, 91].

CSF2 is a monomeric glycoprotein, primarily expressed in the lung and brain [92, 93]. By binding to its receptors, CSF2RA and CSF2RB subunits, it initiates multiple signaling pathways that control cell survival, proliferation, and functional activation [94]. Type 2 alveolar epithelial cells (AT2) are the major source of CSF2 in the lung, both prenatally and postnatally. AT2 initiate CSF2 expression during lung organogenesis, supporting the proliferation of fetal monocytes that seed the embryonic lungs and their differentiation into AMs [15, 95]. CSF2 deficiency significantly reduces the population of AMs in mice [15, 96].

CSF2 and CSF1 generate macrophages with distinct cytokine profiles and transcription factor activities. *In vitro*, CSF2-regulated macrophages produce more pro-inflammatory cytokines, such as TNF-α, IL-6, IL-12p70 and IL-23, and show higher enhanced nuclear factor-κB (NF-κB) and AP-1 activation, while CSF1-regulated macrophages produce more IL-10 and CCL2 [97]. However, these cytokines also can work together to regulate macrophage diversity rather than acting alone or antagonize each other. The differentiation of GMPs is controlled by cytokines such as CSF1, CSF2, CSF3 (Granulocyte colony stimulating factor, G-CSF), which regulate transcription factors, like PU.1 and C/EBPα to guide cell fate [98]. Balanced signaling between CSF1R and CSF2R is crucial for microglial homeostasis. CSF1R signaling supports microglial survival, while CSF2R activation promotes their functional activation and responsiveness to environmental cues [99]. In the lung, CSF2 stimulates AM proliferation and differentiation, also enhancing their responsiveness to CSF1 [100].

Several chemokines also participate in monocyte/macrophage migration, infiltration and development. Monocyte chemoattractant protein-1 (MCP-1), also known as CCL2, is primarily expressed and upregulated by inflammatory and endothelial cells. By binding to CCR2, $CCR2^{+}$ inflammatory monocytes are recruited to various tissues in response to proinflammatory stimuli and tissue injury [101, 102]. Furthermore, CCL2 enhances efferocytosis of apoptotic cells by macrophages through a Rac1-PI3 kinase-dependent mechanism, which is crucial for resolving acute lung inflammation [103]. Other chemokines, such as CCL7, CCL8, and CCL12, also interact with CCR2 to enhance monocyte recruitment [104, 105].

The CX3CR1/CX3CL1 axis is also involved in the differentiation of myeloid precursors into the macrophage/DC lineage. $CX3CR1^{+}$ pre-macrophages are present in the YS from embryonic day 8.5 (E8.5) and migrate to the embryo, peaking around E10.5 and ceasing by E14.5 [106]. While CX3CR1 deficiency does not affect the development of monocytes, conventional DCs (cDCs) and plasmacytoid DCs (pDCs), it selectively impairs the recruitment of blood monocytes to the spleen during acute inflammation [107]. CX3CL1 is released from apoptotic lymphocytes, attracting macrophages to facilitate efficient clearance of apoptotic cells [108]. In skin wound healing, CX3CR1 mediates macrophage and fibroblast accumulation at the wound site, promoting tissue repair through the release of profibrotic and angiogenic factors [109].

1.3.3. Niche and tissue resident-macrophage specific transcription factors

Macrophages exhibit remarkable functional diversity, adapting to specific microenvironments [110]. RTM differentiation and identity are determined by two distinct classes of transcription factors [111].

First, lineage-determining transcription factors, such as PU.1, MYB or ZEB2, are thought to establish core macrophage programs and control their common features [112-117]. Cell surface proteins such as MerTK, Adgre1 (F4/80), CX3CR1, Fcγ receptors (e.g., *Fcgr1*, encoding CD64), PRRs, and phagocytic receptors, which are expressed by almost all RTM populations, can be seen as part of a macrophage core identity and instruct cells to perform

common macrophage functions, like phagocyting particles, pathogens, and dying cells, secreting cytokines/chemokines and initiating immune responses [10, 26, 118].

Second, tissue-specific microenvironmental or niche signals can also instruct macrophages to express signal-dependent transcription factors that drive their tissue-specific identity in different tissues [26, 119, 120]. For example, in the **liver**, KC identity genes are *Nr1h3* (encoding LXR-α), *Spic*, *Id1*, *Id3,* and *Irf7* [121]. Following KC depletion, BM monocytes can repopulate their niche and differentiate into monocyte-derived KCs, which are genetically and functionally similar to their embryonic counterparts [122]. Hepatocytes contribute to this process by inducing DNA3 (ID3) in monocytes. Endothelial cells and stellate cells can synergistically activate LXR-α via a NOTCH signaling pathway or/and a TGFβ signaling pathway [85, 121]. These liver niche signals are essential for the differentiation and maintenance of KCs. In the **spleen**, RPMs are specialized in phagocytosing senescent erythrocytes and recycling heme-associated iron [123, 124]. SPI-C, a PU.1-related transcription factor, plays an important role in the development of RPMs [125]. In monocytes, SPI-C expression is constitutively inhibited by the transcriptional repressor BACH1. Heme induces proteasome-dependent BACH1 degradation, enabling SPI-C expression and subsequent differentiation of monocytes into RPMs [123]. RPMs are primarily generated during embryogenesis and maintained throughout adulthood, with their development and survival regulated by factors such as IRF8/4, heme oxygenase-1, and CSF1 [124].

1.4. Lung tissue-resident macrophages

Mammalian lungs are at the interface between the host and the external world and are continuously exposed to pathogens, allergens, microbial products and other insults entering via the air or the blood. Lung health is crucial for vital gas exchanges, providing oxygen to the bloodstream and removing carbon dioxide in excess from the body. In order to allow efficient gas diffusion and to support life, the airways must be permeable, and the air-blood barrier must remain very thin. Therefore, the lung immune system has evolved as a sophisticated surveillance and defense system to sustain physiological functions and host protection [126].

Dedicated to these tasks, two main populations of RTMs exist in the steady-state lung: AMs and interstitial macrophages (IMs) [127, 128]. Based on their anatomical location, macrophages situated in the alveolar lumen are referred to as AMs, while "non-alveolar" macrophages are mainly present in the lung interstitium, defined as IMs. In 1950, Kaplan *et al.* indeed identified a "non-alveolar" macrophage population, which they termed phagocytic septal cells [129]. In the early 1970s, van Furth and Cohn identified AMs as the main lung RTM population [3] and for decades, macrophages in the interstitium were considered as a transition state between monocytes and AMs [130-132]. The development of tools and techniques for lung tissue digestion and single cell isolation allowed many improvement in our understanding of lung IMs [133]. It is now well-established that IMs represent a distinct RTM population residing in the lung parenchyma [134-137]. A detailed comparison between AMs and IMs is provided in Table 1.

Table 1. Comparison between lung AMs and IMs.

Feature		AMs	IMs
Morphology [138]	Size & shape	Larger size more pseudopodia	Smaller size irregularly shaped nuclei
Marker expression (mice) [139-144]	High expression	MerTK, F4/80, CD36, CD64	
		CD206, SiglecF, CD11c	CD11b, CD86, CD14, CX3CR1
	Intermediate/ variable expression	CD115, CD169, MHC II	
		CD86, CD14	CD206, CCR2, Lyve1, CD11c
	Absent/low expression	CD103, CD24, Ly6C, Zbtb46	
Marker expression (human) [145, 146]	Shared markers	CD68, HLA-DR (MHC II), CD11b	
	Identification markers	CD169	CD36
Location [147, 148]	In the lung	Airway lumen	Interstitium near bronchi, nerves, and blood vessels
Origins [15, 16, 137, 144, 147, 149-152]	Origin (steady state)	Fetal liver-derived mononuclear cells that settle in the airway lumen before and after birth	Embryonic origin of the YS and postnatal contribution of the BM
	Maintenance	Self-sustaining, with minimal contribution from circulating monocytes in young adults, but gradually replacing the AM pool with age	Replenished by circulating monocytes over time
Biological Functions [137, 153, 154]	Steady state	Recycling of surfactant molecules and removal of debris	Maintaining of lung homeostasis, constantly secreting IL-10; Antigen presentation
	Inflammatory situation	Pro-inflammation Cytokines secretion and ROS	Secreting IL-10, wound healing and tissue repair.

In brief, AMs are larger and more homogeneous than IMs. They also exhibit a stronger adherence potential to vitronectin and fibronectin-coated surfaces [153], and show a higher phagocytic activity against inhaled particulates as compared to IMs [153, 155]. Because the alveolar space is constantly exposed to harmless antigens (like dust, pollen, and commensals), overactivation would cause massive inflammation and tissue damage. Thus, AMs have lower MHC II, and focus more on phagocytosis, and AM express low B7 costimulatory molecules, which are necessary for T cell activation [156]. Conversely, IMs are positioned deeper in the tissue, closer to blood vessels and lymphatics, and may serve as a "second line" defense. IMs express more MHC II, like DCs, and can bridge innate and adaptive immunity by presenting antigens to naive T lymphocytes and inducing regulatory T cells (Tregs) [41], while other reports suggest that they contribute to local Th2 activation [157].

AMs rely on CSF2 produced by AT2 during their development from fetal liver monocytes that colonize the lungs during embryonic development, which then mature perinatally [15, 95, 158]. CSF2 is also essential for the maintenance of AMs in adult lungs at steady state [95]. Such embryonically-derived AMs exhibit a unique transcriptomic profile and are relatively stable. However, perturbations observe in inflammation or aging can lead to their replacement by monocyte-derived AMs [152, 159]. Neonatal neutrophil-derived 12-hydroxyeicosatetraenoic acid (12-HETE) is essential for AM self-renewal and longevity [160], while histone deacetylase 3 (HDAC3) regulates AM development, homeostasis, and maturation [161]. Additionally, TGFβ plays a crucial role in AM development and homeostasis through an autocrine signaling loop. TGFβ signaling, along with CSF2, upregulates PPAR-γ, a key transcription factor for AM development [158] (Figure 1). Other transcription factors, like Bach1 and Bach2, work complementarily to maintain normal AM function, with Bach2 being the major contributor [162]. C/EBPβ regulates AM identity, proliferation, phagocytosis, and lipid metabolism, particularly through the induction of *Pparg* isoform 2 expression in conjunction with CSF2 signaling [163]. AMs can clear lipoprotein-containing alveolar surfactant produced by AT2, an essential component of alveolar homeostasis [111]. The absence of CSF2, Bach2 and C/EBPβ in mice

leads to pulmonary alveolar proteinosis (PAP), a condition characterized by the accumulation of surfactant in the lungs [163-165].

IMs arise from diverse sources, including YS primitive progenitors and adult BM monocytes [128]. These progenitors can colonize vacant niches and differentiate into functional IMs, regardless of their origin, and CSF1 and CCL2 participate in this process [166, 167]. The transcription factors MafB and c-Maf play pivotal roles in IM development and differentiation. Indeed, we recently found that MafB regulates the transition from monocyte proliferation to IM subset specification, while c-Maf specifically controlled the identity of the $CD206^{+}$ IM subsets [167] (Figure 1). Additional information about IM heterogeneity can be found below. Notably, MafB and c-Maf expression is induced by CSF1 but reduced by CSF2 [168-170]. Other studies have shown that MafB-deficient macrophages exhibited reduced C1q expression and impaired efferocytosis [171]. C-Maf is essential for IL-10 production in macrophages, directly binding to the IL-10 promoter [172]. It also binds to a conserved non-coding sequence of the *Csf1r* gene, promoting M2-like macrophage polarization and T cell suppression [173]. Additionally, in an LPS-induced injury model, endothelial cells can secrete Rspondin 3, which instructs IM transition through metabolic-epigenetic reprogramming, promoting an anti-inflammatory phenotype and resolving inflammatory injury [174]. Further studies are required to elucidate the interactions and mechanisms between transcription factors and lung niche signals in the regulation of IM development in the steady-state lung.

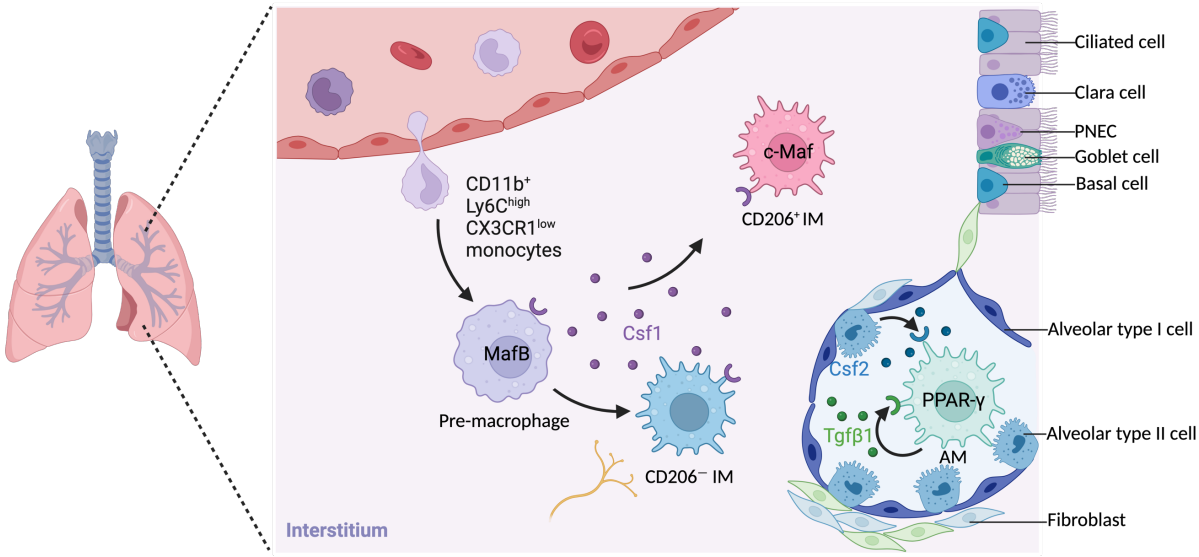

Figure 1. Localization and developmental regulation of lung macrophages in adult mice*. In the lung, embryonic AMs can be maintained through self-renewal within the alveolar lumen. AMs rely on AT2-derived CSF2, as well as TGFβ secreted in an autocrine manner, which sustain AM identity by upregulating the transcription factor PPARγ [158]. IMs are constantly replaced by monocytes in adults. Their development is orchestrated by the master transcription factor MafB [167]. Within the lung interstitium, IMs can be classified into two major subpopulations based on CD206 expression and their anatomical location. CD206^{+} IMs are primarily located near bronchial interstitium and blood vessel, CD206^{-} IMs are found in proximity to nerves [147, 148].*

1.4.1. Lung interstitial macrophages

1.4.1.1 IM heterogeneity

Until recently, IMs were considered as a homogenous population and were mainly investigated in functional studies [128, 139, 144, 175]. According to a report by Gibbings et al., mouse IMs are more heterogenous than previously thought and can be categorized into three subsets based on their expression of CD11c and MHC II: CD11c^{lo}MHC II^{lo} (IM1), CD11c^{lo}MHC II^{hi} (IM2), CD11c^{hi}MHC II^{hi} (IM3) [141]. To define IM subsets more comprehensively, Chakarov et al. and Schyns et al. performed single-cell RNA sequencing (scRNA-seq) on mouse bulk IMs and identified two distinct IM subpopulations, CD206^{-}Lyve-1^{-}MHC II^{hi} IM and

CD206^{+}Lyve-1^{+}MHC II^{lo} IM [147, 148]. Gene expression profiling revealed that CD206^{+}Lyve-1^{+}MHC II^{lo} IMs resembled IM1/IM2, while CD206^{-}Lyve-1^{-}MHC II^{hi} IM shared similarities with IM3. While up to 10 different IM subsets have been identified based on distinct chemokine expression profiles [176], a consensus seems to emerge that IMs can be primarily categorized into two main subsets, namely CD206^{+} IMs and CD206^{-} IMs occupying distinct niches [147, 148, 176, 177].

Schyns *et al.* showed that CD206^{+} IMs predominately populated the peribronchial and perivascular interstitium, where they produced high levels of chemokines and immunosuppressive cytokines, such as IL10 [147]. Conversely, CD206^{-} IMs were primarily located in the alveolar interstitium and associated with nerves, exhibited features of antigen-presenting cells [41, 147]. In human lungs, a distinct population of HLA-DR^{+}CD169$^{-/lo}$CD206$^{+/int}$ cells has been identified, exhibiting a size intermediate between AMs and monocytes, potentially representing human IMs [178]. Human IMs are predominantly found in alveolar septa (78%), with smaller populations around small vessels (14%) and airways (7%) [179].

1.4.1.2 IM ontogeny

IM ontogeny is complex and involves both embryonic and postnatal origins. Tan and Krasnow used genetic lineage tracing in *Runx1*^{CreER} transgenic mice and found that a subset of yolk-sac-derived pre-macrophages seeds the lung at E10.5, persisting as primitive IMs in specific niches [137]. A second wave, originating from BM-derived monocytes, emerges postnatally, forming definitive IMs distributed throughout the lung [137, 144]. Unlike AMs, which self-maintain [15, 16, 149], IMs are partially replenished by circulating monocytes, as shown by parabiosis studies [137, 180]. Further complexity arises from IM heterogeneity, with distinct subpopulations exhibiting different turnover rates [141]. Upon inflammation, LPS- and HDM-induced IMs are derived from CCR2-dependent Ly6C^{+} classical blood monocytes, similar as steady state IMs [142, 144]. Notably, CpG-DNA exposure can drive IM expansion from CCR2-independent Ly6C^{+} monocytes residing in the lung or spleen, independently of classical recruitment pathways [144].

1.4.1.3 IM function

At steady-state and in models of allergic airway inflammation, IMs produce high levels of IL-10, which can inhibit DC-driven Th2 responses to inhaled antigens [139]. Exposure to bacterial CpG-DNA can expand regulatory IMs from splenic and local monocytes, conferring protection against allergic airway inflammation in an IL-10-dependent manner [144]. IMs constitutively produce IL-10 through TLR4/MyD88 pathway activation, independent of microbiota, and their IL-10 production increases in response to house dust mite (HDM) challenge [142]. Transferred wild-type (WT) IMs can reduce neutrophilic inflammation and Th2/Th17-mediated responses in HDM treated $Il10^{-/-}$ mice [142]. Hence, these findings support the importance of IMs in lung homeostasis and in the prevention of immune-mediated allergic airway inflammation.

Li et al. identified distinct chemokine-expressing IM subsets and demonstrated that depletion of $CD206^{hi}$ IMs led to reduced inflammatory cell recruitment, diminished tertiary lymphoid structure (TLS) formation, and fewer germinal center B cells in allergen- and infection-driven inflammation models [176]. These TLS, also known as tertiary lymphoid organs (TLOs), are organized aggregates of immune cells that form in response to chronic immune stimulation [181]. However, the role of IMs in response to bacterial infections and their relationship with TLSs remains insufficiently explored.

Considering that IMs highly express Arginase-1 and $CD206^{+}$ IMs express markers typical of “M2” macrophages, they may play in pulmonary fibrosis. In bleomycin-induced models, IMs emerge as the predominant macrophage population during early stages to activate fibroblasts and promote differentiation in myofibroblasts, exhibiting a phenotypic shift from pro-inflammatory ($Ly6C^{+}$ IMs) to anti-inflammatory and pro-fibrotic ($CD206^{+}$ IMs) over time [182, 183]. Particularly $C1q^{+}$ IMs are distributed around fibrotic nodules and possess these properties [184]. The depletion of IMs using a clinically available CSF1R neutralizing antibody has been shown to reduce radiation-induced lung fibrosis in mice [185]. Single-cell RNA sequencing revealed that monocyte-derived IMs display a pro-fibrotic gene expression profile and interact with fibroblasts through TGFβ, secreted phosphoprotein 1 (SPP1), and platelet-

derived growth factor (PDGF) signaling pathways [186]. Treatment with anti-TNFα antibodies has been shown to reduce both pro-inflammatory and pro-fibrotic IM populations, potentially offering therapeutic benefits [183]. In another context, Chakarov et al. showed that diphtheria toxin (DT)-induced depletion of $CD206^{+}$ IMs in $Lyve1^{Cre/GFP}Slco2b1^{flox/DTR}$ chimeric mice resulted in exacerbated neutrophilic inflammation and lung fibrosis after bleomycin exposure [148]. Hence, further research is needed to fully elucidate the specific contributions of IMs to the pathogenesis of lung fibrosis.

During influenza infection, IMs actively proliferate and serve as the primary producer of IL-10 [177]. Unlike AMs, which drastically decrease in infected mice, IMs are primarily responsible for clearing apoptotic AT2 via efferocytosis [187, 188]. These findings challenge the earlier assumption that AMs were the main efferocytic cells [189, 190].

Importantly, in most of the models used to address IM functions, and under these circumstances of exposure, monocytes can also be recruited to the lung and contribute to a pool of recruited macrophages that often overlap phenotypically with IMs [19, 191, 192]. Such convoluted landscape can complicate the interpretation of findings about the precise contributions of resident IMs vs. recruited macrophages in various lung disorders. Hence, the potential tissue-supportive and homeostatic functions of IMs at steady-state are still unclear. In the future, a deeper understanding of the diverse roles of IMs could offer potential therapeutic strategies for treating pulmonary diseases.

1.4.2. Experimental models available to study macrophage and IM biology

***Lyz2^{Cre}* mice**. The *Lyz2* gene encodes lysozyme 2 (also known as lysozyme M), an enzyme primarily expressed in myeloid cells, including DCs, monocytes, macrophages, neutrophils, and AT2 [193, 194]. It's frequently employed as a deleter line for gene deletion with the myeloid lineage. In the lung, *Lyz2^{Cre}* can target AMs and IMs with a high efficiency [167, 194, 195]. However, recent studies have revealed limitations and unexpected expression patterns with this model. *Lyz2^{Cre}*-mediated recombination has been observed in brain neurons and retinal ganglion cells, raising concerns about its specificity [193, 196]. In the retina, *Lyz2^{Cre}*

is strongly expressed in microglia/resident macrophages of neonatal mice and to a lesser extent in adult mice [196]. The model has also shown incomplete deletion of target genes in inflammatory settings, with a subset of macrophages resisting *Lyz2*^{Cre}-mediated deletion due to lower *Lyz2* expression [197].

***Csf1r*^{Cre} mice**, The *Csf1r* gene encodes a tyrosine kinase receptor crucial for macrophage differentiation and hematopoiesis [198]. *Csf1r*^{Cre} targets AMs and IMs in the lung with high efficiency but also targets lymphocytes with over 80% efficiency [195]. This broad targeting range can complicate studies aiming for macrophage-specific gene manipulation.

***Cx3cr1*^{Cre} *and* ^{CreER} models.** The constitutive *Cx3cr1*^{Cre} system is widely used for gene manipulation in microglia and macrophages but can have unintended effects. For instance, in early postnatal microglia, Cre induction leads to activation, increased phagocytosis, and DNA damage, causing aberrant synaptic pruning and later anxiety [199]. Of note, the tamoxifen-inducible *Cx3cr1*^{CreER} mice have been successfully used to study microglial functions, such as their role in promoting learning-dependent synapse formation through brain-derived neurotrophic factor (BDNF) signaling [200]. In lung macrophages, tamoxifen treatment of *Cx3cr1*^{CreER} efficiently targeted 90% of IMs but did not target AMs [195].

***Tmem119* reporter and *Tmem119*^{CreERT2} mice**. These mice have been developed for specific labeling and manipulation of microglia [201]. Indeed, a *Tmem119*^{tdTomato} reporter mouse model allows for selective visualization of microglia throughout the CNS [202]. While these models primarily focus on microglia, the expression of Tmem119 in lung IMs suggests potential applications in pulmonary studies as well (see below) [167].

CD68-rtTA. This system utilizes the CD68 promoter to drive expression of the reverse tetracycline transactivator (rtTA), enabling doxycycline-inducible gene expression in macrophages [203]. It allows for inducible and selective targeting of CD11b^{+} MNPs in the murine lung, specifically recruited macrophages and RTMs. It achieves approximately 75% efficiency with IMs but not AMs [193, 204].

***Tmem119^{Cre}Cx3cr1$^{LSL-DTR}$* (IM^{DTR}) mice**. Vanneste et al, found Cx3cr1 and Tmem119 were highly expressed in IMs. To investigate the development of lung IMs from monocytes, we crossed *Cx3cr1$^{LSL-DTR}$* mice (*LSL, Lox-STOP-Lox)* with in-house developed *Tmem119^{Cre}* mice, enabling diphtheria toxin receptor (DTR) expression specifically in Tmem119^{+} CX3CR1^{+} IMs. A single injection of 50 ng DT selectively depletes IMs in the lung, with no significant impact on other RTM populations. Depletion of IMs is evident within 2 days post-DT injection, and such empty niche is then repleted with newly differentiated IMs, to such an extent that IM levels are restored to normal levels between 7 and 14 days post-DT, indicating a transient and specific effect [167]. The combination of such irradiated IM^{DTR} model with thorax protection and reconstitution with genetically deficient BM cells represents a unique model to study IM development from monocytes while leaving embryonically-derived AM untouched.

***Lyz2^{Cre} Slco2b1$^{flox/DTR}$* (SLCO) mice**. Chakarov et al identified high *Slco2b1* expression in lung macrophages and crossed *Slco2b1$^{flox/DTR}$* to *Lyz2^{Cre}* mice (*Lyz2^{Cre} Slco2b1$^{flox/DTR}$*), called SLCO mice. The MerTK^{+}CD64^{+} population (AMs and IMs) was totally depleted post-DT treatment within 16 hours. Other myeloid and lymphoid populations were unaffected by DT treatment. The repopulation kinetics differed between AMs and IMs, with IMs rapidly repopulating following monocyte infiltration, while AMs required 21 days to start repopulating and normalized levels after 120 days post-DT. *Lyve1$^{Cre/GFP}$Slco2b1$^{flox/DTR}$* mouse model was generated specifically to target Lyve1^{+}MHCII^{lo} macrophages, *Lyve1$^{Cre/GFP}$Slco2b1$^{flox/DTR}$* BM transferred to CD45.1 mice, and Lyve1^{hi}MHCII^{lo} IM depletion was then observed 24 hours after DT injection [148].

Specific depletion of CD206^{+} IMs was recently observed in DT-treated ***Pf4^{cre}R26$^{EYFP+DTR}$*** and ***Pf4^{cre}R26^{EYFP}Cx3cr1^{DTR}*** mice, which led to diminished inflammatory cell recruitment, reduced TLS formation and fewer germinal center B cells in models of allergen- and infection-driven inflammation [176]. Ural et al. crossed the *Cd169^{Cre}* mice to *Cx3cr1$^{LSL-DTR}$* mice to specifically deplete CD169^{+} IMs (nerve-associated IMs) but not AMs. Absence of CD169^{+} IMs in DT-treated influenza-infected *Cd169^{Cre}Cx3cr1$^{LSL-DTR}$* mice led to elevated inflammation as compared to controls [177].

Lung IMs can also be depleted using anti-CSF1R inhibition (PLX5622) or neutralizing CSF1R antibodies [166, 177, 185]. IMs numbers are also significantly decreased in *Csf1r*$^{-/-}$ mice [177, 205], as the CSF1/CSF1R signaling axis is critical for IM survival and maintenance. Notably, anti-F4/80 antibodies have also been shown to efficiently deplete IMs without targeting AMs [139, 206]. While competitive chimeric studies using *Ccr2*$^{-/-}$ and WT BM cells supported that IMs derived from CCR2-dependent BM monocytes [167], *Ccr2*$^{-/-}$ mice only display difference in IM or AM numbers in aged mice, which may be due to compensatory mechanisms [144, 207].

In conclusion, while various experimental models exist and have revealed important insights into lung IM biology, they suffer from limitations and indicate that additional efforts and more sophisticated models, such as a transgenic mouse model that would specifically target specific IM subsets, are needed to more thoroughly and specifically study IMs in the future.

2. TGFβ signaling

2.1. TGFβ signaling pathway

TGFβ is a pleiotropic cytokine that regulates various cellular processes, including cell growth, differentiation, apoptosis, as well as immune responses [208, 209]. TGFβ signaling pathway integrates into the cellular networks through interactions with other signaling cascades, enabling cell- and tissue-specific effects [208]. Its effects on various immune cells are context-dependent and vary based on the cellular environment, timing, and location [209], which shows the importance of TGFβ in maintaining immune homeostasis and mediating responses to infection and tissue damage.

TGFβ superfamily represents a broad group of secreted signaling proteins comprising 33 distinct genes in mammals, including TGFβs, bone morphogenetic proteins (BMPs), activins, and growth differentiation factors (GDFs) [210-212]. Among these, TGFβ is the most extensively studied, with three primary isoforms identified in mammals: TGFβ1, TGFβ2, and TGFβ3 [211].

The TGFβ superfamily proteins are synthesized as prepropeptide precursors and secreted as homo- or heterodimers, playing crucial roles in diverse developmental and physiological pathways [211]. Studies using knockout mice have revealed distinct functions for each TGFβ isoform. TGFβ1 null mutants show defects in vasculogenesis, hematopoiesis, and germ cell development [211, 213]. TGFβ2 knockout mice exhibit multiple developmental defects, including reduced seminiferous cords and increased ovarian germ cells [213]. TGFβ3 null mutants display delayed pulmonary and defective palate development [211]. Expression patterns of these isoforms vary during embryogenesis, with TGFβ1 predominantly expressed in mesodermal components, TGFβ2 in facial mesenchyme and epithelial layers, and TGFβ3 in prevertebral tissue and lung epithelia. All three isoforms are expressed in bone tissues, but with distinct spatial and temporal patterns [214].

TGFβ is synthesized as a precursor protein that undergoes intracellular modification, including the cleavage of the C-terminal pro-region, known as latency-associated peptide (LAP) [215]. The mature TGFβ dimer noncovalently associates with LAP to form the small latent complex (SLC) [216], which masks the receptor-binding site and renders TGFβ biologically inactive [215]. The secreted complex of TGFβ and LAP can be bound by latent TGFβ binding protein (LTBP), forming a large latent complex (LLC), which is targeted to ECM [217]. The leucine-rich repeat-containing protein 32 (LRRC32), also known as glycoprotein-A repetitions predominant protein (GARP), together with LRRC33, tether SLCs to the cell surface [218-220]. Cell types that highly express LRRC can be found in Table 2. Importantly, these ligands are secreted as latent complexes that require activation to bind their receptors [221]. Activation can occur through integrin-dependent or integrin-independent mechanisms. TGFβ activation by integrins requires the binding of the integrins to an arginylglycylaspartic acid (RGD) sequence within the LAP of TGFβ1 and TGFβ3, a feature absent in latent TGFβ2 [221, 222]. Among the integrins, αVβ6 and αVβ8 are the most extensively studied TGFβ activators, expressed by the cell types in Table 2 [223]. Integrin-independent activation can be achieved through ROS, with LTGFβ1 being uniquely sensitive to ROS-mediated activation via a redox switch centered at methionine 253 in LAPβ1 [224]. Others integrin-independent activators

include acids, bases, proteases, and thrombospondin-1 (TSP-1) [225]. These diverse pathways ensure precise control of TGFβ activation in response to specific cellular and environmental cues (Figure 2).

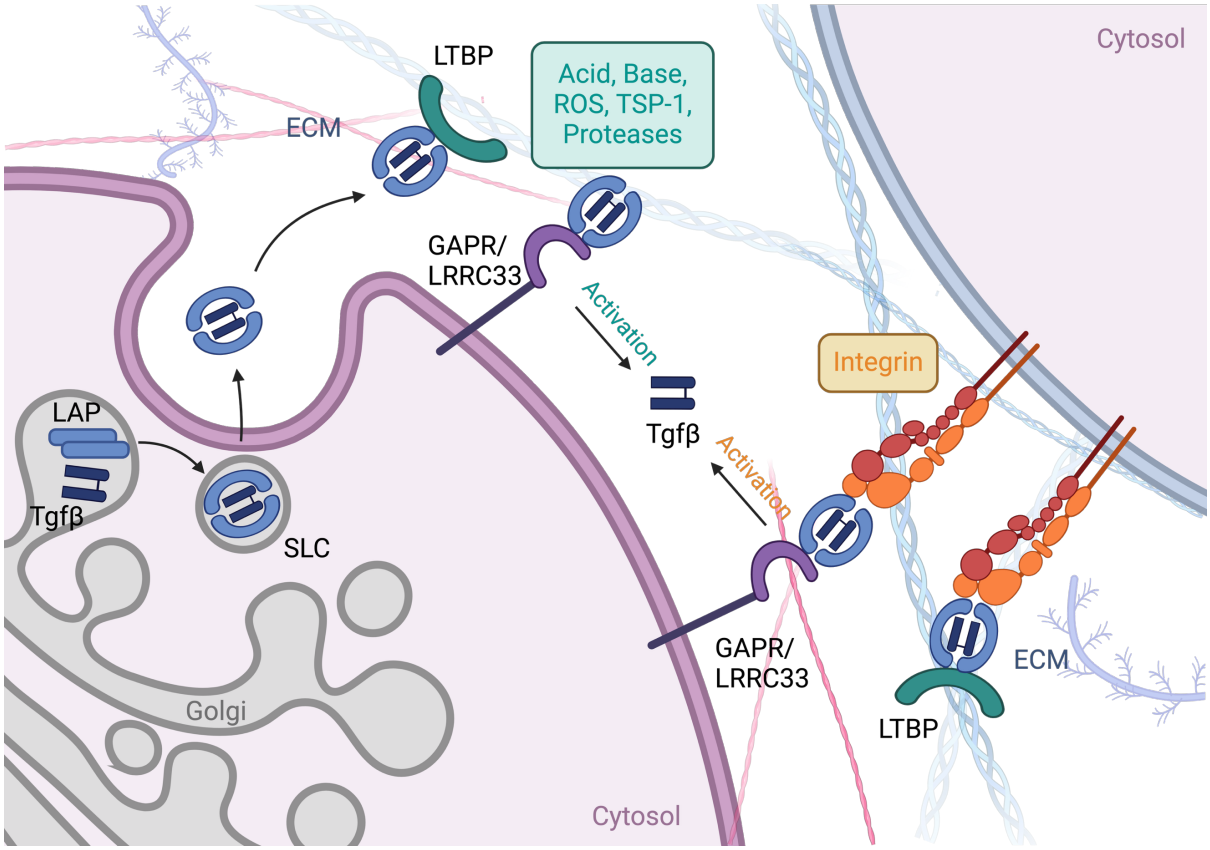

Figure 2. TGFβ activation and regulation. *TGFβ is synthesized as an inactive precursor, where the mature TGFβ dimer remains bound to the latency-associated peptide (LAP), forming the small latent complex (SLC) [215, 216]. SLC can associate with latent TGFβ binding proteins (LTBP) to form the large latent complex (LLC), which is stored in the extracellular matrix (ECM) [217]. Additionally, LRRC32 (GARP) and LRRC33 tether SLC to the cell surface, controlling TGFβ availability [218-220]. Activation of latent TGFβ is required for receptor binding and occurs through integrin-dependent or integrin-independent mechanisms [221]. Non-integrin activation can occur via reactive oxygen species (ROS), proteases, acids, bases, or thrombospondin-1 (TSP-1) [224, 225].*

Table 2. Cell types expressing TGFβ binding proteins and integrins.

	Expressed cells
LRRC32(GAPR) [226]	Tregs, platelets and endothelium
LRRC33 [227]	Macrophages, DCs, and B cells
Integrin αVβ6 [228]	Epithelial cells
Integrin αVβ8 [229-234]	Epithelial cells, fibroblasts, macrophages, DCs, Tregs, and different kinds of tumor cells

The TGFβ signaling pathway is highly conserved across species and involves a series of well-coordinated events that transmit signals from the cell surface to the nucleus, ultimately influencing gene expression [235-237]. The pathway is initiated when TGFβ ligands bind to a heteromeric complex of TGFβ receptor type I and type II serine/threonine kinase receptors on the cell surface [238]. The receptors include the TGFβ receptor type II (TGFβRII), exhibiting constitutive kinase activity and, upon TGFβ ligand binding, phosphorylates and activates the TGFβ receptor type I (TGFβR1/ALK5), thus activating its kinase activity [239, 240]. TGFβ receptor type III (TGFBRIII/β-glycan) interacts with the TGFβ3, resulting to the phosphorylation of TGFβRIII cytoplasmic domain. This interaction facilitates the assembly of an active signaling complex between type I and auto phosphorylated type II receptors [241]. While TGFβRI and TGFBRII possess serine/threonine and tyrosine kinase activities, TGFβRIII lacks kinase activity. TGFβ1 and TGFβ3 bind to TGFβRII with higher affinity than to TGFβRI, whereas TGFβ2 has low binding affinity for both receptors [242]. Mice lacking TGFβ receptors exhibit severe developmental defects. *Tgfbr1* knockout leads to embryonic lethality and female reproductive tract abnormalities [243], while *Tgfbr2* deletion in cranial neural crest cells causes craniofacial malformations, including cleft palate, due to aberrant noncanonical TGFβ signaling [244]. *Tgfbr3*-null mice die at embryonic day E14.5 due to impaired coronary vasculogenesis and epicardial defects [245].

Following ligand-receptor interaction, intracellular TGFβ signaling transduction is activated through canonical and non-canonical pathways [246]. The canonical TGFβ signaling pathway, also referred to as Suppressors of Mothers against Decapentaplegic (SMAD) signaling, begins with the activation of TGFβRI, which phosphorylates receptor-regulated SMAD proteins (R-SMADs), specifically SMAD2 and SMAD3. Phosphorylated SMAD2 and SMAD3 then form a complex with the common-mediator SMAD (Co-SMAD), SMAD4 [247]. The SMAD2/3-SMAD4 complex translocates into the nucleus, where it functions as transcription factor by binding to specific DNA sequences known as SMAD-binding elements (SBEs) [248]. SMAD complexes cooperate with other transcription factors, coactivators and corepressors to modulate gene expression [248, 249].

TGFβ signaling can also activate SMAD-independent pathways, such as ERK, p38 mitogen-activated protein kinase (MAPK), PI3K/AKT, NF-κB, and Rho guanosine triphosphatase (GTPase) signaling, contributing to its diverse biological effects [246].

TGFβ signaling is tightly regulated by negative feedback mechanisms to prevent excessive or prolonged signaling. In the canonical pathway, SMAD6 and SMAD7, as inhibitory SMADs (I-SMADs), can be induced by TGFβ signaling to inhibit the phosphorylation of R-SMADs and disrupt the receptor complex [248, 249]. I-SMADs can recruit ubiquitin ligases (e.g., Smurf1, Smurf2) to the receptor complex, leading to its ubiquitination and degradation [250].

In conclusion, the TGFβ signaling pathway is a complex and tightly regulated network that influences a wide array of cellular functions and processes, and understanding its components and mechanisms will help elucidating its roles in physiology and disease pathogenesis.

2.2. TGFβ in immune regulation

TGFβ is a pleiotropic cytokine that plays essential roles in immune regulation, tissue homeostasis, and development. TGFβ can act on various structural and immune cells, including epithelial cells, lymphocytes, natural killer (NK) cells, mononuclear phagocytes (MNPs) and granulocytes, influencing their proliferation, differentiation, survival and functions [251]. Its functions are highly context-dependent, ranging from promoting immune tolerance and tissue repair to driving fibrosis and immune suppression in pathological conditions, including cancer and chronic inflammation [209, 251]. Given its broad impact on various biological processes, TGFβ has been extensively studied in different organ systems. The complex effects of TGFβ on the immune system make it an attractive but also complex target for therapeutic interventions [251, 252].

In this chapter, we will specifically focus on its roles in the lung, where it critically influences lung development, repair and disease progression, and in macrophage biology, where it shapes cellular differentiation, activation, and function.

2.3. TGFβ in lung physiology and pathology

2.3.1. TGFβ in lung development and repair

TGFβ is produced by various cells in the lung, including macrophages, epithelial cells, endothelial cells and fibroblasts [253, 254]. All three TGFβ isoforms are highly expressed during normal lung development [255].

During lung organogenesis, TGFβ modulates epithelial cell proliferation, differentiation and migration, and can induce epithelial-mesenchymal transition (EMT) and orchestrate ECM remodeling. These processes ensure the proper formation of the bronchial tree and the alveolarization [237, 256-258]. TGFβ can promote the differentiation of mesenchymal cells into smooth muscle cells, fibroblasts and myofibroblasts, which are essential for maintaining the structural integrity of the lung [259-262]. Type 1 alveolar epithelial cells (AT1) and AT2 are crucial components of the lung alveoli. Thin and squamous AT1 cover most of the alveolar surface and facilitate gas exchanges. In contrast, cuboidal AT2 produce surfactant and function as stem cells for alveolar repair and regeneration [263]. The transdifferentiation of AT2 to AT1 is regulated by opposing TGFβ and BMP signaling. TGFβ promotes this process by repressing AT2-specific gene expression while weakly inducing AT1-specific gene expression, while BMP signaling delays this process [264]. Deletion of *Tgfbr2* in AT1 during late lung development results in their reprogramming into AT2, causing persistent alterations in pulmonary architecture into adulthood [265]. TGFβ also inhibits the expression of surfactant proteins (SPs) A, B, and C in human AT2 [266].

2.3.2. TGFβ in lung diseases

In various pulmonary pathologies, increased TGFβ expression often precedes abnormalities in lung function and is closely associated with disease severity [255].

Following lung injury, TGFβ is rapidly upregulated and orchestrates tissue repair by promoting fibroblast proliferation and ECM production [267]. It promotes the proliferation and migration of fibroblasts and myofibroblasts to the site of injury, leading to the production of ECM proteins such as collagen [268-270]. This matrix deposition is crucial for wound healing

and the restoration of lung architecture. However, prolonged dysregulation in TGFβ signaling can result in structural alterations that impair gas exchange and lung function, as observed in conditions such as bronchopulmonary dysplasia and chronic obstructive pulmonary disease (COPD) [271]. AMs have been recently shown to secrete TGFβ2 to maintain cancer cells in a dormant state along with persistent macrophage-cancer cell interactions via TGFβRIII receptor [272].

During the early stages of injury, TGFβ secretion decreases, allowing for increased proliferation of AT2 [215]. However, as repair progresses, TGFβ levels rise, halting AT2 proliferation and promoting cell cycle arrest [273]. This process is essential for maintaining the balance between proliferation and differentiation of alveolar progenitor cells. As mentioned above, TGFβ possess potent anti-inflammatory effects and contribute to resolve inflammation and to the transition from the inflammatory phase to the repair phase [274].

In asthma, TGFβ contributes to airway remodeling through subepithelial fibrosis, smooth muscle hypertrophy, and increased mucus production [275]. It also activates and is produced by eosinophils, perpetuating inflammation [276]. In COPD, TGFβ initially promotes tissue repair but can lead to abnormal remodeling and emphysema development when dysregulated [275]. In idiopathic pulmonary fibrosis (IPF), a progressive lung disease characterized by excessive ECM deposition and impaired lung function, TGFβ production increases prior to collagen synthesis and is secreted by AMs [277-279]. Activated TGFβ exacerbates epithelial apoptosis, EMT, and transformation of fibroblasts and fibrocytes into apoptosis-resistant myofibroblasts, culminating in excessive ECM deposition and fibrosis [280]. TGFβ also exhibits immune-suppressive actions, potentially increasing susceptibility to infections in fibrotic lung diseases [281]. Altogether, by regulating cell proliferation, differentiation, apoptosis, and matrix homeostasis, TGFβ appears to be a master regulator of respiratory health and disease [282], shown in Figure 3.

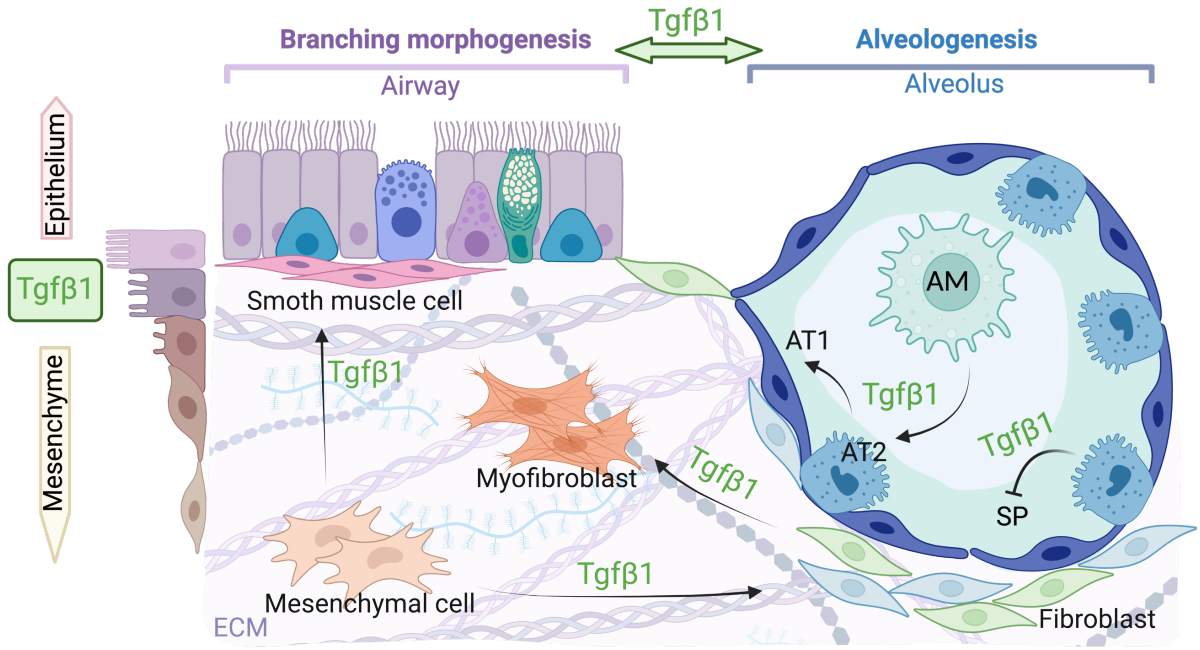

Figure 3. TGFβ in lung physiology and pathology. *First, TGFβ controls epithelial-mesenchymal interactions, essential for branching morphogenesis and alveologenesis during lung development. Second, TGFβ promotes the differentiation of mesenchymal cells into smooth muscle cells, fibroblasts, and myofibroblasts, contributing to lung structure and repair. Third, it regulates epithelial cell differentiation, suppressing AT2 gene expression and reducing surfactant protein (SP) secretion. Fourth, AM-derived TGFβ is a key modulator of immune cell development, maintaining its homeostasis and regulating epithelial cell function.*

2.4. TGFβ signaling in macrophage biology

In the **lung**, the development of both embryonic and postnatal BM-derived AMs relies on TGFβ signaling through an autocrine loop, which can upregulate PPAR-γ expression in concert with CSF2 [158]. Yu et al., observed increased SP-D and protein levels in the bronchoalveolar lavage (BAL) fluid of mice with a myeloid-restricted deficiency in *Tgfbr2*, which lack AMs despite normal CSF2 levels [158], a phenotypic reminiscent to the one observed in *Csf2*-deficient mice [164]. In a model of bleomycin-induced pulmonary inflammation, AMs can secrete large amounts of active TGFβ1 [283]. Activated AMs also produce TNF-α, which stimulates AT2 to secrete CSF2. CSF2 and TGFβ1 can then promote epithelial cell

proliferation, facilitate the transdifferentiation of AT2 into AT1, and contributes to alveolar repair through Stat5-dependent autocrine signaling [284, 285].

Liver sinusoidal endothelial TGFβ and Notch ligand DLL4, along with endogenous LXR ligands, are essential for inducing and maintaining a KC identity [121]. TGFβ signaling suppresses pro-inflammatory responses in KCs by inhibiting the production of cytokines such as IL-1β, IL-6, and TNF-α, while promoting anti-inflammatory IL-10 expression [286, 287]. This regulation occurs through the modulation of NF-κB signaling and the promotion of M2-type macrophage polarization [287]. TGFβ also influences KC-mediated liver regeneration and fibrosis by activating hepatic stellate cells [288]. Furthermore, TGFβ signaling in KCs contributes to attenuating liver ischemia-reperfusion injury by suppressing MMP production [286].

In the **epidermis**, TGFβ can induce the transcription factor Id2 and Runx3 in LCs [289]. TGFβ1 null mice lack epidermal LCs, demonstrating its essential role in LC development or in their epidermal localization [290]. TGFβ1 is produced by epidermal keratinocytes and LCs themselves. BM transfer or local injection of TGFβ1-producing cells can restore LCs in TGFβ1-deficient mice, suggesting both paracrine and autocrine effects of TGFβ1 on LC differentiation [291]. Interestingly, TGFβ1 enhances IL-12 production by CD40-stimulated LCs, potentially influencing the Th1-Th2 balance, while CSF2 inhibits this effect. The relative amounts of TGFβ1 and GM-CSF in the skin microenvironment may thus modulate LC function through regulation of IL-12 secretion [292].

In the **bone**, osteoclasts, specialized bone-resorbing cells, develop from the monocyte/macrophage lineage [293]. TGFβ exhibits a dual role in osteoclastogenesis, with effects dependent on the concentration and the cellular context. At low concentrations, TGFβ stimulates osteoclast differentiation by increasing the RANKL/OPG ratio in stromal cells and enhancing RANK expression in osteoclast precursors [294, 295]. Smad3 signaling appears to have a stimulatory effect on osteoclast formation [296]. TGFβ also directly promotes osteoclast formation in hematopoietic cell cultures treated with RANKL and CSF1 [297]. However, at high concentrations, TGFβ inhibits osteoclast differentiation by suppressing CSF1 expression and

the RANKL/OPG ratio in stromal cells [294]. Additionally, TGFβ directly inhibits osteoclastogenesis by reducing the expression of osteoclast-specific genes and NFAT1 through Smad1 signaling [296]. These findings highlight the complex regulatory role of TGFβ in osteoclastogenesis. Latent TGFβ1, which is abundant in the bone matrix, is released and activated by osteoclasts to specifically induce migration of mesenchymal stem cells (MSCs) to bone-resorptive sites [298]. Furthermore, osteoclast-specific TGFβ receptor signaling is essential for coupling bone resorption to bone formation by inducing Wnt1 secretion. Age-related decreases in skeletal TGFβ availability may contribute to reduced coupling of these processes [299].

In the **gut**, TGFβ regulates the differentiation of Ly6C^{hi} monocytes to intestinal macrophages, enabling them to adapt to their environment [300, 301]. Resident intestinal macrophages in healthy adults are inflammation-anergic due to TGFβ-mediated dysregulation of NF-κB signaling, maintaining an ideal profile for their coexistence with gut microbiota [302]. Myeloid TGFβ signaling contributes to colitis-associated tumorigenesis by promoting macrophage recruitment and inflammatory cytokine production [303]. TGFβ, particularly the TGFβ2 isoform, suppresses inflammatory cytokine production in intestinal macrophages during fetal and neonatal development, protecting against necrotizing enterocolitis [304]. TGFβ depletion from human colonic mucosa results in IL-12 secretion from macrophages, DCs, and epithelial cells, thereby potentially contributing to inflammatory bowel disease (IBD) [305]. Recent studies have revealed the complexity of intestinal macrophage populations. Contrary to previous beliefs, long-lived macrophages, identified by Tim-4 expression, are present in both the lamina propria (LP) and the submucosal/muscularis (S/M) regions [306, 307]. CD163 distinguishes long-lived S/M from LP macrophages, and TGFβ affects spatial distribution of CD163^{+} macrophages [306].

Nerve-associated macrophages (NAM)

Nerve-associated muscularis macrophage in the intestine can shape the enteric nervous system (ENS). In early life, muscularis macrophages refine the ENS by pruning synapses and

phagocytosing neurons, while later adopting a neuro-supportive phenotype instructed by ENS-derived TGFβ. Nerve-associated muscularis macrophage are characterized by upregulation of canonical microglia genes and the high expression of tight junction protein F11r. *In vitro* studies have demonstrated that BMDMs treated with TGFβ1, TGFβ2, or TGFβ3 also exhibit high levels of F11r expression [308]. The muscularis macrophage-neuron interaction can influence intestinal motility and provides tissue protection during injury and infection. However, this interaction can also contribute to gastrointestinal disorders like post-operative ileus [309]. This dynamic interplay between macrophages, the ENS, and TGFβ signaling is crucial for intestinal homeostasis and protection against inflammatory conditions.

In the **skin**, a subset of dermal macrophages interacts with sensory nerves, contributing to myelin surveillance [310, 311]. TGFβ is locally activated through physical interaction with nerves and integrin-mediated cleavage. After injury, TGFβ-driven skin macrophages support nerve regeneration [312].

Recent studies have highlighted the importance of TGFβ signaling in regulating microglial development, homeostasis, and reactivity [313]. Both murine and human studies have identified TGFβ as a key environmental cue that facilitates the transition from YS progenitors to parenchymal microglia [314]. NG2 glia were reported as essential for the maintenance of the microglia-specific gene expression signature by secreting TGFβ2, including markers like Tmem119, P2ry12, and Sall1 [315, 316]. Astrocyte-secreted TGFβ promotes microglia to generate primitive branches [317]. MSCs also secrete TGFβ, modulating microglial activity by shifting them from a pro-inflammatory state to an anti-inflammatory phenotype, which may help resolve neuroinflammation [318]. Importantly, TGFβ1-deficient mice lack microglia but exhibit no changes in brain-associated macrophages (BAM) [319]. The loss of TGFβ signaling in microglia is associated with neuronal dysfunction and cognitive deficits. LRRC33 enables localized TGFβ activation by integrin αVβ8 [227]. This activation does not involve the release of TGFβ from its latent form, allowing for highly specific and localized signaling [320]. LRRC33-mediated TGFβ activation is crucial for maintaining microglial homeostasis and proper CNS function, with deficiencies linked to neurological issues [227, 321]. Radial glia-expressed

integrin αVβ8 also contributes to activation of TGFβ1 on microglia, promoting their development [322]. This activation involves both canonical (Smad-dependent) and non-canonical pathways, with the latter partially suppressing disease-associated gene expression in microglia [322]. Beyond the CNS, TGFβ signaling also regulates retinal microglia, underscoring its broader significance in neuroimmune interactions [323]. These findings highlight the tight regulation of TGFβ signaling in microglial function and nervous system health. Macrophages regulated by TGFβ signaling can be found in Table 3.

Table 3. Contribution of TGFβ signaling to macrophage biology

Cell type	Location	TGFβ1 source	Function
AMs	Lung alveoli	AMs, autocrine [158]	AM development, SP-D secretion in the lung [158].
KCs	Liver	Endothelial cells [121]	KC identity and function, liver homeostasis [121, 286, 287].
LCs	Epidermis	Keratinocytes and LCs, autocrine and paracrine [291]	Regulation transcription factors and LCs location, Th1-Th2 differentiation [289, 290, 292].
Osteoclasts	BM	Osteoclasts [298]	Osteoclast differentiation and migration of MSC [294, 296-298].
Intestinal macrophages	Intestine	Leukocytes, stromal and epithelial cells [324]	Intestine homeostasis, and intestinal macrophage location [300, 301, 306].
Muscularis macrophages	Intestine Muscularis	ENS [308, 309]	Muscularis macrophage's identity and intestine homeostasis [308, 309].
Skin macrophages	Skin dermis	Neurons [312]	Myelin surveillance and Nerve regeneration [310-312].
Microglia	Nervous system	NG2 glia [315, 316, 325]	Microglial development, homeostasis, and reactivity [313, 315, 316, 325].

3. Lung endothelial cells

The intricate structure of the mammalian lung has evolved to optimize gas exchange within a limited space [326]. The lung structure includes non-respiratory airways (trachea, bronchi, bronchioles), and respiratory zones, mainly constituted of alveoli, these tiny air sacs surrounded by blood capillaries where oxygen and carbon dioxide exchange occur. The lung interstitium refers to the delicate, thin network of connective tissue that lies (1) between the alveolar epithelium and the capillary endothelium in the respiratory zones, and (2) underneath the airway epithelium. It provides structural support to the airways and alveoli and contains a mixture of fibroblasts, extracellular matrix (collagen, elastin), immune cells (like IMs), and blood and lymphatic vessels. We further elaborate on lung endothelial cells below, which represent an important actor of our research.

Pulmonary endothelial cells, which form the inner lining of all blood vessels, perform diverse functions, including facilitating the movement of immune cells across the vascular barrier, maintaining the balance between coagulation and bleeding, regulating the delivery of metabolites to surrounding tissues, and contributing to vascular regeneration and expansion following injury [327]. Classical markers of lung ECs include PECAM1 (CD31) [328-330], CDH5 (VE-cadherin) [331], CLDN5, and ERG [332]. CLDN5, a tight junction protein, is regulated by the transcription factor ERG, essential for maintaining endothelial barrier function [333]. ERG also regulates other endothelial-specific genes, including VE-cadherin [333].

The pulmonary endothelium comprises three main types of endothelial cells: capillary endothelial cells, vascular endothelial cells, and lymphatic endothelial cells [334]. Capillary endothelial cells can be further divided into two specialized subtypes: aerocytes, which facilitate leukocyte trafficking and gas exchange through their thin, expansive morphology, and general capillary endothelial cells (gCap), which can regulate the vasomotor tone and act as stem/progenitor cells [334]. In lung capillaries, endothelial cells express angiogenesis-related genes, including VEGF receptors, angiopoietin-2, and Tie receptors [335]. Blood vessel endothelial cells include both arterial and venous endothelial subtypes [336]. Arterial endothelial cells regulate vascular tone and respond to mechanical forces, while venous

endothelial cells contribute to fluid exchanges and leukocyte extravasation [337], The von Willebrand factor (vWF) is a widely used blood vessel endothelial cell marker, with higher expression in venous compared to arterial endothelial cells. Arterial endothelial cells express EphrinB2, while venous endothelial cells express EphB4 [338]. Lymphatic endothelial cells contribute to the lymphatic network that is essential for fluid drainage and immune surveillance [339]. These cells express specific markers, including Prox1, Lyve1, Podoplanin (Pdpn), and CD90.2 [340, 341].

Together, these endothelial cell populations form a complex and dynamic interface between the circulatory, respiratory, and immune systems. Understanding their specialized functions and their interactions with other lung structural and immune cells is fundamental for our understanding of lung physiology, immune regulation, tissue repair, and the pathogenesis of various pulmonary disorders.

An important interplay exists between endothelial cells and macrophages. Indeed, endothelial cells have been shown to provide CSF1 for the expansion of macrophage colonies from progenitors [342]. Apoptotic endothelial cells can release MFG-E8, which reprograms macrophages into an anti-inflammatory phenotype through STAT-3 phosphorylation [343]. TGFβ family related cytokines released from endothelial cells are also important in modulating macrophage chemotaxis and proliferation within the wound microenvironment [344]. In the liver, sinusoidal endothelial TGFβ has been shown to regulate KC identity [121]. Recent studies have also highlighted a role for endothelial cells in regulating lung macrophage function and tissue repair. Lung endothelial cells can secrete Rspondin3, which activates Wnt-β-catenin signaling in IMs in an LPS-induced injury model, leading to metabolic-epigenetic reprogramming that promotes anti-inflammatory responses and attenuates lung injury [174]. The endothelial-macrophage interaction is thought to be a dynamic two-way interaction. Indeed, AM secretory products can also enhance endothelial cell chemokine production during hypoxia and reoxygenation, amplifying inflammatory responses [345].

OBJECTIVES

OBJECTIVES

Our laboratory has a long-standing interest in understanding the biology of lung IMs, which has remained an enigmatic lung cell population for decades, as opposed to AMs. The development of scRNA-seq technologies and of specific transgenic models of IM depletion allowed us to investigate IM biology with more resolution and precision. Indeed, in 2019, we identified two transcriptionally and functionally distinct IM subsets in the steady-state lung, highlighting their heterogeneity and potential immunomodulatory roles [147]. $CD206^{+}$ IMs are primarily anti-inflammatory, while $CD206^{-}$ IMs have antigen presentation capabilities [41, 147]. In 2023, we also found that MafB was a major transcription factor limiting local monocyte proliferation and driving development of both IM subsets [167]. Others have in parallel explored the heterogeneity and the anti-inflammatory functions of IMs in disease models [139, 144, 148, 176, 346].

The objective of my PhD thesis work was to fill two gaps in IM biology. First, the niche cellular and molecular signals that regulate IM development, maintenance, and identity remain completely unknown. Second, the homeostatic functions of IMs in the steady-state lung remain unclear, limiting our understanding of their roles beyond core macrophage functions.

To address these questions, we undertook a multidisciplinary approach integrating: conditional knockout and unique transgenic mice to analyze the role of niche signals in IM development in vivo; single-cell and bulk RNA sequencing to characterize IM transcriptome changes that occur in response to niche signals; *in vitro* cell culture assays to assess the impact of niche signals on IM identity features; flow cytometry, RT-qPCR, and immunofluorescence to assess the contribution of niche signals to IM identity and spatial location. By elucidating the niche-instructive signals and associated signaling pathways that control IM development and identity beyond CSF1, our work would fill a fundamental gap of knowledge of lung IM biology and in their homeostatic functions.

EXPERIMENTAL SECTION

The findings of this study have been published in *Science Immunology* 10(106):eadr4977. doi: 10.1126/sciimmunol.adr4977.

Endothelial-driven TGFβ signaling supports lung interstitial macrophage development from monocytes

W. Peng[1,2], D. Vanneste[1,2], D. Bejarano[3], J. Abinet[1,2], M. Meunier[1,2], C. Radermecker[1,2], F. Perin[4], D. Cataldo[4], F. Bureau[2,5], A. Schlitzer[3], Q. Bai[1,6,*] & T. Marichal[1,2,7,*]

[1] Laboratory of Immunophysiology, GIGA Institute, University of Liège; Liège, Belgium

[2] Faculty of Veterinary Medicine, University of Liège; Liège, Belgium

[3] Quantitative Systems Biology, Life and Medical Sciences (LIMES) Institute, University of Bonn, Bonn, Germany

[4] Laboratory of Tumor and Development Biology, GIGA Institute, University of Liège; Liège, Belgium

[5] Laboratory of Cellular and Molecular Immunology, GIGA Institute, University of Liège; Liège, Belgium

[6] PhyMedExp INSERM 1046, University of Montpellier, Montpellier, France

[7] Walloon Excellence in Life Sciences and Biotechnology (WELBIO) Department, WEL Research Institute; Wavre, Belgium

[*] These authors contributed equally to this work and are co–last authors.

EXPERIMENTAL SECTION

1. Materials and methods

Mice

All experiments, unless otherwise specified, were performed on age-matched 8–12-wk-old male and female mice on the C57BL/6 background. In this study, the following mice were used on the C57BL/6 background: CD45.2 WT (The Jackson Laboratory), CD45.1 WT (The Jackson Laboratory, 002014), *Lyz2*^{Cre} (The Jackson Laboratory, 004781), *Mafb*$^{fl/fl}$ [167], *Tgfbr2*$^{fl/fl}$ (The Jackson Laboratory, 012603), *Cdh5*^{CreERT2} (Taconic Biosciences, 13073), *Tgfb1*$^{fl/fl}$ (The Jackson Laboratory, 065809), and *Tmem119*^{Cre} *Cx3cr1*$^{LSL\text{-}DTR/+}$ mice, called IM^{DTR} mice [167]. Myeloid-restricted *Tgfbr2* or *Mafb* depletion was achieved by crossing *Tgfbr2*$^{fl/fl}$ or *Mafb*$^{fl/fl}$ mice with *Lyz2*^{Cre} mice. CD45.1/CD45.2 IM^{DTR} mice were generated by crossing CD45.1 *Tmem119*^{Cre} with CD45.2 *Cx3cr1*$^{LSL\text{-}DTR}$ mice. *Cdh5*^{CreERT2} and *Tgfb1*$^{fl/fl}$ mice were crossed to produce *Cdh5*^{CreERT2} *Tgfb1*$^{fl/fl}$ mice.

Mice were housed under specific pathogen-free conditions and maintained in a 12-h light–dark cycle with food and water ad libitum. Experiments were reviewed and approved by the Institutional Animal Care and Use Committee of the University of Liège (ethical approval #1956). The ‘Guide for the Care and Use of Laboratory Animals’, prepared by the Institute of Laboratory Animal Resources, National Research Council, and published by the National Academy Press, as well as European and local legislations, was followed carefully. Accordingly, the temperature and relative humidity were 21°C and 45-60%, respectively.

Bone marrow, blood and tissue single-cell suspension preparation

Blood was collected via retro-orbital plexus bleeding from terminally anesthetized mice. For BM cells collection, mice were sacrificed via cervical dislocation, femurs and tibias were dissected and cleaned of soft tissue. Distal and proximal ends were opened to flush out BM cells. After centrifugation, cell pellets were resuspended in ice-cold PBS (Thermo Fisher, 14190094) containing 10 mM EDTA (Merck Millipore, 1084181000), and single-cell

suspension were abstained by filtering through a 70 µm cell strainer (Corning, 352350). To isolate lung leukocytes, lungs were finely minced with razor blades and digested for 1 h at 37 °C in digestion medium No.1, consisting of 5% vol/vol FBS (Thermo Fisher, 10270098), 1 mg/mL collagenase A (Sigma, 14190094) and 0.05 mg/mL DNase I (Sigma, 11284932001) in HBSS (Lonza, BE10-508F). After 45 mins of digestion, the suspension was passed through an 18-gauge needle to dissociate cell aggregates. Ice-cold PBS (Thermo Fisher, 14190094) with 10 mM EDTA (Merck Millipore, 1084181000) was added to stop the digestion, and cell suspensions were filtered using a 70 µm cell strainer (Corning, 352350). Mononuclear leukocytes from lungs were enriched using a Percoll density gradient (GE Healthcare, 17089101), with cells collected from the 1.080:1.038 g/mL interface. For heart single-cell suspensions, the same digestion procedure was used as described for lung leukocytes, but without applying a Percoll gradient. Ear single-cell suspensions were prepared by harvesting the ears from the base, splitting them into dorsal and ventral layers, and placing them in HBSS containing 5 U/mL Dispase (Sigma, D4693) for 90 min at 37 °C. Ear tissues were cut into small pieces using razor blades and further digested for 1 h at 37°C in digestion medium No.1, following the same procedure as for lung leukocytes but without applying a Percoll gradient.

To isolate lung structural cells, mice were administrated i.t with 1 mL digestion medium No.2 (1 U/mL Dispase (Merck Millipore, D4693), 4 U/mL Elastase (Merck Millipore, E1250) and 0.05 mg/mL DNase 1 in HBSS) for 1 min. The entire lung with the trachea was harvested and digested for 30 mins at 37 °C in 1 ml digestion medium No.2. Subsequently, the lungs were minced into small pieces using razor blades and further digested as described above with digestion medium No.1 (HBSS containing 5% vol/vol FBS, 1 mg/mL collagenase A, and 0.05 mg/mL DNase I) for 30 mins at 37°C to obtain a single-cell suspension.

In vivo treatments with chemicals and antibodies

For DT-induced depletion of IMs, IM^{DTR} mice were administered a single i.p. injection of 50 ng DT (List Biological Labs, 150), while control mice were injected with PBS. In TgfβR inhibitor experiments, IM^{DTR} mice received three i.p. injection of 1 mg/kg body weight

LY364947 (Selleckchem, S2805) in 200 µl PBS at days 2, 4 and 6 post-DT. Control mice were injected with 200 µl PBS i.p..

For assessment of cell localization in the lung, 1 µg of FITC-conjugated anti-mouse CD45.2 (clone 104, BD Biosciences, 564616) was injected i.v. 10 minutes before, and 1 µg of APC-conjugated anti-mouse CD45.2 (clone 104, BD Biosciences, 558702) was injected i.t. 5 min before sacrifice to distinguish intravascular (CD45-FITC$^+$ CD45-APC$^-$), parenchymal (CD45-FITC$^-$ CD45-APC$^-$) and airway (CD45-FITC$^-$ CD45-APC$^+$) cells.

To achieve endothelial-specific *Tgfb1* deletion, four-week-old *Cdh5*^{CreERT2} *Tgfb1*$^{fl/fl}$ mice or *Tgfb1*$^{fl/fl}$ control were fed tamoxifen diet (0.25 g/kg, SAFE, E8404A01R 00008) for 4 weeks, then were fed with normal diet afterwards.

Flow cytometry

Cells (0.5 - 5 × 10^6) were pre-incubated with Mouse Fc Block (BD Biosciences, 553142) to avoid nonspecific binding to Fc receptors and then stained with appropriate antibodies at 4 °C in the dark for 10 mins. Unless otherwise instructed, all antibodies are diluted 1:100 for staining at 4 °C for 30 mins. Cell viability was assessed using LIVE/DEAD Fixable Near-IR (775) stain (Thermo Fisher, L34976), and cell apoptosis was detected by Annexin V after surface staining, according to the manufacturer's instructions. TgfβRII (R&D Systems, FAB532P), Cx3cr1 (R&D systems, FAB5825G) and Tmem119 (ThermoFisher, 12-6119-82) stainings were performed at 37 °C for 30 mins with a 1:50 dilution. Intracellular cytokine staining was performed using an intracellular staining set (ThermoFisher, 00-5523-00). For Ki-67 staining, cells were permeabilized and stained extracellularly using FITC Mouse Anti-Ki-67 Set (BD Biosciences, 556026). Annexin V/PI stainings were performed at room temperature for 15 min. The cell suspensions were analyzed with an LSRFortessa (BD Biosciences). FlowJo software (BD Biosciences) was used for data analysis. For the bulk and scRNA-seq experiments, lung CD45.1$^-$CD45.2$^+$Ly6G$^-$SiglecF$^-$CD11b$^+$SSC^{lo}CD64$^+$ Macs were sorted using a Sony MA900. To generate conditioned medium (CM), endothelial cells (CD45$^-$CD31$^+$Epcam$^-$), epithelial

cells ($CD45^-CD31^-Epcam^+$) and stromal cells ($CD45^-CD31^-Epcam^-$) were sorted using a FACSAria III (BD Biosciences). The list of antibodies used can be found in the Table S1.

Generation of BM (competitive) chimeras

Eight-week-old CD45.1/CD45.2 IM^{DTR} mice were anesthetized via i.p. injection of ketamine (75 mg/kg body weight; Dechra, 804132) and xylazine (10 mg/kg body weight; Bayer, 0076901) in 200 µl PBS. The thoracic cavity was shielded with a 0.6-cm-thick lead cover, and the mice were lethally irradiated with two doses of 6 Gy, 15 mins apart. Following recovery from anesthesia, the mice were reconstituted by i.v. administration of 10^7 BM cells from CD45.2 *Tgfbr2*$^{fl/fl}$ mice or CD45.2 *Lyz2*^{Cre} *Tgfbr2*$^{fl/fl}$ mice. For mixed BM chimeras, mice received an i.v. injection with 10^7 BM cells consisting of 50 % CD45.1 WT cells and 50% CD45.2 *Lyz2*^{Cre} *Tgfbr2*$^{fl/fl}$ cells. Nine-week-old *Cdh5*^{CreERT2} *Tgfb1*$^{fl/fl}$ mice were lethally irradiated with two doses of 4 Gy, 15 mins apart. The mice were injected i.v. with 10^7 BM cells from CD45.1.2 WT mice after 2 h irradiation and were treated with 0.05 mg/ml of enrofloxacin (Baytril, Bayer) in drinking water for 4 weeks from the day of irradiation.

***Ex vivo* BM Mo and BMDM experiments**

To generate conditioned medium (CM), FACS-sorted lung endothelial cells, epithelial cells and stromal cells were cultured in RPMI medium (ThemoFisher, 21875-034) containing 10% vol/vol FBS, 50 U/ml Penicillin-Streptomycin (ThemoFisher, 15070-063), 1 mM sodium pyruvate (ThemoFisher, 11360-070), 1 × MEM NEAA (ThemoFisher, 11140-035) and 50 µM 2-Mercaptoethanol (ThemoFisher, 31350-010) at 37 °C. After 12 h, the conditioned medium was collected by centrifugation to obtain the supernatant. BM $Ly6C^+$ monocytes were isolated from mice using the Monocyte Isolation Kit (Miltenyi Biotec, 130-100-629). These monocytes were then treated with CM, while the control monocytes were cultured in the medium at 37 °C for 48 h. BM Mo were then collected and RNA was extracted by Trizol.

BM $Ly6C^+$ monocytes were isolated from *Tgfbr2*$^{fl/fl}$, *Lyz2*^{Cre} *Tgfbr2*$^{fl/fl}$, *Mafb*$^{fl/fl}$, *Lyz2*^{Cre} *Mafb*$^{fl/fl}$ mice and treated with or without 20 ng/ml Tgfβ1 together with 40 ng/ml Csf1 or Csf2 at 37 °C for 48h. All samples were analyzed by flow cytometry or RT-qPCR.

For co-culture experiments, endothelial cells were isolated from mouse lung single cell suspensions using the CD31 MicroBeads Kit (Miltenyi Biotec, 130-097-418) and co-cultured with BM Mo from *Tgfbr2*$^{fl/fl}$ or *Lyz2*^{Cre} *Tgfbr2*$^{fl/fl}$ mice with 40 ng/ml Csf1 at 37 °C for 48h. One co-culture group from *Tgfbr2*$^{fl/fl}$ mice were treated with 5 μM TgfβR inhibitor LY-364947(Selleckchem, S2805). The ratio of endothelial cells and BM Mo was 2:1 in Fig. 2 H-J and 1:2 in Fig. 5 J-L.

For the generation of BMDM, BM Mo were treated with 40 ng/ml Csf1 on first day, and the medium containing 40 ng/ml Csf1 was changed twice at day 3 and day 5 day. At day 7, 95% cells were F4/80^{+}CD11b^{+} as confirmed by flow cytometry.

Immunofluorescence

For lung immunofluorescence staining, lungs were perfused with 10 mL PBS via the left ventricle and collected. Lungs were fixed in 4% paraformaldehyde (Thermo Fisher, F/1501/PB15) at 4 °C for 24 h. Subsequently, the fixed lungs were cryoprotected in 30% sucrose (VWR, Avantor, 57-50-1) in PBS at 4 °C for 4 h. Following cryoprotection, the lungs were embedded in optimal cutting temperature compound (OCT; Tissue-Tek, 4583) and stored at -80 °C overnight. The lung OCT sections were cut into 7-μm-thick sections and blocked-in methanol 100% (Merck, 67-56-1) at -20 °C for 20 mins. For staining, samples were incubated overnight at 4 °C in blocking buffer (PBS with 0.3% Triton X-100 (Merck, 648466) and 2% donkey serum (Sigma Aldrich, D9663)) containing rat anti-mouse antibodies CD68 (Bio-rad, MCA1957GA), mouse anti-mouse antibodies directed against Tgfβ1 (R&D Systems, MAB2402), rabbit anti-mouse antibodies directed against Erg (Abcams, ab92513) at a 1:100 dilution, FITC-conjugated anti-mouse antibodies against vWF (Santa Cruz, sc-365712) at a 1:75 dilution. After washing with PBS, the samples were incubated with secondary antibodies: anti-rat IgG antibodies conjugated with AF488 (ThermoFisher, A-11034), anti-mouse IgG antibodies conjugated with AF750 (ThermoFisher, A-21037) and anti-rabbit IgG antibodies conjugated with AF647 (BioLegend, 405416) in blocking buffer at a 1:500 dilution in the dark at room temperature for 2 h. Finally, samples were washed with PBS, mounted with 10 μl

ProLong Antifade reagent with DAPI (ThermoFisher, P36966) on glass slides, and stored at room temperature in the dark overnight. All samples were analyzed using spectral fluorescence microscopy. Images shown in Fig. 5F were acquired on an LSM 880 inverted confocal microscope using Plan-Apochromat 40x/1.3 Oil objectives. Fluorophores were excited simultaneously at 405/488/561/633 nm with detection wavelength at 350-499/380-548/573-627/659-735 with Airyscan in Zeiss SuperResolution mode and unidirectional acquisition. Images shown in Fig. 8E were acquired on an LSM 980 inverted confocal microscope using Plan-Apochromat 63x/1.4 Oil objectives. Fluorophores were excited simultaneously at 405/488/639 nm with detection wavelength at 350-499/380-548/659-735 with GaAsP-PMT in Zeiss FastAiryScanSheppardSum SR-4y:4.2 mode and bidirectional acquisition. Analysis was performed with Zeiss Blue software 3.6.

The cell distance analysis was performed by Imaris 9.5. The $CD68^+$ cells and $Tgf\beta1^+Erg^+$ cells were identified by the intensity of fluorescence. The distance of $Tgf\beta1^+Erg^+$-$CD68^+$ cells pairs was calculated the minimum surface distance from $Tgf\beta1^+Erg^+$ cells to $CD68^+$ cells. All images in Imaris were performed in batch mode with the same algorithm.

Real-time quantitative PCR

Total RNA was extracted from the samples using TRIzol reagent (ThermoFisher, 10296010). cDNA was synthesized using with RevertAid H Minus First Strand cDNA Synthesis Kit (ThermoFisher, K1631), RT-qPCR was performed using SYBR green supermix (Bio-rad, 1725121). The cycle threshold (CT) values obtained from triplicate qPCR reactions were extracted from the QuantStudio 5 (ThemoFisher) and transferred onto spreadsheets for analysis using the relative quantification method $2^{-\Delta\Delta CT}$.The primers for the test genes are listed in Table. Primers.

CODEX staining

Five μm-thick slices of frozen lungs from chimeric IM^{DTR} mice (Fig. 6A) were prepared and used for CODEX staining, as described [347]. Briefly, after drying the sections, they were fixed for 10 min in ice-cold acetone. After fixation, coverslips were transferred to hydration buffer

and subsequently photobleached twice for 45 min each. Afterwards, sections were blocked and stained with a 28-plex CODEX antibody panel overnight at 4°C. Samples were washed twice with staining buffer, fixed in ice-cold methanol for 5 min, washed with 1 x PBS, and fixed with BS3 fixative for 20 min (ThermoFisher, 21580). After washing off the fixative, the samples were stored at 4°C before imaging.

CODEX imaging, processing and analysis

Frozen lung sections from chimeric IM^{DTR} mice were prepared for CODEX staining using a 28-plex antibody panel. Following fixation, photobleaching, and blocking, samples were stained overnight and processed for imaging. CODEX imaging was performed using a widefield fluorescence microscope, capturing multiple channels with z-spacing of 1.5 µm. Raw files were processed for background subtraction, stitching, and cell segmentation.

Cell populations were identified and classified using fluorescence markers and a strategy akin to flow cytometry (Table. CODEX phenotypes), and downstream analyses were performed.

Coverslips and reporter plate were equilibrated at room temperature for 30 min before imaging. A multicycle CODEX experiment was performed using a Zeiss Axio Observer widefield fluorescence microscope with a 20x objective (NA 0.85), and the 405, 488, 568, and 647 nm channels. A z-spacing of 1.5 µm was used for acquisition. Raw files were exported using the CODEX Instrument Manager (Akoya Biosciences) and processed with CODEX Processor v1.7 (Akoya Biosciences). Processing included background subtraction, stitching, shading, shading correction, and cell segmentation.

Images were inspected and analyzed using the CODEX MAV (Akoya Biosciences) plugin in Fiji. Regions out of focus were removed for the analysis. Cells were selected using the DAPI counterstain and subsequently classified using a similar strategy to the one used in flow cytometry. Mature IMs were defined as $CD45.2^{+}CD45.1^{-}Lin^{-}CD11b^{+}SiglecF^{-}F4/80^{+}Ly6C^{-}MerTK^{+}MHCII^{+}CD206^{+}$cells. Monocytes were defined as $CD45.2^{+}CD45.1^{-}Lin^{-}CD11b^{+}SiglecF^{-}F4/80^{+}$ $Ly6C^{+/lo}CD64^{+/lo}MerTK^{lo/-}$ cells.

After cell classification, the generated .csv files were exported to CytoMAP [348] and cell interactions of monocytes and IMs with other immune and structural cells (Table. CODEX phenotypes) were calculated using Pearson correlation.

To determine the distribution of monocytes and IMs interstitial macrophages in the major anatomical areas of the lung, images were exported to QuPath. The perivascular, peribronchial, interstitial spaces and the adventitial cuffs were manually annotated in the whole image. Afterwards cells were detected using the DAPI counterstain and multiple classifiers were established using the single stains and used to gate the same populations as above. To calculate the distances between $Tgf\beta^{+}$ or $Tgf\beta^{-}$ endothelial cells ($CD45^{-}EpCAM^{-}PDGFRa^{-}CD31^{+}$) and IMs and monocytes, the nearest distance between centroids was calculated.

ELISA, Collagen and Proteome Assays

Lungs of chimeric IM^{DTR} mice were perfused with 10 mL PBS through the right ventricle and isolated. The dissected lungs were snap frozen in liquid nitrogen and homogenized using a tissue homogenizer (IKA) in 360 µl ice-cold lysis buffer (40 mM Tris-HCl (pH 7.4), 150 mM NaCl, 10% glycerol and protease inhibitor cocktail (Sigma, 11697498001)). The samples were added 1% NP-40 (Sigma, 74385), then centrifuged for 20 mins at 4 °C, and supernatants were collected after centrifugation. The protein concentration was determined by Pierce BCA Protein Assay Kit (Thermo Fisher), following to the manufacturer's instructions. The supernatants were stored at -80 °C. Tgfβ1, IL-10 and soluble collagen level were quantified in lung homogenates using Tgfβ1 Human/Mouse Uncoated ELISA Kit (Thermo Fisher, 88-8350-88), IL-10 Mouse uncoated ELISA Kit (Thermo Fisher, 88-7105-88), mouse Elastin ELISA Kit (Novusbio, NBP3-06918) and Sircol Soluble Collagen Assay Kit (Biocolor, S1000), respectively, according to the manufacturer's instructions.

For Proteome profiler assay, 200 ng total protein were tested for the presence of cytokines and chemokines using a proteome profiler mouse XL cytokine array (R&D Systems), according

to manufacturer instructions. Results were visualized using an ImageQuant LAS 4000 (GE Healthcare) and analyzed using ImageJ software.

Lung function measurements

Mice were anesthetized i.p. with sodium pentobarbital (Nembutal) at a dose of 50 mg/kg. The trachea was surgically exposed via dissection of the neck region. An 18-gauge blunt metal cannula, known for its typical resistance of 0.18 cmH_2Os/mL, was inserted into trachea and secured using a nylon suture to ensure stability. Subsequently, the mice were connected to the flexiVent computer-controlled piston ventilator (SCIREQ) through the cannula. This connection was facilitated by the FX adaptor Y-tubing. The ventilator was set to standard parameters for murine ventilation: a positive end expiratory pressure (PEEP) at 3 cmH^2O, a tidal volume of 10 mL/kg, a respiratory rate of 150 breaths per minute, and a fraction of inspired oxygen of 0.21, which corresponds to room air. Respiratory mechanics were evaluated using the forced oscillation technique (FOT) and the latest version of the flexiVent operating software (flexiWare version 8.1.3).

Lung histology and histopathological measurements

Lungs were fixed in 5% formalin, paraffin-embedded, and cut into 5-µm sections that were then stained with hematoxylin and eosin (H&E) before analysis. Full lung sections images were acquired on an Axioscan 7(Zeiss, 20×).

The size of alveoli was assessed with the method of mean linear intercept (MLI), as described [349, 350]. Briefly, lung tissues and alveolar walls were identified by thresholding (Huang thresholding) on hematoxylin and eosin (H&E)-stained lung images. Horizontal test lines were generated by overlaying line grids onto lung field images at 50% opacity, using image flattening to isolate measurement regions. Chord lengths were identified with color thresholding and measured with the “analyze particles” function in Fiji/ImageJ, and results were exported for statistical analyses. For each image, three zones of alveoli were randomly selected and only the cords within these regions were counted with "ROI tool".

The clusters of perivascular infiltrating leukocytes were identified in H&E-stained lung images as described [351, 352]. Briefly, only the leukocyte clusters larger than 50 μm in size and adjacent to the small arterioles or venules (i.e., less than 100 μm in diameter) were counted in each lung section. The count number were then normalized by the corresponding lung area, yielding normalized values expressed as foci per unit area.

Bulk RNA sequencing analyses

Lung CD45.1$^-$CD45.2$^+$Ly6G$^-$SiglecF$^-$CD11b$^+$SSC^{lo}CD64$^+$ IMs were FACS-sorted from chimeric IM^{DTR} mice (Fig. 6A) using the gating strategy shown in fig. S7A into TRIzol reagent (Thermo Fisher, 10296010). Total RNA was extracted with the standard TRIzol RNA extraction protocol. RNA quality and quantity were evaluated using a 2100 bioanalyzer (Agilent) and the Quant-iT RiboGreen RNA Assay Kit (Thermo Fisher, R11490). One hundred nanograms of RNA was used to generate the libraries using the TruSeq Stranded mRNA kit (Illumina, 20020594). These libraries were sequenced on an Illumina NovaSeq sequencer on an SP flow cell. Sequence alignment with the mouse genome (GRCm38), sequence counting, and quality control were performed using the nf-core/rnaseq pipeline.

RNA-seq data were analyzed by R (version 4.3.3) using R Bioconductor (3.18) and DESeq2 package (version 1.42.1). To correct for potential batch effects, the ComBat function from the sva package (v3.50.0). Differential expression analysis was performed using the DESeq2 package (v1.42.1). Gene set enrichment analysis (GSEA) was conducted using the clusterProfiler package (v4.10.1). Molecular Signatures Database (MSigDB) gene sets were supplied by msigdbr package (v7.5.1).

Single cell RNA sequencing and analyses

Lung CD45.1$^-$CD45.2$^+$Ly6G$^-$SiglecF$^-$CD11b$^+$SSC^{lo}CD64$^+$ cells were FACS-sorted from lung single-cell suspensions pooled from 5 chimeric IM^{DTR} mice, as for the bulk RNA-seq analysis. For each sample, an aliquot of Trypan blue-treated cells was examined under the microscope for counting, viability and aggregate assessment following FACS sorting. Viability was above 90% for all samples and no aggregates were observed. Cells from each group were

then labelled with TotalSeq anti-mouse hashtags (BioLegend, TotalSeq-B0301 for donor *Tgfbr2*$^{fl/fl}$ group and TotalSeq-B0303 for doner *Lyz2*^{cre} *Tgfbr2*$^{fl/fl}$ group) before being pooled. Pooled cells were centrifuged, and pellet was resuspended in calcium- and magnesium-free PBS containing 0.4 mg/ mL UltraPure BSA (Thermo Fisher Scientific). For library preparation, approximately 10 000 cells were loaded into the Chromium iX (10x Genomics), in which they were partitioned, their polyA RNAs captured and barcoded using Chromium Next GEM Single Cell 3' Reagent Kits v3.1 (10x Genomics). The cDNAs were amplified and libraries compatible with Illumina sequencers were generated using Chromium Next GEM Single Cell 3' Reagent Kits v3.1 with Feature Barcoding technology for Cell Surface Protein (10x Genomics). For Hash Tag Oligonucleotide (TotalSeq B anti-mouse Antibody, Biolegend) library, primers for cDNA amplification and index PCR are provided in Chromium Single Cell 3' Feature Barcode Library Kit (10x Genomics). The libraries were sequenced on an Illumina NovaSeq 6000 on an S4 cell flow (read 1, 150 cy; read 2, 150 cy; index 1, 10 cy; index 2, 10 cy) at a depth of ~25,000 reads per cell.

The Cell Ranger (v8.0) application (10x Genomics) was then used to demultiplex the BCL files into FASTQ files (cellranger mkfastq), to perform alignment (to Cell Ranger human genome references 3.0.2 GRCm38/build 97), filtering, UMI counting and to produce gene-barcode matrices for each sample (cellranger multi).

Filtered matrix files were used for further scRNA-seq analyses with R Bioconductor (3.18) and Seurat (5.1.0). Filtered matrices containing cell IDs and feature names in each sample were used to build a Seurat object. We performed a quality control by filtering out the cells with less than 200 detected genes, the genes detected in less than 3 cells and the cells exhibiting more than 10% of mitochondrial genes. Gene counts were normalized by default method “LogNormalize” with scale factor 10000 and log-transformation. Four clusters were obtained using FindClusters function (Seurat package) and characterized by expression of cell type-specific genes. For differential expression analysis, expression in each gene was compared using FindMarkers function (Seurat package) and the genes with adjusted *P* value < 0.05 and logFC > 0.5 were considered as significant up-regulated genes. Gene-ontology enrichment

analysis and gene set enrichment analysis (GSEA) were performed using clusterProfiler package.

Analysis of published single-cell RNA sequencing data

NicheNet analysis [353] was applied to previously published single-cell RNA sequencing data [147]. The cell types were defined by SingleR package. We used the ligand-receptor network included in NicheNetR package to predict ligand activity. To perform the NicheNet analysis, receiver cell population were set as classical monocytes developing into IMs, whereas the sender cell population was set as endothelial cells. Only genes expressed with in at least 10% of cells in one cluster will be used to calculated ligand activity.

InAct molecular interaction database (inact-micluster) was used to construct mouse ligand-receptor network. Briefly, only *mus musculus* genes were filtered and annotated with Gene Ontology (GO). Only interaction pair with interactor.a (ligands) annotated by “extracellular region part” (GO: 0044421), plasma membrane (GO: 0005886), or “plasma membrane part” (GO:0044459), and interactor.b (receptors) annotated by “plasma membrane” (GO:0005886), “plasma membrane region” (GO:0098590) or “plasma membrane part” (GO:0044459) were considered as ligand-receptor interaction pairs. A final 2957 ligand-receptor pairs were generated.

Ligand-receptor activities between cell types were calculated using our previously published single-cell RNA sequencing data [147]. The relative activity of each ligand-receptor pair was calculated by multiplying the average expression of ligand gene and receptor gene. ChordDiagram was made with package circlize package.

The pseudotime trajectory of monocyte-to-IM development was previously reported [167] and analyzed using monocle3 package (1.0.0). Briefly, cells were clustered using the cluster_cells function with UMAP coordinates. The pseudotime trajectories were constructed with the learn_graph and order_cells functions. The starting cells (root cells) were selected to ensure correct trajectory inference. Gene expression across the pseudotime and differential expression was estimated by tradeSeq package (v1.4.0). To infer the contribution of Csf1 and

Tgfβ1 during monocyte-to-IM development, target genes regulated by Csf1 and Tgfβ1 were derived from a previously established ligand-target interaction matrix (NicheNetr package). Specifically, the top 100 target genes for each ligand, ranked by interaction score, were selected. A ligand-specific gene signature was then defined by identifying genes that were both among the top 100 targets of the ligand and differentially expressed along the monocyte-to-macrophage trajectory. These ligand-specific signatures were evaluated in the scRNA-seq dataset by using the AddModuleScore function (Seurat). Both signatures were evaluated along pseudotime on the global monocyte-to-IM trajectory. The Tgfβ1 target gene signature was then measured separately for each lineage of $CD206^{+}$ and $CD206^{-}$ IMs.

Statistical analysis

Graphs were prepared with GraphPad Prism 10 (GraphPad software) or R Bioconductor (3.5.1). Data distribution was assumed to be normal when parametric tests were performed. No data were excluded from the analyses. Statistical analyses were performed with Prism 9 (GraphPad software), and with R Bioconductor (3.5.1) and Seurat package for scRNA-seq data, respectively. The statistical analyses performed for each experiment are indicated in the respective figure legends. We considered a *P* value lower than 0.05 to be significant (*, $P < 0.05$; **, $P < 0.01$; ***, $P < 0.001$; ****, $P < 0.0001$; ns, not significant).

Antibodies

Name	Source	Cat. Number
Anti-mouse C1qA Monoclonal Antibody (Mouse, clone JL-1), biotin conjugated	Bio-techne	NBP1-51140B
Anti-mouse CD3 Monoclonal Antibody (Hamster, clone 2H5), PE conjugated	BD Biosciences	553064
Anti-mouse CD19 Monoclonal Antibody (Rat, clone 6D5), BV421 conjugated	BD Biosciences	115537
Anti-mouse CD11b Monoclonal Antibody (Rat, clone M1/70), BUV395 conjugated	BD Biosciences	563553
Anti-mouse CD11b Monoclonal Antibody (Rat, clone M1/70), PE-Cy7 conjugated	BD Biosciences	552850
Anti-mouse CD11c Monoclonal Antibody (Hamster, clone HL3), BV786 conjugated	BD Biosciences	563735
Anti-mouse CD16/32 (Mouse BD Fc Block™) Monoclonal Antibody (Rat, clone 2.4G2), unconjugated	BD Biosciences	553142
Anti-mouse CD31 Monoclonal Antibody (Rat, clone 390), BV421 conjugated	BD Biosciences	563356
Anti-mouse CD31 Monoclonal Antibody (Rat, clone 390), AF647 conjugated	BioLegend	102416
Anti-mouse CD45.1 Monoclonal Antibody (Mouse, clone A20), BUV395 conjugated	BD Biosciences	565212
Anti-mouse CD45.2 Monoclonal Antibody (Mouse, clone 104), BUV395 conjugated	BD Biosciences	564616
Anti-mouse CD45.2 Monoclonal Antibody (Mouse, clone 104), FITC conjugated	BD Biosciences	561874
Anti-mouse CD45.2 Monoclonal Antibody (Mouse, clone 104), PE-Cy7 conjugated	BD Biosciences	560696
Anti-mouse CD45.2 Monoclonal Antibody (Mouse, clone 104), PerCP-Cy5.5 conjugated	BD Biosciences	552950

Anti-mouse CD45.2 Monoclonal Antibody (Mouse, clone 104), APC conjugated	BD Biosciences	558702
Anti-mouse CD64 Monoclonal Antibody (Mouse, clone X54-5/7.1), BV421 conjugated	BioLegend	139309
Anti-mouse CD68 Recombinant Monoclonal Antibody (Rat, clone FA-11), unconjugated	Bio-rad	MCA1957GA
Anti-mouse CD90.2 Monoclonal Antibody (Rat, clone 30H12), AF700 conjugated	BioLegend	105320
Anti-mouse CD90.2 Monoclonal Antibody (Rat, clone 53-21), BV786 conjugated	BD Biosciences	564365
Anti-mouse CD115 (CSF1R) Monoclonal Antibody (Rat, clone AFS98), PerCP-Cy5.5 conjugated	BioLegend	135526
Anti-mouse CD170 (SiglecF) Monoclonal Antibody (Rat, clone E50-2440), PE-CF594 conjugated	BD Biosciences	562757
Anti-mouse CD206 (MMR) Monoclonal Antibody (Rat, clone C068C2), AF488 conjugated	BioLegend	141710
Anti-mouse CD206 (MMR) Monoclonal Antibody (Rat, clone C068C2), AF647 conjugated	BioLegend	141712
Anti-mouse CD206 (MMR) Monoclonal Antibody (Rat, clone C068C2), BV785 conjugated	Sony Biotechnology	1308645
Anti-mouse CD206 (MMR) Monoclonal Antibody (Rat, clone C068C2), PE-Cy7 conjugated	BioLegend	141720
Anti-mouse CD326 (Epcam) Monoclonal Antibody (Rat, clone G8.8), APC-Cy7 conjugated	BioLegend	118217
Anti-mouse CD326 (Epcam) Monoclonal Antibody (Rat, clone G8.8), BV510 conjugated	BD Biosciences	747748
Anti-mouse Cx3cr1 Polyclonal Antibody (Goat), AF488 conjugated	R&D systems	FAB5825G
Anti-mouse Erg Recombinant Monoclonal Antibody (Rabbit), unconjugated	Abcam	ab92513

Anti-mouse F4/80 Monoclonal Antibody (Rat, clone BM8), PE conjugated	Sony Biotechnology	1215550
Anti-mouse F4/80 Monoclonal Antibody (Rat, clone BM8), BV650 conjugated	BioLegend	123149
Anti-mouse FceR1a Monoclonal Antibody (Hamster, clone MAR-1), BUV737 conjugated	BD Biosciences	751766
Anti-mouse I-A/I-E (MHC-II) Monoclonal Antibody (Rat, clone M5/114.15.2), AF700 conjugated	ThermoFisher	56-5321-80
Anti-mouse I-A/I-E (MHC-II) Monoclonal Antibody (Rat, clone M5/114.15.2), PerCP-Cy5.5 conjugated	Sony Biotechnology	1138125
Anti-mouse Ki-67 Monoclonal Antibody (Mouse), FITC conjugated	BD Biosciences	51-36524X
Anti-mouse LAP(TGF-β1) Monoclonal Antibody (Mouse, clone HK1.4), PE conjugated	BioLegend	141403
Anti-mouse Ly6C Monoclonal Antibody (Rat, clone HK1.4), AF700 conjugated	BioLegend	128024
Anti-mouse Ly6C Monoclonal Antibody (Rat, clone AL-21), PE-CF594 conjugated	BD Biosciences	562728
Anti-mouse Ly6G Monoclonal Antibody (Rat, clone 1A8), AF488 conjugated	BioLegend	127625
Anti-mouse Ly6G Monoclonal Antibody (Rat, clone 1A8), APC conjugated	BD Biosciences	560599
Anti-mouse MafB Recombinant Monoclonal Antibody (Rabbit, clone BLR046F), unconjugated	Bethyl Laboratories Inc.	A700-046
Anti-mouse NK1.1 Monoclonal Antibody (Mouse, clone PK136), FITC conjugated	BD Biosciences	553164
Anti-mouse TGF-beta 1 Monoclonal Antibody (Mouse, clone 9016EC), unconjugated	R&D Systems	MAB2402

Anti-mouse TGF-beta RI/ALK-5 Monoclonal Antibody (Rat, clone 141231), PE conjugated	R&D Systems	FAB5871P
Anti-mouse TGF-beta RII Polyclonal Antibody (Goat), PE conjugated	R&D Systems	FAB532P
Anti-mouse Tmem119 Monoclonal Antibody (Mouse, clone V3RT1GOsz), PE conjugated	ThermoFisher	12-6119-82
Anti-mouse von Willebrand Factor/vWF Monoclonal Antibody (Mouse, clone C-12), FITC conjugated	Santa Cruz Biotechnology	sc-365712 FITC
Anti-rabbit IgG (H+L) Cross-Adsorbed Secondary Polyclonal Antibody (Goat), AF488 conjugated	ThermoFisher	A-11034
Anti-rabbit IgG (H+L) Cross-Adsorbed Secondary Polyclonal Antibody (Donkey), AF647 conjugated	BioLegend	406414
Anti-mouse IgG (H+L) Cross-Adsorbed Secondary Polyclonal Antibody (Goat), AF750 conjugated	ThermoFisher	A-21037
Anti-rat IgG (H+L) Cross-Adsorbed Secondary Polyclonal Antibody (Goat), AF647 conjugated	BioLegend	405416
Anti-mouse IgG1, κ Isotype Control (Mouse), PE conjugated	BD Biosciences	555749
Anti-mouse IgG1, κ Isotype Control (Mouse), FITC conjugated	BD Biosciences	51-35404X
Anti-mouse IgG1, κ Isotype Control (Goat), PE conjugated	R&D Systems	IC108P

Antibodies for CODEX panel

Name	**Source**	**Cat. Number**
Anti-mouse CD64 (Rat, clone X54-5/7.1)	BioLegend	139302
Anti-mouse CD31 (Rat, clone MEC13.3)	BioLegend	102502
Anti-mouse SMA (Mouse, clone 1A4)	BioLegend	904601

Anti-mouse CD90.2 (Rat, clone Thy-1.2)	BioLegend	140302
Anti-mouse F4/80 (Rat, clone BM8)	ThermoFisher	14-4801-95
Anti-mouse Ly6C (Rat, clone HK1.4)	BioLegend	128002
Anti-mouse EpCAM (Rat, clone G8.8)	BioLegend	118202
Anti-mouse CD8a (Rat, clone 53-6.7)	BioLegend	100702
Anti-mouse PDGFRa (Rat, clone APA5)	ThermoFisher	14-1401-82
Anti-mouse CD11c (Rat, clone N418)	BioLegend	117302
Anti-mouse TCRβ (Rat, clone H57-597)	BioLegend	109202
Anti-mouse Ly6G (Rat, clone 1A8)	BioLegend	127602
Anti-mouse CD206 (Rat, clone MR5D3)	Bio-rad	MCA2235GA
Anti-mouse CD169 (Rat, clone 3D6.112)	BioLegend	142402
Anti-I-A/I-E (Rat, clone M5/114.15.2)	BioLegend	107602
Anti-mouse NK1.1 (Mouse, clone PK136)	BioLegend	108702
Anti-mouse CD11b (Rat, clone M1/70)	BioLegend	101202
Anti-mouse CD301b (Rat, clone URA1)	BioLegend	146802
Anti-human/mouse/rat TGFβ (Mouse, clone 1D11.16.8)	Novus Biologicals	NBP3-07718
Anti-mouse MerTK (Rat, clone DS5MMER)	ThermoFisher	14-5751-82
Anti-mouse CD4 (Rat, clone RM4-5)	BioLegend	100506
Anti-mouse CD19 (Rat, clone 6D5)	BioLegend	115502
Anti-mouse Xcr1 (Rat, clone ZET)	BioLegend	148202
Anti-mouse CD26 (Rat, clone H194-112)	BioLegend	137802
Anti-mouse SiglecF (Rat, clone 1RNM44N)	ThermoFisher	14-1702-82
Anti-mouse PDGFRβ (Rat, clone APB5)	BioLegend	136002
Anti-mouse CD45.1 (Mouse, clone A20)	BioLegend	110702
Anti-mouse CD45.2 (Rat, clone 104)	BioLegend	109802

Reagents

Name	Source	Cat. Number
Annexin V, conjugated FITC	BD Bioscience	560931
Annexin V, conjugated APC	ThermoFisher	A35110
Annexin V Binding Buffer, 10X	BD Bioscience	556454
ArC™ Amine Reactive Compensation Bead Kit	ThermoFisher	A10628
Baytrill (enrofloxacine)	Bayer	616300
Bovine Serum Albumin (BSA)	Sigma	A7906
Brilliant Stain Buffer	BD Bioscience	563794
Collagenase A, from Clostridium histolyticum	Sigma	11088793001
cOmplete™ Protease Inhibitor Cocktail	Sigma	11697498001
Diphtheria Toxin (DT), from *Corynebacterium diphtheriae*	List Biological Labs	150
DNase I	Sigma	11284932001
dNTP	ThermoFisher	N8080260
Donkey serum	Sigma	D9663
Dispase II	Merck Millipore	D4693
DPBS	ThermoFisher	14190094
EDTA	Merck Millipore	1084181000
Elastase from porcine pancreas	Merck Millipore	E1250
FastGene 100 bp DNA Marker	NIPPON Genetics	MWD100
Fetal Bovine Serum (FBS)	ThermoFisher	10270098
Glycerol	ThermoFisher	158920025
GoTaq G2 Hot Start Taq Polymerase	Promega	M7401
HBSS with Phenol Red	Lonza	BE10-508F
IsoFlo (Isoflurane)	Zoetis	B506

KAPA Express Extract	Merck	KK7100
LY-364947	Selleckchem	S2805
MEM NEAA	ThemoFisher	11140-035
Methanol	Merck	67-56-1
Nimatek (Ketamine)	Dechra	804132
Nonidet P 40 Substitute	Sigma	74385
O.C.T. Compound	Tissue-Tek	4583
OneComp eBeads	ThermoFisher	01-1111-41
Paraformaldehyde	ThermoFisher	F/1501/PB15
Percoll	GE Healthcare	17089101
Penicillin-Streptomycin	ThemoFisher	15070-063
ProLong Antifade Mountant with DAPI	ThermoFisher	P36966
Rompun (Xylazine)	Bayer	0076901
Sodium pyruvate	ThemoFisher	11360-070
Sucrose	Merck	57-50-1
Streptavidin, PE-CF594 conjugated	BD Biosciences	BD Biosciences
Recombinant Mouse TGF-beta 1 Protein	R&D Systems	7666-MB-005
0.25g/kg Tamoxifen mouse food	SAFE	E8404A01R 00008
Tris(hydroxymethyl)aminomethane	Merck Millipore	108382
TRIzol Reagent	ThermoFisher	10296010
Triton X-100	Merck	648466
Tween-20	ThermoFisher	233360010
Recombinant Murine M-CSF	ThermoFisher	315-02
RPMI 1640 Medium	ThermoFisher	21875-034
2-Mercaptoethanol	ThemoFisher	31350-010

CD11b MicroBeads, human and mouse	Miltenyi Biotec	130-049-601
CD31 MicroBeads, mouse	Miltenyi Biotec	130-097-418
Mouse Elastin ELISA Kit (Colorimetric)	Novusbio	NBP3-06918
IL-10 Mouse Uncoated ELISA Kit	ThermoFisher	88-7105-88
iTaq Universal SYBR Green Supermix	Bio-rad	1725121
LIVE/DEAD™ Fixable Near-IR Dead Cell Stain Kit, for 633 or 635 nm excitation	BD Biosciences	L34976
Foxp3 / Transcription Factor Staining Buffer Set	ThermoFisher	00-5523-00
Monocyte Isolation Kit (BM), mouse	Miltenyi Biotec	130-100-629
Pierce™ BCA Protein Assay Kit	ThermoFisher	23225
Quick-DNA™ Microprep Kit	ZYMO RESEARCH	D3020
TGF beta-1 Human/Mouse Uncoated ELISA Kit	ThermoFisher	88-8350-88
RevertAid H Minus First Strand cDNA Synthesis Kit	ThermoFisher	K1631
RNA Clean & Concentrator™-5	ZYMO RESEARCH	R1013
Sircol Soluble Collagen Assay Kit	Biocolor	S1000
VascuLife® EnGS-Mv Microvascular Endothelial Kit	CellSystems	LL-0004

Reagents for CODEX staining

Name	**Source**	**Cat. Number**
CODEX staining kit	Akoya Biosciences	7000008
CODEX conjugation kit	Akoya Biosciences	7000009
CODEX Buffer	Akoya Biosciences	7000001
Nuclear staining	Akoya Biosciences	7000003

BS3 fixative	ThermoFisher	21580
Acetone	Sigma	650501-1L
Methanol Free Formaldehyde	Sigma	28908
Methanol for HPLC >99.9%	Sigma	34860-1L-R

Barcodes and reporters for CODEX

Name	**Source**	**Cat. Number**
BX005 – RX005	Akoya Biosciences	5450024
BX006 – RX006	Akoya Biosciences	5450027
BX007 – RX007	Akoya Biosciences	5450015
BX010 – RX010	Akoya Biosciences	5450016
BX013 – RX013	Akoya Biosciences	5450017
BX014 – RX014	Akoya Biosciences	5450025
BX015 – RX015	Akoya Biosciences	5350001
BX016 – RX016	Akoya Biosciences	5150001
BX017 – RX017	Akoya Biosciences	5250001
BX019 – RX019	Akoya Biosciences	5450002
BX021 – RX021	Akoya Biosciences	5350002
BX022 – RX022	Akoya Biosciences	5150003
BX023 – RX023	Akoya Biosciences	5250003
BX024 – RX024	Akoya Biosciences	5350003
BX026 – RX026	Akoya Biosciences	5250004
BX027 – RX027	Akoya Biosciences	5350004
BX028 – RX028	Akoya Biosciences	5450005
BX030 – RX030	Akoya Biosciences	5350005
BX031 – RX031	Akoya Biosciences	5150006

BX033 – RX033	Akoya Biosciences	5350006
BX034 – RX034	Akoya Biosciences	5150007
BX037 – RX037	Akoya Biosciences	5150008
BX040 – RX040	Akoya Biosciences	5450009
BX041 – RX041	Akoya Biosciences	5250008
BX042 – RX042	Akoya Biosciences	5350008
BX043 – RX043	Akoya Biosciences	5150010
BX047 – RX047	Akoya Biosciences	5250009
BX049 – RX049	Akoya Biosciences	5450012

Primers

Gene name		5’ → 3’
Actb	F	AATCGTGCGTGACATCAAAG
	R	GGATTCCATACCCAAGAAGG
Csf1r	F	TGGATGCCTGTGAATGGCTCTG
	R	GTGGGTGTCATTCCAAACCTGC
Tmem119	F	ACTACCCATCCTCGTTCCCTGA
	R	TAGCAGCCAGAATGTCAGCCTG
Tgfbr1	F	CATTCACCACCGTGTGCCAAATGA
	R	ACCTGATCCAGACCCTGATGTTGT
Tgfbr2	F	CGACTTGACCTGTTGCCTGT
	R	CGTCTGCTTGAACGACTCCA
Tgfb1	F	TGACGTCACTGGAGTTGTACGG
	R	GGTTCATGTCATGGATGGTGC
C1qc	F	AAGGACGGGCATGATGGACTCC
	R	TTTCCCACGGTGGCCAGGCAT

Mafb	F	AGACAGGCTTTGCGTCCTAA
	R	TGCCAATGTGTGGGTTTCTA
Cx3cr1	F	GTGAGACTGGGTGAGTGACTGG
	R	CGAGGACCACCAACAGATTT
Pparg	F	GTGATGGAAGACCACTCGCATT
	R	CCATGAGGGAGTTAGAAGGTTC
Csf2ra	F	CAGTTTGAGGTCCAGTGGCAGA
	R	CCAGTGCTTCATCCTCGTGTCG
Car4	F	ACTGCCCAGTATCTCCAAACCC
	R	CAGTTTGGTGTGGTTAGTGAGCC
Crebpb	F	CAACCTGGAGACGCAGCACAAG
	R	GCTTGAACAAGTTCCGCAGGGT
Il17a	F	CAGACTACCTCAACCGTTCCAC
	R	TCCAGCTTTCCCTCCGCATTGA
Il1b	F	TGGACCTTCCAGGATGAGGACA
	R	GTTCATCTCGGAGCCTGTAGTG
Ccl5	F	TGCAGAGGACTCTGAGACAGC
	R	GAGTGGTGTCCGAGCCATA
Tnfa	F	CCACGTCGTAGCAAACCAC
	R	TTTGAGATCCATGCCGTTG
Il6	F	TACCACTTCACAAGTCGGAGGC
	R	CTGCAAGTGCATCATCGTTGTTC
Ifng	F	CAGCAACAGCAAGGCGAAAAAGG
	R	TTTCCGCTTCCTGAGGCTGGAT
Mafb$^{fl/fl}$ *genotyping*	F	TCCATCCATCTTGGGAAAAG
	R	TCAGGACTGGGCTGCTAGTT

Tgfbr2$^{fl/fl}$ *genotyping*		TATGGACTGGCTGCTTTTGTATTC
		TGGGGATAGAGGTAGAAAGACATA
		TATTGGGTGTGGTTGTGGACTTTA
Cr3cr1$^{LSL\text{-}DTR}$ *genotyping*		TCCAATTGTTCACCCTTTCA
		ACCAACAGATTTCCCACCAG
		CTCCAGACTGCCTTGGGAAAA
LyzM^{Cre} *genotyping*		CCCAGAAATGCCAGATTACG
		CTTGGGCTGCCAGAATTTCTC
		TTACAGTCGGCCAGGCTGAC
Chd5^{CreERT2} *genotyping*		GCCTGCATTACCGGTCGATGCAACGA
		GTGGCAGATGGCGCGGCAACACCATT
		GAGACTCTGGCTACTCATCC
		CCTTCAGCAAGAGCTGGGGAC
Tgfb1$^{fl/fl}$ *genotyping*		TGC ACA GTA CCT CAT GCA CA
		GGG GTG GAG ACA GAC TGG AA

Software

Software	**Producer**	**Reference**
Flowjo v10.8.1	BD	https://www.flowjo.com/
Prism 10	GraphPad Software	https://www.graphpad.com/scientific-software/prism/
Adobe Illustrator 2021	Adobe	
R	The R Foundation	https://www.r-project.org/
ImageJ 1.54	National Institutes of Health	http://imagej.org/
Imaris 9.5	Oxford Instruments	https://imaris.oxinst.com/
Qupath 0.5.0		https://qupath.github.io/

CODEX instrument manager	Akoya Biosciences	
CODEX Processor	Akoya Biosciences	
CODEX MAV	Akoya Biosciences	
CytoMAP		[348]

CODEX phenotypes

Cell type	**Markers**
Monocyte	$CD45.2^{+}$ $CD45.1^{-}$ Lin^{-} $CD11b^{+}$ $SiglecF^{-}$ $F4/80^{+}$ $Ly6C^{+/lo}$ $CD64^{+/lo}$ $MerTK^{lo/-}$
IM	$CD45.2^{+}$ $CD45.1^{-}$ Lin^{-} $CD11b^{+}$ $SiglecF^{-}$ $F4/80^{+}$ $Ly6C^{-}$ $MerTK^{+}$ $MHCII^{+}$
$CD206^{-}$ IM	$CD45.2^{+}$ $CD45.1^{-}$ Lin^{-} $CD11b^{+}$ $SiglecF^{-}$ $F4/80^{+}$ $Ly6C^{-}$ $MerTK^{+}$ $MHCII^{+}CD206^{-}$
$CD206^{+}$ IM	$CD45.2^{+}$ $CD45.1^{-}$ Lin^{-} $CD11b^{+}$ $SiglecF^{-}$ $F4/80^{+}$ $Ly6C^{-}$ $MerTK^{+}$ $MHCII^{+}$ $CD206^{+}$
AM	$CD45^{+}$ Lin^{-} $F4/80^{+}$ $CD64^{+}$ $CD11c^{+}$ $SiglecF^{+}$
DC1	$CD45^{+}$ Lin^{-} $F4/80^{-}$ $CD26^{+}$ $MHCII^{+}$ $CD11c^{+}$ $Xcr1^{+}$
DC2	$CD45^{+}$ Lin^{-} $F4/80^{-}$ $CD26^{+}$ $MHCII^{+}$ $CD11c^{+}$ $CD11b^{+}$
Eosinophil	$CD45^{+}$ Lin^{-} $CD64^{-}$ $CD11c^{-}$ $SiglecF^{+}$
Neutrophil	$CD45^{+}$ Lin^{-} $F4/80^{-}$ $Ly6G^{+}$ $CD11b^{+}$
B cell	$CD45^{+}$ $TCR\beta^{-}$ $CD19^{+}$
T cell	$CD45^{+}$ $CD19^{-}$ $TCR\beta^{+}$
ILC	$CD45^{+}$ $TCR\beta^{-}$ $CD19^{-}$ $CD127^{+}$
Endothelial cell	$CD45^{-}$ $CD31^{+}$ $EpCAM^{-}$ $PDGFRa^{-}$
Fibroblast	$CD45^{-}$ $CD31^{-}$ $EpCAM^{-}$ $PDGFRa^{+}$
Epithelial cell	$CD45^{-}$ $CD31^{-}$ $EpCAM^{+}$ $PDGFRa^{-}$

2. Results

2.1. Lung endothelial Tgfβ1-interstitial macrophage Tgfβ receptor interactions are inferred from NicheNet analyses

We aimed to predict putative ligand-receptor interactions between sender lung structural cells and receiver IMs from single cell transcriptomic data using NicheNet analyses [353]. To this end, we employed previously published single cell RNA-sequencing (scRNA-seq) data of lung IM subsets, Ly6C$^+$ classical monocytes (cMo) (i.e., the precursors of IMs), and non-hematopoietic niche cells including endothelial, epithelial and stromal cells analyzed at steady-state in C57BL/6 WT mice [147] (fig. S1). The top interactions between ligands expressed by niche cells and the corresponding receptors on IMs were visualized using a Circos plot [354], where the strength of the interaction is related to the thickness of the connecting arrows (Fig. 1A). *Csf1*, coding for Csf1 or macrophage colony-stimulating factor (M-CSF), was expressed by the three niche cell populations and was predicted to be involved in IM development via Csf1r signaling, consistent with previous findings [167, 177]. Of note, a substantial interaction was also predicted between endothelial cell-derived *Tgfb1* and IMs (Fig. 1A). Further analysis of target genes triggered by Tgfβ1 signaling within receiver IMs revealed a high regulatory potential for the receptors *Tgfbr1* and *Tgfbr2*, as well as for various migration-related genes associated with integrin binding (i.e., *Itgb1*, *Itga4*, *Itgb5*, *Icam2*, *Itgax*, *Fn1*, *Igf1*, *Itga5*, *Calr*, *Thbs1*, *Icam1*) (Fig. 1B). Moreover, *Tgfb1* expression in the scRNA-seq data [147] was significantly higher in endothelial cells as compared to epithelial or stromal cells (Fig 1C).

Tgfβ1 can bind to membrane Tgfβ receptor II (TgfβRII) subunit, allowing cooperative binding to TgfβRI and downstream signaling [355]. We assessed *Tgfbr1* and *Tgfbr2* expression in lung cMo, AMs, CD206$^-$ IMs and CD206$^+$ IMs thanks to previously published bulk RNA-seq data [167] and found that AMs and IMs expressed significantly higher levels of *Tgfbr1* and *Tgfbr2* as compared to cMo (Fig. 1D). We next evaluated the protein expression of TgfβRI and TgfβRII on lung myeloid cells from WT mice by flow cytometry (fig. S2A). We found that lung monocytes, AMs and IMs expressed TgfβRI, whose levels were significantly lower in both IM

subsets as compared to AMs or cMo (fig. S2, B and C). Interestingly, while lung cMo and Ly6C^{-} patrolling monocytes (pMo) expressed low levels of TgfβRII, its expression was elevated in AMs and in IMs, especially in the CD206^{+} IM subset (Fig. 1, E and F). Lung neutrophils (Neu), conventional dendritic cells (cDCs) and blood myeloid cells also expressed significantly lower levels of TgfβRII as compared to lung IMs (fig. S2, D and E). Together, our results indicate that IMs could be effective responders to Tgfβ signals through the Tgfβ-TgfβRII signaling pathway, and that endothelial cells may represent an important source of Tgfβ1.

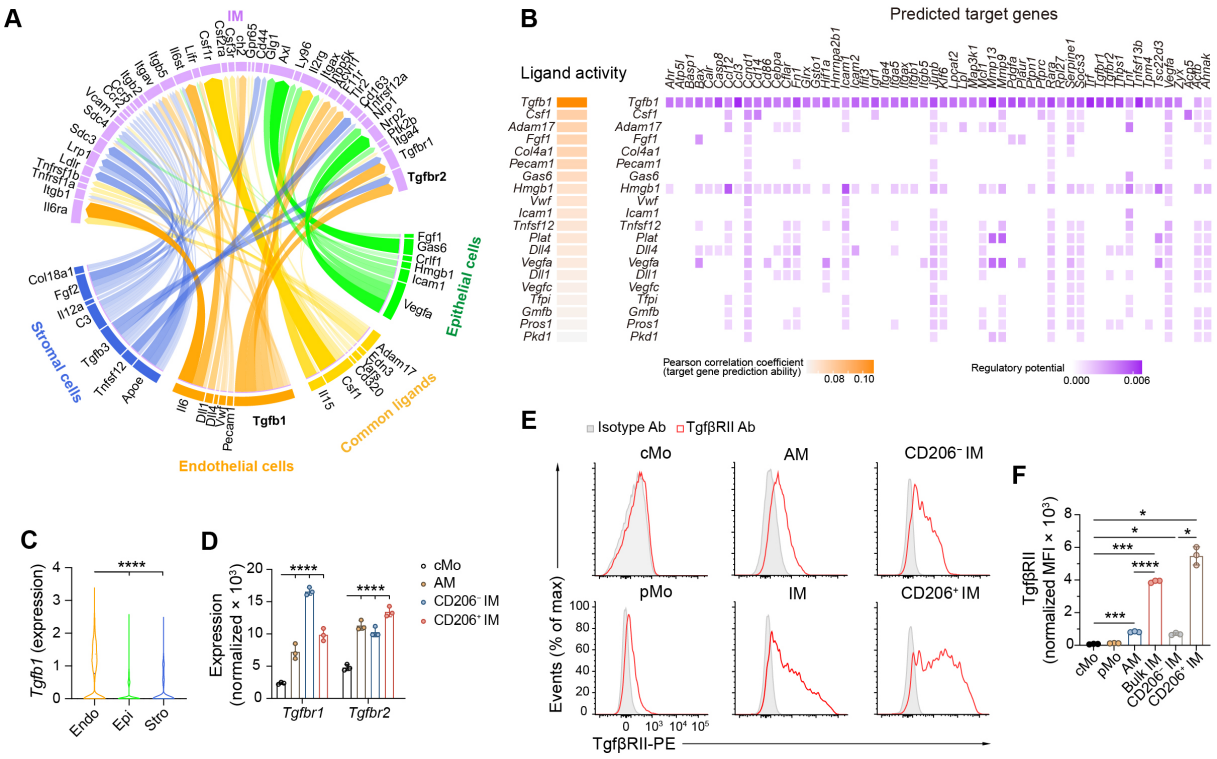

Fig. 1. Endothelial Tgfβ1-IM Tgfβ receptor interactions are predicted from NicheNet analyses during IM development. (**A**) Circos plot depicting the putative interactions between structural cell-derived ligands (bottom) and IM-intrinsic receptors (top), evaluated by NicheNet analysis of scRNA-seq data of lung monocytes, IMs and structural cells from naïve C57BL/6 WT mice [147]. Opacity of the arrows correlates with the interaction score. (**B**) Heatmap depicting predicted ligand activity within lung endothelial cells and IM-intrinsic target gene activation during IM development, based on NicheNet analyses as in (A). (**C**) Expression of *Tgfb1* within lung primary endothelial cells (Endo), epithelial cells (Epi) and stromal cells (Stro), extracted from the scRNA-seq data, as in (A), and depicted by violin plots (height: expression; width: abundance of cells). (**D**) Expression of *Tgfbr1* and *Tgfbr2* within lung cMo, AMs, CD206^{-} IMs and CD206^{+} IMs of naïve C57BL/6 WT mice, extracted by bulk RNA-seq data analyses [167]. (**E**) Representative histograms and (**F**) bar graph showing normalized MFI of TgfβRII expression in lung cMo, pMo, AMs and IMs from naïve C57BL/6 WT mice. (D,F) Data show mean +/- SEM (D) *n* = 3 biological replicates of FACS-sorted cells; (F) Data are representative of 3 independent experiments (*n* = 3 mice). *P* values were calculated using (C) a one-way ANOVA with Games-Howell's post hoc tests or (D) a two-way ANOVA with Dunnett's post hoc tests or (F) a one-way ANOVA with Dunnett's post hoc tests. *, *P*<0.05; ***, *P*<0.001; ****, *P*<0.0001. MFI, mean fluorescence intensity.

2.2. Lung endothelial Tgfβ1 triggers a core lung IM identity on Csf1-grown monocytes and Macs ex vivo

We sought to investigate the potential impact of soluble factors released from primary lung endothelial, epithelial, and stromal cells on monocyte differentiation and the acquisition of a distinct lung IM profile. To this end, $CD45^{-}EpCam^{-}CD31^{+}$ endothelial cells, $CD45^{-}EpCam^{+}CD31^{-}$ epithelial cells and $CD45^{-}EpCam^{-}CD31^{-}$ stromal cells were FACS-sorted from a lung single cell suspension of WT mice (fig. S2F), cultured for 12 hours and their supernatants were collected. Bone marrow-derived monocytes (BM Mo) were isolated from the BM of WT mice, cultured in basal medium (Ctrl) or conditioned medium (CM) from endothelial cells (CM-Endo), epithelial cells (CM-Epi) or stromal cells (CM-Stro) for 48 hours and subjected to bulk RNA sequencing (Fig. 2A). Principal component analysis (PCA) showed distinct clustering patterns for BM Mo exposed to distinct CM, indicating unique gene expression profiles induced by each CM (Fig. 2B). We generated gene set signatures of lung $CD206^{+}$ IMs, $CD206^{-}$ IMs and AMs based on our previously published scRNA-seq data (*10*) and mapped these signatures to CM-stimulated BM Mo using Gene Set Enrichment Analysis (GSEA) (*24*). Of note, CM-Endo and CM-Stro triggered an enrichment in an IM signature regardless of the IM subset, but CM-Endo was the only treatment that stimulated a specific IM signature while refraining an AM signature (Fig. 2C). These data suggested that lung endothelial cells release soluble signals that can imprint a specific IM signature.

Next, we investigated whether recombinant Tgfβ1 was sufficient to imprint the trajectory of Csf1-grown BM Mo towards a lung IM profile. As opposed to AMs, bulk IMs can be uniquely defined by an elevated expression of Cx3cr1, Tmem119, MafB and C1q [147, 167, 176]. Hence, BM Mo from WT (i.e., $Tgfbr2^{fl/fl}$) mice were cultured with Csf1 in the presence of absence of Tgfβ1 for 48 hours and the expression of IM identity genes and proteins were evaluated by RT-qPCR and flow cytometry, respectively (Fig. 2D). We found that Tgfβ1 significantly upregulated the transcript levels of *Mafb*, *C1qc*, *Cx3cr1*, *Tmem119* and *Csf1r* in Csf1-treated BM Mo, while it had no effect on *Tgfbr2* expression and downregulated the expression of the AM-specific transcription factor *Pparg* (Fig. 2E). At the protein level, we also found significantly

increased expression of MafB, C1qa, Cx3cr1 and Tmem119 in Tgfβ1-treated Csf1-grown WT BM Mo as compared to untreated controls (Fig. 2, F and G). To evaluate the impact of Tgfβ signaling through TgfβRII in this model, we used myeloid-specific *Tgfbr2*-deficient mice by crossing *Tgfbr2*$^{fl/fl}$ mice with mice expressing the Cre recombinase under the control of the myeloid Lyz2 promoter (called *Lyz2*^{Cre} mice). A significant decrease in *Tgfbr2* expression and a partial excision of the floxed allele were observed in BM Mo from *Lyz2*^{Cre} *Tgfbr2*$^{fl/fl}$ mice as compared to *Tgfbr2*$^{fl/fl}$ littermate controls (fig. S3). Of note, the induction of IM identity marker genes and proteins were all significantly decreased in Tgfβ1-treated *Tgfbr2*-deficient Csf1-grown BM Mo as compared to the WT counterparts, while Tgfβ1-triggered downregulation of *Pparg* was no longer observed in the absence of *Tgfbr2* (Fig. 2E-G). We also generated WT or *Tgfbr2*-deficient BM-derived macrophages (BMDMs) and treated them from day 7 till day 9 of culture with Tgfβ1 (fig. S4A-C). Interestingly, we also observed Tgfβ1-triggered and TgfβRII-mediated increases in the expression of IM-specific markers on differentiated BMDMs, as seen in BM Mo (fig. S4, D and E). Treatment of BM Mo with Csf2 and Tgfβ1, two cytokines required for AM development and identity [15, 95, 158], triggered an AM-associated signature independently of the concomitant presence of Csf1 (fig. S5, A and B) and did not induce expression of IM signature genes. Of note, the addition of Csf2 to Csf1- or Tgfβ1- and Csf1-grown BM Mo exerted a substantial inhibitory effect on the expression of IM signature genes and *Tgfbr2* (fig. S5, C and D). Altogether, these results show that, in the presence of Csf1, Tgfβ1 can signal through TgfβRII to imprint a core IM signature in differentiating BM Mo or in BMDMs.

Finally, we asked whether co-culture of Csf1-grown BM Mo with lung primary endothelial cells (Endo) would trigger a similar IM signature and whether such signature was dependent on TgfβRII (Fig. 2H). We found that co-culture of BM Mo with Endo induced a significant increase in the expression of the IM markers Cx3cr1, Tmem119, MafB and C1qa (Fig. 2, I and J). Of note, such induction of IM identity was abolished in the presence of LY364947, a Tgfβ receptor inhibitor, and was significantly decreased in BM Mo from *Lyz2*^{Cre} *Tgfbr2*$^{fl/fl}$ mice as compared to BM Mo from *Tgfbr2*$^{fl/fl}$ controls (Fig. 2, I and J).

Our *ex vivo* results demonstrate that in the presence of Tgfβ1 and Csf1, or lung primary endothelial cells, BM Mo can acquire a lung IM-specific profile during macrophage differentiation. Notably, such IM identity is dependent on myeloid-intrinsic Tgfβ receptor signaling.

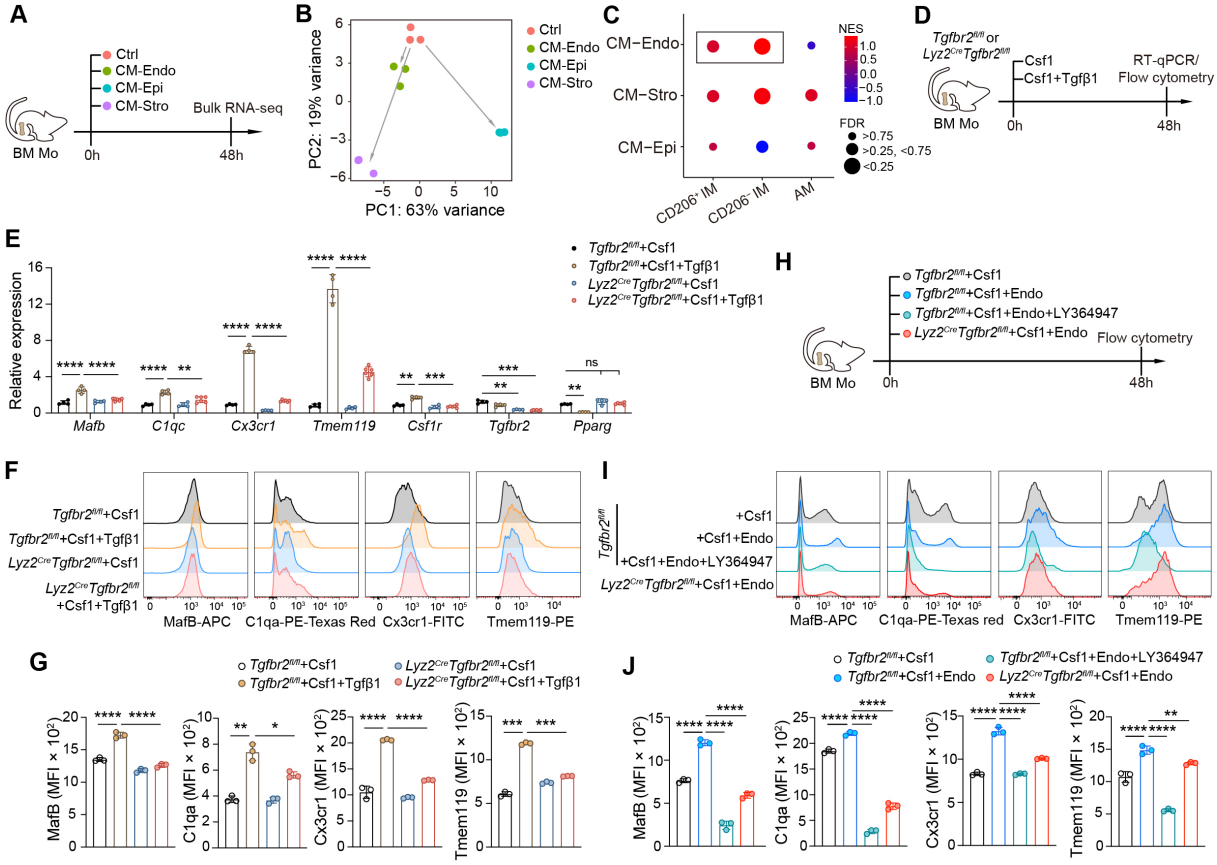

Fig. 2. Lung endothelial Tgf1 triggers a core IM signature on Csf1-grown BM Mo and BMDMs. (**A**) Experimental outline for (B, C). BM Mo from WT mice were cultured in basal medium (Ctrl) or conditioned medium (CM) from lung primary endothelial (CM-Endo), epithelial (CM-Epi) or stromal (CM-Stro) cells and subjected to bulk RNA-seq analyses 48 hours later. (**B**) Principal Component Analysis (PCA) plot of the BM Mo bulk RNA-seq data, as in (A). (**C**) Gene Set Enrichment Analysis (GSEA) comparing the transcriptome of CM-stimulated BM Mo, as in (A), with signature gene sets characteristic of CD206^{+} IMs, CD206^{-} IMs and AMs. (**D**) Experimental outline for (E-G). BM Mo from *Tgfbr2*$^{fl/fl}$ or *Lyz2*^{Cre} *Tgfbr2*$^{fl/fl}$ mice were stimulated with Csf1 or Csf1 + Tgfβ1 for 48 hours and were analyzed by RT-qPCR and flow cytometry. (**E**) Relative mRNA expression of the indicated genes in BM Mo, as in (D). (**F**) Representative histograms and (**G**) bar graph showing MFI of MafB, C1qa, Cx3cr1 and Tmem119 expression in BM Mo, as in (D). (**H**) Experimental outline for (I, J). Csf1-grown BM Mo from WT mice were co-cultured with or without lung primary endothelial cells (Endo) in the presence or absence of the TgfβR inhibitor LY364947 and were analyzed by flow cytometry 48 hours later. (**I**) Representative histograms and (**J**) bar graph showing MFI of MafB, C1qa, Cx3cr1 and Tmem119 expression in BM Mo, as in (H). (E,G,J) Data show mean +/- SEM and are representative of 3 independent experiments (*n* = 3-6 replicates from 2 to 3 mice). *P* values were calculated using (E) a two-way ANOVA with Tukey's post hoc tests, (G, J) a one-way ANOVA with Dunnett's post hoc tests. *, *P*<0.05; **, *P*<0.01; ***, *P*<0.001; ****, *P*<0.0001. MFI, mean fluorescence intensity; ns, not significant. FDR, Falso Discovery Rate; NES, Normalized Enrichment Score.

2.3. Myeloid Tgfβ receptor signaling mediates lung IM development and identity *in vivo*

Next, we employed *Tmem119*^{Cre} *Cx3cr1*$^{LSL\text{-}DTR}$ mice (i.e., IM^{DTR} mice) (*11*), in which diphteria toxin (DT) treatment causes a bolus depletion of the IM niche that is rapidly refilled by cMo-derived *de novo* IMs. In order to evaluate the contribution of Tgfβ receptor signaling to IM development, we combined DT-triggered IM niche depletion in IM^{DTR} mice with intraperitoneal (i.p.) injections of the Tgfβ receptor inhibitor LY363947 at days 2, 4 and 6 post-DT (Fig. 3A). At day 7 post-DT, we found that numbers of lung cMo and IMs were significantly lower in LY363947-treated IM^{DTR} mice as compared to PBS-treated controls, while numbers of pMo and AMs remained unchanged (Fig. 3B). Of note, Tgfβ receptor inhibition was associated with a significant decrease in numbers of both CD206^{-} IMs and CD206^{+} IMs (fig. S6A). Interestingly, this was associated with a significant increase in the proportion of apoptotic Annexin V^{+} lung cMo and IMs in LY364947-treated mice as compared to vehicle-treated counterparts (fig. S6B). Of note, the proportion of blood Ly6C^{+} cMo was higher in LY363947-treated IM^{DTR} mice as compared to PBS-treated counterparts and the viability of BM and blood cMo were not affected by LY363947 (fig. S6, C and D). These results suggested that Tgfβ receptor signaling impacted lung cMo and IM survival capacity, and was important for lung cMo recruitment or lung IM differentiation.

To assess whether myeloid-intrinsic Tgfβ receptor signaling played a role in either lung cMo recruitment or IM differentiation from cMo *in vivo*, we generated BM competitive chimeras in thorax-protected CD45.1/CD45.2 IM^{DTR} mice engrafted with a 1:1 BM cell mix from CD45.1 WT and CD45.2 *Lyz2*^{Cre} *Tgfbr2*$^{fl/fl}$ mice (Fig. 3C). At week 4 post-transfer, donor chimerism of blood cMo exceeded 80 %, while AM donor chimerism was below 5%, indicating efficient BM donor reconstitution and thorax protection, respectively (Fig. 3, D and E). Seven days post-DT, we found that more than 85 % of IMs were of donor origin, confirming efficient depletion and BM reconstitution (Fig. 3, D and E) and we evaluated the donor chimerism of lung cMo and IM subsets. Lung cMo of donor origin arose equally from CD45.1 WT and CD45.2 *Lyz2*^{Cre} *Tgfbr2*$^{fl/fl}$ cells, indicating that lung cMo recruitment was independent of Tgfβ receptor (Fig. 3, D-F).

However, we found that CD45.1 WT BM cells had a competitive advantage over CD45.2 *Lyz2*^{Cre} *Tgfbr2*$^{fl/fl}$ cells to become IMs, regardless of the IM subset, suggesting that TgfβRII-deficient monocytes, once in the lung, failed to fully differentiate into IMs and reconstitute the IM pool (Fig. 3, D-F).

To further characterize lung monocytes and macrophages in the absence of myeloid-intrinsic TgfβRII, we compared their numbers, localization and identity by flow cytometry between myeloid-restricted *Tgfbr2*-deficient mice and littermate controls. First, we found that IMs from *Lyz2*^{Cre} *Tgfbr2*$^{fl/fl}$ mice exhibited a 60% reduction in *Tgfbr2* expression as compared to those from littermate controls (fig. S7A). Second, no abnormalities were found in the blood leukocyte composition of such transgenic mice (fig. S7B). As expected, AM numbers were significantly lower in *Lyz2*^{Cre} *Tgfbr2*$^{fl/fl}$ mice as compared to controls [158] (Fig. 3G). Notably, IM numbers were also significantly lower in *Lyz2*^{Cre} *Tgfbr2*$^{fl/fl}$ mice as compared to controls (Fig. 3G). The remaining IMs in *Lyz2*^{Cre} *Tgfbr2*$^{fl/fl}$ mice exhibited a higher percentage of Annexin V^{+} cells as compared to control IMs, supporting that IMs are more sensitive to apoptosis in the absence of TgfβRII signaling (fig. S7C). The percentage of Ki-67^{+} cells was also significantly higher in IMs from *Lyz2*^{Cre} *Tgfbr2*$^{fl/fl}$ mice as compared to control IMs, suggesting that reduced cell proliferation does not account for the lower IM numbers in these mice (fig. S7D). Interestingly, flow-cytometry-based UMAP plot representation of monocytes and macrophages highlighted the appearance of a distinct cell population in *Lyz2*^{Cre} *Tgfbr2*$^{fl/fl}$ mice (Fig. 3H). Back-gating analysis identified this population as Ly6C^{+}CD64^{+} monocytes (called CD64^{+} Mo) (Fig 3I), whose numbers were significantly increased in *Lyz2*^{Cre} *Tgfbr2*$^{fl/fl}$ mice as compared to littermate controls (Fig. 3G). The phenotype of CD64^{+} Mo was reminiscent to that of transitioning CD64^{+} monocytes that appear during IM development in IM^{DTR} mice [167], but could also correspond to inflammatory monocytes or macrophages recruited when inflammation is present [144, 147]. Hence, we evaluated the expression of pro-inflammatory genes on lung extracts of *Lyz2*^{Cre} *Tgfbr2*$^{fl/fl}$ and littermate control mice and found no evidence of inflammation in the absence of myeloid *Tgfbr2* in 8-12-week-old mice (fig. S7E). Next, we assessed the localization of CD64^{+} Mo. To this end, we labeled intravascular cells by

intravenous (i.v.) injection of anti-CD45-FITC antibodies 10 minutes before sacrifice, and airway cells by intratracheal (i.t.) injection of anti-CD45-APC antibodies 5 minutes before sacrifice. As expected, most cMo and pMo were intravascular, most AMs were in the airway lumen and most IMs were parenchymal, regardless of the mouse genotype (fig. S7, F and G). Interestingly, while the few lung CD64$^+$ Mo present in control mice were mostly intravascular, 70% of lung CD64$^+$ Mo from *Lyz2^{Cre} Tgfbr2$^{fl/fl}$* mice were parenchymal (Fig. 3, J and K). These data further support the idea that, while monocyte entry in the tissue is not affected in the absence of intrinsic *Tgfbr2,* monocyte-to-IM differentiation is impaired and blocked at an early differentiation stage that accumulates in the tissue. Finally, we found that both CD64$^+$ Mo and IMs from *Lyz2^{Cre} Tgfbr2$^{fl/fl}$* mice exhibited a significant decrease in the expression of Cx3cr1 and Tmem119 in as compared to CD64$^+$ Mo and IMs from littermate control mice (Fig. 3, L and M), supporting a loss of IM identity in the absence of myeloid *Tgfbr2*. Numbers of heart and skin macrophages were, however, similar between *Lyz2^{Cre} Tgfbr2$^{fl/fl}$* and control mice (fig. S7 H-J), suggesting that myeloid-intrinsic Tgfβ receptor signaling may play a more dominant role in the lung compared to other organs.

Altogether, these results demonstrate that intrinsic TgfβR signaling plays an important role for lung IM development and to imprint a core IM identity *in vivo*.

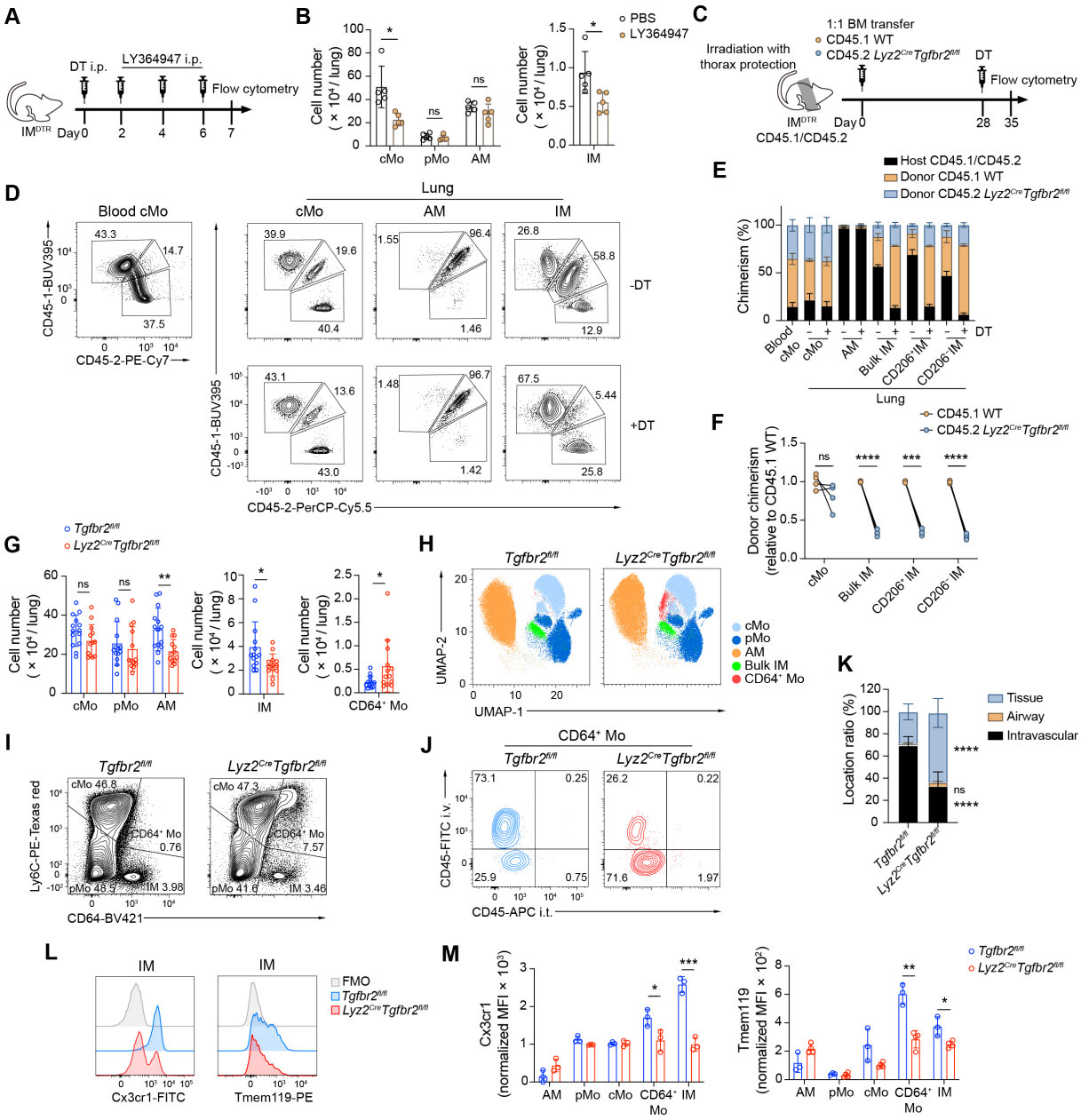
A
DT i.p.
LY364947 i.p.
Flow cytometry
IM^DTR
Day 0 2 4 6 7
B
PBS
LY364947
Cell number (× 10⁴ / lung)
cMo pMo AM
IM
C
1:1 BM transfer
CD45.1 WT
CD45.2 Lyz2^Cre Tgfbr2^fl/fl
Irradiation with thorax protection
DT
Flow cytometry
IM^DTR
CD45.1/CD45.2
Day 0 28 35
D
Blood cMo
Lung
cMo AM IM
-DT
+DT
CD45-1-BUV395
CD45-2-PE-Cy7
CD45-2-PerCP-Cy5.5
E
Host CD45.1/CD45.2
Donor CD45.1 WT
Donor CD45.2 Lyz2^Cre Tgfbr2^fl/fl
Chimerism (%)
Blood cMo cMo AM Bulk IM CD206⁺IM CD206⁻IM
DT
Lung
F
CD45.1 WT
CD45.2 Lyz2^Cre Tgfbr2^fl/fl
Donor chimerism (relative to CD45.1 WT)
cMo Bulk IM CD206⁺IM CD206⁻IM
G
Tgfbr2^fl/fl
Lyz2^Cre Tgfbr2^fl/fl
Cell number (× 10⁴ / lung)
cMo pMo AM IM CD64⁺ Mo
H
Tgfbr2^fl/fl
Lyz2^Cre Tgfbr2^fl/fl
UMAP-1
UMAP-2
cMo
pMo
AM
Bulk IM
CD64⁺ Mo
I
Tgfbr2^fl/fl
Lyz2^Cre Tgfbr2^fl/fl
Ly6C-PE-Texas red
CD64-BV421
cMo 46.8
CD64⁺ Mo 0.76
pMo 48.5
IM 3.98
cMo 47.3
CD64⁺ Mo 7.57
pMo 41.6
IM 3.46
J
CD64⁺ Mo
Tgfbr2^fl/fl
Lyz2^Cre Tgfbr2^fl/fl
CD45-FITC i.v.
CD45-APC i.t.
73.1 0.25 25.9 0.75
26.2 0.22 71.6 1.97
K
Tissue
Airway
Intravascular
Location ratio (%)
Tgfbr2^fl/fl
Lyz2^Cre Tgfbr2^fl/fl
L
IM
IM
FMO
Tgfbr2^fl/fl
Lyz2^Cre Tgfbr2^fl/fl
Cx3cr1-FITC
Tmem119-PE
M
Cx3cr1 (normalized MFI × 10³)
Tmem119 (normalized MFI × 10²)
AM pMo cMo CD64⁺ Mo IM
Tgfbr2^fl/fl
Lyz2^Cre Tgfbr2^fl/fl

Fig. 3. Tgfβ receptor inhibition and myeloid-restricted *Tgfbr2* deficiency impede monocyte-to-IM development and IM identity *in vivo*. (**A**) Experimental outline for (B, C). IM^{DTR} mice were treated intraperitoneally (i.p.) at day 0 with DT and at days 2, 4 and 6 with PBS or the TgfβR inhibitor LY364947, and lung myeloid cell numbers and viability were evaluated by flow cytometry at day 7 post-DT. (**B**) Absolute numbers of lung cMo, pMo, AMs and IMs, as in (A). (**C**) Experimental outline for (D-F). Naïve CD45.1/CD45.2 IM^{DTR} mice were lethally irradiated with thorax protection and were reconstituted with a 1:1 mix of CD45.1 WT and CD45.2 *Lyz2*^{Cre} *Tgfbr2*$^{fl/fl}$ BM cells, were injected with DT or PBS 28 days later, and the chimerism was assessed at day 35. (**D**) Representative CD45.1 and CD45.2 contour plots and (**E**) bar graph showing % of host CD45.1/CD45.2, donor CD45.1 WT and donor CD45.2 *Lyz2*^{Cre} *Tgfbr2*$^{fl/fl}$ chimerism in the indicated cell populations, as in (C). (**F**) Quantification of donor CD45.2 *Lyz2*^{Cre} *Tgfbr2*$^{fl/fl}$ chimerism relative to donor CD45.1 WT chimerism in the indicated cell populations, as in (D). (**G**) Absolute numbers of the indicated lung myeloid cell populations evaluated by flow cytometry in *Lyz2*^{Cre} *Tgfbr2*$^{fl/fl}$ mice and in *Tgfbr2*$^{fl/fl}$ littermate controls, as depicted by individual values and violin plots (height: cell numbers; width: abundance of cells). (**H**) Representative UMAP plots of lung $CD45^+CD11b^+$ and/or $CD11c^+$ cells analyzed by flow cytometry in *Lyz2*^{Cre} *Tgfbr2*$^{fl/fl}$ mice and in *Tgfbr2*$^{fl/fl}$ littermate controls (merged data from 2 mice per group). (**I**) Representative flow cytometry Ly6C and CD64 plots of lung $CD45^+SSC^{lo}CD11b^+F4/80^+$ cells from *Lyz2*^{Cre} *Tgfbr2*$^{fl/fl}$ mice and *Tgfbr2*$^{fl/fl}$ littermate controls. (**J**) Representative CD45-i.v. and CD45-i.t. plots of lung $CD45^+SSC^{lo}CD11b^+F4/80^+Ly6C^+CD64^+$ cells (i.e., $CD64^+$ Mo) from *Lyz2*^{Cre} *Tgfbr2*$^{fl/fl}$ mice and *Tgfbr2*$^{fl/fl}$ littermate controls injected with anti-CD45-FITC Ab i.v. and anti-CD45-APC Ab i.t. before sacrifice. (**K**) Percentages of tissue ($CD45\text{-}i.v.^-/CD45\text{-}i.t.^-$), airway ($CD45\text{-}i.v.^-/CD45\text{-}i.t.^+$) and intravascular ($CD45\text{-}i.v.^+/CD45\text{-}i.t.^-$) $CD64^+$ Mo, as in (K). (**L**) Representative histograms and (**M**) bar graph showing MFI of Cx3cr1 and Tmem119 expression in (M) IMs and (N) the indicated lung myeloid cell populations of *Lyz2*^{Cre} *Tgfbr2*$^{fl/fl}$ mice and *Tgfbr2*$^{fl/fl}$ littermate controls, evaluated by flow cytometry. (B,E,F,G,K,M) Data show (B,E,M) mean +/- SEM and are representative of 2-3 independent experiments (*n* = 3-6 mice), and (F) individual mice are representative of 3 independent experiments (*n* = 4 mice), (G,K) mean +/- SEM are pooled from 4 independent experiments (*n* = 8-14 mice). *P* values were calculated using (B,M) a unpaired Student's *t* test, (F) a paired multiple *t* test, (G) a Wilcoxon rank sum test or (K) a two-way ANOVA with Sidak's post-hoc tests. *, $P<0.05$; **, $P<0.01$; ***, $P<0.001$; ****, $P<0.0001$. Ab, antibody; MFI, mean fluorescence intensity; ns, not significant.

2.4. Tgfβ1 acts in synergy with Csf1 to trigger a MafB-dependent IM identity

We have recently shown that the transcription factor MafB was important for IM development [167]. First, we asked whether Tgfβ1 could trigger MafB expression. WT BM Mo were cultured with Tgfβ, Csf1, or Tgfβ and Csf1 for 48 hours and the expression of *Mafb* and IM identity genes was evaluated by RT-qPCR. Freshly isolated BM Mo were used as controls (Fig. 4A). We observed that, while Tgfβ1 or Csf1 alone could trigger *Mafb*, the combination of both treatments was the most potent in upregulating *Mafb* expression, which correlated with the most significant induction of the IM identity genes *C1qc*, *Cx3cr1*, *Tmem119* and *Csf1r* (Fig. 4B). Of note, Csf1 treatment significantly increased *Tgfbr2* expression, while Tgfβ1 treatment alone did not trigger expression of *Csf1r* nor *Tgfbr2* (Fig. 4B), suggesting that engagement of Csf1 signaling licenses IMs for the action of Tgfβ1. Further supporting this hypothesis, we found that the increase in target gene signature score downstream of Csf1 preceded the increase in target gene signature score downstream of Tgfβ1 along the trajectory of monocyte-to-IM development [167] (Fig. 4C).

Second, we asked whether Tgfβ1-mediated induction of IM identity was dependent on MafB. We isolated BM Mo from myeloid-restricted Mafb-deficient mice [167] (*Lyz2*^{Cre} *Mafb*$^{fl/fl}$ mice) and littermate controls and cultured them with Csf1 in the presence of absence of Tgfβ1 for 48 hours (Fig. 4D). The absence of *Mafb* mRNA was confirmed in BM Mo from *Lyz2*^{Cre} *Mafb*$^{fl/fl}$ mice (Fig. 4E). We found that, in the absence of MafB, Tgfβ1 treatment was no longer able to trigger an IM identity profile, as shown by the absence of upregulation of *C1qc*, *Cx3cr1* and *Csf1r* in MafB-deficient BM Mo and a significant decrease in *Tmem119* expression in MafB-deficient BM Mo as compared to WT BM Mo (Fig. 4E). Moreover, *Tgfbr2* expression itself was significantly decreased in the absence of MafB, suggesting that MafB could also directly or indirectly regulate *Tgfbr2* expression (Fig. 4E). This was further evidenced when we looked at the differential expression of *Mafb*, *Tgfbr2* and target genes downstream of TgfβRII signaling along the trajectory of monocyte-to-IM development [167]. Of note, *Mafb* and *Tgfbr2* displayed a similar pattern of upregulation during the differentiation trajectories, and the progressive increase in target gene signature score downstream of Tgfβ1 was observed in

both CD206^{-} IM and CD206^{+} IM differentiation pathways, supporting Tgfβ signaling engagement in both subsets (Fig. 4F). Moreover, many predicted target genes downstream of TgfβRII signaling with the highest regulatory potential (Fig. 1B) were upregulated over the course of monocyte-to-IM development (Fig. 4G), and their expression was significantly lower in *Mafb*-deficient IMs from *Lyz2*^{Cre} *Mafb*$^{fl/fl}$ mice [167] as compared to the WT counterparts (Fig. 4H). Finally, we quantified TgfβRII expression on IMs from *Lyz2*^{Cre} *Mafb*$^{fl/fl}$ and control mice and, while IMs from *Lyz2*^{Cre} *Mafb*$^{fl/fl}$ mice expressed detectable levels TgfβRII, we found a significantly lower TgfβRII expression on IMs from *Lyz2*^{Cre} *Mafb*$^{fl/fl}$ mice as compared to the WT counterparts (Fig. 4, I and J), indicating that MafB could regulate TgfβRII expression in IMs. Altogether, these data support that Tgfβ1-Tgfβ receptor interactions can activate MafB-dependent pathways, which then regulates IM-intrinsic TgfβRII expression and TgfβRII-dependent signaling events to mediate full development of mature IMs, in concert with Csf1.

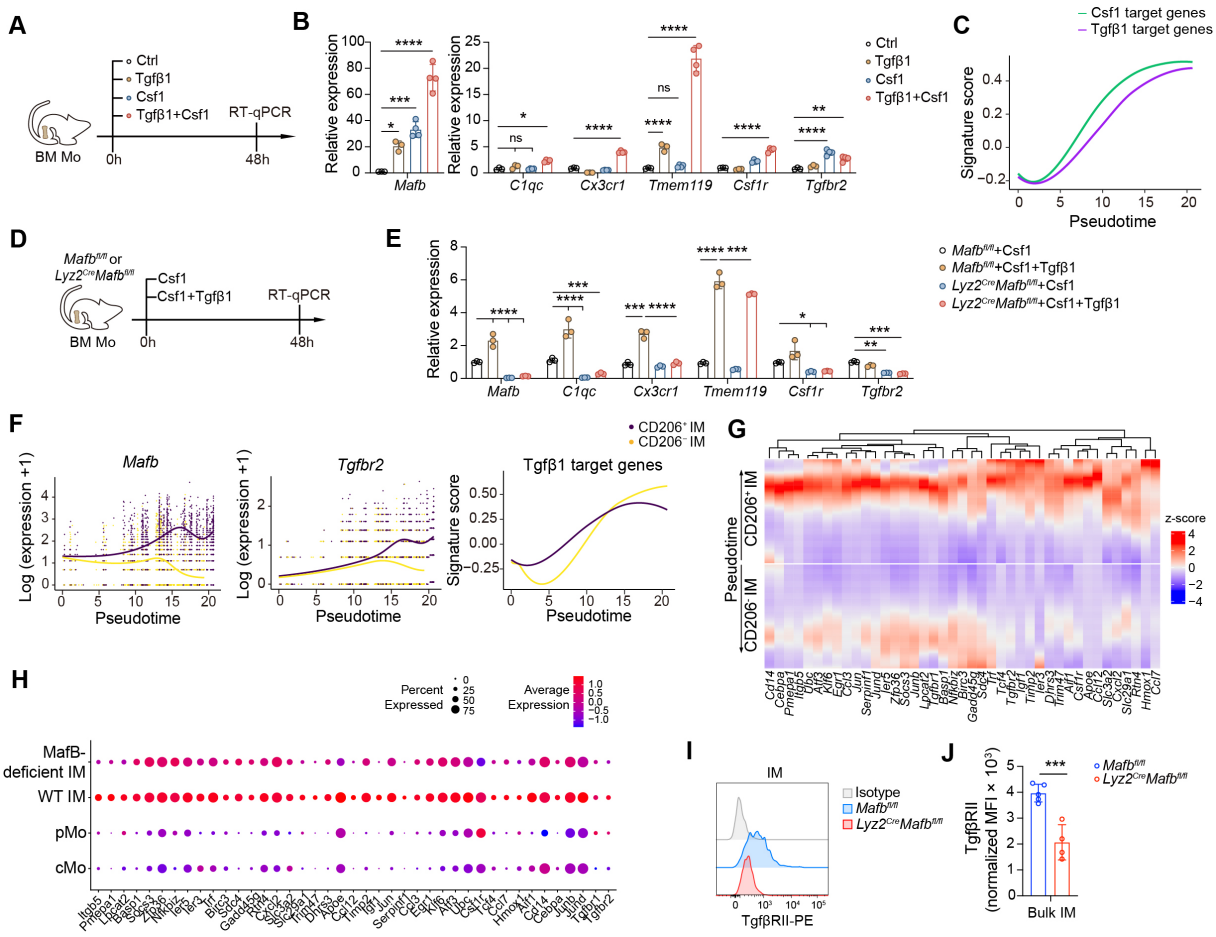
A
Ctrl
Tgfβ1
Csf1
Tgfβ1+Csf1
RT-qPCR
BM Mo
0h
48h
B
Relative expression
Mafb
C1qc
Cx3cr1
Tmem119
Csf1r
Tgfbr2
Ctrl
Tgfβ1
Csf1
Tgfβ1+Csf1
C
Csf1 target genes
Tgfβ1 target genes
Signature score
Pseudotime
D
Mafb fl/fl or Lyz2Cre Mafb fl/fl
Csf1
Csf1+Tgfβ1
RT-qPCR
BM Mo
0h
48h
E
Relative expression
Mafb
C1qc
Cx3cr1
Tmem119
Csf1r
Tgfbr2
Mafb fl/fl +Csf1
Mafb fl/fl +Csf1+Tgfβ1
Lyz2Cre Mafb fl/fl +Csf1
Lyz2Cre Mafb fl/fl +Csf1+Tgfβ1
F
CD206+ IM
CD206- IM
Mafb
Tgfbr2
Tgfβ1 target genes
Log (expression +1)
Signature score
Pseudotime
G
CD206+ IM
CD206- IM
Pseudotime
z-score
H
Percent Expressed
Average Expression
MafB-deficient IM
WT IM
pMo
cMo
I
IM
Isotype
Mafb fl/fl
Lyz2Cre Mafb fl/fl
TgfβRII-PE
J
TgfβRII (normalized MFI × 10³)
Bulk IM
Mafb fl/fl
Lyz2Cre Mafb fl/fl

Fig. 4. Reciprocal regulation of MafB- and Tgfβ receptor-dependent pathways in IMs. (**A**) Experimental outline for (B). BM Mo from WT C57BL/6 mice were stimulated with Tgfβ1, Csf1 or Csf1 + Tgfβ1 for 48 hours and were analyzed by RT-qPCR. Freshly isolated BM Mo were used as controls. (**B**) Relative mRNA expression of the indicated genes in BM Mo, as in (A). (**C**) Signature scores of Csf1 and Tgfβ1 target genes along pseudotime during monocyte-to-IM development, based on the scRNA-seq mapping of monocyte-to-IM trajectory [167]. (**D**) BM Mo from *Mafb*$^{fl/fl}$ or *Lyz2*^{Cre} *Mafb*$^{fl/fl}$ mice were stimulated with Csf1 or Csf1 + Tgfβ1 for 48 hours and were analyzed by RT-qPCR. (**E**) Relative mRNA expression of the indicated genes in BM Mo, as in (D). (**F**) Expression of *Mafb* (left)*, Tgfbr2* (middle), and signature scores of Tgfβ1 target genes (right) along pseudotime evaluated by TradeSeq in monocyte-to-IM trajectories (both CD206^{-} and CD206^{+} IM trajectories) [167]. (**G**) Heatmap showing expression of the indicated genes along pseudotime during monocyte-to-IM trajectories, as in (F). (**H**) Dot plot showing average expression and % of cells expressing the indicated genes in clusters of classical monocytes (cMo), patrolling monocytes (pMo), WT IMs and MafB-deficient IMs, based on previously published scRNA-seq data [167]. (**I**) Representative histograms and (**J**) bar graph showing normalized MFI of TgfβRII expression in lung from *Lyz2*^{Cre} *Mafb*$^{fl/fl}$ mice or *Mafb*$^{fl/fl}$ littermate controls. (B,E,J) Data shown mean +/- SEM and are representative of 3 independent experiments (*n* = 3 replicates from different mice in (B) and (E), *n* =4-5 mice in (J)). *P* values were calculated using (B) a two-way ANOVA with Dunnett's post hoc tests, (E) a two-way ANOVA with Tukey's post hoc tests or (J) a two-tailed unpaired Student's *t* test. *, *P*<0.05; **, *P*<0.01; ***, *P*<0.001; ****, *P*<0.0001. MFI, mean fluorescence intensity; ns, not significant.

2.5. vWF$^+$ blood vessel endothelial cells release Tgfβ1 to shape IM development and identity

Next, we sought to identify the precise source of Tgfβ1 necessary for IM development *in vivo*. First, we assessed intracellular expression of latent Tgfβ1 in lung structural cells at steady-state by flow cytometry (fig. S2F). No Tgfβ1-expressing cells were found in CD45$^-$EpCam$^+$CD31$^-$ epithelial cells nor in CD45$^-$EpCam$^-$CD31$^-$ stromal cells (Fig. 5, A and B). However, we found a substantial proportion of Tgfβ1$^+$ cells within CD45$^-$EpCam$^-$CD31$^+$ endothelial cells, which was restricted to the vWF$^+$ blood vessel compartment but not the CD90.2$^+$ lymphatic nor the vWF$^-$CD90.2$^-$ capillary compartment [356] (Fig. 5, A and B). We reasoned that such latent Tgfβ1 would be more released in the lung microenvironment when the IM niche is refilling. To evaluate this possibility, we depleted IMs by DT treatment in IM^{DTR} mice and followed the percentage of Tgfβ1$^+$ cells within vWF$^+$ endothelial cells during IM niche replenishment. Interestingly, we found a significant decrease in such percentage at days 3, 5 and 7 post-DT, while levels were back to baseline at day 14 post-DT (Fig. 5, C and D), consistent with the idea that vWF$^+$ endothelial cells release more latent Tgfβ1 when IM development from monocytes is accelerated. Accordingly, the levels of latent Tgfβ1 found in lungs of DT-treated IM^{DTR} mice at day 4 post-DT were significantly higher as compared to those found in lungs of PBS-treated IM^{DTR} mice (Fig. 5E). Next, we performed immunostainings of CD68$^+$ myeloid cells and Erg1$^+$Tgfβ1$^+$ endothelial cells on lung sections from IM^{DTR} mice that were treated or not with DT 4 days before. Of note, CD68$^+$ myeloid cells were found in the vicinity of Erg1$^+$Tgfβ1$^+$ endothelial cells (Fig. 5F) and we observed a significant increase in pairs of CD68$^+$ myeloid cells and Erg1$^+$Tgfβ1$^+$ endothelial cells that were distant from less than 10 µm in lungs from DT-treated IM^{DTR} mice as compared to PBS-treated controls (Fig. 5G). These data suggested that vWF$^+$ blood vessel endothelial cells could release Tgfβ1 and interacted more closely with tissue monocytes differentiating into IMs during niche refilling.

Lastly, we sought to formally address the contribution of endothelial Tgfβ1 to IM development and identity *ex vivo* and *in vivo*. To this end, we crossed tamoxifen-inducible *Cdh5^{CreERT2}* with *Tgfb1$^{fl/fl}$* mice to obtain *Cdh5^{CreERT2} Tgfb1$^{fl/fl}$* mice that would be conditionally

deficient in *Tgfb1* in endothelial cells upon tamoxifen treatment. After weaning, *Cdh5*^{CreERT2} *Tgfb1*$^{fl/fl}$ and *Tgfb1*$^{fl/fl}$ littermate controls were fed tamoxifen for 28 days, followed by a normal diet. At day 49 post-weaning, we confirmed a significant decrease in *Tgfb1* mRNA levels within FACS-sorted lung CD45^{-}EpCam^{-}CD31^{+} endothelial cells from tamoxifen-fed *Cdh5*^{CreERT2} *Tgfb1*$^{fl/fl}$ compared to controls (Fig. 5, H and I). Similarly, the percentage of Tgfβ1^{+} cells within vWF^{+} endothelial cells and the levels of latent Tgfβ1were significantly lower in lungs from tamoxifen-fed *Cdh5*^{CreERT2} *Tgfb1*$^{fl/fl}$ mice as compared to controls (Fig. 5, H and I). We co-cultured BM Mo with Csf1 and FACS-sorted Endo from tamoxifen-fed *Cdh5*^{CreERT2} *Tgfb1*$^{fl/fl}$ mice or control counterparts and found that Endo-triggered induction of the IM markers Cx3cr1, Tmem119, MafB and C1qa was significantly lower when Tgfβ1 was knocked down in Endo (Fig. 5J-L). In a separate cohort of mice, in order to create a context in which the IM niche is in need of refilling, we lethally irradiated mice at day 35 post-weaning to deplete hematopoietic cells and IMs and reconstituted them with donor CD45.1/CD45.2 BM cells (Fig. 5H). At day 14 post-reconstitution, the majority of blood cells and 50% of CD45^{+} lung cells were of donor origin, regardless of the host genotype (fig. S8), and *In vivo*, both the numbers and the percentage of donor IMs within CD45^{+} cells were significantly decreased in *Cdh5*^{CreERT2} *Tgfb1*$^{fl/fl}$ mice as compared to littermate controls (Fig. 5M), demonstrating that IM development was impaired when endothelial Tgfβ1 expression was decreased. In addition, expression levels of Cx3cr1 and Tmem119 identity markers were significantly decreased in IMs from *Cdh5*^{CreERT2} *Tgfb1*$^{fl/fl}$ mice as compared to those from control mice (Fig. 5, N and O), indicating that endothelial Tgfβ1 can shape IM identity. Altogether, these data provided evidence that vWF^{+} blood vessel endothelial cells represent an important source of Tgfβ1 to dictate IM development and identity.

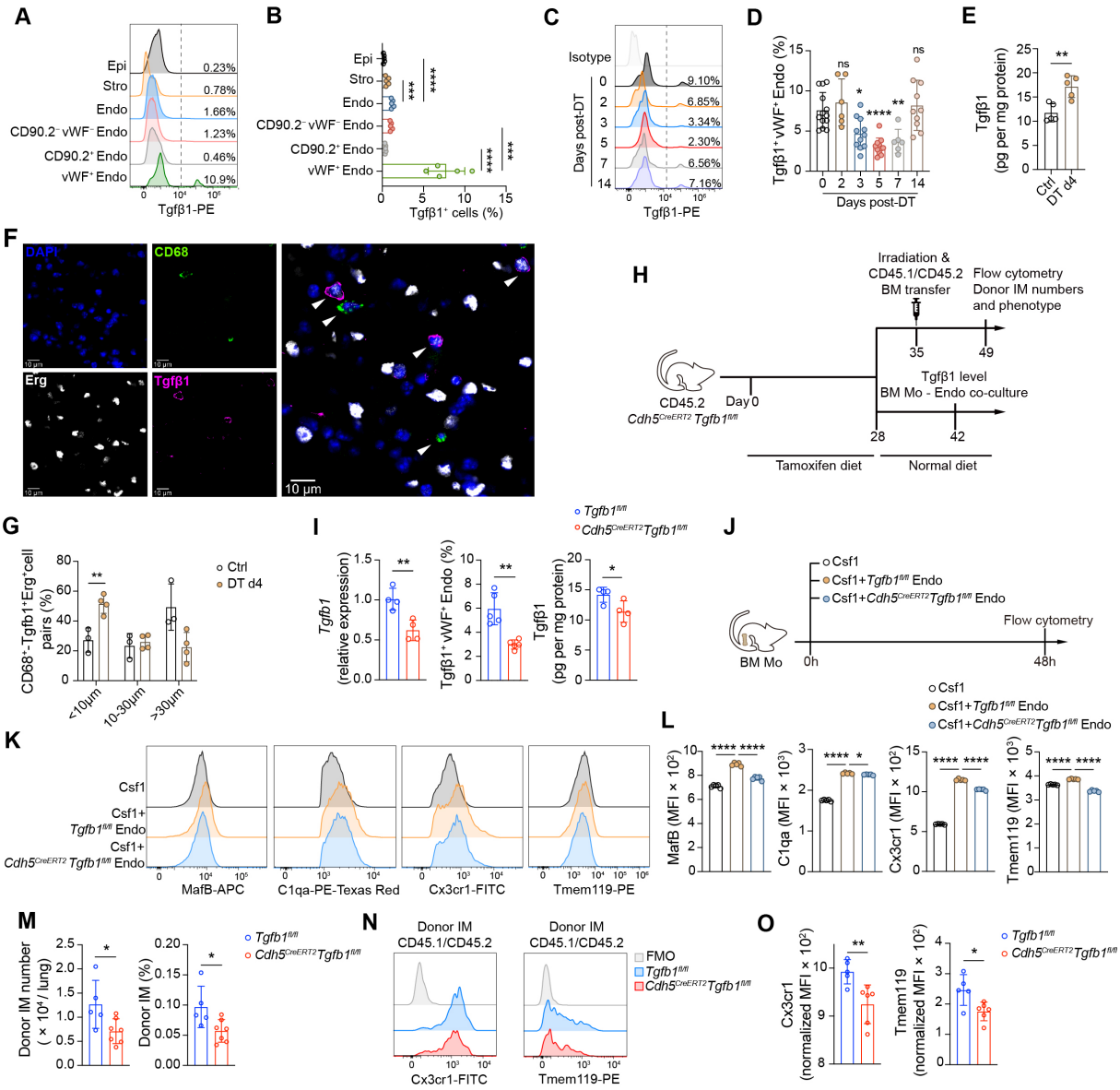
A
Epi
Stro
Endo
CD90.2⁻ vWF⁻ Endo
CD90.2⁺ Endo
vWF⁺ Endo
0.23%
0.78%
1.66%
1.23%
0.46%
10.9%
Tgfβ1-PE
B
Tgfβ1⁺ cells (%)
C
Isotype
Days post-DT
9.10%
6.85%
3.34%
2.30%
6.56%
7.16%
Tgfβ1-PE
D
Tgfβ1⁺ vWF⁺ Endo (%)
Days post-DT
E
Tgfβ1 (pg per mg protein)
Ctrl
DT d4
F
DAPI
CD68
Erg
Tgfβ1
10 μm
H
Irradiation & CD45.1/CD45.2 BM transfer
Flow cytometry Donor IM numbers and phenotype
CD45.2 Cdh5CreERT2 Tgfb1fl/fl
Day 0
35
49
Tgfβ1 level BM Mo - Endo co-culture
28
42
Tamoxifen diet
Normal diet
G
CD68⁺-Tgfb1⁺Erg⁺cell pairs (%)
Ctrl
DT d4
<10μm
10-30μm
>30μm
I
Tgfb1 (relative expression)
Tgfβ1⁺ vWF⁺ Endo (%)
Tgfβ1 (pg per mg protein)
Tgfb1fl/fl
Cdh5CreERT2Tgfb1fl/fl
J
Csf1
Csf1+Tgfb1fl/fl Endo
Csf1+Cdh5CreERT2Tgfb1fl/fl Endo
Flow cytometry
BM Mo
0h
48h
K
Csf1
Csf1+ Tgfb1fl/fl Endo
Csf1+ Cdh5CreERT2 Tgfb1fl/fl Endo
MafB-APC
C1qa-PE-Texas Red
Cx3cr1-FITC
Tmem119-PE
L
Csf1
Csf1+Tgfb1fl/fl Endo
Csf1+Cdh5CreERT2Tgfb1fl/fl Endo
MafB (MFI × 10²)
C1qa (MFI × 10³)
Cx3cr1 (MFI × 10²)
Tmem119 (MFI × 10³)
M
Donor IM number (× 10⁴ / lung)
Donor IM (%)
Tgfb1fl/fl
Cdh5CreERT2Tgfb1fl/fl
N
Donor IM CD45.1/CD45.2
Donor IM CD45.1/CD45.2
FMO
Tgfb1fl/fl
Cdh5CreERT2Tgfb1fl/fl
Cx3cr1-FITC
Tmem119-PE
O
Cx3cr1 (normalized MFI × 10²)
Tmem119 (normalized MFI × 10²)
Tgfb1fl/fl
Cdh5CreERT2Tgfb1fl/fl

Fig. 5. Lung vWF$^+$ endothelial-derived Tgfβ1 contributes to IM development and identity. (**A**) Representative histogram of latent Tgfβ1 expression in lung EpCam$^+$CD31$^-$ epithelial cells (Epi), CD45$^-$EpCam$^-$CD31$^-$ stromal cells (Stro) and CD45$^-$EpCam$^-$CD31$^+$ endothelial cells (Endo), assessed by flow cytometry in C57BL/6 WT mice. Endo were further divided into CD90.2$^-$vWF$^-$ capillary, CD90.2$^+$ lymphatic and vWF$^+$ blood vessel Endo. (**B**) Bar graph showing the percentage of Tgfβ1$^+$ cells in the indicated cell populations, as in (A). (**C**) Representative histogram of latent Tgfβ1 expression in lung vWF$^+$ blood vessel Endo, assessed by flow cytometry at days 0, 2, 3, 5, 7 and 14 post-DT in DT-treated IM^{DTR} mice. (**D**) Bar graph showing the percentage of Tgfβ1$^+$ cells within lung vWF$^+$ blood vessel Endo, as in (C), as depicted by individual values and violin plots (height: %; width: abundance of cells). (**E**) Levels of latent Tgfβ1, assessed by ELISA on lung extracts from PBS-treated (Ctrl) and DT-treated IM^{DTR} mice at day 4 post-treatment. (**F**) Representative confocal microscopy images of CD68$^+$ mononuclear phagocytes and Tgfβ1$^+$Erg$^+$ Endo in lungs of DT-treated IM^{DTR} mice at day 4 post-DT. (**G**) Percentages of CD68$^+$ mononuclear phagocytes - Tgfβ1$^+$Erg$^+$ Endo according to the distance separating the 2 cell types in lungs from PBS-treated (control) or DT-treated IM^{DTR} mice at day 4 post-DT (DT d4). (**H**) Experimental outline for (I-O). CD45.2 *Cdh5^{CreERT2} Tgfb1$^{fl/fl}$* mice or *Tgfb1$^{fl/fl}$* controls were fed tamoxifen from day 0 to day 28, were lethally irradiated and reconstituted with CD45.1 WT BM cells at day 35 and analyzed at day 49. (**I**) *Tgfb1* expression assessed by RT-qPCR (left) and percentage of Tgfβ1$^+$ cells (middle) in FACS-sorted Endo, and levels of latent Tgfβ1 assessed by ELISA on lung extracts from chimeric *Cdh5^{CreERT2} Tgfb1$^{fl/fl}$* mice or *Tgfb1$^{fl/fl}$* controls, as in (H). (**J**) Experimental outline for (K, L). Csf1-grown BM Mo from WT mice were co-cultured with or without lung primary endothelial cells (Endo) from tamoxifen-fed chimeric *Cdh5^{CreERT2} Tgfb1$^{fl/fl}$* mice or *Tgfb1$^{fl/fl}$* controls and were analyzed by flow cytometry 48 hours later. (**K**) Representative histograms and (**L**) bar graph showing MFI of MafB, C1qa, Cx3cr1 and Tmem119 expression in BM Mo, as in (J). (**M**) Bar graph showing the numbers (left) and percentages (right) of CD45.1 donor IMs from chimeric *Cdh5^{CreERT2} Tgfb1$^{fl/fl}$* mice or *Tgfb1$^{fl/fl}$* controls, assessed by flow cytometry. (**N**) Representative histograms and (**O**) bar graph showing MFI of Cx3cr1 and Tmem119 expression in IMs from chimeric *Cdh5^{CreERT2} Tgfb1$^{fl/fl}$* mice or *Tgfb1$^{fl/fl}$* controls, assessed by flow cytometry. (B,D,E,G,I,L,M,O) Data show (B,E,G,I,L,M,O) mean +/- SEM and are representative of 3 independent experiments (n=3-7 mice), (D) mean +/- SEM are pooled from 4 independent experiments (*n* = 6-13 mice). *P* values were calculated using (B,D,L) a one-way ANOVA with Dunnett's post-hoc tests, (E,I,M,O) a two-tailed unpaired Student's *t* test or (G) a two-way ANOVA with Sidak's post-hoc tests. *, *P*<0.05; **, *P*<0.01; ****, *P*<0.0001. MFI, mean fluorescence intensity; ns, not significant.

2.6. Myeloid *Tgfbr2* deficiency is associated with a proliferative and dysfunctional profile in IMs

Next, we wondered about the functional consequences of IM-specific *Tgfbr2* deficiency for IM functional profile. To this end, we generated a mouse strain in which AMs would retain TgfβRII expression while IMs would be deficient. Briefly, CD45.1/CD45.2 IM^{DTR} mice were lethally irradiated with thorax protection and were fully reconstituted with BM cells either from CD45.2 $Tgfbr2^{fl/fl}$ mice or from CD45.2 $Lyz2^{Cre}$ $Tgfbr2^{fl/fl}$ mice (Fig. 6A). Four weeks later, chimeric IM^{DTR} mice were treated with DT to specifically empty the IM niche and trigger IM niche refilling from either control or *Tgfbr2*-deficient monocytes. We confirmed that AMs and IMs were of host and donor origin in those chimeric mice, respectively (Fig. 6B). Bulk RNA-seq was performed on reconstituted $CD45.1^{-}CD45.2^{+}Ly6G^{-}SiglecF^{-}CD11b^{+}SSC^{lo}CD64^{+}$ cells at day 10 post-DT (fig. S9A) and knock-down of *Tgfbr2* exon 2 was confirmed (fig. S9B). Principal Component Analysis (PCA) and unsupervised hierarchical clustering showed that control IMs clustered separately from *Tgfbr2*-deficient IMs (Fig. 6, C and D). Differential expression (DE) analyses showed 79 upregulated genes in WT IMs and 152 upregulated genes in *Tgfbr2*-deficient IMs (adjusted P value < 0.05 and $\log_2$ fold change > or < 1, respectively) (Fig. 6E). First, we confirmed the downregulation of the IM identity genes *Cx3cr1* and *Tmem119* in the absence of *Tgfbr2* (Fig. 6F). Second, Gene Set Enrichment Analyses (GSEA) were performed to infer biological responses that were enriched (positive normalized enrichment score [NES]) or defective (negative NES) in the absence of Tgfβ receptor (Fig. 6G). Genes known to be upregulated or downregulated upon Tgfβ1 stimulation were significantly enriched in *Tgfbr2*-sufficient or deficient IMs, respectively, validating the model (Fig. 6G). Of note, *Tgfbr2*-deficient IMs were enriched in responses related to cell cycling and proliferation, further supporting that, in the absence of *Tgfbr2*, IMs are blocked in a premature proliferative stage that precedes IM differentiation [167] (Fig. 6G). Moreover, responses related to cell-cell adhesion were enriched in *Tgfbr2*-deficient IMs (Fig. 6G). Conversely, a range of responses associated with homeostatic and immunoregulatory functions of macrophages were enriched in *Tgfbr2*-sufficient IMs, such as the activation of mTORC1 signaling [357], antigen processing

and presentation [41], and a signature of tolerogenic macrophages (Fig. 6G). ScRNA-seq analysis of lung CD45.1^{-}CD45.2^{+}Ly6G^{-}SiglecF^{-}CD11b^{+}SSC^{lo}CD64^{+} cells isolated at day 90 post-DT from myeloid-intrinsic *Tgfbr2*-deficient chimeric IM^{DTR} mice indicated an accumulation of monocytes (*Ly6c2, Ccr2, Irf8*) expressing *Fcgr4*, reminiscent of tissue monocytes [147], at the expense of CD206^{-} IMs (*Cd72, Cd74, H2-Eb1*) and CD206^{+} IMs (*Mrc1, Folr2*), when compared to controls (Fig. 6H-J). DE and gene Ontology (GO) analyses highlighted an enrichment, in monocytes from *Tgfbr2*-deficient chimeric IM^{DTR} mice, in the response to type II interferons (*Irf1, Cxcl9, Stat1*), in cell-cell adhesion (*Vasp, Sdc4, Ccl5*), in cell proliferation (*Mif, Cd38*) and in apoptotic signaling as compared to those from *Tgfbr2*-sufficient controls (Fig. 6, K and L), supporting that tissue monocytes substantially contribute the transcriptional changes observed by bulk RNA-seq. Our data thus support that TGFβ receptor signaling is essential for the differentiation and homeostatic functions of IMs, preventing their accumulation in an immature, proliferative state.

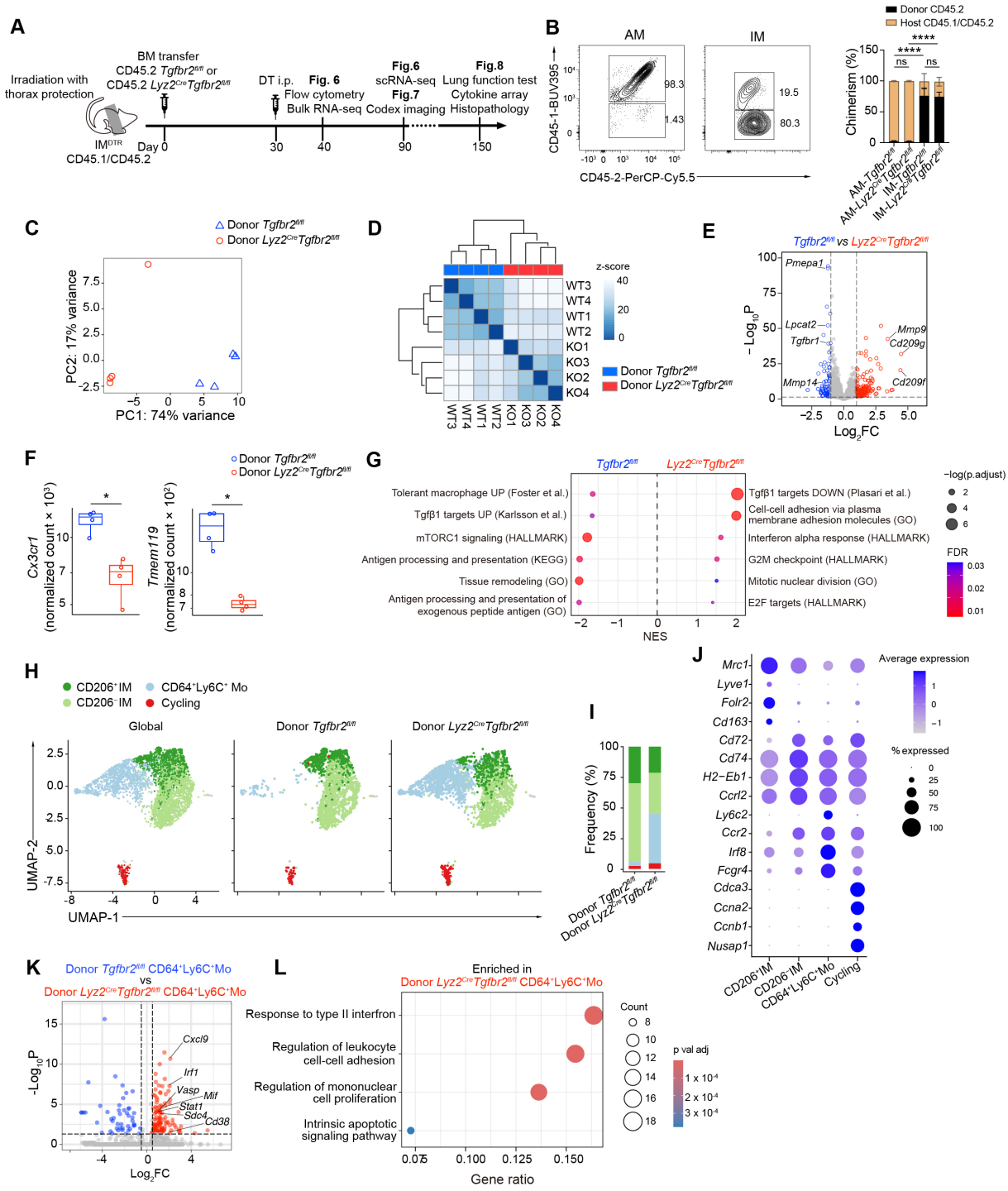
A
Irradiation with thorax protection
BM transfer
CD45.2 Tgfbr2fl/fl or
CD45.2 Lyz2CreTgfbr2fl/fl
IMDTR
CD45.1/CD45.2
Day 0
DT i.p.
30
Fig. 6
Flow cytometry
Bulk RNA-seq
40
Fig.6
scRNA-seq
Fig.7
Codex imaging
90
Fig.8
Lung function test
Cytokine array
Histopathology
150
B
AM
IM
CD45-1-BUV395
CD45-2-PerCP-Cy5.5
98.3
1.43
19.5
80.3
Donor CD45.2
Host CD45.1/CD45.2
Chimerism (%)
ns
****
AM-Tgfbr2fl/fl
AM-Lyz2CreTgfbr2fl/fl
IM-Tgfbr2fl/fl
IM-Lyz2CreTgfbr2fl/fl
C
Donor Tgfbr2fl/fl
Donor Lyz2CreTgfbr2fl/fl
PC2: 17% variance
PC1: 74% variance
D
z-score
WT3
WT4
WT1
WT2
KO1
KO3
KO2
KO4
Donor Tgfbr2fl/fl
Donor Lyz2CreTgfbr2fl/fl
E
Tgfbr2fl/fl vs Lyz2CreTgfbr2fl/fl
Pmepa1
Lpcat2
Tgfbr1
Mmp14
Mmp9
Cd209g
Cd209f
−Log10P
Log2FC
F
Donor Tgfbr2fl/fl
Donor Lyz2CreTgfbr2fl/fl
Cx3cr1
(normalized count × 10³)
Tmem119
(normalized count × 10²)
G
Tgfbr2fl/fl
Lyz2CreTgfbr2fl/fl
Tolerant macrophage UP (Foster et al.)
Tgfβ1 targets UP (Karlsson et al.)
mTORC1 signaling (HALLMARK)
Antigen processing and presentation (KEGG)
Tissue remodeling (GO)
Antigen processing and presentation of exogenous peptide antigen (GO)
Tgfβ1 targets DOWN (Plasari et al.)
Cell-cell adhesion via plasma membrane adhesion molecules (GO)
Interferon alpha response (HALLMARK)
G2M checkpoint (HALLMARK)
Mitotic nuclear division (GO)
E2F targets (HALLMARK)
NES
−log(p.adjust)
FDR
H
CD206+ IM
CD206- IM
CD64+Ly6C+ Mo
Cycling
Global
Donor Tgfbr2fl/fl
Donor Lyz2CreTgfbr2fl/fl
UMAP-2
UMAP-1
I
Frequency (%)
Donor Tgfbr2fl/fl
Donor Lyz2CreTgfbr2fl/fl
J
Mrc1
Lyve1
Folr2
Cd163
Cd72
Cd74
H2-Eb1
Ccrl2
Ly6c2
Ccr2
Irf8
Fcgr4
Cdca3
Ccna2
Ccnb1
Nusap1
CD206+IM
CD206-IM
CD64+Ly6C+Mo
Cycling
Average expression
% expressed
K
Donor Tgfbr2fl/fl CD64+Ly6C+Mo
vs
Donor Lyz2CreTgfbr2fl/fl CD64+Ly6C+Mo
Cxcl9
Irf1
Vasp
Mif
Stat1
Sdc4
Cd38
-Log10P
Log2FC
L
Enriched in
Donor Lyz2CreTgfbr2fl/fl CD64+Ly6C+Mo
Response to type II interfron
Regulation of leukocyte cell-cell adhesion
Regulation of mononuclear cell proliferation
Intrinsic apoptotic signaling pathway
Count
p val adj
Gene ratio

Fig. 6. Disruption of IM-intrinsic TgfβRII signaling is associated with an IM immature and dysfunctional profile. (**A**) Experimental outline. Thorax-protected CD45.1/CD45.2 IM^{DTR} mice were lethally irradiated and reconstituted with BM cells from either CD45.2 *Tgfbr2*$^{fl/fl}$ mice (group "Donor *Tgfbr2*$^{fl/fl}$") or *Lyz2*^{Cre} *Tgfbr2*$^{fl/fl}$ mice (group "Donor *Lyz2*^{Cre} *Tgfbr2*$^{fl/fl}$). Chimeric mice injected 4 weeks later with DT i.p. and analyzed at days 10 (chimerism of AMs and IMs and bulk RNA-seq analysis of IMs), 60 (scRNA-seq analysis of IMs and CODEX analysis) and 120 after DT (lung function, histopathology, proteome profiling). (**B**) Representative flow cytometry CD45.1 and CD45.2 plots (left) and chimerism (right) of AMs and IMs, assessed at day 10 post-DT, as in (A). (**C**) PCA plot showing the transcriptional identity of IMs, evaluated by bulk RNA-seq at day 10 post-DT, as in (A). *n*= 4 replicates per group, each replicate representing a pool of IMs sorted from 3 mice in 2 independent sorting experiments. (**D**) Unsupervised hierarchical clustering of IMs analyzed by bulk RNA-seq, as in (A). (**E**) Volcano plot depicting the differentially expressed (DE) genes between *Tgfbr2*-sufficient and *Tgfbr2*-deficient IMs, as in (A). (**F**) Bar graphs showing expression of the indicated DE genes between *Tgfbr2*-sufficient and *Tgfbr2*-deficient IMs, as in (A). (**G**) GSEA analyses of *Tgfbr2*-sufficient and *Tgfbr2*-deficient IMs, as in (A). The Normalized Enrichment Score (NES) and, False Discovery Rate (FDR) are shown for each process. (**H**) Global and genotype-specific UMAP plots depicting the transcriptional identity of lung $CD45.1^{-}CD45.2^{+}Ly6G^{-}SiglecF^{-}CD11b^{+}SSC^{lo}CD64^{+}$ cells isolated from donor *Tgfbr2*$^{fl/fl}$ and donor *Lyz2*^{Cre} *Tgfbr2*$^{fl/fl}$ chimeric IM^{DTR} mice at day 60 post-DT, as in (A) (n=5 pooled mice per group). (**I**) Histogram showing the frequency of each cluster for cells from donor *Tgfbr2*$^{fl/fl}$ and donor *Lyz2*^{Cre} *Tgfbr2*$^{fl/fl}$ chimeric IM^{DTR} mice. (**J**) Dot plots showing average expression of the indicated genes and the percentages of cells expressing the genes within each cluster. (**K**) Volcano plot depicting DE genes between the monocyte cluster from donor *Tgfbr2*$^{fl/fl}$ and donor *Lyz2*^{Cre} *Tgfbr2*$^{fl/fl}$ chimeric IM^{DTR} mice. (**L**) Dot plot showing Gene Ontology (GO) enrichment results comparing $CD64^{+}Ly6C^{+}$ monocyte coming from donor *Tgfbr2*$^{fl/fl}$ and donor *Lyz2*^{Cre} *Tgfbr2*$^{fl/fl}$ chimeric IM^{DTR} mice. (B,F) Data show mean +/- SEM and (B) are representative of 2 independent experiments (*n* = 5 mice); (F) represent 4 biological replicates of FACS-sorted cells. *P* values were calculated using (B) a two-way ANOVA with Tukey's post-hoc tests or (E,F,K) a Wilcoxon rank sum test. (E,K) Significantly expressed genes were defined by $\log_2FC >$ 0.5 and adjusted *P* value < 0.05. *, *P*<0.05; ****, *P*<0.0001. MFI, mean fluorescence intensity; ns, not significant.

2.7. Myeloid Tgfβ receptor signaling drives monocyte and IM spatial organization in the lung microenvironment

Next, we used codetection by indexing (CODEX)-enabled multiplex imaging to investigate how monocyte and IM spatial niche occupancies were affected by the loss of TGFβ receptor signaling [358, 359]. Using a 28-parameter staining panel, we identified donor monocytes and IMs (fig. S10) as well as other lung immune and structural cell types using common markers (Table S2). Within the donor $CD45.1^{-}CD45.2^{+}$ population, we observed a higher proportion of monocytes in lungs from myeloid-intrinsic *Tgfbr2*-deficient chimeric IM^{DTR} mice compared to *Tgfbr2*-sufficient controls (Fig. 7A), confirming our flow cytometry and scRNA-seq data. Interestingly, monocytes predominantly accumulated in the adventitial cuffs surrounding larger blood vessels (Fig. 7, B and C), which are composed of vWF^{+} endothelial cells [356]. We next examined how cell interactions between monocytes, IMs and their microenvironment were influenced by the loss of IM-intrinsic TGFβ receptor signaling. The interaction scores of monocytes with endothelial cells and fibroblasts, and to a lesser with epithelial cells, were reduced in lungs from myeloid-intrinsic *Tgfbr2*-deficient chimeric IM^{DTR} mice as compared to the *Tgfbr2*-sufficient controls (Fig. 7D). A similar reduction in interaction score with endothelial cells was observed for *Tgfbr2*-deficient IMs (Fig. 7D), consistent with a role for TGFβ receptor signaling in the positioning of monocytes and IMs in dedicated niches. We also found that the interaction score of monocytes with IMs was higher in the absence myeloid TgfβRII (Fig. 7D), suggesting that IMs were retained in close proximity to monocytes and failed to migrate properly towards their specific niches. Interestingly, in control lungs, monocytes were significantly closer to $Tgfβ^{+}$ endothelial cells than to $Tgfβ^{-}$ endothelial cells, supporting a preferential interaction (Fig. 7, E and F). However, the distance between monocytes and Tgfβ-producing endothelial cells was markedly increased in the absence of myeloid TgfβRII (Fig. 7, E and F). These data suggested that TGFβ receptor signaling is crucial for guiding monocytes and IMs to their dedicated niches and facilitating interactions with lung structural cells.

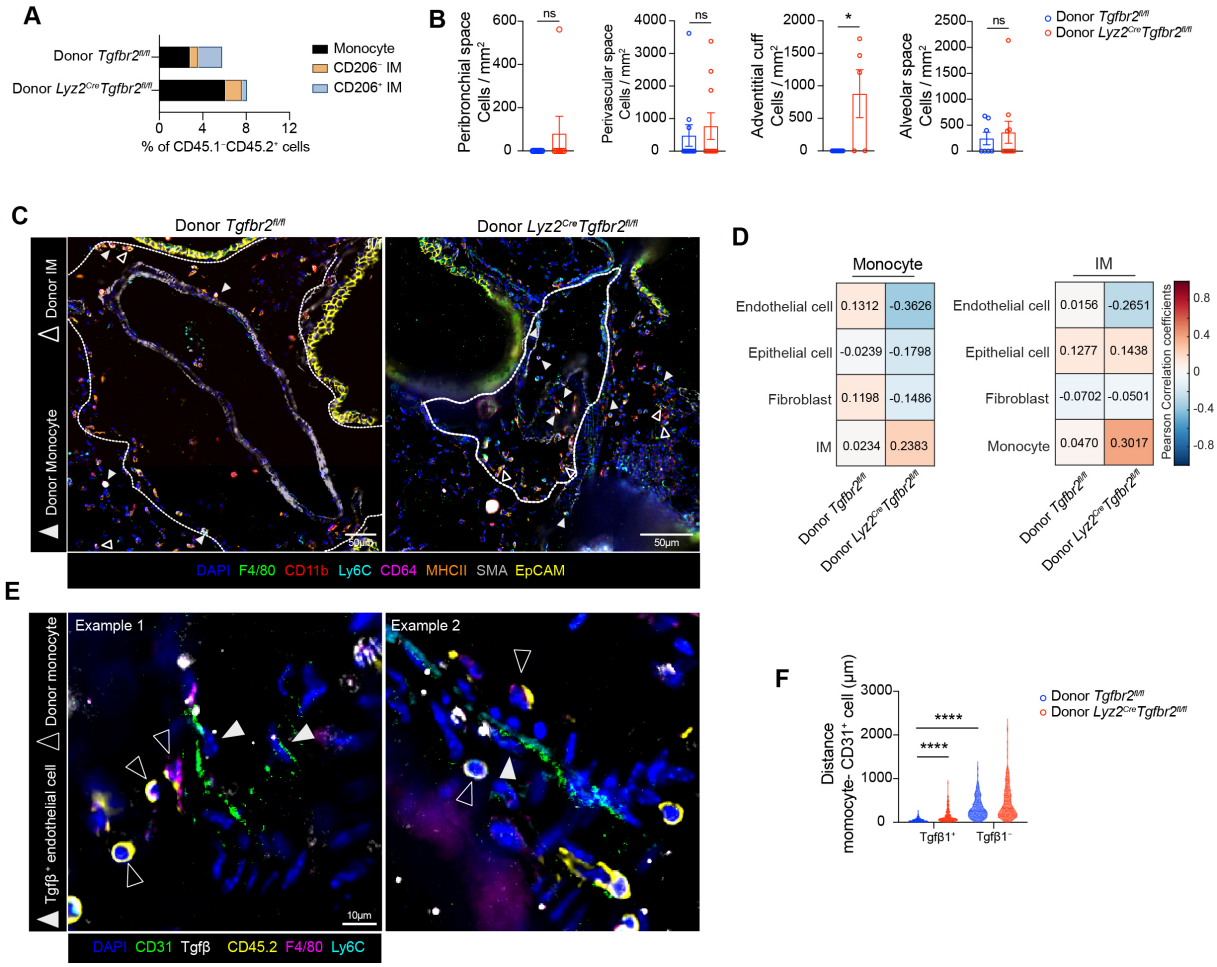

Fig. 7. Tgfβ receptor signaling in monocytes and IMs regulates niche occupancy and interactions with lung structural cells. (**A**) Bar graphs showing the proportion of monocytes and IM subsets within donor CD45.1$^-$CD45.2$^+$ cells, as in (Fig. 6A). (**B**) Bar graphs showing the cell numbers of CD45.1$^-$CD45.2$^+$ monocytes in the 4 anatomical area, peribronchial space, perivascular space, adventitial cuff and alveolar space, as in (Fig. 6A). (**C**) Representative imaging showing adventitial cuffs in donor *Tgfbr2*$^{fl/fl}$ and donor *Lyz2*^{Cre} *Tgfbr2*$^{fl/fl}$ chimeric IM^{DTR} mice lung with presence of CD45.1$^-$CD45.2$^+$ monocytes and IMs, as in (Fig. 6A). (**D**) The interaction score of CD45.1$^-$CD45.2$^+$ monocyte or IM with indicated cell in donor *Tgfbr2*$^{fl/fl}$ and donor *Lyz2*^{Cre} *Tgfbr2*$^{fl/fl}$ chimeric IM^{DTR} mice lung, as in (Fig. 6A). (**E**) The proximity between CD45.1$^-$CD45.2$^+$ monocyte and Tgfβ$^+$CD31$^+$cells in donor *Lyz2*^{Cre} *Tgfbr2*$^{fl/fl}$ chimeric IM^{DTR} mice lung, as in (Fig. 6A). (**F**) Violin plots showing the shortest distance between CD45.1$^-$CD45.2$^+$ monocyte with Tgfβ$^+$CD31$^+$cells or Tgfβ$^-$CD31$^+$cells in donor *Tgfbr2*$^{fl/fl}$ and donor *Lyz2*^{Cre} *Tgfbr2*$^{fl/fl}$ chimeric IM^{DTR} mice lung, as in (Fig. 6A). (B,F) Data show mean +/- SEM. *P* values were calculated using a Wilcoxon rank sum test. *, *P*<0.05; ****, *P*<0.0001. ns, not significant. Scale bars: (C) 50 μm; (E) 10 μm.

2.8. Myeloid-intrinsic *Tgfbr2*-deficient mice prematurely develop lung aging-associated abnormalities

To assess the consequences of IM-intrinsic *Tgfbr2* deficiency on lung homeostasis, we performed lung function measurement, histopathological analyses and protein quantification in chimeric IM^{DTR} mice whose IMs were sufficient or deficient in *Tgfbr2,* at 4 months post-DT (Fig. 6A). Of note, we showed in fig. S2, D and E, that blood myeloid cells, lung neutrophils and lung DCs expressed significantly lower levels of TgfβRII as compared to IMs, indicating that they are unlikely to represent major confounding factors in the model. We noticed a substantial death of chimeric IM^{DTR} mice in the absence of myeloid *Tgfbr2* from 2 months post-DT (fig. S11A), in line with previous reports suggesting that myeloid *Tgfbr2* deficiency can trigger stroke [360]. Importantly, we only analyzed mice that were healthy without weight loss or other signs of morbidity. First, we found that lungs from myeloid-intrinsic *Tgfbr2*-deficient mice displayed significantly higher inspiratory capacity, higher compliance and lower elastance as compared to control lungs (Fig. 8A; fig. S11B), a phenotype that was similarly observed in 18-month-old WT mice as compared to 2-month-old WT mice (Fig. 8A; fig. S11B). These data are consistent with the hypothesis that, in the absence of *Tgfbr2* on IMs, lungs develop age-related functional abnormalities. Second, a higher degree of alveolar dilatation was observed in lungs of donor $Lyz2^{Cre}$ $Tgfbr2^{fl/fl}$ mice as compared to donor $Tgfbr2^{fl/fl}$ mice (Fig. 8, B and C), a phenotype similar to senile hyperinflation [361]. Third, perivascular accumulation of leukocytes, among which $CD68^+$ monocytic cells close to vWF^+ endothelial cells, was observed in lungs of donor $Lyz2^{Cre}$ $Tgfbr2^{fl/fl}$ mice (Fig. 8, B, D and E). Of note, at the protein level, lungs of donor $Lyz2^{Cre}$ $Tgfbr2^{fl/fl}$ mice contained significantly lower levels of many cytokines, chemokines and growth factors as compared to those of donor $Tgfbr2^{fl/fl}$ mice (Fig. 8E), supporting an impairment of lung immune surveillance when IMs cannot engage Tgfb receptor pathways. Moreover, lungs of donor $Lyz2^{Cre}$ $Tgfbr2^{fl/fl}$ chimeric mice displayed lower levels of IL-10, an immunosuppressive cytokine produced by IMs [139, 144, 147, 148] (Fig. 8F), lower levels of elastin (Fig. 8G) and higher levels of soluble collagen (Fig. 8H) as compared to those of donor $Tgfbr2^{fl/fl}$ mice. Altogether, these data supported that disruption of IM-specific TgfβRII

signaling has a profound impact on the lung immunoregulatory environment and triggers age-related changes.

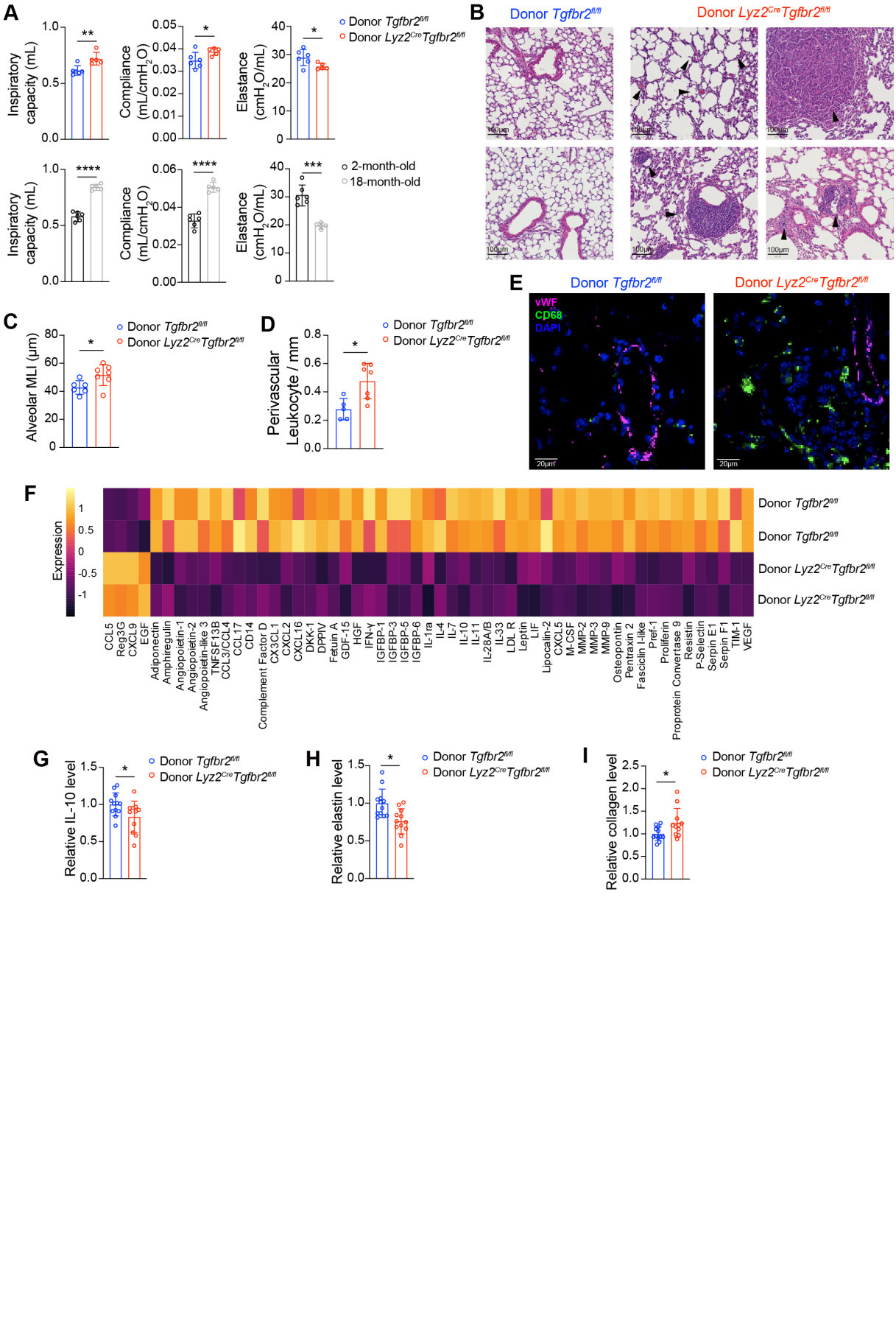
A
Inspiratory capacity (mL)
Compliance (mL/cmH2O)
Elastance (cmH2O/mL)
Donor Tgfbr2fl/fl
Donor Lyz2CreTgfbr2fl/fl
2-month-old
18-month-old
B
Donor Tgfbr2fl/fl
Donor Lyz2CreTgfbr2fl/fl
C
Alveolar MLI (μm)
D
Perivascular Leukocyte / mm
E
vWF
CD68
DAPI
F
Expression
CCL5
Reg3G
CXCL9
EGF
Adiponectin
Amphiregulin
Angiopoietin-1
Angiopoietin-2
Angiopoietin-like 3
TNFSF13B
CCL3/CCL4
CCL17
CD14
Complement Factor D
CX3CL1
CXCL2
CXCL16
DKK-1
DPPIV
Fetuin A
GDF-15
HGF
IFN-γ
IGFBP-1
IGFBP-3
IGFBP-5
IGFBP-6
IL-1ra
IL-4
IL-7
IL-10
IL-11
IL-28A/B
IL-33
LDL R
Leptin
LIF
Lipocalin-2
CXCL5
M-CSF
MMP-2
MMP-3
MMP-9
Osteopontin
Pentraxin 2
Fasciclin I-like
Pref-1
Proliferin
Proprotein Convertase 9
Resistin
P-Selectin
Serpin E1
Serpin F1
TIM-1
VEGF
G
Relative IL-10 level
H
Relative elastin level
I
Relative collagen level

Fig. 8. IM-intrinsic *Tgfbr2* deficiency triggers age-related lung functional, structural and immune abnormalities. (**A**) Invasive measurements of inspiratory capacity, lung compliance and lung elastance in donor *Tgfbr2*$^{fl/fl}$ or donor *Lyz2*^{Cre} *Tgfbr2*$^{fl/fl}$ chimeric IM^{DTR} mice at day 120 after DT, as in Fig. 6A, and in 2-month-old or 18-month-old C57BL/6 WT mice. (**B**) Representative Hematoxylin & Eosin staining of lung sections of chimeric IM^{DTR}, as in (A). (**C**) Alveolar dilatation assessed through measurements of alveolar MLI in lungs of chimeric IM^{DTR}, as in (B). (**D**) Quantification of perivascular leukocyte infiltration in lungs of chimeric IM^{DTR}, as in (B). (**E**) Representative confocal microscopy pictures of lung sections of chimeric IM^{DTR}, as in (B). Pictures are representative of one of 6 mice, each giving similar results. (**F**) Heatmap depicting the relative abundance of the indicated proteins in lung extracts from chimeric IM^{DTR} mice at day 120 post-DT, as in (A). (**G-I**) Levels of (G) IL-10, (H) elastin and (I) soluble collagen in lung extracts from chimeric IM^{DTR} mice, as in (A). (A,C,D,G,H,I) Data show mean +/- SEM, (A,C,D) are representative of 2 independent experiments (*n* = 5-7 mice) or (G,H,I) are pooled from 2 independent experiments (*n* = 11-12 mice). (F) Data represent biological replicates of FACS-sorted cells. (A,C,D,G,H,I) *P* values were calculated using a two-tailed unpaired Student's *t* test. *, *P*<0.05; ***, *P*<0.001; **, *P*<0.01; ****, *P*<0.0001. MLI, mean linear intercept; MFI, mean fluorescence intensity.

2.9. Supplementary figures

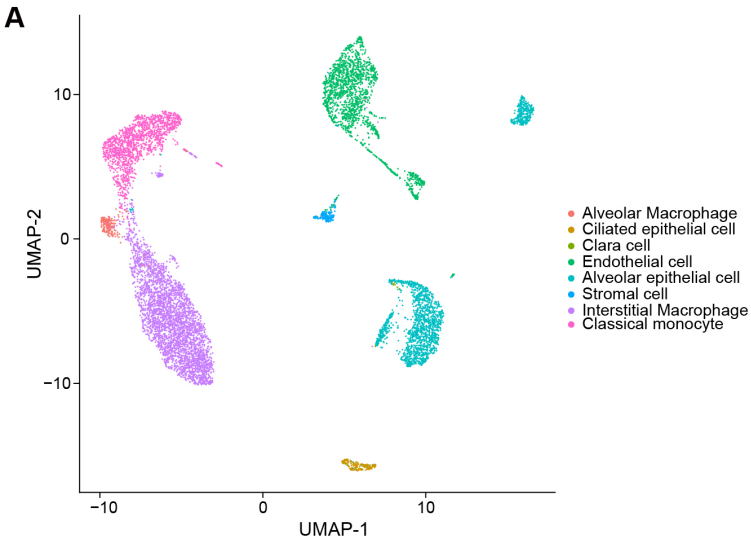

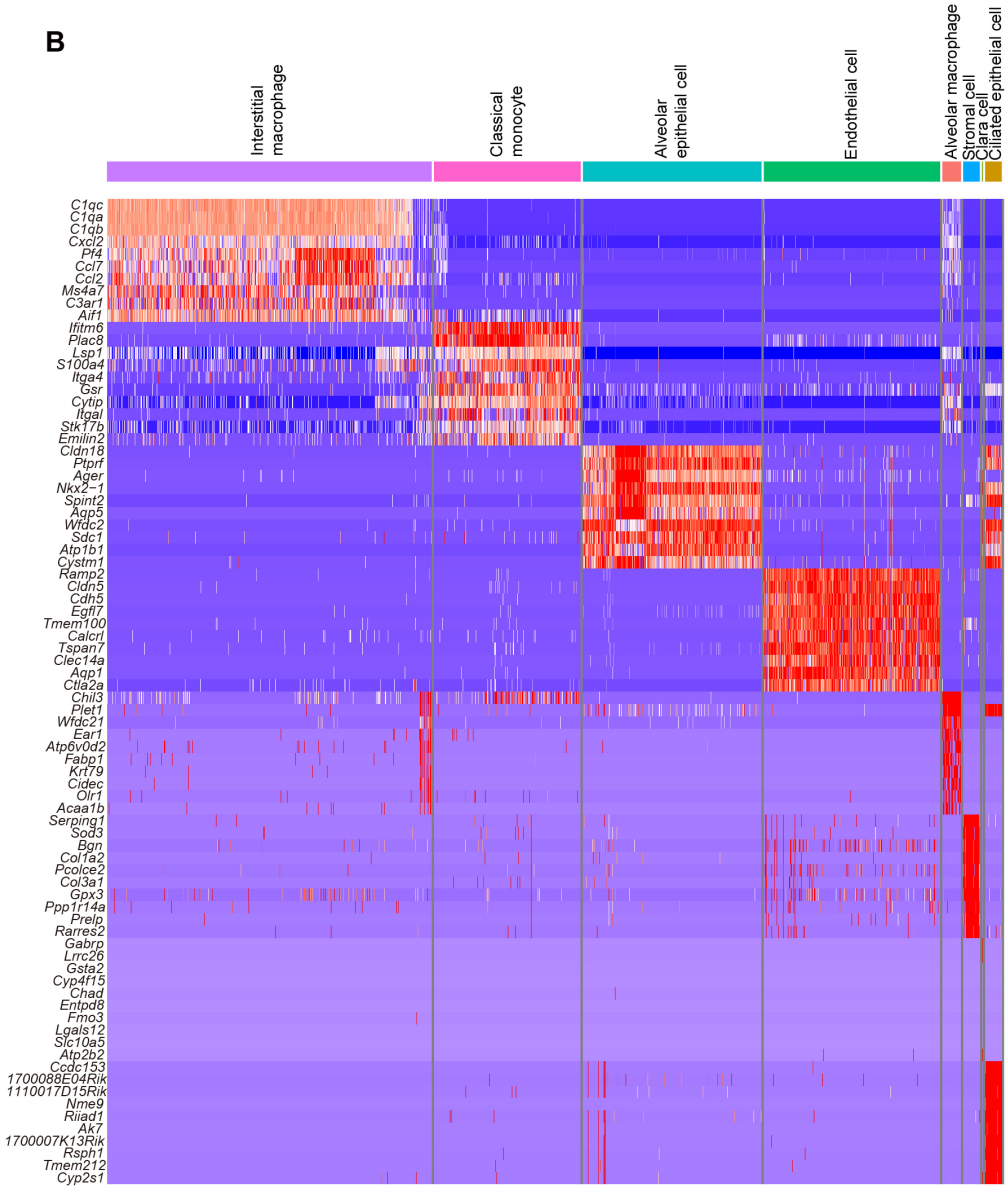

Fig. S1. Transcriptional identity of lung structural and myeloid cells analyzed by NicheNet analyses. (**A**) UMAP plot depicting the transcriptional identity of lung structural cells and myeloid cells from steady-state C57BL/6 WT mice [175], as analyzed by scRNA-seq and used for NicheNet analyses shown in Fig. 1, A and B. (**B**) Heatmap depicting the top 10 upregulated genes in each cluster, as in (A).

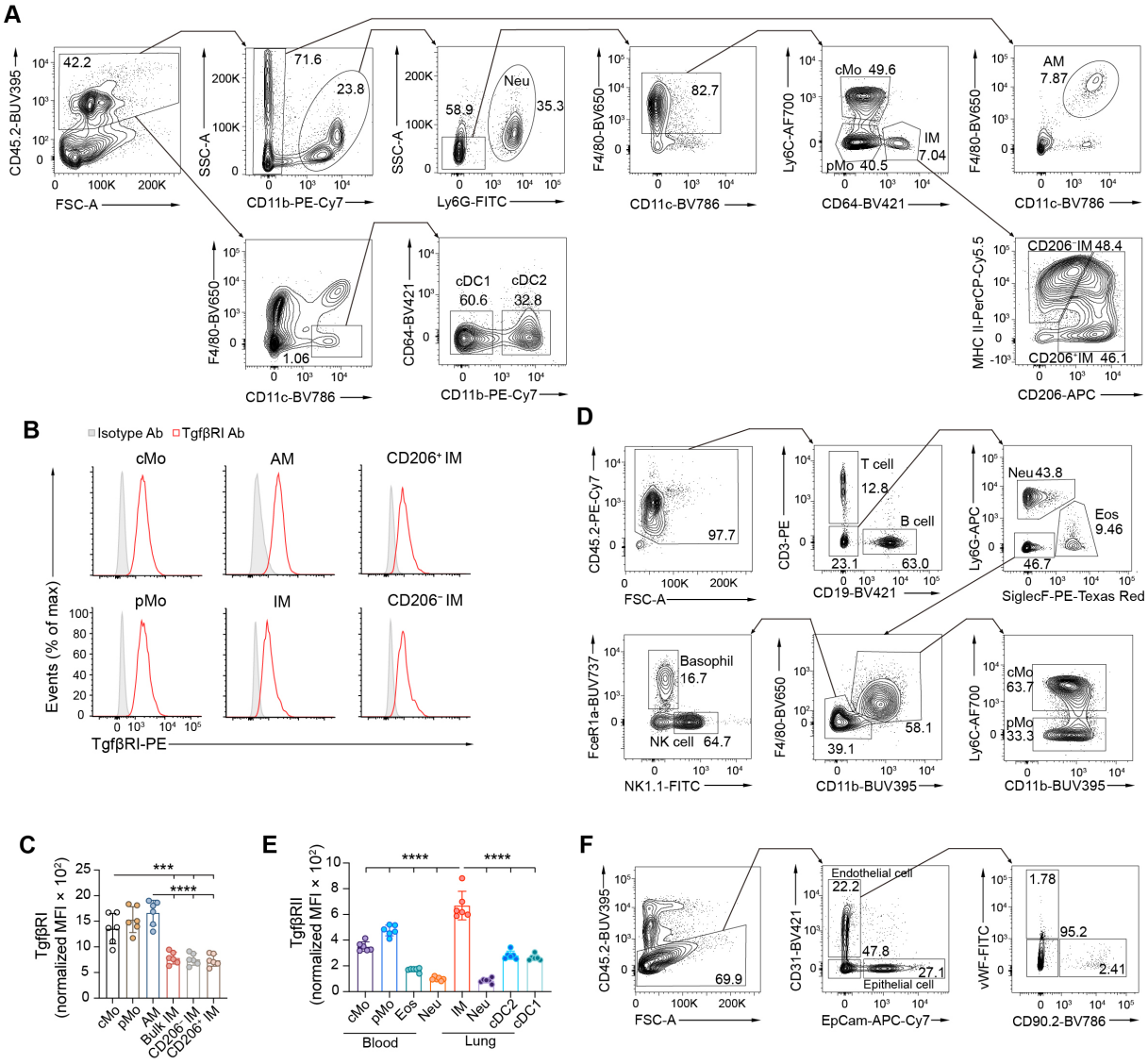

Fig. S2. Flow cytometry gating strategies and expression of Tgfβ receptors by blood and lung myeloid cells. (**A**) Representative flow cytometry gating strategy to delineate lung myeloid cells in lungs of naïve C57BL/6 WT mice. (**B**) Representative histograms and (**C**) bar graph showing normalized MFI of TgfβRI expression in lung cMo, pMo, AMs and IMs, as in (A). (**D**) Representative flow cytometry gating strategy to delineate blood leukocyte populations in naïve C57BL/6 WT mice. (**E**) Bar graph showing normalized MFI of TgfβRII expression in the indicated cell populations from naïve C57BL/6 WT mice. (**F**) Representative flow cytometry gating strategy showing live CD45$^-$EpCam$^+$CD31$^-$ epithelial cells, CD45$^-$EpCam$^-$CD31$^-$ stromal cells and CD45$^-$EpCam$^-$CD31$^+$ endothelial cells, further divided into vWF$^+$CD90.2$^-$ blood vessel, vWF$^-$CD90.2$^+$ lymphatic and vWF$^-$CD90.2$^-$ capillary endothelial cells. (C,E) Data show mean +/- SEM and are representative of 2 independent experiments (n = 5 mice). P values were calculated using (C) a one-way ANOVA with Tukey's post hoc tests or (E) a one-way ANOVA with Dunnett's post hoc tests. ***, P<0.001; ****, P<0.0001. cDC1, type 1 conventional dendritic cell; cDC2, type 2 conventional dendritic cell; Eos, eosinophil; MFI, mean fluorescence intensity; Neu, neutrophil.

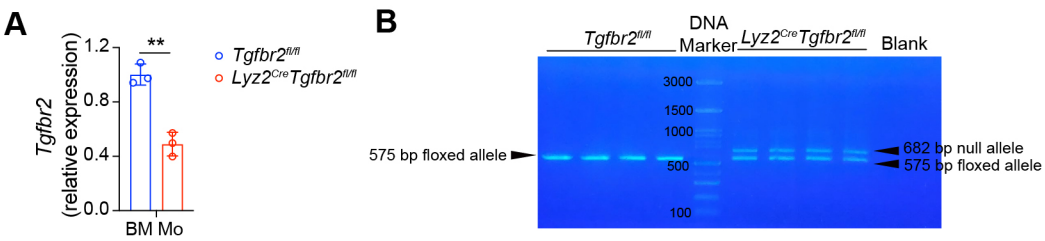

Fig. S3. Efficiency of *Tgfbr2* deletion in BM Mo from *Lyz2*^{Cre} *Tgfbr2*$^{fl/fl}$ mice. (**A**) mRNA expression of *Tgfbr2* in BM Mo from *Lyz2*^{Cre} *Tgfbr2*$^{fl/fl}$ mice and *Tgfbr2*$^{fl/fl}$ littermate controls. (**B**) PCR blot of genomic DNA extracted from BM Mo from *Lyz2*^{Cre} *Tgfbr2*$^{fl/fl}$ mice and *Tgfbr2*$^{fl/fl}$ littermate controls. (A) Data show mean +/- SEM and are representative of 3 independent experiments (n = 3 mice). P values were calculated using an unpaired two-tailed Student's t test. **, P<0.01.

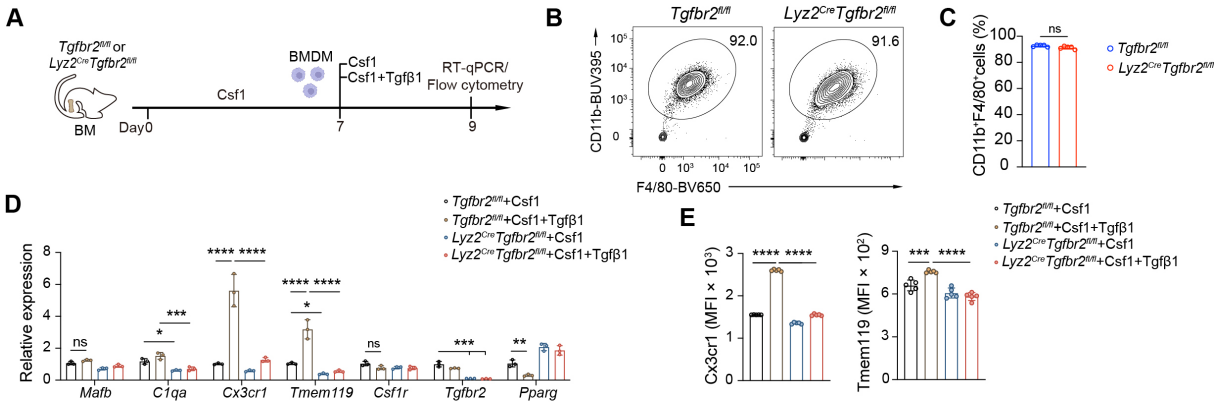

Fig. S4. Stimulation of Csf1-grown BM-derived Macs (BMDMs) with Tgfβ1 triggers a core IM identity. (**A**) Experimental outline for (B-D). BM cells from *Tgfbr2*$^{fl/fl}$ or *Lyz2*^{Cre} *Tgfbr2*$^{fl/fl}$ mice were derived into BMDMs with Csf1 for 7 days, were stimulated with Csf1 or Csf1 + Tgfβ1 for 48 hours and were analyzed by RT-qPCR and flow cytometry. (**B**) Representative CD11b and F4/80 flow cytometry histograms and (**C**) quantification of the % of CD11b^{+}F4/80^{+} Macs in BMDMs, assessed at day 7, as in (A). (**D**) Relative mRNA expression of the indicated genes in BMDMs, as in (A). (**E**) Bar graph showing MFI of Cx3cr1 and Tmem119 expression in BMDMs, as in (A). (C,D,E) Data shown mean +/- SEM and are representative of 3 independent experiments [n = 5 replicates from 2-3 mice in (C) and (E); n = 3 replicates from 2-3 mice in (D)]. *P* values were calculated using (C) an unpaired two-tailed Student's *t* test or (D) a two-way ANOVA with Tukey's post hoc tests or (E) a one-way ANOVA with Dunnett's post hoc tests. *, *P*<0.05; **, *P*<0.01; ***, *P*<0.001; ****, *P*<0.0001. MFI, mean fluorescence intensity; ns, not significant.

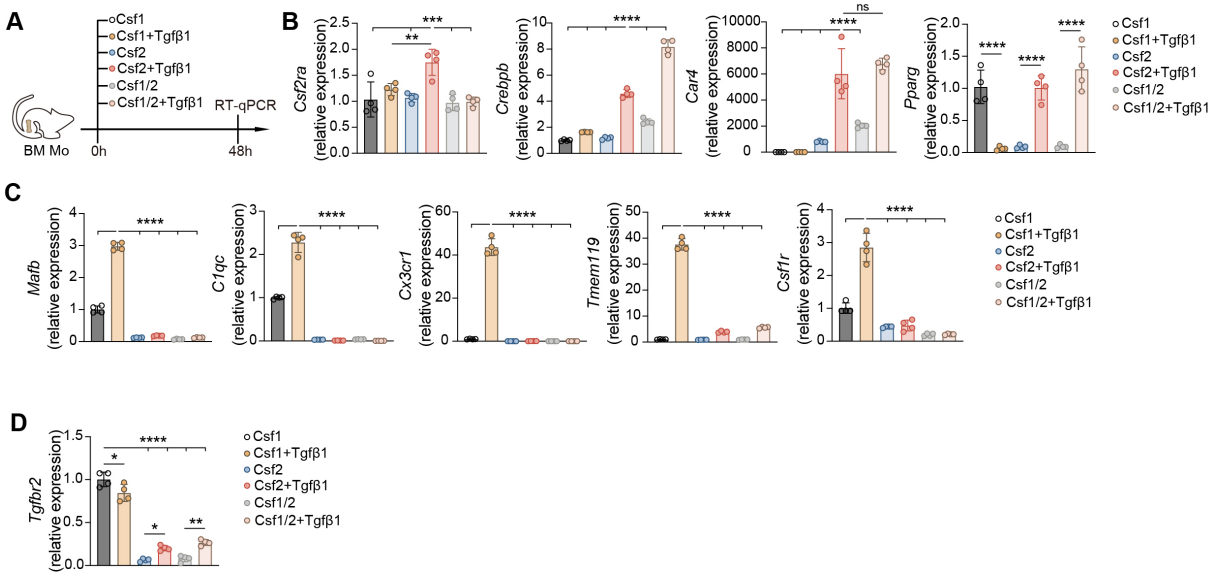

Fig. S5. Csf2 and Tgfβ1 drive AM-associated gene expression while suppressing IM-specific signature in BM Mo. (**A**) Experimental outline for (B-D). BM Mo from C57BL/6 WT mice were stimulated with Csf1, Csf1 + Tgfβ1, Csf2, Csf2 + Tgfβ1, Csf1/Csf2 or Csf1/Csf2 + Tgfβ1 for 48 hours and were analyzed by RT-qPCR. (**B**) Relative mRNA expression of the indicated AM-associated genes in BM Mo, as in (A). (**C**) Relative mRNA expression of the indicated IM-associated genes in BM Mo, as in (A). (**D**) Relative mRNA expression of *Tgfbr2* in BM Mo, as in (A). (B-D) Data show mean +/- SEM and independent replicates are representative from 2 independent *ex vivo* experiments (*n* = 4 replicates from 2-3 mice). *P* values were calculated using (B, C) a one-way ANOVA with Dunnett's post hoc tests or (D) a one-way ANOVA with Tukey's post hoc tests. *, *P*<0.05; **, *P*<0.01; ***, *P*<0.001; ****, *P*<0.0001. ns, not significant.

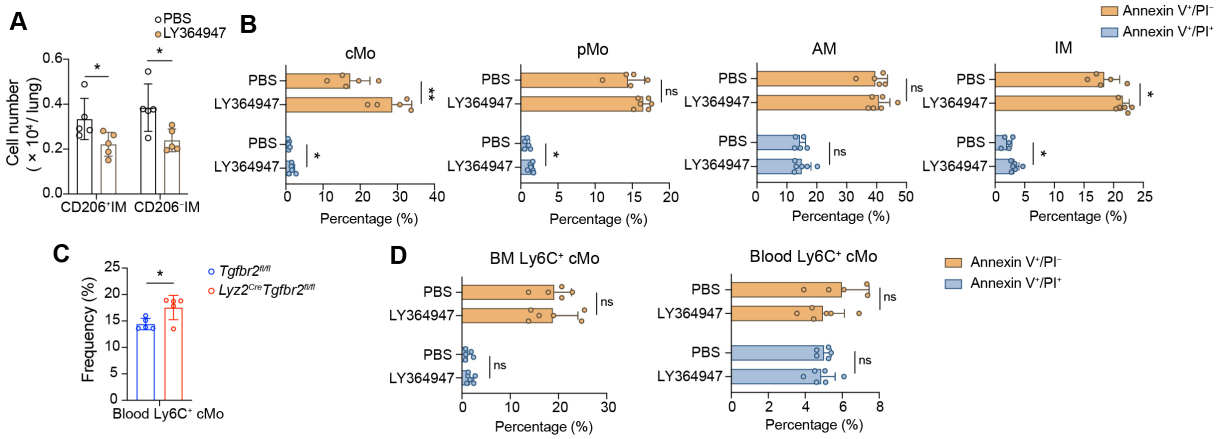

Fig. S6. Numbers of IM subsets and viability of Ly6C$^+$ cMo, Ly6C$^-$ pMo, AMs and IMs in LY363947-treated IM-depleted IM^{DTR} mice at day 7 post-DT. (**A**) Absolute numbers of CD206$^+$ IMs and CD206$^-$ IMs in LY363947-treated and vehicle-treated IM-depleted IM^{DTR} mice at day 7 post-DT. (**B**) Bar graphs showing the percentages of annexin V$^+$/PI$^-$ (early apoptotic) and annexin V$^+$/PI$^+$ (late apoptotic) cells within lung cMo, pMo, AMs and IMs in LY363947-treated and vehicle-treated IM-depleted IM^{DTR} mice at day 7 post-DT. (**C**) Bar graph showing percentages of blood CD45$^+$CD11b$^+$Ly6C$^+$ cMo, as in (B). (**D**) Bar graphs showing the frequency of annexin V$^+$/PI$^-$ (early apoptotic) and annexin V$^+$/PI$^+$ (late apoptotic) within BM and blood cMo, as in (B). (A,B,C,D) Data show mean +/- SEM and are representative 2 independent experiments (n = 5-6 mice). P values were calculated using (A,B,C,D) an unpaired two-tailed Student's t test. *, P<0.05; **, P<0.01 ns, not significant.

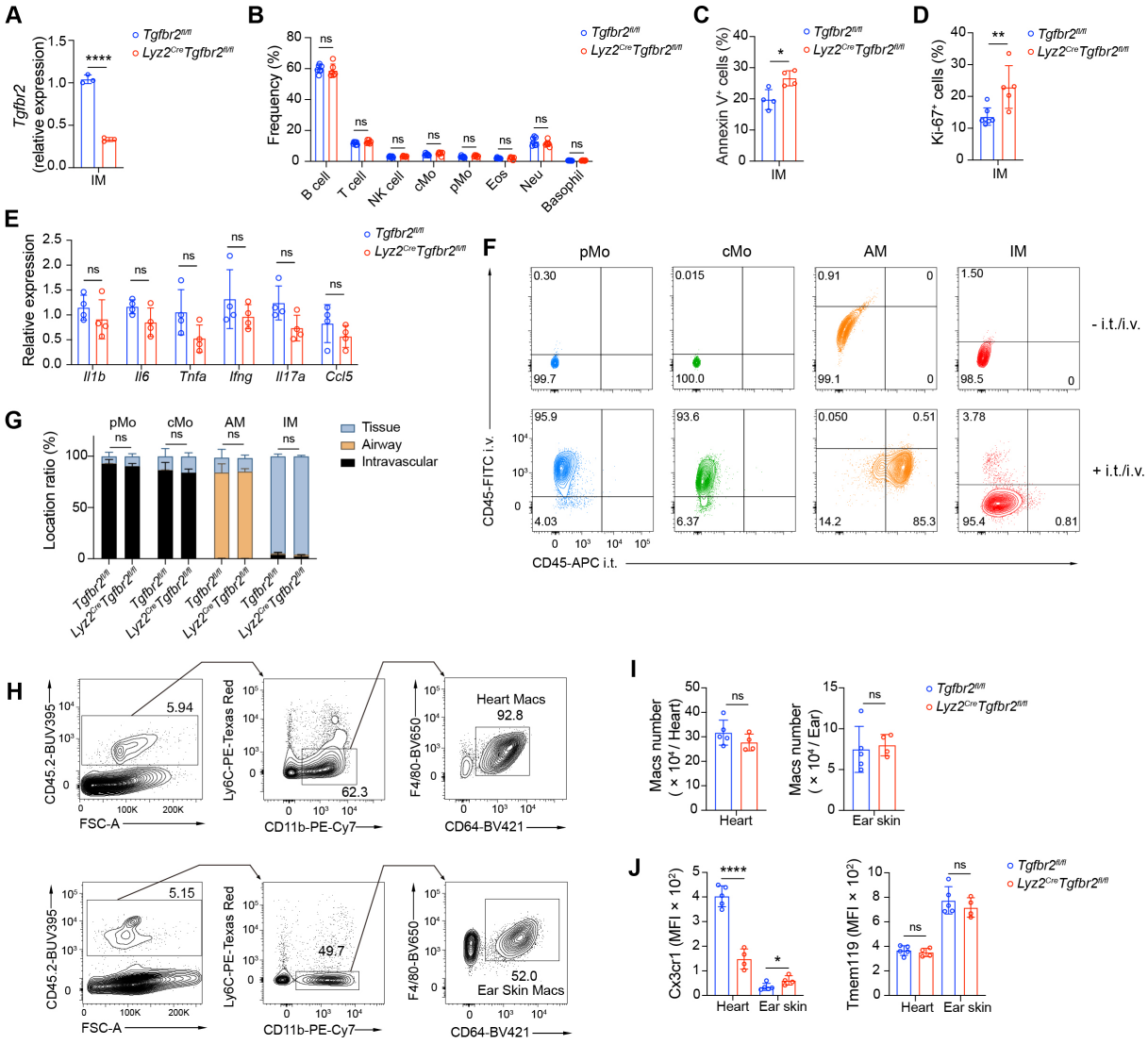
A
B
C
D
E
F
G
H
I
J
Tgfbr2 (relative expression)
Frequency (%)
Annexin V+ cells (%)
Ki-67+ cells (%)
Relative expression
Location ratio (%)
Tissue
Airway
Intravascular
pMo
cMo
AM
IM
- i.t./i.v.
+ i.t./i.v.
CD45-FITC i.v.
CD45-APC i.t.
CD45.2-BUV395
Ly6C-PE-Texas Red
CD11b-PE-Cy7
F4/80-BV650
CD64-BV421
FSC-A
Heart Macs
92.8
Ear Skin Macs
52.0
Macs number (× 10⁴/ Heart)
Macs number (× 10⁴/ Ear)
Cx3cr1 (MFI × 10²)
Tmem119 (MFI × 10²)
Heart
Ear skin
B cell
T cell
NK cell
cMo
pMo
Eos
Neu
Basophil
Il1b
Il6
Tnfa
Ifng
Il17a
Ccl5
Tgfbr2fl/fl
Lyz2CreTgfbr2fl/fl

Fig. S7. Analysis of 2-month-old myeloid-restricted *Tgfbr2*-deficient mice. (**A**) mRNA expression of *Tgfbr2* in lung IMs from *Lyz2*^{Cre} *Tgfbr2*$^{fl/fl}$ mice and *Tgfbr2*$^{fl/fl}$ littermate controls, assessed by RT-qPCR. (**B**) Bar graph showing percentages of the indicated blood leukocyte populations in *Lyz2*^{Cre} *Tgfbr2*$^{fl/fl}$ mice and *Tgfbr2*$^{fl/fl}$ littermate controls, assessed by flow cytometry and using the gating strategy shown in fig. S2D. (**C**) Percentage of Annexin V^{+} cells and (**D**) percentage of Ki67^{+} cells in IMs from *Lyz2*^{Cre} *Tgfbr2*$^{fl/fl}$ mice and *Tgfbr2*$^{fl/fl}$ littermate controls. (**E**) mRNA expression of the indicated genes in lungs from *Lyz2*^{Cre} *Tgfbr2*$^{fl/fl}$ mice and *Tgfbr2*$^{fl/fl}$ littermate controls, assessed by RT-qPCR. (**F**) Representative CD45-i.v. and CD45-i.t. plots of lung cMo, pMo, AMs and IMs from *Lyz2*^{Cre} *Tgfbr2*$^{fl/fl}$ mice and *Tgfbr2*$^{fl/fl}$ littermate controls injected with anti-CD45-FITC and anti-CD45-APC Ab i.v. and i.t. before sacrifice, respectively. (**G**) Percentages of tissue (CD45-i.v.$^{-}$/CD45-i.t.$^{-}$), airway (CD45-i.v.$^{-}$/CD45-i.t.$^{+}$) and intravascular (CD45-i.v.$^{+}$/CD45-i.t.$^{-}$) cMo, pMo, AMs and IMs, as in (F). (**H**) Representative flow cytometry gating strategy to delineate heart and ear skin macrophages (Macs) of *Lyz2*^{Cre} *Tgfbr2*$^{fl/fl}$ mice and *Tgfbr2*$^{fl/fl}$ littermate controls. (**I**) Absolute numbers, (**J**) Cx3cr1 and Tmem119 expression levels of heart and ear skin Macs, as in (H). (A,B,C,D,E,G,I,J) Data show mean +/- SEM (A,B,C,E,G,I,J) are representative of 2 independent experiments (n = 4-5 mice) and (D) are pooled from 2 independent experiments (n = 5-7 mice). P values were calculated using (A,B,C,D,E,I,J) an unpaired two-tailed Student's t test or (G) a two-way ANOVA with Sidak's post-hoc tests. *, P<0.05; **, P<0.01; ****, P<0.0001. ns, not significant.

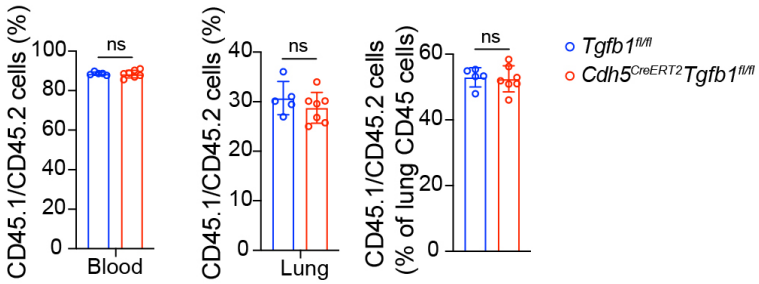

Fig. S8. Donor CD45.1/CD45.2 chimerism in the blood and lung of chimeric *Cdh5*^{CreERT2} *Tgfb1*$^{fl/fl}$ mice. *Cdh5*^{CreERT2} *Tgfb1*$^{fl/fl}$ and *Tgfb1*$^{fl/fl}$ littermate controls were fed tamoxifen for 28 days, followed by a normal diet. At day 35, mice were lethally irradiated and reconstituted with donor CD45.1/CD45.2 BM cells and the chimerism was evaluated in the blood and in the lung at day 49. Data shown mean +/- SEM and are representative of 2 independent experiments (*n* = 5-7 mice). *P* values were calculated using an unpaired two-tailed Student's *t* test. ns, not significant.

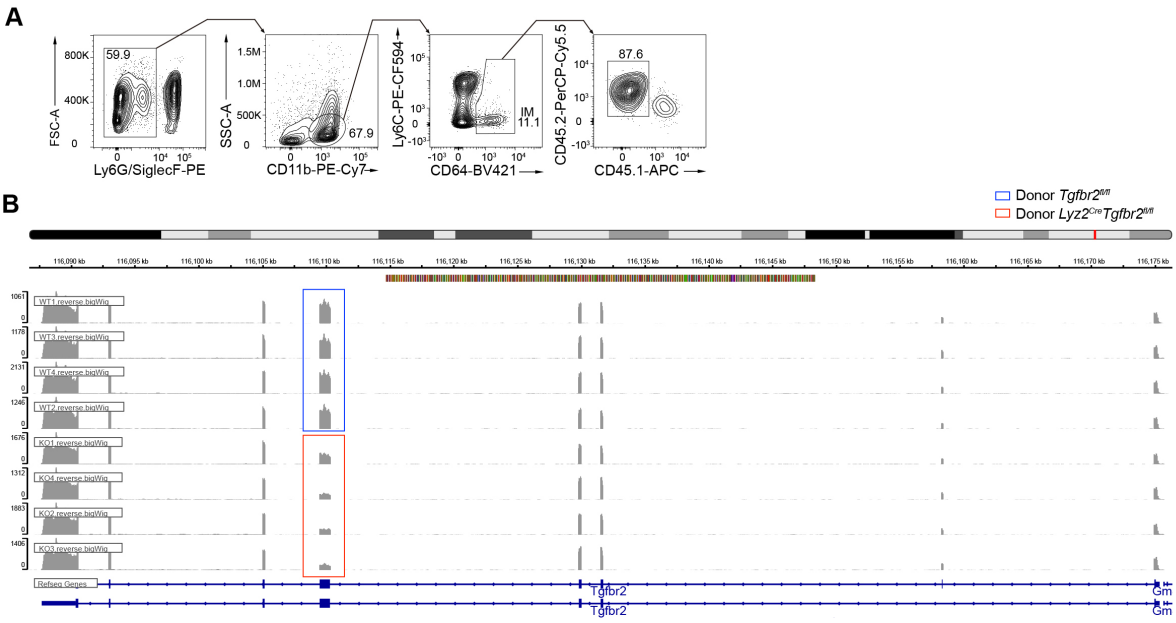

Fig. S9. *Tgfbr2* depletion in donor IMs from donor *Tgfbr2*$^{fl/fl}$ or donor *Lyz2*^{Cre} *Tgfbr2*$^{fl/fl}$ chimeric IM^{DTR} mice. (**A**) Flow cytometry sorting strategy to isolate donor IMs for bulk and scRNA-seq analyses. (**B**) *Tgfbr2* gene sequencing results in IMs from donor *Tgfbr2*$^{fl/fl}$ or donor *Lyz2*^{Cre} *Tgfbr2*$^{fl/fl}$ chimeric IM^{DTR} mice.

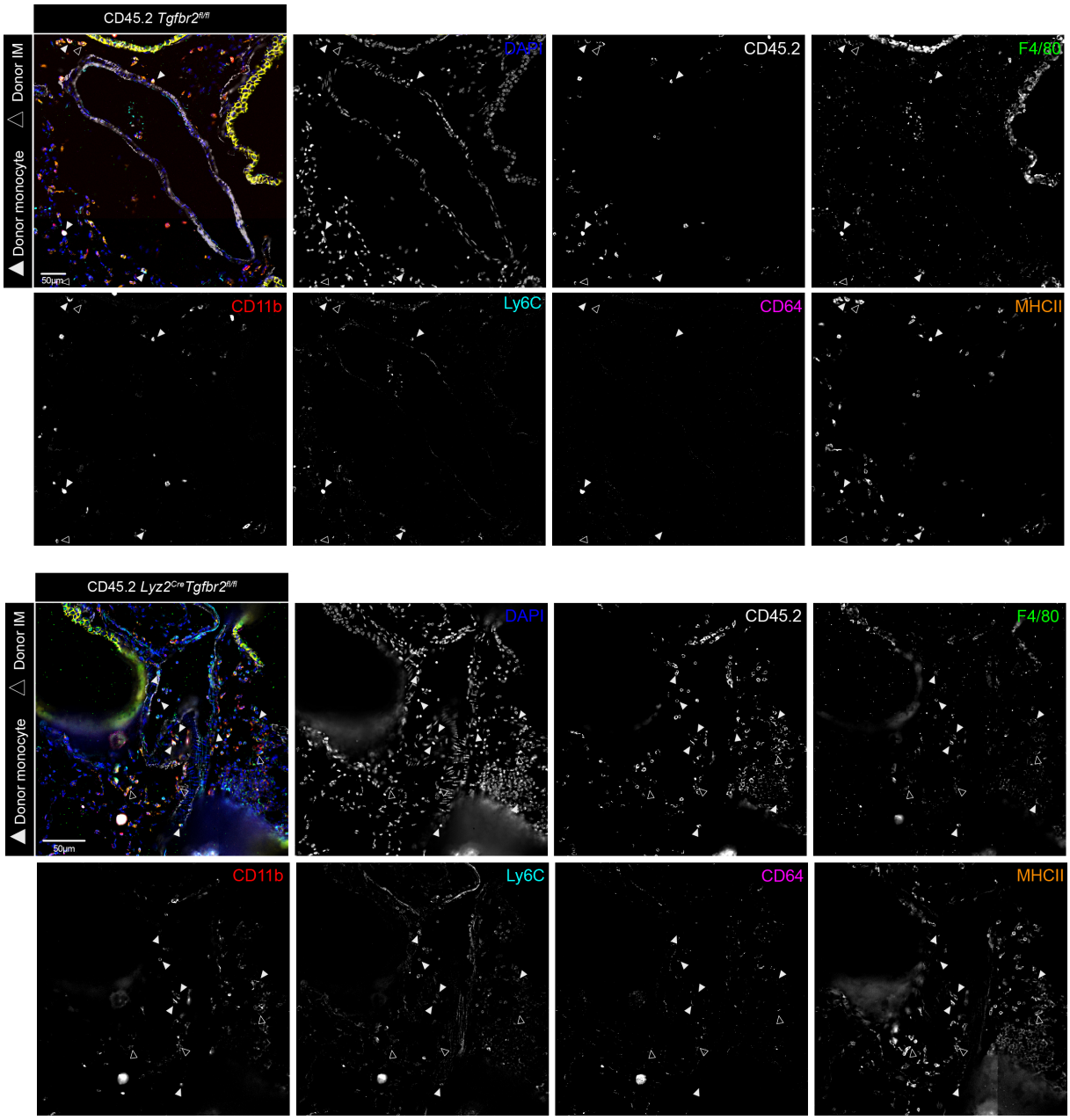

Fig. S10. Identification of donor CD45.1^{-}CD45.2^{+} monocytes and IMs in lungs of donor *Tgfbr2*$^{fl/fl}$ and donor *Lyz2*^{Cre} *Tgfbr2*$^{fl/fl}$ chimeric IM^{DTR} mice. Representative pictures showing individual labeling of markers used to define donor CD45.1^{-}CD45.2^{+} monocytes and IMs in lungs of donor *Tgfbr2*$^{fl/fl}$ and donor *Lyz2*^{Cre} *Tgfbr2*$^{fl/fl}$ chimeric IM^{DTR} mice, as in Fig. 6A. Scale bars: 50 μm.

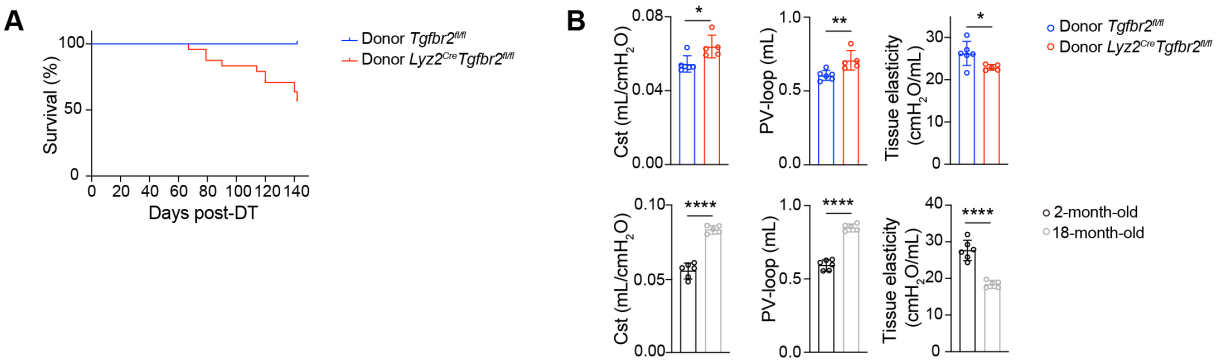

Fig. S11. Survival and lung function of donor *Tgfbr2*$^{fl/fl}$ or donor *Lyz2*^{Cre} *Tgfbr2*$^{fl/fl}$ chimeric IM^{DTR} mice. (**A**) Survival curve of donor *Tgfbr2*$^{fl/fl}$ or donor *Lyz2*^{Cre} *Tgfbr2*$^{fl/fl}$ chimeric IM^{DTR} mice. (**B**) Invasive measurements of quasi-static compliance (Cst), pressure-volume loops (PV-loop) and tissue elasticity in chimeric IM^{DTR} mice 3 months after DT, as in Fig. 6A), and in 2-month-old or 18-month-old C57BL/6 WT mice. (B) Data show mean +/- SEM and are representative of 2 independent experiments (n = 5-6 mice). P values were calculated using an unpaired two-tailed Student's t test. *, P<0.05; **, P<0.01; ****, P<0.0001.

DISCUSSION

DISCUSSION

In this study, we found that blood vessel-associated vWF$^+$ endothelial cells provide TGFβ1 to monocytes entering the lung tissue, enabling their transition toward functional IMs. Using a combination of ex vivo experiments and multiple transgenic mouse models, we demonstrated that endothelial-derived TGFβ signaling is critical for regulating IM identity, in part through collaboration with CSF1 to upregulate the master transcription factor MafB. Disruption of myeloid-intrinsic TGFβ receptor signaling resulted in the accumulation of monocytes and immature IMs in adventitial cuffs, impaired IM development, altered niche occupancy, and was associated with changes in the lung immunoregulatory environment and age-related abnormalities. By employing novel technologies such as Codex imaging, we further revealed that TGFβ signaling modulates the spatial organization of monocyte-to-IM differentiation in the lung. Functionally, the loss of TGFβ receptor signaling in IMs compromised immune surveillance and contributed to structural deterioration resembling lung aging. Altogether, our findings uncover a previously unrecognized endothelial–myeloid crosstalk involving TGFβ1–TGFβ receptor interactions, which continuously supports IM differentiation from monocytes in adult mice (Conclusion figure) and highlight the essential role of lung IMs, shaped by TGFβ signaling, in preserving tissue architecture and immune homeostasis under steady-state conditions.

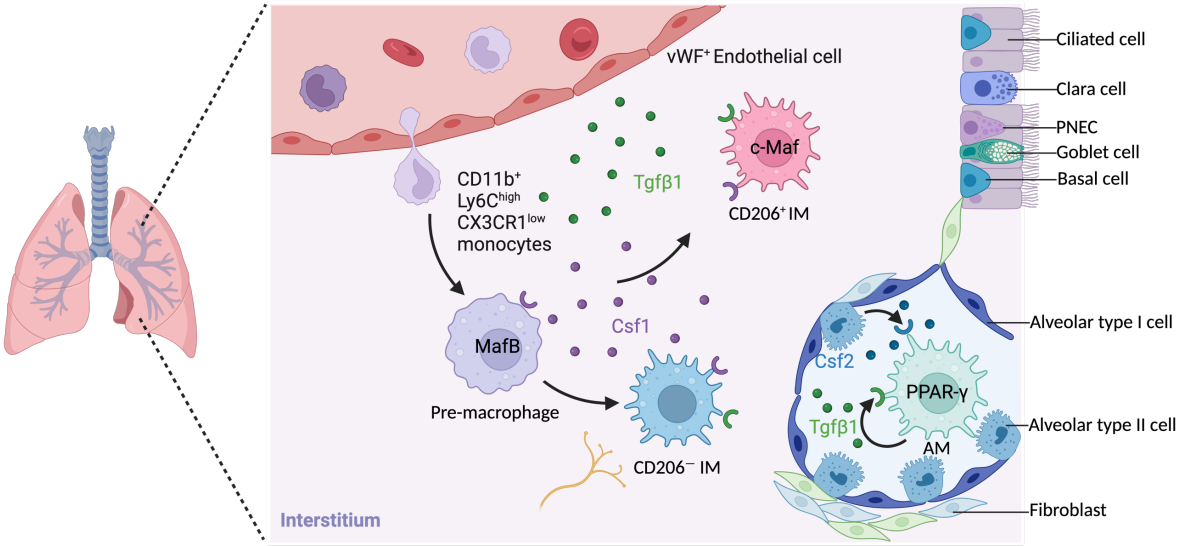

Conclusion figure. Endothelial Tgfβ signaling cooperates with CSF1 to regulate monocyte-derived IM identity and development.

Endothelial Tgfβ1 regulates IM development and identity

Ex vivo, we used BM monocytes cultured with growth factors (Csf1, Csf2) and Tgfβ1, or with conditioned medium from lung structural cells, or with endothelial cells, and focused on the expression of four key identity markers of IMs: Cx3cr1, Tmem119, MafB, and C1q to understand the effect of endothelial-derived Tgfβ in driving IM differentiation and identity.

MafB, a transcription factor essential for IM differentiation, plays a pivotal role in regulating the expression of complement component C1q, crucial for macrophage efferocytosis [171]. MafB-deficient macrophages exhibit reduced C1q expression and impaired efferocytosis, which can lead to increased glomerular autoimmunity. Consistent with these findings, Vanneste et al. demonstrated that the absence of MafB significantly reduces C1q expression in IMs, as observed in scRNA-seq data [167]. We further validated that *Mafb*-deficient IMs exhibit diminished phagocytic activity *ex vivo* (data not shown). Beyond its roles in IM biology, MafB is implicated in various macrophage-related diseases, including atherosclerosis, obesity, and ischemic stroke [362].

Cx3cr1, the receptor for fractalkine (CX3CL1), is widely expressed in RTMs, including microglia and IMs [167]. The CX3CR1-CX3CL1 axis facilitates monocyte and macrophage adhesion to blood vessels and plays a role in maintaining macrophage homeostasis, and TGFβ signaling enhances CX3CR1 expression, promoting the homeostatic state of macrophages [363]. In the CNS, CX3CR1 mediates neuron-glia communication, which is essential for maintaining CNS function [364]. Disruption of TGFβ signaling in $CX3CR1^{+}$ monocyte-derived macrophages can lead to severe consequences, including demyelinating diseases [363]. Mechanistically, TGFβ1 increases steady-state levels of CX3CR1 mRNA without altering its half-life, potentially through two SBEs identified in the rat CX3CR1 promoter [365].

Tmem119 is a well-established marker for microglia, distinguishing them from other macrophage populations [316, 319]. TGFβ signaling directly regulates *Tmem119* expression during the postnatal maturation of microglia. Activation of TGFβ receptors leads to the translocation of SMAD2/3 complexes to the nucleus, where they bind to regulatory elements in the *Tmem119* promoter, driving its expression [366]. This highlights the importance of TGFβ

signaling in maintaining microglial identity and function. Interestingly, Vanneste et al. demonstrated that IMs also exhibit high expression of Tmem119 [167]. By employing an intersectional strategy of both *Tmem119* and *Cx3cr1* expression, they were able to specifically deplete IMs using low doses of DT without affecting microglia, highlighting the utility of these markers in studying IM biology. Additionally, we found that *Tmem119*$^{CreER\text{-}Tomato}$ reporter mice serve as an effective tool for tracking IMs *in vivo* (data not shown). These findings suggest that Tmem119 is not only a marker for microglia but also a valuable marker of IMs.

AMs are known to be regulated by TGFβ1 with CSF2 [15]. *Ex vivo* experiments revealed several intriguing observations regarding the interplay between Tgfβ1, CSF1, and CSF2 in regulating macrophage differentiation and identity. Indeed, BM monocytes treated with Tgfβ1 in combination with either CSF1 or CSF2 differentially upregulated genes associated either with IMs or AMs, respectively (fig. S5). Specifically, CSF2 suppressed IM-related gene signatures, while CSF1, in conjunction with Tgfβ1, inhibited *Pparg* expression. Notably, only the combination of CSF2 and Tgfβ1 increased *Csf2ra* expression, whereas *Csf1r* expression was upregulated exclusively under CSF1 and Tgfβ1 treatment. This suggests that these signaling pathways enable cells to respond more robustly to CSF2 or CSF1, depending on the specific combination of cytokines (fig. S5). Daassi et al. demonstrated that MafB and c-Maf expression were induced by IL-10 but suppressed by CSF2 [170]. This underscores macrophage identity is not fixed but dynamically shaped by environmental cues, mediated via the selective activation of enhancers [59, 60]. The presence of Csf1 or Csf2 may shape chromatic accessibility of AM-specific loci or IM-associated loci, then Tgfβ1 can bind and upregulate the expression of specific identity genes.

Viola et al. investigated how three TGFβ isoforms imprinted the nerve-associated muscularis macrophages phenotype and quantified expression of muscularis macrophages subset marker genes in BMDMs following 24 h stimulation with TGFβ1, TGFβ2 or TGFβ3 [308]. In addition, skin macrophages have been shown to be regulated by all TGFβ isoforms in a recent paper [312]. In fact, these 3 isoforms, depending on the dose, could also upregulate IM

identity markers with similar efficiency *in vitro* (data not shown), suggesting redundant or overlapping functions among these isoforms in regulating IM and other RTM phenotypes.

In vivo study, we investigated the role of Tgfβ signaling in the regulation of IM development and identity in the lung. First, we identified that TgfβRII, a critical membrane receptor for Tgfβ signaling, is highly expressed in IMs compared to other lung myeloid cell populations (Fig. 1 D, F and fig. S2E). This observation was supported by scRNA-seq data from previous studies [367]. To further explore the functional role of Tgfβ signaling in IMs, *Lyz2*^{Cre} *Tgfbr2*$^{fl/fl}$ mice were generated to impair *Tgfbr2* expression in myeloid cells. Although this model was not entirely specific to IMs, as *Lyz2* would also target other myeloid cells (neutrophils, monocytes, AMs), we found lower expression of TgfβRII in these cells (Fig. 1 D, F and fig. S2E). However, this model was not completely efficient in abrogating *Tgfbr2* expression in monocytes and IMs (fig. S3A and fig. S7A), and we only observed moderate reduction in the total number of IMs (Fig. 3G). Notably, Yu et al. previously demonstrated that, while AM development depends on TGFβ signaling, AM numbers gradually normalized in same *Lyz2*^{Cre} *Tgfbr2*$^{fl/fl}$ mice as the mice aged [158]. We postulate that a similar compensatory mechanism may occur for IMs.

The experiments assessing IM numbers in *Lyz2*^{Cre} *Tgfbr2*$^{fl/fl}$ mice also examined CD64^{+} monocyte numbers, which were increased in *Lyz2*^{Cre} *Tgfbr2*$^{fl/fl}$ mice compared to controls (Fig. 3G). Previous studies have reported the presence of a "waterfall" population (CD64^{+} monocytes) under inflammatory conditions [144, 183]. 12-16-week-old *Lyz2*^{Cre} *Tgfbr2*$^{fl/fl}$ mice did not exhibit significant upregulation of inflammation-related genes compared with *Tgfbr2*$^{fl/fl}$ mice (fig. S7E), suggesting that the observed effects were not driven by inflammation. Instead, we found that the absence of Tgfβ signaling impaired the differentiation of IMs, as evidenced by the accumulation of transitional cells (Ly6C^{+}CD64^{+} monocytes) in the interstitium (Fig. 3, J and K) and lower expression of IM signature markers Cx3cr1 and Tmem119 in CD64^{+} monocytes and IMs from *Lyz2*^{Cre} *Tgfbr2*$^{fl/fl}$ mice compared to controls (Fig. 3, L and M). These findings further support impaired IM development and identity in the absence of myeloid *Tgfbr2* under homeostatic conditions.

CD206^{-} IMs express lower levels of TgfβRII compared to CD206^{+} IMs, suggesting that CD206^{+} IMs might rely more on TGFβ receptor signaling for their development. However, our findings in fig. S6A show that i.p injections of the TgfβR inhibitor LY363947 at days 2, 4, and 6 post-DT in IM^{DTR} mice lead to a significant and comparable reduction in both CD206^{-} and CD206^{+} IMs (fig. S6A). Bioinformatic analyses further revealed a progressive increase in the signature score of Tgfβ1 target genes along pseudotime in the differentiation pathways of both CD206^{-} and CD206^{+} IMs, strongly supporting Tgfβ signaling in the development of both subsets (Fig. 4F). Additionally, competitive chimera experiment demonstrated a clear advantage of WT over *Tgfbr2*-deficient BM cells during the repopulation of both IM subsets after DT treatment (Fig. 3, E and F). Through scRNA-seq analysis, we identified two distinct IM subsets that were significantly reduced in the *Tgfbr2*-deficient IMs (Fig. 6, H and I). These subsets were defined using additional identity markers of IM beyond those used in flow cytometry analysis. Taken together, these results provide evidence that Tgfβ receptor signaling is required for the development and maintenance of both IM subsets.

Furthermore, these findings align with our previous work on MafB dependency in IMs [167]. Vanneste et al. shows MafB expression and inferred activity were lower in CD206^{-} IMs compared to CD206^{+} IMs. Despite this difference, myeloid-intrinsic *Mafb* deletion affected both subsets, as demonstrated in BM mixed chimera experiments. Similarly, although CD206^{-} IMs express lower levels of TgfβRII than CD206^{+} IMs, Tgfβ receptor antagonism or deletion impacts both subsets. These findings are consistent with the idea that Tgfβ receptor signaling plays a crucial role at an early stage of monocyte-to-macrophage differentiation, prior to subset divergence, much like the role previously described for MafB.

To address potential confounding effects associated with the *Lyz2*^{Cre} model, especially related to AM-intrinsic *Tgfbr2*, we employed a unique chimeric mouse model in which CD45.1^{+} CD45.2^{+} IM^{DTR} mice were irradiated with thorax protection (Fig. 6A). In this model, AMs were predominantly derived from host cells, while most IMs originated from donor BM cells after DT treatment. This experimental design enabled us to specifically investigate the role of Tgfβ signaling in IM, avoiding the confounding effects of Tgfβ signaling in regulating AMs. scRNA-

seq analysis revealed a significant enrichment in the population of $CD64^{+}$ $Ly6C^{+}$ monocytes/IMs in the *Tgfbr2*-deficient group. These cells exhibited elevated levels of apoptosis and proliferation (Fig. 6L), a phenotype reminiscent of observations in *Mafb*-deficient IMs in our previous work [167]. Additionally, CODEX imaging demonstrated that the spatial location of monocytes and monocytes/IMs interactions with endothelial cells were markedly disrupted in the absence of IM-intrinsic TGFβ signaling (Fig. 7 B and D). These findings indicate that Tgfβ signaling not only governs IM development but also plays a critical role in their spatial integration within the lung microenvironment, which is consistent with the research that TGFβ modulates the spatial positioning of intestinal macrophages [306].

Endothelial TGFβ signaling in the lung

Through NicheNet analysis, we identified *Tgfb1* and *Csf1* as the top ligands involved in endothelial cell-IM interactions (Fig. 1B). Our findings revealed that endothelial cells, particularly those lining blood vessels, express high levels of Tgfβ1 in mice (Fig. 1C, 5A and B). Co-culture of endothelial cells with microglia induces CX3CR1 expression [368], which aligns with our *ex vivo* experiment (Fig. 2 H-J and Fig. 5 J-L). In Fig. 5, $Cdh5^{CreERT2}$ $Tgfb1^{fl/fl}$ mice data highlight the specific role of endothelial cells in regulating IMs via Tgfβ signaling. When IMs were depleted, endothelial cells released more Tgfβ1 to the tissue, which recruits monocytes from the bloods and promotes their differentiation into IMs (Fig. 5 C-E). This mechanism mirrors the observed dynamics of CSF1 levels during the survival and proliferation phases of macrophages. Administration of recombinant CSF1 in mice led to increased macrophage content in the liver, peritoneal cavity, and spleen, as well as a significant rise in circulating monocytes [369]. Similarly, CSF1 treatment in rats resulted in increased macrophage populations in bone marrow, liver, spleen, and lung [370]. However, the precise mechanisms of endothelial cells that sense and maintain TGFβ signal and IM niche in the lung remain unclear. Drawing parallels to the CSF1 hypothesis [23], we speculate that dying IMs or neighboring macrophages may provide signals to the niche, triggering either the proliferation of resident macrophages or the differentiation of circulating monocytes. Future studies should

focus on elucidating the molecular cues that enable endothelial cells to sense empty niche and coordinate macrophage recruitment and differentiation.

Despite these findings, several important questions remain to be explored:

TGFβ activation mechanism in endothelial cell and IM interactions. Previous research shows that fluid shear stress stimulates endothelial cells to upregulate TGFβ1 transcription and production, a process modulated by potassium channel activity [371]. Beyond TGFβ1, endothelial cells also express other members of the TGFβ family, such as BMP-10 and Activin A, which signal through the ALK-1 receptor. Notably, Activin A has been proposed to act as an endogenous regulator of TGFβ function in endothelial cells by competitively binding to ALK-1 [372]. Understanding of endothelial TGFβ activation mechanism in IMs is needed to better regulated IM differentiation.

Role of IMs in endothelial cell and lung homeostasis. AMs can respond to AT2-derived epithelial CSF2 and autocrine TGFβ [15, 158]. In turn, they can provide a benefit to the tissue, recycle surfactant, and regulate tissue regeneration by producing growth factors such as TGFβ [373]. Further research is needed to clarify the mechanisms by which IMs maintain lung homeostasis, especially with regards to their reciprocal interactions with endothelial cells.

Other sources of TGFβ1 and niche signals in disease states. In normal human lung, immunohistochemical analyses have identified TGFβ1 expression in the epithelial cells of bronchi, bronchioles, and alveoli [374]. Under pathological conditions, such as during bleomycin-induced pulmonary fibrosis, the expression of TGFβ1 is significantly upregulated, with myofibroblasts, fibroblasts, and eosinophils emerging as the primary sources of this increased expression [375]. In our study, we focus on the mouse steady-state lung. However, in disease models, other cellular sources of TGFβ1 or other niche signals may also contribute to monocyte recruitment and IM development. This process is more complex than previously understood. Investigating the interplay between endothelial cells and other TGFβ1-producing cells in disease model could provide deeper insights into the developing targeted therapies that modulate IM development and function, thereby influencing the progression of pulmonary diseases.

The known activation mechanisms in different cell types are summarized below in Table 1. The activation mechanisms of TGFβ1 in our study remain to be discovered.

Table 1. TGFβ1 activation mechanism in different cell types.

Cell type	TGFβ1 activation mechanism
Endothelial cells	Plasmin on endothelial cell surfaces is necessary for LTGFβ activation [376].
Epithelial cells	Cortical actin/myosin activate latent TGFβ via the αvβ6 integrin, triggered by G-protein coupled receptor agonists and involving Rho Kinase and mechanical tension [377].
Fibroblasts	Myofibroblast contraction can directly activate latent TGFβ1 from the ECM through integrin-mediated processes [378]. Sirt1 regulates canonical TGFβ signaling to control fibroblast activation and tissue fibrosis [379]. Shear forces can activate latent TGFβ1 released from fibroblasts involving thiol-disulfide exchange and requiring the presence of LTBP1 [380].
AMs	The association of TSP-1/latent TGFβ1 complex with CD36 is necessary to the activation of latent TGFβ1 [381].
Microglia	LRRC33 functions as a milieu molecule on microglia surfaces, enabling highly localized, integrin-αVβ8-dependent TGFβ activation [227].
Osteoblasts	As the bone matrix deposited by osteoblasts contains abundant TGFβ in its latent form. the acidic environment created by osteoclasts offers an ideal condition for TGFβ activation [382]. Proteolytic cleavage of LTBP1 by osteoclasts, involving serine proteases and MMPs, is a cellular mechanism for releasing TGFβ from bone matrix [383].
Platelets	Thrombin-stimulated platelets activate latent TGFβ1 through a furin-like proprotein convertase, independent of classical activation pathways involving TSP-1 or plasmin [384]. Shear forces (similar as fibroblasts) [380].
Tregs	Tregs suppress immune cells within proximity by activating latent TGFβ1 presented by GARP to integrin αVβ8 on their surface [385]. ROS activate latent TGFβ1 [386].

Targeting the mechanisms of TGFβ signaling has led to the development of several promising therapeutic strategies. One such target is GARP, a transmembrane protein expressed on Tregs and platelets. GARP binds and activates latent TGFβ1, a process critical for maintaining peripheral tolerance and preventing inflammatory diseases [387]. Recent studies have demonstrated increased GARP expression in the BM and spleen of mice with

primary myelofibrosis. Blocking GARP:TGFβ1 with monoclonal antibodies (Livmoniplimab) reduced fibrosis and suppressed the clonal expansion of transformed cells in PMF models, highlighting its therapeutic potential for fibrotic diseases [388]. The therapeutic applications of GARP:TGFβ1 blockade extend beyond PMF, with potential uses in cancer immunotherapy and the treatment of inflammatory diseases [389]. Monoclonal antibodies targeting GARP:TGFβ1 complexes have shown significant potential in preclinical studies. For instance, these antibodies inhibit the immunosuppressive activity of Tregs in vivo, offering a promising approach for cancer immunotherapy [390]. Additionally, massive TGFβ-targeting therapies are already in clinical trials for fibrosis and cancer, Pirfenidone and Nintedanib suppress TGFβ-induced transcription, which is already used in patients for IPF treatment [391, 392].

Evidence that IM can prevent the development of age-related abnormities

In Fig. 8, we observed that *Tgfbr2*-deficient IMs significantly impact lung structure and function, with phenotypes closely resembling those of aging lungs. There are structural and functional changes.

Structurally, the aging lung undergoes significant alterations, including alveolar distension (Fig. 8 B and C), enlargement of alveolar ducts, loss of elasticity (Fig. 8A), elastin degradation (Fig. 8H) [393-395].These changes lead to increased alveolar pore size and frequency, as well as interstitial modifications such as focal collagen deposition (Fig. 8I) [396].

Functionally, the aging respiratory system experiences a stiffening of the chest wall due to calcification of ribs and costal cartilage [361], and intercostal muscle mass and force decline, impairing respiratory function [397]. These structural and functional changes lead to increased residual volume (Fig. 8A), decreased forced vital capacity, and diminished respiratory muscle strength, impairing effective cough and airway clearance [361, 398]. Aging lungs also exhibit increased alveolar dead space and ventilation-perfusion imbalances, potentially reducing blood oxygen levels [398].

Moreover, aging is associated with diminished mucociliary clearance, characterized by slower ciliary beat frequency and altered mucus properties [399]. This impairment increases

susceptibility to respiratory infections and chronic airway diseases [399, 400]. Exercise capacity declines with age, accompanied by reduced ventilatory responses to hypoxia and hypercapnia [398, 401]. Aging also impairs innate immunity, predisposing the elderly to pulmonary inflammation [397]. The diminished regenerative capacity of the aging respiratory system increases susceptibility to acute and chronic lung diseases [402]. Notably, aging is associated with an increased prevalence and severity of small airway dysfunction, even in non-smokers [403]. Additionally, aging confers a profibrotic phenotype on fibroblasts, exacerbating fibro-genic responses in the lungs [404]. We observed a slight increase in collagen deposition, indicating a heightened risk of fibrosis (Fig. 8H).

Moreover, the levels of many cytokines and growth factors, including IL-10, were reduced in the absence of IM-intrinsic *Tgfbr2*, potentially compromising immune surveillance and tissue integrity. IMs may directly or indirectly regulate the ECM by modulating ECM-degrading enzymes such as MMPs, which were decreased in lungs containing *Tgfbr2*-deficient IMs, or by producing IL-10, know to regulate ECM deposition [405, 406]. While their cellular source remains to be identified, other factors found to be decreased in lungs with *Tgfbr2*-deficient IMs are potential suppressors of fibroblast-driven collagen deposition, such as adiponectin [407], HGF [408] or pentraxin-2 [409]. Finally, IMs may also play a role in preserving the integrity of the alveolar-capillary barrier by interacting with epithelial and endothelial cells. Loss of TgfβR signaling in IMs may disrupt their ability to occupy dedicated niches and to promote the production of growth factors and cytokines that maintain endothelial and epithelial integrity and functions, including adiponectin [410], angiopoietin-1 [411], amphiregulin [412] and lipocalin-2 [413]. Identifying the precise IM-driven mechanisms involved, and whether specific IM subsets preferentially carry out such homeostatic functions, represent interesting avenues for future research, suggesting impaired immune surveillance and tissue repair capacity in whole lung.

Neuro-immune interactions

TGFβ plays a crucial role in regulating NAMs, such as muscularis macrophages, skin macrophage and microglia. Neurons can indeed produce TGFβ, and in turn, TGFβ-driven NAM

contribute to neuro-immune crosstalk in health and diseases [308, 312, 315, 323, 363, 414]. Such NAMs exhibit a high expression of CX3CR1 and a regulation by TGFβ, similarly to IMs. Of note, a specific subset of IMs, termed nerve- and airway-associated IMs, has been identified and is characterized by a high expression of CD169 and a close association with airways and sympathetic nerves [177]. These YS-derived, self-renewing IMs require CSF1 for development and play an immunoregulatory role during lung inflammation. Depletion of IMs, including NAMs, attenuates Th2 cell responses in asthma models and reduces radiation-induced lung fibrosis [185, 206]. In our study, IMs exhibit decreased Cx3cr1 expression in *Lyz2*^{Cre} *Tgfbr2*$^{fl/fl}$ mice. Based on the gating strategy, the nerve-associated IMs are MerTK^{+}CD64^{+}F4/80^{+}Ly6C^{-}CX3CR1^{+}CD169^{+}, suggesting that TGFβ signaling may also regulate CD169^{+} IMs [177]. Further research will be needed to understand the commonalities between such NAMs and their potential regulation by TGFβ1, particularly in the context of neuro-immune interactions.

Broader Clinical Implications and Future Perspectives

Our study uncovers a previously unrecognized endothelial–macrophage axis that is essential for maintaining lung immune homeostasis and structural integrity through TGFβ1-mediated signaling. These findings may have important clinical implications, particularly in the context of chronic pulmonary diseases such as COPD, IPF and age-related lung dysfunction. The disruption of IM development observed upon impaired TGFβ signaling mirrors several features of lung aging and suggests that a decline in endothelial-driven niche support may contribute to tissue degeneration, chronic inflammation, and fibrosis. Therapeutically, strategies aiming to restore or enhance endothelial-derived TGFβ1 signaling could offer new avenues to preserve lung architecture, promote regenerative responses, and modulate immune surveillance without broadly suppressing immunity.

Beyond the lung, our work raises the exciting possibility that similar vascular–macrophage circuits operate in other tissues, including the central nervous system and peripheral barrier sites. Understanding how vascular niches orchestrate macrophage behavior could provide a

conceptual framework for developing precision therapies that selectively target tissue-specific macrophage subsets. Future research should focus on elucidating how this endothelial-IM axis adapts to injury, infection, and aging, and whether its manipulation can be leveraged to prevent or reverse the progression of inflammatory, fibrotic, and degenerative diseases. Ultimately, deciphering the molecular dialogue between endothelial cells and immune cells may open new therapeutic horizons for promoting organ resilience across the lifespan.

REFERENCES

REFERENCES

1. Metchnikoff, E., *Untersuchungen über die mesodermalen Phagocyten einiger Wirbeltiere.* Biol Zentralbl, 1883. **3**: p. 560.
2. Wynn, T.A., A. Chawla, and J.W. Pollard, *Macrophage biology in development, homeostasis and disease.* Nature, 2013. **496**(7446): p. 445-455.
3. van Furth, R. and Z.A. Cohn, *The origin and kinetics of mononuclear phagocytes.* The Journal of experimental medicine, 1968. **128**(3): p. 415-435.
4. Hume, D.A., *Differentiation and heterogeneity in the mononuclear phagocyte system.* Mucosal immunology, 2008. **1**(6): p. 432-441.
5. Epelman, S., K.J. Lavine, and G.J. Randolph, *Origin and functions of tissue macrophages.* Immunity, 2014. **41**(1): p. 21-35.
6. Frame, J.M., K.E. McGrath, and J. Palis, *Erythro-myeloid progenitors:"definitive" hematopoiesis in the conceptus prior to the emergence of hematopoietic stem cells.* Blood Cells, Molecules, and Diseases, 2013. **51**(4): p. 220-225.
7. Palis, J., et al., *Development of erythroid and myeloid progenitors in the yolk sac and embryo proper of the mouse.* Development, 1999. **126**(22): p. 5073-5084.
8. Palis, J. and M.C. Yoder, *Yolk-sac hematopoiesis: the first blood cells of mouse and man.* Experimental hematology, 2001. **29**(8): p. 927-936.
9. Hoeffel, G., et al., *C-Myb+ erythro-myeloid progenitor-derived fetal monocytes give rise to adult tissue-resident macrophages.* Immunity, 2015. **42**(4): p. 665-678.
10. Mass, E., et al., *Specification of tissue-resident macrophages during organogenesis.* Science, 2016. **353**(6304): p. aaf4238.
11. Ajami, B., et al., *Local self-renewal can sustain CNS microglia maintenance and function throughout adult life.* Nature neuroscience, 2007. **10**(12): p. 1538-1543.
12. Ginhoux, F., et al., *Fate mapping analysis reveals that adult microglia derive from primitive macrophages.* Science, 2010. **330**(6005): p. 841-845.
13. Merad, M., et al., *Langerhans cells renew in the skin throughout life under steady-state conditions.* Nature immunology, 2002. **3**(12): p. 1135-1141.
14. Schulz, C., et al., *A lineage of myeloid cells independent of Myb and hematopoietic stem cells.* Science, 2012. **336**(6077): p. 86-90.
15. Guilliams, M., et al., *Alveolar macrophages develop from fetal monocytes that differentiate into long-lived cells in the first week of life via GM-CSF.* Journal of Experimental Medicine, 2013. **210**(10): p. 1977-1992.
16. Hashimoto, D., et al., *Tissue-resident macrophages self-maintain locally throughout adult life with minimal contribution from circulating monocytes.* Immunity, 2013. **38**(4): p. 792-804.
17. Bain, C.C., et al., *Constant replenishment from circulating monocytes maintains the macrophage pool in the intestine of adult mice.* Nat Immunol, 2014. **15**(10): p. 929-937.
18. Blériot, C., S. Chakarov, and F. Ginhoux, *Determinants of Resident Tissue Macrophage Identity and Function.* Immunity, 2020. **52**(6): p. 957-970.
19. Guilliams, M. and F.R. Svedberg, *Does tissue imprinting restrict macrophage plasticity?* Nature immunology, 2021. **22**(2): p. 118-127.

20. Hume, D.A., K.M. Irvine, and C. Pridans, *The mononuclear phagocyte system: the relationship between monocytes and macrophages.* Trends in immunology, 2019. **40**(2): p. 98-112.
21. Liu, Z., et al., *Fate Mapping via Ms4a3-Expression History Traces Monocyte-Derived Cells.* Cell, 2019. **178**(6): p. 1509-1525 e19.
22. Mould, K.J., et al., *Airspace macrophages and monocytes exist in transcriptionally distinct subsets in healthy adults.* American Journal of Respiratory and Critical Care Medicine, 2021. **203**(8): p. 946-956.
23. Guilliams, M., et al., *Establishment and Maintenance of the Macrophage Niche.* Immunity, 2020. **52**(3): p. 434-451.
24. Yona, S. and S. Jung, *Monocytes: subsets, origins, fates and functions.* Curr Opin Hematol, 2010. **17**(1): p. 53-9.
25. Pridans, C., et al., *Transcriptomic Analysis of Rat Macrophages.* Front Immunol, 2020. **11**: p. 594594.
26. Gautier, E.L., et al., *Gene-expression profiles and transcriptional regulatory pathways that underlie the identity and diversity of mouse tissue macrophages.* Nature immunology, 2012. **13**(11): p. 1118-1128.
27. Liu, L., et al., *An optimized flow cytometry panel for classifying macrophage polarization.* Journal of Immunological Methods, 2022. **511**: p. 113378.
28. Hirayama, D., T. Iida, and H. Nakase, *The Phagocytic Function of Macrophage-Enforcing Innate Immunity and Tissue Homeostasis.* Int J Mol Sci, 2017. **19**(1).
29. Mass, E., et al., *Tissue-specific macrophages: how they develop and choreograph tissue biology.* Nat Rev Immunol, 2023. **23**(9): p. 563-579.
30. Uribe-Querol, E. and C. Rosales, *Phagocytosis: Our Current Understanding of a Universal Biological Process.* Front Immunol, 2020. **11**: p. 1066.
31. Melcarne, C., B. Lemaitre, and E. Kurant, *Phagocytosis in Drosophila: From molecules and cellular machinery to physiology.* Insect Biochem Mol Biol, 2019. **109**: p. 1-12.
32. Myers, K.V., S.R. Amend, and K.J. Pienta, *Targeting Tyro3, Axl and MerTK (TAM receptors): implications for macrophages in the tumor microenvironment.* Mol Cancer, 2019. **18**(1): p. 94.
33. Wanke, F., et al., *Ligand-dependent kinase activity of MERTK drives efferocytosis in human iPSC-derived macrophages.* Cell Death Dis, 2021. **12**(6): p. 538.
34. Heit, B., T. Tasnim, and A. Le Lam, *MER Tyrosine Kinase Mediates Efferocytosis Through a Novel β2 Integrin-Activating Signalling Pathway.* The Journal of Immunology, 2021.
35. Yanagihashi, Y., et al., *Mouse macrophages show different requirements for phosphatidylserine receptor Tim4 in efferocytosis.* Proc Natl Acad Sci U S A, 2017. **114**(33): p. 8800-8805.
36. N, A.G. and A. Hidalgo, *Nuclear Receptors and Clearance of Apoptotic Cells: Stimulating the Macrophage's Appetite.* Front Immunol, 2014. **5**: p. 211.
37. Westman, J., S. Grinstein, and P.E. Marques, *Phagocytosis of Necrotic Debris at Sites of Injury and Inflammation.* Front Immunol, 2019. **10**: p. 3030.
38. Tran, N. and E.L. Mills, *Redox regulation of macrophages.* Redox Biol, 2024. **72**: p. 103123.
39. Baran, C.P., et al., *The role of ROS and RNS in regulating life and death of blood monocytes.* Curr Pharm Des, 2004. **10**(8): p. 855-66.
40. Guerriero, J.L., *Macrophages: Their Untold Story in T Cell Activation and Function.* Int Rev Cell Mol Biol, 2019. **342**: p. 73-93.
41. Legrand, C., et al., *Lung Interstitial Macrophages Can Present Soluble Antigens and Induce Foxp3(+) Regulatory T Cells.* Am J Respir Cell Mol Biol, 2024. **70**(6): p. 446-456.

42. Peppelenbosch, M.P., et al., *Macrophages present pinocytosed exogenous antigen via MHC class I whereas antigen ingested by receptor-mediated endocytosis is presented via MHC class II.* J Immunol, 2000. **165**(4): p. 1984-91.
43. Harding, C.V. and R. Song, *Phagocytic processing of exogenous particulate antigens by macrophages for presentation by class I MHC molecules.* J Immunol, 1994. **153**(11): p. 4925-33.
44. Morris, D.L., et al., *Adipose tissue macrophages function as antigen-presenting cells and regulate adipose tissue CD4+ T cells in mice.* Diabetes, 2013. **62**(8): p. 2762-72.
45. Xu, Y., et al., *Macrophages transfer antigens to dendritic cells by releasing exosomes containing dead-cell-associated antigens partially through a ceramide-dependent pathway to enhance CD4(+) T-cell responses.* Immunology, 2016. **149**(2): p. 157-71.
46. Muntjewerff, E.M., L.D. Meesters, and G. van den Bogaart, *Antigen Cross-Presentation by Macrophages.* Front Immunol, 2020. **11**: p. 1276.
47. Ito, T., et al., *Notch system in the linkage of innate and adaptive immunity.* J Leukoc Biol, 2012. **92**(1): p. 59-65.
48. Ito, T., et al., *The linkage of innate and adaptive immune response during granulomatous development.* Front Immunol, 2013. **4**: p. 10.
49. Lee, M.S. and Y.J. Kim, *Signaling pathways downstream of pattern-recognition receptors and their cross talk.* Annu Rev Biochem, 2007. **76**: p. 447-80.
50. Hamerman, J.A., K. Ogasawara, and L.L. Lanier, *Cutting edge: Toll-like receptor signaling in macrophages induces ligands for the NKG2D receptor.* J Immunol, 2004. **172**(4): p. 2001-5.
51. Ito, T., et al., *The critical role of Notch ligand Delta-like 1 in the pathogenesis of influenza A virus (H1N1) infection.* PLoS Pathog, 2011. **7**(11): p. e1002341.
52. Martinez, F.O., et al., *Macrophage activation and polarization.* Front Biosci, 2008. **13**: p. 453-61.
53. Arango Duque, G. and A. Descoteaux, *Macrophage cytokines: involvement in immunity and infectious diseases.* Front Immunol, 2014. **5**: p. 491.
54. Fujiwara, N. and K. Kobayashi, *Macrophages in inflammation.* Curr Drug Targets Inflamm Allergy, 2005. **4**(3): p. 281-6.
55. Lee, K., *M1 and M2 polarization of macrophages: a mini-review.* Medical Biological Science and Engineering, 2019. **2**: p. 1-5.
56. Smith, T.D., et al., *Regulation of macrophage polarization and plasticity by complex activation signals.* Integr Biol (Camb), 2016. **8**(9): p. 946-55.
57. Ruscitti, C., et al., *Recruited atypical Ly6G(+) macrophages license alveolar regeneration after lung injury.* Sci Immunol, 2024. **9**(98): p. eado1227.
58. Sica, A. and A. Mantovani, *Macrophage plasticity and polarization: in vivo veritas.* J Clin Invest, 2012. **122**(3): p. 787-95.
59. Gosselin, D., et al., *Environment drives selection and function of enhancers controlling tissue-specific macrophage identities.* Cell, 2014. **159**(6): p. 1327-40.
60. Glass, C.K., *Genetic and genomic approaches to understanding macrophage identity and function.* Arterioscler Thromb Vasc Biol, 2015. **35**(4): p. 755-62.
61. Pollard, J.W., *Trophic macrophages in development and disease.* Nat Rev Immunol, 2009. **9**(4): p. 259-70.
62. Van Nguyen, A. and J.W. Pollard, *Colony stimulating factor-1 is required to recruit macrophages into the mammary gland to facilitate mammary ductal outgrowth.* Dev Biol, 2002. **247**(1): p. 11-25.

63. Nucera, S., D. Biziato, and M. De Palma, *The interplay between macrophages and angiogenesis in development, tissue injury and regeneration.* Int J Dev Biol, 2011. **55**(4-5): p. 495-503.
64. Pang, C., et al., *Macrophage infiltration into adipose tissue may promote angiogenesis for adipose tissue remodeling in obesity.* Am J Physiol Endocrinol Metab, 2008. **295**(2): p. E313-22.
65. Oishi, Y. and I. Manabe, *Macrophages in inflammation, repair and regeneration.* Int Immunol, 2018. **30**(11): p. 511-528.
66. Rodero, M.P. and K. Khosrotehrani, *Skin wound healing modulation by macrophages.* Int J Clin Exp Pathol, 2010. **3**(7): p. 643-53.
67. Lu, P., et al., *Extracellular matrix degradation and remodeling in development and disease.* Cold Spring Harb Perspect Biol, 2011. **3**(12).
68. Ravanti, L. and V.M. Kähäri, *Matrix metalloproteinases in wound repair (review).* Int J Mol Med, 2000. **6**(4): p. 391-407.
69. Lévesque, J.P., et al., *Macrophages form erythropoietic niches and regulate iron homeostasis to adapt erythropoiesis in response to infections and inflammation.* Exp Hematol, 2021. **103**: p. 1-14.
70. Sukhbaatar, N. and T. Weichhart, *Iron Regulation: Macrophages in Control.* Pharmaceuticals (Basel), 2018. **11**(4).
71. Korolnek, T. and I. Hamza, *Macrophages and iron trafficking at the birth and death of red cells.* Blood, 2015. **125**(19): p. 2893-7.
72. Vogt, A.S., et al., *On Iron Metabolism and Its Regulation.* Int J Mol Sci, 2021. **22**(9).
73. Nairz, M., et al., *"Pumping iron"-how macrophages handle iron at the systemic, microenvironmental, and cellular levels.* Pflugers Arch, 2017. **469**(3-4): p. 397-418.
74. Hoeffel, G. and F. Ginhoux, *Fetal monocytes and the origins of tissue-resident macrophages.* Cell Immunol, 2018. **330**: p. 5-15.
75. Shepard, J.L. and L.I. Zon, *Developmental derivation of embryonic and adult macrophages.* Curr Opin Hematol, 2000. **7**(1): p. 3-8.
76. Ng, L.G., et al., *Origin and Heterogeneity of Tissue Myeloid Cells: A Focus on GMP-Derived Monocytes and Neutrophils.* Annu Rev Immunol, 2023. **41**: p. 375-404.
77. Ginhoux, F. and S. Jung, *Monocytes and macrophages: developmental pathways and tissue homeostasis.* Nat Rev Immunol, 2014. **14**(6): p. 392-404.
78. Guilliams, M., A. Mildner, and S. Yona, *Developmental and Functional Heterogeneity of Monocytes.* Immunity, 2018. **49**(4): p. 595-613.
79. Terry, R.L. and S.D. Miller, *Molecular control of monocyte development.* Cell Immunol, 2014. **291**(1-2): p. 16-21.
80. Yáñez, A., et al., *Granulocyte-Monocyte Progenitors and Monocyte-Dendritic Cell Progenitors Independently Produce Functionally Distinct Monocytes.* Immunity, 2017. **47**(5): p. 890-902.e4.
81. Muñoz-Garcia, J., et al., *The twin cytokines interleukin-34 and CSF-1: masterful conductors of macrophage homeostasis.* Theranostics, 2021. **11**(4): p. 1568-1593.
82. Wang, Y., et al., *IL-34 is a tissue-restricted ligand of CSF1R required for the development of Langerhans cells and microglia.* Nat Immunol, 2012. **13**(8): p. 753-60.
83. Tian, Y., et al., *Elevated serum and synovial fluid levels of interleukin-34 in rheumatoid arthritis: possible association with disease progression via interleukin-17 production.* J Interferon Cytokine Res, 2013. **33**(7): p. 398-401.

84. Greter, M., et al., *Stroma-derived interleukin-34 controls the development and maintenance of langerhans cells and the maintenance of microglia.* Immunity, 2012. **37**(6): p. 1050-1060.
85. Bonnardel, J., et al., *Stellate Cells, Hepatocytes, and Endothelial Cells Imprint the Kupffer Cell Identity on Monocytes Colonizing the Liver Macrophage Niche.* Immunity, 2019. **51**(4): p. 638-654.e9.
86. Chitu, V. and E.R. Stanley, *Colony-stimulating factor-1 in immunity and inflammation.* Curr Opin Immunol, 2006. **18**(1): p. 39-48.
87. Nandi, S., et al., *Developmental and functional significance of the CSF-1 proteoglycan chondroitin sulfate chain.* Blood, 2006. **107**(2): p. 786-95.
88. Yao, G.Q., et al., *Selective deletion of the soluble Colony-Stimulating Factor 1 isoform in vivo prevents estrogen-deficiency bone loss in mice.* Bone Res, 2017. **5**: p. 17022.
89. Dai, X.M., et al., *Incomplete restoration of colony-stimulating factor 1 (CSF-1) function in CSF-1-deficient Csf1op/Csf1op mice by transgenic expression of cell surface CSF-1.* Blood, 2004. **103**(3): p. 1114-23.
90. Lenzo, J.C., et al., *Control of macrophage lineage populations by CSF-1 receptor and GM-CSF in homeostasis and inflammation.* Immunol Cell Biol, 2012. **90**(4): p. 429-40.
91. Dai, X.-M., et al., *Targeted disruption of the mouse colony-stimulating factor 1 receptor gene results in osteopetrosis, mononuclear phagocyte deficiency, increased primitive progenitor cell frequencies, and reproductive defects.* Blood, 2002. **99**(1): p. 111-120.
92. Cohen, M., et al., *Lung Single-Cell Signaling Interaction Map Reveals Basophil Role in Macrophage Imprinting.* Cell, 2018. **175**(4): p. 1031-1044.e18.
93. Komuczki, J., et al., *Fate-Mapping of GM-CSF Expression Identifies a Discrete Subset of Inflammation-Driving T Helper Cells Regulated by Cytokines IL-23 and IL-1β.* Immunity, 2019. **50**(5): p. 1289-1304.e6.
94. Hercus, T.R., et al., *The GM-CSF receptor family: mechanism of activation and implications for disease.* Growth Factors, 2012. **30**(2): p. 63-75.
95. Gschwend, J., et al., *Alveolar macrophages rely on GM-CSF from alveolar epithelial type 2 cells before and after birth.* J Exp Med, 2021. **218**(10).
96. Nishinakamura, R., et al., *The pulmonary alveolar proteinosis in granulocyte macrophage colony-stimulating factor/interleukins 3/5 beta c receptor-deficient mice is reversed by bone marrow transplantation.* J Exp Med, 1996. **183**(6): p. 2657-62.
97. Fleetwood, A.J., et al., *Granulocyte-macrophage colony-stimulating factor (CSF) and macrophage CSF-dependent macrophage phenotypes display differences in cytokine profiles and transcription factor activities: implications for CSF blockade in inflammation.* J Immunol, 2007. **178**(8): p. 5245-52.
98. Weston, B.R., L. Li, and J.J. Tyson, *Mathematical Analysis of Cytokine-Induced Differentiation of Granulocyte-Monocyte Progenitor Cells.* Front Immunol, 2018. **9**: p. 2048.
99. Chitu, V., et al., *Microglial Homeostasis Requires Balanced CSF-1/CSF-2 Receptor Signaling.* Cell Rep, 2020. **30**(9): p. 3004-3019.e5.
100. Chen, B.D., M. Mueller, and T.H. Chou, *Role of granulocyte/macrophage colony-stimulating factor in the regulation of murine alveolar macrophage proliferation and differentiation.* J Immunol, 1988. **141**(1): p. 139-44.
101. Lin, J., V. Kakkar, and X. Lu, *Impact of MCP-1 in atherosclerosis.* Curr Pharm Des, 2014. **20**(28): p. 4580-8.
102. Tsou, C.L., et al., *Critical roles for CCR2 and MCP-3 in monocyte mobilization from bone marrow and recruitment to inflammatory sites.* J Clin Invest, 2007. **117**(4): p. 902-9.

103. Tanaka, T., et al., *Monocyte chemoattractant protein-1/CC chemokine ligand 2 enhances apoptotic cell removal by macrophages through Rac1 activation.* Biochem Biophys Res Commun, 2010. **399**(4): p. 677-82.
104. Gouwy, M., et al., *Synergy between coproduced CC and CXC chemokines in monocyte chemotaxis through receptor-mediated events.* Mol Pharmacol, 2008. **74**(2): p. 485-95.
105. Kuscher, K., et al., *Synergy-inducing chemokines enhance CCR2 ligand activities on monocytes.* Eur J Immunol, 2009. **39**(4): p. 1118-28.
106. Stremmel, C., et al., *Author Correction: Yolk sac macrophage progenitors traffic to the embryo during defined stages of development.* Nat Commun, 2018. **9**(1): p. 3699.
107. Auffray, C., et al., *CX3CR1+ CD115+ CD135+ common macrophage/DC precursors and the role of CX3CR1 in their response to inflammation.* J Exp Med, 2009. **206**(3): p. 595-606.
108. Truman, L.A., et al., *CX3CL1/fractalkine is released from apoptotic lymphocytes to stimulate macrophage chemotaxis.* Blood, 2008. **112**(13): p. 5026-36.
109. Ishida, Y., J.L. Gao, and P.M. Murphy, *Chemokine receptor CX3CR1 mediates skin wound healing by promoting macrophage and fibroblast accumulation and function.* J Immunol, 2008. **180**(1): p. 569-79.
110. Hume, D.A., K.M. Summers, and M. Rehli, *Transcriptional Regulation and Macrophage Differentiation.* Microbiol Spectr, 2016. **4**(3).
111. T'Jonck, W., M. Guilliams, and J. Bonnardel, *Niche signals and transcription factors involved in tissue-resident macrophage development.* Cell Immunol, 2018. **330**: p. 43-53.
112. Athar Aziz, E.S., Sandrine Sarrazin, Michael H. Sieweke, *MafB/c-Maf Deficiency Enables Self-Renewal of Differentiated Functional Macrophages.* SCIENCE, 2009. **326**: p. 867-871.
113. Moriguchi, T., et al., *MafB is essential for renal development and F4/80 expression in macrophages.* Molecular and cellular biology, 2006. **26**(15): p. 5715-5727.
114. Wu, X., et al., *Transcription factor Zeb2 regulates commitment to plasmacytoid dendritic cell and monocyte fate.* Proceedings of the National Academy of Sciences, 2016. **113**(51): p. 14775-14780.
115. Zhang, D.E., et al., *The macrophage transcription factor PU.1 directs tissue-specific expression of the macrophage colony-stimulating factor receptor.* Mol Cell Biol, 1994. **14**(1): p. 373-81.
116. Imperato, M.R., et al., *The RUNX1-PU.1 axis in the control of hematopoiesis.* Int J Hematol, 2015. **101**(4): p. 319-29.
117. Soucie, E.L., et al., *Lineage-specific enhancers activate self-renewal genes in macrophages and embryonic stem cells.* Science, 2016. **351**(6274): p. aad5510.
118. Geissmann, F., et al., *Development of monocytes, macrophages, and dendritic cells.* Science, 2010. **327**(5966): p. 656-661.
119. Guilliams, M. and C.L. Scott, *Does niche competition determine the origin of tissue-resident macrophages?* Nat Rev Immunol, 2017. **17**(7): p. 451-460.
120. Lavin, Y., et al., *Regulation of macrophage development and function in peripheral tissues.* Nature Reviews Immunology, 2015. **15**(12): p. 731-744.
121. Sakai, M., et al., *Liver-Derived Signals Sequentially Reprogram Myeloid Enhancers to Initiate and Maintain Kupffer Cell Identity.* Immunity, 2019. **51**(4): p. 655-670.e8.
122. Scott, C.L., et al., *Bone marrow-derived monocytes give rise to self-renewing and fully differentiated Kupffer cells.* Nature communications, 2016. **7**(1): p. 1-10.
123. Haldar, M., et al., *Heme-mediated SPI-C induction promotes monocyte differentiation into iron-recycling macrophages.* Cell, 2014. **156**(6): p. 1223-1234.

124. Kurotaki, D., T. Uede, and T. Tamura, *Functions and development of red pulp macrophages.* Microbiol Immunol, 2015. **59**(2): p. 55-62.
125. Kohyama, M., et al., *Role for Spi-C in the development of red pulp macrophages and splenic iron homeostasis.* Nature, 2009. **457**(7227): p. 318-321.
126. Kageyama, T., et al., *Physiological and immunological barriers in the lung.* Semin Immunopathol, 2024. **45**(4-6): p. 533-547.
127. Hou, F., et al., *Diversity of Macrophages in Lung Homeostasis and Diseases.* Front Immunol, 2021. **12**: p. 753940.
128. Schyns, J., F. Bureau, and T. Marichal, *Lung Interstitial Macrophages: Past, Present, and Future.* J Immunol Res, 2018. **2018**: p. 5160794.
129. Kaplan, M.H., A.H. Coons, and H.W. Deane, *Localization of antigen in tissue cells: III. Cellular distribution of pneumococcal polysaccharides types II and III in the mouse.* The Journal of Experimental Medicine, 1950. **91**(1): p. 15-30.
130. Blusse van Oud Alblas, A., B. Van der Linden-Schrever, and R. Van Furth, *Origin and kinetics of pulmonary macrophages during an inflammatory reaction induced by intravenous administration of heat-killed bacillus Calmette-Guérin.* The Journal of experimental medicine, 1981. **154**(2): p. 235-252.
131. Cai, Y., et al., *In vivo characterization of alveolar and interstitial lung macrophages in rhesus macaques: implications for understanding lung disease in humans.* The Journal of Immunology, 2014. **192**(6): p. 2821-2829.
132. Landsman, L. and S. Jung, *Lung macrophages serve as obligatory intermediate between blood monocytes and alveolar macrophages.* The Journal of Immunology, 2007. **179**(6): p. 3488-3494.
133. Holt, P.G., et al., *Preparation of interstitial lung cells by enzymatic digestion of tissue slices: preliminary characterization by morphology and performance in functional assays.* Immunology, 1985. **54**(1): p. 139.
134. Cossarizza, A., et al., *Guidelines for the use of flow cytometry and cell sorting in immunological studies.* Eur J Immunol, 2017. **47**(10): p. 1584-1797.
135. Franke-Ullmann, G., et al., *Characterization of murine lung interstitial macrophages in comparison with alveolar macrophages in vitro.* The Journal of Immunology, 1996. **157**(7): p. 3097-3104.
136. Laskin, D.L., B. Weinberger, and J.D. Laskin, *Functional heterogeneity in liver and lung macrophages.* Journal of leukocyte biology, 2001. **70**(2): p. 163-170.
137. Tan, S.Y.S. and M.A. Krasnow, *Developmental origin of lung macrophage diversity.* Development, 2016. **143**(8): p. 1318-1327.
138. Sebring, R.J. and B.E. Lehnert, *Morphometric comparisons of rat alveolar macrophages, pulmonary interstitial macrophages, and blood monocytes.* Experimental lung research, 1992. **18**(4): p. 479-496.
139. Bedoret, D., et al., *Lung interstitial macrophages alter dendritic cell functions to prevent airway allergy in mice.* J Clin Invest, 2009. **119**(12): p. 3723-38.
140. Brody, A.R., et al., *Interstitial pulmonary macrophages produce platelet-derived growth factor that stimulates rat lung fibroblast proliferation in vitro.* Journal of leukocyte biology, 1992. **51**(6): p. 640-648.
141. Gibbings, S.L., et al., *Three unique interstitial macrophages in the murine lung at steady state.* American journal of respiratory cell and molecular biology, 2017. **57**(1): p. 66-76.
142. Kawano, H., et al., *IL-10-producing lung interstitial macrophages prevent neutrophilic asthma.* International immunology, 2016. **28**(10): p. 489-501.
143. Bharat, A., et al., *Flow Cytometry Reveals Similarities Between Lung Macrophages in Humans and Mice.* Am J Respir Cell Mol Biol, 2016. **54**(1): p. 147-9.

144. Sabatel, C., et al., *Exposure to bacterial CpG DNA protects from airway allergic inflammation by expanding regulatory lung interstitial macrophages.* Immunity, 2017. **46**(3): p. 457-473.
145. Evren, E., E. Ringqvist, and T. Willinger, *Origin and ontogeny of lung macrophages: from mice to humans.* Immunology, 2020. **160**(2): p. 126-138.
146. Hoppstädter, J., et al., *Differential cell reaction upon Toll-like receptor 4 and 9 activation in human alveolar and lung interstitial macrophages.* Respiratory research, 2010. **11**(1): p. 1-15.
147. Schyns, J., et al., *Non-classical tissue monocytes and two functionally distinct populations of interstitial macrophages populate the mouse lung.* Nat Commun, 2019. **10**(1): p. 3964.
148. Chakarov, S., et al., *Two distinct interstitial macrophage populations coexist across tissues in specific subtissular niches.* Science, 2019. **363**(6432).
149. Ginhoux, F. and M. Guilliams, *Tissue-resident macrophage ontogeny and homeostasis.* Immunity, 2016. **44**(3): p. 439-449.
150. Gomez Perdiguero, E., et al., *Tissue-resident macrophages originate from yolk-sac-derived erythro-myeloid progenitors.* Nature, 2015. **518**(7540): p. 547-551.
151. Yona, S., et al., *Fate mapping reveals origins and dynamics of monocytes and tissue macrophages under homeostasis.* Immunity, 2013. **38**(1): p. 79-91.
152. McQuattie-Pimentel, A.C., et al., *The lung microenvironment shapes a dysfunctional response of alveolar macrophages in aging.* J Clin Invest, 2021. **131**(4).
153. Johansson, A., et al., *Functional, morphological, and phenotypical differences between rat alveolar and interstitial macrophages.* American journal of respiratory cell and molecular biology, 1997. **16**(5): p. 582-588.
154. Gong, J.L., et al., *Interstitial lung macrophages interact with dendritic cells to present antigenic peptides derived from particulate antigens to T cells.* Immunology, 1994. **81**(3): p. 343.
155. Fathi, M., et al., *Functional and morphological differences between human alveolar and interstitial macrophages.* Exp Mol Pathol, 2001. **70**(2): p. 77-82.
156. Chelen, C.J., et al., *Human alveolar macrophages present antigen ineffectively due to defective expression of B7 costimulatory cell surface molecules.* J Clin Invest, 1995. **95**(3): p. 1415-21.
157. Tang, X.Z., et al., *Bronchus-associated macrophages efficiently capture and present soluble inhaled antigens and are capable of local Th2 cell activation.* Elife, 2022. **11**.
158. Yu, X., et al., *The Cytokine TGF-beta Promotes the Development and Homeostasis of Alveolar Macrophages.* Immunity, 2017. **47**(5): p. 903-912 e4.
159. Kulikauskaite, J. and A. Wack, *Teaching Old Dogs New Tricks? The Plasticity of Lung Alveolar Macrophage Subsets.* Trends Immunol, 2020. **41**(10): p. 864-877.
160. Pernet, E., et al., *Neonatal imprinting of alveolar macrophages via neutrophil-derived 12-HETE.* Nature, 2023. **614**(7948): p. 530-538.
161. Yao, Y., et al., *Histone deacetylase 3 controls lung alveolar macrophage development and homeostasis.* Nat Commun, 2020. **11**(1): p. 3822.
162. Ebina-Shibuya, R., et al., *The double knockout of Bach1 and Bach2 in mice reveals shared compensatory mechanisms in regulating alveolar macrophage function and lung surfactant homeostasis.* The Journal of Biochemistry, 2016. **160**(6): p. 333-344.
163. Dörr, D., et al., *C/EBPβ regulates lipid metabolism and Pparg isoform 2 expression in alveolar macrophages.* Sci Immunol, 2022. **7**(75): p. eabj0140.

164. Notarangelo, L.D. and I. Pessach, *Out of breath: GM-CSFRalpha mutations disrupt surfactant homeostasis.* J Exp Med, 2008. **205**(12): p. 2693-7.
165. Nakamura, A., et al., *Transcription repressor Bach2 is required for pulmonary surfactant homeostasis and alveolar macrophage function.* Journal of Experimental Medicine, 2013. **210**(11): p. 2191-2204.
166. Mohamed, S.H., et al., *CSF1R inhibition by PLX5622 reduces pulmonary fungal infection by depleting MHCII(hi) interstitial lung macrophages.* Mucosal Immunol, 2024. **17**(6): p. 1256-1272.
167. Vanneste, D., et al., *MafB-restricted local monocyte proliferation precedes lung interstitial macrophage differentiation.* Nat Immunol, 2023. **24**(5): p. 827-840.
168. Cuevas, V.D., et al., *MAFB Determines Human Macrophage Anti-Inflammatory Polarization: Relevance for the Pathogenic Mechanisms Operating in Multicentric Carpotarsal Osteolysis.* J Immunol, 2017. **198**(5): p. 2070-2081.
169. Kikuchi, K., et al., *Macrophages Switch Their Phenotype by Regulating Maf Expression during Different Phases of Inflammation.* J Immunol, 2018. **201**(2): p. 635-651.
170. Daassi, D., et al., *Differential expression patterns of MafB and c-Maf in macrophages in vivo and in vitro.* Biochem Biophys Res Commun, 2016. **473**(1): p. 118-124.
171. Tran, M.T.N., et al., *MafB is a critical regulator of complement component C1q.* Nat Commun, 2017. **8**(1): p. 1700.
172. Cao, S., et al., *The protooncogene c-Maf is an essential transcription factor for IL-10 gene expression in macrophages.* J Immunol, 2005. **174**(6): p. 3484-92.
173. Liu, M., et al., *Transcription factor c-Maf is a checkpoint that programs macrophages in lung cancer.* J Clin Invest, 2020. **130**(4): p. 2081-2096.
174. Zhou, B., et al., *The angiocrine Rspondin3 instructs interstitial macrophage transition via metabolic-epigenetic reprogramming and resolves inflammatory injury.* Nat Immunol, 2020. **21**(11): p. 1430-1443.
175. Liegeois, M., et al., *The interstitial macrophage: A long-neglected piece in the puzzle of lung immunity.* Cell Immunol, 2018. **330**: p. 91-96.
176. Li, X., et al., *Coordinated chemokine expression defines macrophage subsets across tissues.* Nat Immunol, 2024. **25**(6): p. 1110-1122.
177. Ural, B.B., et al., *Identification of a nerve-associated, lung-resident interstitial macrophage subset with distinct localization and immunoregulatory properties.* Sci Immunol, 2020. **5**(45).
178. Yu, Y.R., et al., *Flow Cytometric Analysis of Myeloid Cells in Human Blood, Bronchoalveolar Lavage, and Lung Tissues.* Am J Respir Cell Mol Biol, 2016. **54**(1): p. 13-24.
179. Hume, P.S., et al., *Localization of Macrophages in the Human Lung via Design-based Stereology.* Am J Respir Crit Care Med, 2020. **201**(10): p. 1209-1217.
180. Serbina, N.V. and E.G. Pamer, *Monocyte emigration from bone marrow during bacterial infection requires signals mediated by chemokine receptor CCR2.* Nat Immunol, 2006. **7**(3): p. 311-7.
181. Neyt, K., et al., *Tertiary lymphoid organs in infection and autoimmunity.* Trends Immunol, 2012. **33**(6): p. 297-305.
182. Libório-Ramos, S., et al., *Interstitial Macrophages Lead Early Stages of Bleomycin-Induced Lung Fibrosis and Induce Fibroblasts Activation.* Cells, 2023. **12**(3).
183. Venosa, A., et al., *Myeloid cell dynamics in bleomycin-induced pulmonary injury in mice; effects of anti-TNFα antibody.* Toxicol Appl Pharmacol, 2021. **417**: p. 115470.
184. Ogawa, T., et al., *Profibrotic properties of C1q(+) interstitial macrophages in silica-induced pulmonary fibrosis in mice.* Biochem Biophys Res Commun, 2022. **599**: p. 113-119.

185. Meziani, L., et al., *CSF1R inhibition prevents radiation pulmonary fibrosis by depletion of interstitial macrophages.* Eur Respir J, 2018. **51**(3).
186. Wang, S., et al., *Single-Cell RNA Sequencing Reveals Monocyte-Derived Interstitial Macrophages with a Pro-Fibrotic Phenotype in Bleomycin-Induced Pulmonary Fibrosis.* Int J Mol Sci, 2024. **25**(21).
187. David, C., et al., *The deadly dance of alveolar macrophages and influenza virus.* Eur Respir Rev, 2024. **33**(174).
188. Zuttion, M., et al., *Interstitial Macrophages Mediate Efferocytosis of Alveolar Epithelium during Influenza Infection.* Am J Respir Cell Mol Biol, 2024. **70**(3): p. 159-164.
189. Broug-Holub, E., et al., *Alveolar macrophages are required for protective pulmonary defenses in murine Klebsiella pneumonia: elimination of alveolar macrophages increases neutrophil recruitment but decreases bacterial clearance and survival.* Infect Immun, 1997. **65**(4): p. 1139-46.
190. Kooguchi, K., et al., *Role of alveolar macrophages in initiation and regulation of inflammation in Pseudomonas aeruginosa pneumonia.* Infect Immun, 1998. **66**(7): p. 3164-9.
191. Aegerter, H., B.N. Lambrecht, and C.V. Jakubzick, *Biology of lung macrophages in health and disease.* Immunity, 2022. **55**(9): p. 1564-1580.
192. Ruscitti, C., C. Radermecker, and T. Marichal, *Journey of monocytes and macrophages upon influenza A virus infection.* Curr Opin Virol, 2024. **66**: p. 101409.
193. Blank, T. and M. Prinz, *CatacLysMic specificity when targeting myeloid cells?* Eur J Immunol, 2016. **46**(6): p. 1340-2.
194. Miyake, Y., et al., *Protective role of macrophages in noninflammatory lung injury caused by selective ablation of alveolar epithelial type II Cells.* J Immunol, 2007. **178**(8): p. 5001-9.
195. McCubbrey, A.L., et al., *Promoter Specificity and Efficacy in Conditional and Inducible Transgenic Targeting of Lung Macrophages.* Front Immunol, 2017. **8**: p. 1618.
196. Fouda, A.Y., et al., *Utility of LysM-cre and Cdh5-cre Driver Mice in Retinal and Brain Research: An Imaging Study Using tdTomato Reporter Mouse.* Invest Ophthalmol Vis Sci, 2020. **61**(3): p. 51.
197. Vannella, K.M., et al., *Incomplete deletion of IL-4Rα by LysM(Cre) reveals distinct subsets of M2 macrophages controlling inflammation and fibrosis in chronic schistosomiasis.* PLoS Pathog, 2014. **10**(9): p. e1004372.
198. Bonifer, C. and D.A. Hume, *The transcriptional regulation of the Colony-Stimulating Factor 1 Receptor (csf1r) gene during hematopoiesis.* Front Biosci, 2008. **13**: p. 549-60.
199. Sahasrabuddhe, V. and H.S. Ghosh, *Cx3Cr1-Cre induction leads to microglial activation and IFN-1 signaling caused by DNA damage in early postnatal brain.* Cell Rep, 2022. **38**(3): p. 110252.
200. Parkhurst, C.N., et al., *Microglia promote learning-dependent synapse formation through brain-derived neurotrophic factor.* Cell, 2013. **155**(7): p. 1596-609.
201. Kaiser, T. and G. Feng, *Tmem119-EGFP and Tmem119-CreERT2 Transgenic Mice for Labeling and Manipulating Microglia.* eNeuro, 2019. **6**(4).
202. Ruan, C., et al., *A novel Tmem119-tdTomato reporter mouse model for studying microglia in the central nervous system.* Brain Behav Immun, 2020. **83**: p. 180-191.
203. Pillai, M.M., B. Hayes, and B. Torok-Storb, *Inducible transgenes under the control of the hCD68 promoter identifies mouse macrophages with a distribution that differs from the F4/80 - and CSF-1R-expressing populations.* Exp Hematol, 2009. **37**(12): p. 1387-92.

204. McCubbrey, A.L., et al., *Selective and inducible targeting of CD11b+ mononuclear phagocytes in the murine lung with hCD68-rtTA transgenic systems.* Am J Physiol Lung Cell Mol Physiol, 2016. **311**(1): p. L87-l100.
205. Schlitzer, A., et al., *IRF4 transcription factor-dependent CD11b+ dendritic cells in human and mouse control mucosal IL-17 cytokine responses.* Immunity, 2013. **38**(5): p. 970-83.
206. Deng, N., et al., *Anti-F4/80 treatment attenuates Th2 cell responses: Implications for the role of lung interstitial macrophages in the asthmatic mice.* Int Immunopharmacol, 2021. **99**: p. 108009.
207. Zhang, Y., et al., *CCR2(+) Inflammatory Monocytes Are Recruited to Yersinia pseudotuberculosis Pyogranulomas and Dictate Adaptive Responses at the Expense of Innate Immunity during Oral Infection.* Infect Immun, 2018. **86**(3).
208. Lutz, M. and P. Knaus, *Integration of the TGF-beta pathway into the cellular signalling network.* Cell Signal, 2002. **14**(12): p. 977-88.
209. Kelly, A., et al., *Regulation of Innate and Adaptive Immunity by TGFβ.* Adv Immunol, 2017. **134**: p. 137-233.
210. Morikawa, M., R. Derynck, and K. Miyazono, *TGF-β and the TGF-β Family: Context-Dependent Roles in Cell and Tissue Physiology.* Cold Spring Harb Perspect Biol, 2016. **8**(5).
211. Chang, H., C.W. Brown, and M.M. Matzuk, *Genetic Analysis of the Mammalian Transforming Growth Factor-β Superfamily.* Endocrine Reviews, 2002. **23**(6): p. 787-823.
212. Wrana, J.L., *Signaling by the TGFβ superfamily.* Cold Spring Harb Perspect Biol, 2013. **5**(10): p. a011197.
213. Memon, M.A., et al., *Transforming growth factor beta (TGFβ1, TGFβ2 and TGFβ3) null-mutant phenotypes in embryonic gonadal development.* Molecular and Cellular Endocrinology, 2008. **294**(1): p. 70-80.
214. Schmid, P., et al., *Differential expression of TGF beta 1, beta 2 and beta 3 genes during mouse embryogenesis.* Development, 1991. **111**(1): p. 117-30.
215. Khalil, N., *TGF-beta: from latent to active.* Microbes Infect, 1999. **1**(15): p. 1255-63.
216. Walton, K.L., et al., *Two distinct regions of latency-associated peptide coordinate stability of the latent transforming growth factor-beta1 complex.* J Biol Chem, 2010. **285**(22): p. 17029-37.
217. Hyytiäinen, M., C. Penttinen, and J. Keski-Oja, *Latent TGF-beta binding proteins: extracellular matrix association and roles in TGF-beta activation.* Crit Rev Clin Lab Sci, 2004. **41**(3): p. 233-64.
218. Tran, C., et al., *Development of a second-generation antiandrogen for treatment of advanced prostate cancer.* Science, 2009. **324**(5928): p. 787-90.
219. Ma, W., et al., *LRRC33 is a novel binding and potential regulating protein of TGF-β1 function in human acute myeloid leukemia cells.* PLoS One, 2019. **14**(10): p. e0213482.
220. Guo, M., et al., *Mini-Review: GARP, a Putative Potential Molecule in Tumor Immunosuppressive Environment.* Journal of Cancer Treatment and Diagnosis, 2019. **3**: p. 14-18.
221. Shi, M., et al., *Latent TGF-β structure and activation.* Nature, 2011. **474**(7351): p. 343-9.
222. Annes, J.P., D.B. Rifkin, and J.S. Munger, *The integrin alphaVbeta6 binds and activates latent TGFbeta3.* FEBS Lett, 2002. **511**(1-3): p. 65-8.
223. Wipff, P.J. and B. Hinz, *Integrins and the activation of latent transforming growth factor beta1 - an intimate relationship.* Eur J Cell Biol, 2008. **87**(8-9): p. 601-15.
224. Jobling, M.F., et al., *Isoform-specific activation of latent transforming growth factor beta (LTGF-beta) by reactive oxygen species.* Radiat Res, 2006. **166**(6): p. 839-48.

225. Munger, J.S., et al., *The integrin alpha v beta 6 binds and activates latent TGF beta 1: a mechanism for regulating pulmonary inflammation and fibrosis.* Cell, 1999. **96**(3): p. 319-28.
226. Tran, D.Q., et al., *GARP (LRRC32) is essential for the surface expression of latent TGF-beta on platelets and activated FOXP3+ regulatory T cells.* Proc Natl Acad Sci U S A, 2009. **106**(32): p. 13445-50.
227. Qin, Y., et al., *A Milieu Molecule for TGF-β Required for Microglia Function in the Nervous System.* Cell, 2018. **174**(1): p. 156-171.e16.
228. Breuss, J.M., et al., *Expression of the beta 6 integrin subunit in development, neoplasia and tissue repair suggests a role in epithelial remodeling.* J Cell Sci, 1995. **108 (Pt 6)**: p. 2241-51.
229. Mu, D., et al., *The integrin alpha(v)beta8 mediates epithelial homeostasis through MT1-MMP-dependent activation of TGF-beta1.* J Cell Biol, 2002. **157**(3): p. 493-507.
230. Kitamura, H., et al., *Mouse and human lung fibroblasts regulate dendritic cell trafficking, airway inflammation, and fibrosis through integrin αvβ8-mediated activation of TGF-β.* J Clin Invest, 2011. **121**(7): p. 2863-75.
231. Kelly, A., et al., *Human monocytes and macrophages regulate immune tolerance via integrin αvβ8-mediated TGFβ activation.* J Exp Med, 2018. **215**(11): p. 2725-2736.
232. Worthington, J.J., et al., *Intestinal dendritic cells specialize to activate transforming growth factor-β and induce Foxp3+ regulatory T cells via integrin αvβ8.* Gastroenterology, 2011. **141**(5): p. 1802-12.
233. Lainé, A., et al., *Regulatory T cells promote cancer immune-escape through integrin αvβ8-mediated TGF-β activation.* Nature Communications, 2021. **12**(1): p. 6228.
234. Takasaka, N., et al., *Integrin αvβ8-expressing tumor cells evade host immunity by regulating TGF-β activation in immune cells.* JCI Insight, 2018. **3**(20).
235. Tzavlaki, K. and A. Moustakas, *TGF-β Signaling.* Biomolecules, 2020. **10**(3).
236. Weiss, A. and L. Attisano, *The TGFbeta superfamily signaling pathway.* Wiley Interdiscip Rev Dev Biol, 2013. **2**(1): p. 47-63.
237. Kasai, H., et al., *TGF-beta1 induces human alveolar epithelial to mesenchymal cell transition (EMT).* Respir Res, 2005. **6**(1): p. 56.
238. Wrana, J.L., *TGF-beta receptors and signalling mechanisms.* Miner Electrolyte Metab, 1998. **24**(2-3): p. 120-30.
239. Wrana, J.L., et al., *TGF beta signals through a heteromeric protein kinase receptor complex.* Cell, 1992. **71**(6): p. 1003-14.
240. ten Dijke, P., et al., *Characterization of type I receptors for transforming growth factor-beta and activin.* Science, 1994. **264**(5155): p. 101-4.
241. Blobe, G.C., et al., *A novel mechanism for regulating transforming growth factor beta (TGF-beta) signaling. Functional modulation of type III TGF-beta receptor expression through interaction with the PDZ domain protein, GIPC.* J Biol Chem, 2001. **276**(43): p. 39608-17.
242. Vander Ark, A., J. Cao, and X. Li, *TGF-β receptors: In and beyond TGF-β signaling.* Cell Signal, 2018. **52**: p. 112-120.
243. Li, Q., et al., *Transforming growth factor β receptor type 1 is essential for female reproductive tract integrity and function.* PLoS Genet, 2011. **7**(10): p. e1002320.
244. Iwata, J., et al., *Modulation of noncanonical TGF-β signaling prevents cleft palate in Tgfbr2 mutant mice.* J Clin Invest, 2012. **122**(3): p. 873-85.
245. Compton, L.A., et al., *Coronary vessel development is dependent on the type III transforming growth factor beta receptor.* Circ Res, 2007. **101**(8): p. 784-91.

246. Deng, Z., et al., *TGF-beta signaling in health, disease, and therapeutics.* Signal Transduct Target Ther, 2024. **9**(1): p. 61.
247. Moustakas, A., S. Souchelnytskyi, and C.H. Heldin, *Smad regulation in TGF-beta signal transduction.* J Cell Sci, 2001. **114**(Pt 24): p. 4359-69.
248. Itoh, S., et al., *Signaling of transforming growth factor-beta family members through Smad proteins.* Eur J Biochem, 2000. **267**(24): p. 6954-67.
249. Miyazono, K., P. ten Dijke, and C.H. Heldin, *TGF-beta signaling by Smad proteins.* Adv Immunol, 2000. **75**: p. 115-57.
250. Morén, A., et al., *Degradation of the tumor suppressor Smad4 by WW and HECT domain ubiquitin ligases.* J Biol Chem, 2005. **280**(23): p. 22115-23.
251. Wrzesinski, S.H., Y.Y. Wan, and R.A. Flavell, *Transforming growth factor-beta and the immune response: implications for anticancer therapy.* Clin Cancer Res, 2007. **13**(18 Pt 1): p. 5262-70.
252. Letterio, J.J. and A.B. Roberts, *Regulation of immune responses by TGF-beta.* Annu Rev Immunol, 1998. **16**: p. 137-61.
253. Halwani, R., et al., *Role of transforming growth factor-β in airway remodeling in asthma.* Am J Respir Cell Mol Biol, 2011. **44**(2): p. 127-33.
254. Leach, H.G., et al., *Endothelial cells recruit macrophages and contribute to a fibrotic milieu in bleomycin lung injury.* Am J Respir Cell Mol Biol, 2013. **49**(6): p. 1093-101.
255. Bartram, U. and C.P. Speer, *The role of transforming growth factor beta in lung development and disease.* Chest, 2004. **125**(2): p. 754-65.
256. Xu, J., S. Lamouille, and R. Derynck, *TGF-beta-induced epithelial to mesenchymal transition.* Cell Res, 2009. **19**(2): p. 156-72.
257. Kahata, K., V. Maturi, and A. Moustakas, *TGF-β Family Signaling in Ductal Differentiation and Branching Morphogenesis.* Cold Spring Harb Perspect Biol, 2018. **10**(3).
258. Saito, A., M. Horie, and T. Nagase, *TGF-β Signaling in Lung Health and Disease.* Int J Mol Sci, 2018. **19**(8).
259. Gu, W., et al., *Smooth muscle cells differentiated from mesenchymal stem cells are regulated by microRNAs and suitable for vascular tissue grafts.* J Biol Chem, 2018. **293**(21): p. 8089-8102.
260. Hu, B., Z. Wu, and S.H. Phan, *Smad3 mediates transforming growth factor-beta-induced alpha-smooth muscle actin expression.* Am J Respir Cell Mol Biol, 2003. **29**(3 Pt 1): p. 397-404.
261. Kim, K.K., et al., *Alveolar epithelial cell mesenchymal transition develops in vivo during pulmonary fibrosis and is regulated by the extracellular matrix.* Proc Natl Acad Sci U S A, 2006. **103**(35): p. 13180-5.
262. Guo, W., et al., *Abrogation of TGF-beta1-induced fibroblast-myofibroblast differentiation by histone deacetylase inhibition.* Am J Physiol Lung Cell Mol Physiol, 2009. **297**(5): p. L864-70.
263. Chen, Y., Y. Dong, and X. Du, *Lung development: AT1 and AT2 property.* BIOCELL, 2019. **43**: p. 1-5.
264. Zhao, L., M. Yee, and M.A. O'Reilly, *Transdifferentiation of alveolar epithelial type II to type I cells is controlled by opposing TGF-β and BMP signaling.* Am J Physiol Lung Cell Mol Physiol, 2013. **305**(6): p. L409-18.
265. Callaway, D.A., et al., *TGF-β controls alveolar type 1 epithelial cell plasticity and alveolar matrisome gene transcription in mice.* J Clin Invest, 2024. **134**(6).
266. Correll, K.A., et al., *TGF beta inhibits expression of SP-A, SP-B, SP-C, but not SP-D in human alveolar type II cells.* Biochemical and Biophysical Research Communications, 2018. **499**(4): p. 843-848.

267. Grande, J.P., *Role of transforming growth factor-beta in tissue injury and repair.* Proc Soc Exp Biol Med, 1997. **214**(1): p. 27-40.
268. Fine, A. and R.H. Goldstein, *The effect of transforming growth factor-beta on cell proliferation and collagen formation by lung fibroblasts.* J Biol Chem, 1987. **262**(8): p. 3897-902.
269. Clarke, D.L., et al., *Matrix regulation of idiopathic pulmonary fibrosis: the role of enzymes.* Fibrogenesis & Tissue Repair, 2013. **6**(1): p. 20.
270. Cutroneo, K.R., *Gene therapy for tissue regeneration.* J Cell Biochem, 2003. **88**(2): p. 418-25.
271. Morty, R.E., M. Königshoff, and O. Eickelberg, *Transforming growth factor-beta signaling across ages: from distorted lung development to chronic obstructive pulmonary disease.* Proc Am Thorac Soc, 2009. **6**(7): p. 607-13.
272. Dalla, E., et al., *Lung-resident alveolar macrophages regulate the timing of breast cancer metastasis.* Cell, 2024. **187**(23): p. 6631-6648.e20.
273. Riemondy, K.A., et al., *Single cell RNA sequencing identifies TGFβ as a key regenerative cue following LPS-induced lung injury.* JCI Insight, 2019. **5**(8).
274. Gauthier, T., et al., *TGF-β uncouples glycolysis and inflammation in macrophages and controls survival during sepsis.* Sci Signal, 2023. **16**(797): p. eade0385.
275. Kraik, K., et al., *The Role of Transforming Growth Factor-β (TGF-β) in Asthma and Chronic Obstructive Pulmonary Disease (COPD).* Cells, 2024. **13**(15).
276. Moore, B., R.F. Murphy, and D.K. Agrawal, *Interaction of tgf-beta with immune cells in airway disease.* Curr Mol Med, 2008. **8**(5): p. 427-36.
277. Fernandez, I.E. and O. Eickelberg, *The impact of TGF-β on lung fibrosis: from targeting to biomarkers.* Proc Am Thorac Soc, 2012. **9**(3): p. 111-6.
278. Ye, Z. and Y. Hu, *TGF-β1: Gentlemanly orchestrator in idiopathic pulmonary fibrosis (Review).* Int J Mol Med, 2021. **48**(1).
279. Khalil, N. and A.H. Greenberg, *The Role of TGF-β in Pulmonary Fibrosis*, in *Ciba Foundation Symposium 157 - Clinical Applications of TGF-β*. 2007. p. 194-211.
280. Coward, W.R., G. Saini, and G. Jenkins, *The pathogenesis of idiopathic pulmonary fibrosis.* Ther Adv Respir Dis, 2010. **4**(6): p. 367-88.
281. Thomas, B.J., et al., *In the Shadow of Fibrosis: Innate Immune Suppression Mediated by Transforming Growth Factor-β.* Am J Respir Cell Mol Biol, 2016. **55**(6): p. 759-766.
282. Aschner, Y. and G.P. Downey, *Transforming Growth Factor-β: Master Regulator of the Respiratory System in Health and Disease.* Am J Respir Cell Mol Biol, 2016. **54**(5): p. 647-55.
283. Khalil, N., et al., *Regulation of alveolar macrophage transforming growth factor-beta secretion by corticosteroids in bleomycin-induced pulmonary inflammation in the rat.* J Clin Invest, 1993. **92**(4): p. 1812-8.
284. Cakarova, L., et al., *Macrophage tumor necrosis factor-alpha induces epithelial expression of granulocyte-macrophage colony-stimulating factor: impact on alveolar epithelial repair.* Am J Respir Crit Care Med, 2009. **180**(6): p. 521-32.
285. Bhaskaran, M., et al., *Trans-differentiation of alveolar epithelial type II cells to type I cells involves autocrine signaling by transforming growth factor beta 1 through the Smad pathway.* J Biol Chem, 2007. **282**(6): p. 3968-76.

286. Feng, M., et al., *Ex vivo induced regulatory T cells regulate inflammatory response of Kupffer cells by TGF-beta and attenuate liver ischemia reperfusion injury.* Int Immunopharmacol, 2012. **12**(1): p. 189-96.
287. Qian, J., et al., *Mechanism of TGF-β1 inhibiting Kupffer cell immune responses in cholestatic cirrhosis.* Exp Ther Med, 2020. **20**(2): p. 1541-1549.
288. Dewidar, B., et al., *TGF-β in Hepatic Stellate Cell Activation and Liver Fibrogenesis-Updated 2019.* Cells, 2019. **8**(11).
289. Zhang, X., et al., *TGF-β1-induced transcription factor networks in Langerhans cell development and maintenance.* Allergy, 2016. **71**(6): p. 758-764.
290. Borkowski, T.A., et al., *A role for endogenous transforming growth factor beta 1 in Langerhans cell biology: the skin of transforming growth factor beta 1 null mice is devoid of epidermal Langerhans cells.* J Exp Med, 1996. **184**(6): p. 2417-22.
291. Thomas, R.M., et al., *Appearance of Langerhans cells in the epidermis of Tgfb1(-/-) SCID mice: paracrine and autocrine effects of transforming growth factor-beta 1 and -beta 2(1).* J Invest Dermatol, 2001. **117**(6): p. 1574-80.
292. Tada, Y., et al., *Transforming growth factor-beta up-regulates CD40-engaged IL-12 production of mouse Langerhans cells.* Eur J Immunol, 2001. **31**(1): p. 294-300.
293. Kubatzky, K.F., F. Uhle, and T. Eigenbrod, *From macrophage to osteoclast - How metabolism determines function and activity.* Cytokine, 2018. **112**: p. 102-115.
294. Karst, M., et al., *Roles of stromal cell RANKL, OPG, and M-CSF expression in biphasic TGF-beta regulation of osteoclast differentiation.* J Cell Physiol, 2004. **200**(1): p. 99-106.
295. Yan, T., et al., *Regulation of osteoclastogenesis and RANK expression by TGF-beta1.* J Cell Biochem, 2001. **83**(2): p. 320-5.
296. Lee, B., et al., *A dual role of TGF-β in human osteoclast differentiation mediated by Smad1 versus Smad3 signaling.* Immunology Letters, 2019. **206**: p. 33-40.
297. Sells Galvin, R.J., et al., *TGF-beta enhances osteoclast differentiation in hematopoietic cell cultures stimulated with RANKL and M-CSF.* Biochem Biophys Res Commun, 1999. **265**(1): p. 233-9.
298. Crane, J.L. and X. Cao, *Bone marrow mesenchymal stem cells and TGF-β signaling in bone remodeling.* J Clin Invest, 2014. **124**(2): p. 466-72.
299. Weivoda, M.M., et al., *Osteoclast TGF-β Receptor Signaling Induces Wnt1 Secretion and Couples Bone Resorption to Bone Formation.* J Bone Miner Res, 2016. **31**(1): p. 76-85.
300. Schridde, A., et al., *Tissue-specific differentiation of colonic macrophages requires TGFβ receptor-mediated signaling.* Mucosal Immunol, 2017. **10**(6): p. 1387-1399.
301. Bain, C.C. and A. Schridde, *Origin, Differentiation, and Function of Intestinal Macrophages.* Front Immunol, 2018. **9**: p. 2733.
302. Smith, P.D., et al., *Intestinal macrophages and response to microbial encroachment.* Mucosal Immunol, 2011. **4**(1): p. 31-42.
303. Li, J., et al., *Myeloid TGF-β signaling contributes to colitis-associated tumorigenesis in mice.* Carcinogenesis, 2013. **34**(9): p. 2099-108.
304. Maheshwari, A., et al., *TGF-β2 suppresses macrophage cytokine production and mucosal inflammatory responses in the developing intestine.* Gastroenterology, 2011. **140**(1): p. 242-53.
305. Jarry, A., et al., *Loss of interleukin-10 or transforming growth factor β signaling in the human colon initiates a T-helper 1 response via distinct pathways.* Gastroenterology, 2011. **141**(5): p. 1887-96.e1-2.

306. Prise, I.E., et al., *CD163 and Tim-4 identify resident intestinal macrophages across sub-tissular regions that are spatially regulated by TGF-β.* bioRxiv, 2023: p. 2023.08.21.553672.
307. Shaw, T.N., et al., *Tissue-resident macrophages in the intestine are long lived and defined by Tim-4 and CD4 expression.* J Exp Med, 2018. **215**(6): p. 1507-1518.
308. Viola, M.F., et al., *Dedicated macrophages organize and maintain the enteric nervous system.* Nature, 2023. **618**(7966): p. 818-826.
309. De Schepper, S., et al., *Muscularis macrophages: Key players in intestinal homeostasis and disease.* Cell Immunol, 2018. **330**: p. 142-150.
310. Kolter, J., et al., *A Subset of Skin Macrophages Contributes to the Surveillance and Regeneration of Local Nerves.* Immunity, 2019. **50**(6): p. 1482-1497.e7.
311. Kolter, J., K. Kierdorf, and P. Henneke, *Origin and Differentiation of Nerve-Associated Macrophages.* The Journal of Immunology, 2020. **204**(2): p. 271-279.
312. Kolter, J., et al., *Sensory neurons shape macrophage identity via TGF-β signalling.* bioRxiv, 2025: p. 2025.02.06.635770.
313. Li, L., et al., *TGF-β Signaling in Microglia: A Key Regulator of Development, Homeostasis and Reactivity.* Biomedicines, 2024. **12**(11).
314. Barry-Carroll, L. and D. Gomez-Nicola, *The molecular determinants of microglial developmental dynamics.* Nature Reviews Neuroscience, 2024. **25**(6): p. 414-427.
315. Zhang, S.Z., et al., *NG2 glia regulate brain innate immunity via TGF-β2/TGFBR2 axis.* BMC Med, 2019. **17**(1): p. 204.
316. Spittau, B., N. Dokalis, and M. Prinz, *The Role of TGFβ Signaling in Microglia Maturation and Activation.* Trends Immunol, 2020. **41**(9): p. 836-848.
317. Zhang, J., et al., *Priming of microglia with IFN-γ impairs adult hippocampal neurogenesis and leads to depression-like behaviors and cognitive defects.* Glia, 2020. **68**(12): p. 2674-2692.
318. Noh, M.Y., et al., *Mesenchymal Stem Cells Modulate the Functional Properties of Microglia via TGF-β Secretion.* Stem Cells Transl Med, 2016. **5**(11): p. 1538-1549.
319. Butovsky, O., et al., *Identification of a unique TGF-β-dependent molecular and functional signature in microglia.* Nat Neurosci, 2014. **17**(1): p. 131-43.
320. Campbell, M.G., et al., *Cryo-EM Reveals Integrin-Mediated TGF-β Activation without Release from Latent TGF-β.* Cell, 2020. **180**(3): p. 490-501.e16.
321. Peterson, A.J. and M.B. O'Connor, *Lean on Me: Cell-Cell Interactions Release TGF-β for Local Consumption Only.* Cell, 2018. **174**(1): p. 18-20.
322. McKinsey, G.L., et al., *Radial glia promote microglial development through integrin α(V)β(8) -TGFβ1 signaling.* bioRxiv, 2023.
323. Ma, W., et al., *Absence of TGFβ signaling in retinal microglia induces retinal degeneration and exacerbates choroidal neovascularization.* Elife, 2019. **8**.
324. Stolfi, C., et al., *Role of TGF-Beta and Smad7 in Gut Inflammation, Fibrosis and Cancer.* Biomolecules, 2021. **11**(1): p. 17.
325. Liu, M., et al., *Transcription factor c-Maf is essential for IL-10 gene expression in B cells.* Scand J Immunol, 2018. **88**(3): p. e12701.
326. Hsia, C.C., D.M. Hyde, and E.R. Weibel, *Lung Structure and the Intrinsic Challenges of Gas Exchange.* Compr Physiol, 2016. **6**(2): p. 827-95.

327. Liao, J.K., *Linking endothelial dysfunction with endothelial cell activation.* J Clin Invest, 2013. **123**(2): p. 540-1.
328. Newman, P.J., *The role of PECAM-1 in vascular cell biology.* Ann N Y Acad Sci, 1994. **714**: p. 165-74.
329. Vecchi, A., et al., *Monoclonal antibodies specific for endothelial cells of mouse blood vessels. Their application in the identification of adult and embryonic endothelium.* Eur J Cell Biol, 1994. **63**(2): p. 247-54.
330. Vittet, D., et al., *Embryonic stem cells differentiate in vitro to endothelial cells through successive maturation steps.* Blood, 1996. **88**(9): p. 3424-31.
331. Nakano, H., K. Nakano, and D.N. Cook, *Isolation and Purification of Epithelial and Endothelial Cells from Mouse Lung.* Methods Mol Biol, 2018. **1799**: p. 59-69.
332. Schupp, J.C., et al., *Integrated Single-Cell Atlas of Endothelial Cells of the Human Lung.* Circulation, 2021. **144**(4): p. 286-302.
333. Yuan, L., et al., *ETS-related gene (ERG) controls endothelial cell permeability via transcriptional regulation of the claudin 5 (CLDN5) gene.* J Biol Chem, 2012. **287**(9): p. 6582-91.
334. Gillich, A., et al., *Capillary cell-type specialization in the alveolus.* Nature, 2020. **586**(7831): p. 785-789.
335. Favre, C.J., et al., *Expression of genes involved in vascular development and angiogenesis in endothelial cells of adult lung.* Am J Physiol Heart Circ Physiol, 2003. **285**(5): p. H1917-38.
336. dela Paz, N.G. and P.A. D'Amore, *Arterial versus venous endothelial cells.* Cell Tissue Res, 2009. **335**(1): p. 5-16.
337. Krüger-Genge, A., et al., *Vascular Endothelial Cell Biology: An Update.* Int J Mol Sci, 2019. **20**(18).
338. Wang, H.U., Z.F. Chen, and D.J. Anderson, *Molecular distinction and angiogenic interaction between embryonic arteries and veins revealed by ephrin-B2 and its receptor Eph-B4.* Cell, 1998. **93**(5): p. 741-53.
339. Trivedi, A. and H.O. Reed, *The lymphatic vasculature in lung function and respiratory disease.* Front Med (Lausanne), 2023. **10**: p. 1118583.
340. Davis, J.M., et al., *Lymphatic endothelial differentiation in pulmonary lymphangioleiomyomatosis cells.* J Histochem Cytochem, 2013. **61**(8): p. 580-90.
341. Kretschmer, S., et al., *Visualization of intrapulmonary lymph vessels in healthy and inflamed murine lung using CD90/Thy-1 as a marker.* PLoS One, 2013. **8**(2): p. e55201.
342. He, H., et al., *Endothelial cells provide an instructive niche for the differentiation and functional polarization of M2-like macrophages.* Blood, 2012. **120**(15): p. 3152-62.
343. Brissette, M.J., et al., *MFG-E8 released by apoptotic endothelial cells triggers anti-inflammatory macrophage reprogramming.* PLoS One, 2012. **7**(4): p. e36368.
344. Valluru, M., et al., *Transforming Growth Factor-β and Endoglin Signaling Orchestrate Wound Healing.* Front Physiol, 2011. **2**: p. 89.
345. McCourtie, A.S., et al., *Alveolar macrophage secretory products augment the response of rat pulmonary artery endothelial cells to hypoxia and reoxygenation.* Ann Thorac Surg, 2008. **85**(3): p. 1056-60.
346. Dick, S.A., et al., *Three tissue resident macrophage subsets coexist across organs with conserved origins and life cycles.* Sci Immunol, 2022. **7**(67): p. eabf7777.
347. Bayerl, F., et al., *Guidelines for visualization and analysis of DC in tissues using multiparameter fluorescence microscopy imaging methods.* Eur J Immunol, 2023. **53**(11): p. e2249923.
348. Stoltzfus, C.R., et al., *CytoMAP: A Spatial Analysis Toolbox Reveals Features of Myeloid Cell Organization in Lymphoid Tissues.* Cell Rep, 2020. **31**(3): p. 107523.

349. Crowley, G., et al., *Quantitative lung morphology: semi-automated measurement of mean linear intercept.* BMC Pulm Med, 2019. **19**(1): p. 206.
350. Grillet, P.E., et al., *Diastolic Cardiomyopathy Secondary to Experimentally Induced Exacerbated Emphysema.* Am J Respir Cell Mol Biol, 2023. **69**(2): p. 230-241.
351. Singh, B., et al., *Strain-specific differences in perivascular inflammation in lungs in two murine models of allergic airway inflammation.* Clin Exp Immunol, 2005. **141**(2): p. 223-9.
352. Wang, P.M., et al., *Direct leukocyte migration across pulmonary arterioles and venules into the perivascular interstitium of murine lungs during bleomycin injury and repair.* Am J Pathol, 2011. **178**(6): p. 2560-72.
353. Browaeys, R., W. Saelens, and Y. Saeys, *NicheNet: modeling intercellular communication by linking ligands to target genes.* Nature methods, 2020. **17**(2): p. 159-162.
354. Krzywinski, M., et al., *Circos: an information aesthetic for comparative genomics.* Genome Res, 2009. **19**(9): p. 1639-45.
355. Wrana, J.L., et al., *Mechanism of activation of the TGF-beta receptor.* Nature, 1994. **370**(6488): p. 341-7.
356. Grant, D., et al., *Comprehensive phenotyping of endothelial cells using flow cytometry 1: Murine.* Cytometry A, 2021. **99**(3): p. 251-256.
357. Li, Q., et al., *Activation of mTORC1 by LSECtin in macrophages directs intestinal repair in inflammatory bowel disease.* Cell Death Dis, 2020. **11**(10): p. 918.
358. Black, S., et al., *CODEX multiplexed tissue imaging with DNA-conjugated antibodies.* Nature Protocols, 2021. **16**(8): p. 3802-3835.
359. Goltsev, Y., et al., *Deep Profiling of Mouse Splenic Architecture with CODEX Multiplexed Imaging.* Cell, 2018. **174**(4): p. 968-981.e15.
360. Hollander, M.C., et al., *Attenuation of Myeloid-Specific TGFβ Signaling Induces Inflammatory Cerebrovascular Disease and Stroke.* Circ Res, 2017. **121**(12): p. 1360-1369.
361. Sharma, G. and J. Goodwin, *Effect of aging on respiratory system physiology and immunology.* Clin Interv Aging, 2006. **1**(3): p. 253-60.
362. Hamada, M., et al., *Role of MafB in macrophages.* Exp Anim, 2020. **69**(1): p. 1-10.
363. Lund, H., et al., *Fatal demyelinating disease is induced by monocyte-derived macrophages in the absence of TGF-β signaling.* Nat Immunol, 2018. **19**(5): p. 1-7.
364. Sheridan, G.K. and K.J. Murphy, *Neuron-glia crosstalk in health and disease: fractalkine and CX3CR1 take centre stage.* Open Biol, 2013. **3**(12): p. 130181.
365. Chen, S., et al., *TGF-beta1 upregulates CX3CR1 expression and inhibits fractalkine-stimulated signaling in rat microglia.* J Neuroimmunol, 2002. **133**(1-2): p. 46-55.
366. Attaai, A., et al., *Postnatal maturation of microglia is associated with alternative activation and activated TGFβ signaling.* Glia, 2018. **66**(8): p. 1695-1708.
367. Angelidis, I., et al., *An atlas of the aging lung mapped by single cell transcriptomics and deep tissue proteomics.* Nat Commun, 2019. **10**(1): p. 963.
368. Lee, Y.S., et al., *CX(3)CR1 differentiates F4/80(low) monocytes into pro-inflammatory F4/80(high) macrophages in the liver.* Sci Rep, 2018. **8**(1): p. 15076.
369. Hume, D.A., et al., *The effect of human recombinant macrophage colony-stimulating factor (CSF-1) on the murine mononuclear phagocyte system in vivo.* J Immunol, 1988. **141**(10): p. 3405-9.

370. Irvine, K.M., et al., *Analysis of the impact of CSF-1 administration in adult rats using a novel Csf1r-mApple reporter gene.* J Leukoc Biol, 2020. **107**(2): p. 221-235.
371. Ohno, M., et al., *Fluid shear stress induces endothelial transforming growth factor beta-1 transcription and production. Modulation by potassium channel blockade.* J Clin Invest, 1995. **95**(3): p. 1363-9.
372. Hawker, J., et al., *Endothelial Cells Express Activin A which may serve as an antagonist to TGFβ binding to Activin-Like Kinase 1 Receptor.* The FASEB Journal, 2020. **34**(S1): p. 1-1.
373. Vannella, K.M. and T.A. Wynn, *Mechanisms of Organ Injury and Repair by Macrophages.* Annu Rev Physiol, 2017. **79**: p. 593-617.
374. Kang, Y., et al., *Enhanced tumorigenesis and reduced transforming growth factor-beta type II receptor in lung tumors from mice with reduced gene dosage of transforming growth factor-beta1.* Mol Carcinog, 2000. **29**(2): p. 112-26.
375. Zhang, H.Y., et al., *Lung fibroblast alpha-smooth muscle actin expression and contractile phenotype in bleomycin-induced pulmonary fibrosis.* Am J Pathol, 1996. **148**(2): p. 527-37.
376. Sato, Y., et al., *The mechanism for the activation of latent TGF-beta during co-culture of endothelial cells and smooth muscle cells: cell-type specific targeting of latent TGF-beta to smooth muscle cells.* J Cell Biol, 1993. **123**(5): p. 1249-54.
377. Giacomini, M.M., et al., *Epithelial cells utilize cortical actin/myosin to activate latent TGF-β through integrin αvβ6-dependent physical force.* Experimental Cell Research, 2012. **318**(6): p. 716-722.
378. Wipff, P.J., et al., *Myofibroblast contraction activates latent TGF-beta1 from the extracellular matrix.* J Cell Biol, 2007. **179**(6): p. 1311-23.
379. Zerr, P., et al., *Sirt1 regulates canonical TGF-β signalling to control fibroblast activation and tissue fibrosis.* Ann Rheum Dis, 2016. **75**(1): p. 226-33.
380. Ahamed, J., et al., *In vitro and in vivo evidence for shear-induced activation of latent transforming growth factor-beta1.* Blood, 2008. **112**(9): p. 3650-60.
381. Yehualaeshet, T., et al., *Activation of rat alveolar macrophage-derived latent transforming growth factor beta-1 by plasmin requires interaction with thrombospondin-1 and its cell surface receptor, CD36.* Am J Pathol, 1999. **155**(3): p. 841-51.
382. Xu, X., et al., *Transforming growth factor-β in stem cells and tissue homeostasis.* Bone Research, 2018. **6**(1): p. 2.
383. Dallas, S.L., et al., *Proteolysis of latent transforming growth factor-beta (TGF-beta)-binding protein-1 by osteoclasts. A cellular mechanism for release of TGF-beta from bone matrix.* J Biol Chem, 2002. **277**(24): p. 21352-60.
384. Blakytny, R., et al., *Latent TGF-beta1 activation by platelets.* J Cell Physiol, 2004. **199**(1): p. 67-76.
385. Liénart, S., et al., *Structural basis of latent TGF-β1 presentation and activation by GARP on human regulatory T cells.* Science, 2018. **362**(6417): p. 952-956.
386. Amarnath, S., et al., *Endogenous TGF-beta activation by reactive oxygen species is key to Foxp3 induction in TCR-stimulated and HIV-1-infected human CD4+CD25- T cells.* Retrovirology, 2007. **4**: p. 57.
387. Metelli, A., et al., *Immunoregulatory functions and the therapeutic implications of GARP-TGF-β in inflammation and cancer.* J Hematol Oncol, 2018. **11**(1): p. 24.
388. Lecomte, S., et al., *Therapeutic activity of GARP:TGF-β1 blockade in murine primary myelofibrosis.* Blood, 2023. **141**(5): p. 490-502.

389. Stockis, J., O. Dedobbeleer, and S. Lucas, *Role of GARP in the activation of latent TGF-β1.* Mol Biosyst, 2017. **13**(10): p. 1925-1935.
390. Cuende, J., et al., *Monoclonal antibodies against GARP/TGF-β1 complexes inhibit the immunosuppressive activity of human regulatory T cells in vivo.* Sci Transl Med, 2015. **7**(284): p. 284ra56.
391. Richeldi, L., et al., *Efficacy and safety of nintedanib in idiopathic pulmonary fibrosis.* N Engl J Med, 2014. **370**(22): p. 2071-82.
392. King, T.E., Jr., et al., *A phase 3 trial of pirfenidone in patients with idiopathic pulmonary fibrosis.* N Engl J Med, 2014. **370**(22): p. 2083-92.
393. Sicard, D., et al., *Aging and anatomical variations in lung tissue stiffness.* Am J Physiol Lung Cell Mol Physiol, 2018. **314**(6): p. L946-l955.
394. Kononov, S., et al., *Roles of mechanical forces and collagen failure in the development of elastase-induced emphysema.* Am J Respir Crit Care Med, 2001. **164**(10 Pt 1): p. 1920-6.
395. Meiners, S., O. Eickelberg, and M. Königshoff, *Hallmarks of the ageing lung.* Eur Respir J, 2015. **45**(3): p. 807-27.
396. Mack, S.M., et al. *Lung Anatomy and Aging*. 2020.
397. Lalley, P.M., *The aging respiratory system—Pulmonary structure, function and neural control.* Respiratory Physiology & Neurobiology, 2013. **187**(3): p. 199-210.
398. Lee, S., S. Yim, and H.C. Kim, *Aging of the respiratory system.* Kosin Medical Journal, 2016. **31**: p. 11.
399. Bailey, K.L., *Aging Diminishes Mucociliary Clearance of the Lung.* Adv Geriatr Med Res, 2022. **4**(2).
400. Kuek, L.E. and R.J. Lee, *First contact: the role of respiratory cilia in host-pathogen interactions in the airways.* American Journal of Physiology-Lung Cellular and Molecular Physiology, 2020. **319**(4): p. L603-L619.
401. Posner, J.D., et al., *Exercise capacity in the elderly.* Am J Cardiol, 1986. **57**(5): p. 52c-58c.
402. Cho, S.J. and H.W. Stout-Delgado, *Aging and Lung Disease.* Annu Rev Physiol, 2020. **82**: p. 433-459.
403. Dai, C., et al., *The association between small airway dysfunction and aging: a cross-sectional analysis from the ECOPD cohort.* Respir Res, 2022. **23**(1): p. 229.
404. Pardo, A. and M. Selman, *Lung Fibroblasts, Aging, and Idiopathic Pulmonary Fibrosis.* Ann Am Thorac Soc, 2016. **13 Suppl 5**: p. S417-s421.
405. Moroguchi, A., et al., *Interleukin-10 suppresses proliferation and remodeling of extracellular matrix of cultured human skin fibroblasts.* Eur Surg Res, 2004. **36**(1): p. 39-44.
406. Reitamo, S., et al., *Interleukin-10 modulates type I collagen and matrix metalloprotease gene expression in cultured human skin fibroblasts.* J Clin Invest, 1994. **94**(6): p. 2489-92.
407. Marangoni, R.G., et al., *Adiponectin is an endogenous anti-fibrotic mediator and therapeutic target.* Sci Rep, 2017. **7**(1): p. 4397.
408. Crestani, B., et al., *Hepatocyte growth factor and lung fibrosis.* Proc Am Thorac Soc, 2012. **9**(3): p. 158-63.
409. Pilling, D. and R.H. Gomer, *Persistent lung inflammation and fibrosis in serum amyloid P component (APCs-/-) knockout mice.* PLoS One, 2014. **9**(4): p. e93730.
410. Nakanishi, K., et al., *Involvement of endothelial apoptosis underlying chronic obstructive pulmonary disease-like phenotype in adiponectin-null mice: implications for therapy.* Am J Respir Crit Care Med, 2011. **183**(9): p. 1164-75.
411. Jeansson, M., et al., *Angiopoietin-1 is essential in mouse vasculature during development and in response to injury.* J Clin Invest, 2011. **121**(6): p. 2278-89.

412. Monticelli, L.A., et al., *Innate lymphoid cells promote lung-tissue homeostasis after infection with influenza virus.* Nature Immunology, 2011. **12**(11): p. 1045-1054.
413. Saiga, H., et al., *Lipocalin 2-dependent inhibition of mycobacterial growth in alveolar epithelium.* J Immunol, 2008. **181**(12): p. 8521-7.
414. Dobbertin, A., et al., *Neurons promote macrophage proliferation by producing transforming growth factor-beta2.* J Neurosci, 1997. **17**(14): p. 5305-15.

PUBLICATION LIST

PUBLICATION LIST

- **Wen Peng**, Domien Vanneste, David Bejarano, Joan Abinet, Margot Meunier, Coraline Radermecker, Fabienne Perin, Didier Cataldo, Fabrice Bureau, Andreas Schlitzer, Qiang Bai, Thomas Marichal. Endothelial-driven TGFβ signaling supports lung interstitial macrophage development from monocytes. ***Science Immunology***. 2025; 10.1126/sciimmunol.adr4977.

- Domien Vanneste, Qiang Bai, Shakir Hasan, **Wen Peng**, Dimitri Pirottin, Joey Schyns, Pauline Maréchal, Cecilia Ruscitti, Margot Meunier, Zhaoyuan Liu, Céline Legrand, Laurence Fievez, Florent Ginhoux, Coraline Radermecker, Fabrice Bureau, Thomas Marichal. MafB-restricted local monocyte proliferation precedes lung interstitial macrophage differentiation. ***Nature Immunology***. 2023; 10.1038/s41590-023-01468-3.

- Xiaofan Yang, Ting Huang, Tiantian Wang, Hongbo Gao, Haitao Zhang, **Wen Peng**, Jiacong Zhao, Shujing Hu, Panpan Lu, Zhongsi Hong, Bo Li, Kai Deng. MAT2A-mediated S-Adenosylmethionine level in $CD4^+$ T cells regulates HIV-1 latent infection. ***Frontiers in Immunology***. 2021; 12: 745784.

- **Wen Peng**, Zhongsi Hong, Xi Chen, Hongbo Gao, Zhuanglin Dai, Jiacong Zhao, Wen Liu, Dan Li, Kai Deng. Thiostrepton reactivates latent HIV-1 through the p-TEFb and NF-κB pathways mediated by heat shock response. ***Antimicrobial Agents and Chemotherapy***. 2020; 10.1128/AAC.02328-19.

APPENDIX

MACROPHAGES

Endothelial-driven TGFβ signaling supports lung interstitial macrophage development from monocytes

Wen Peng[1,2], Domien Vanneste[1,2], David Bejarano[3], Joan Abinet[1,2], Margot Meunier[1,2], Coraline Radermecker[1,2], Fabienne Perin[4], Didier Cataldo[4], Fabrice Bureau[2,5], Andreas Schlitzer[3], Qiang Bai[1,6]†*, Thomas Marichal[1,2,7]†*

Lung interstitial macrophages (IMs) are monocyte-derived parenchymal macrophages whose tissue-supportive functions remain unclear. Despite progress in understanding lung IM diversity and transcriptional regulation, the signals driving their development from monocytes and their functional specification remain unknown. Here, we found that lung endothelial cell–derived Tgfβ1 triggered a core Tgfβ receptor–dependent IM signature in mouse bone marrow–derived monocytes. Myeloid-specific impairment of Tgfβ receptor signaling severely disrupted monocyte-to-IM development, leading to the accumulation of perivascular immature monocytes, reduced IM numbers, and a loss of IM-intrinsic identity, a phenomenon similarly observed in the absence of endothelial-specific Tgfβ1. Mice lacking the Tgfβ receptor in monocytes and IMs exhibited altered monocyte and IM niche occupancy and hallmarks of aging including impaired immunoregulation, hyperinflation, and fibrosis. Our work identifies a Tgfβ signaling–dependent endothelial-IM axis that shapes IM development and sustains lung integrity, providing foundations for IM-targeted interventions in aging and chronic inflammation.

INTRODUCTION

In the lung, resident tissue macrophages (RTMs) represent the major immune compartment at steady state and are thought to exert important tissue-supportive, homeostatic, and immune functions. Depending on their localization, two main RTM populations exist, with alveolar macrophages (AMs) residing in the alveolar lumen and interstitial macrophages (IMs) populating the lung parenchyma (*1*–*3*). AMs have been extensively studied and are known to be long-lived, self-maintaining RTMs whose development and maintenance require type 2 alveolar epithelial cell (AT2)–derived granulocyte-macrophage colony-stimulating factor (also called Csf2) and AM-intrinsic transforming growth factor–β1 (Tgfβ1). Such microenvironmental signals trigger sustained expression of peroxisome proliferator–activated receptor–γ (PPAR-γ) and imprint a niche-specific functional specification important for host defense and surfactant homeostasis (*4*–*7*).

Conversely, IMs are less numerous, less accessible, and more enigmatic cells (*2*, *8*). Our understanding of IM development and diversity has benefited from the analysis of their transcriptomic profile at the single-cell level and the development of transgenic tools allowing their specific depletion (*9*–*14*). Although up to 10 different IM subsets have been recently proposed (*12*), a consensus seems to have emerged that IMs can be primarily categorized into two main subsets, namely, $CD206^+$ IMs and $CD206^-$ IMs, which occupy distinct niches (*9*, *10*, *12*, *14*). Parabiosis, bone marrow (BM) chimeras and fate-mapping studies have shown that both IM subsets are slowly replenished by classical monocytes (cMos) in adult mice (*9*–*11*, *15*). IM development from monocytes requires the activity of the transcription factor MafB and relies on Csf1 receptor signaling when the IM niche is in need of replenishment (*11*). Moreover, mature IMs share a core signature characterized by elevated expression of MafB, the fractalkine receptor Cx3cr1, the transmembrane protein 119 (Tmem119), and the complement component 1q (C1q) (*10*–*12*). According to the macrophage niche model, these findings are consistent with the idea that as-yet-unknown signals released from the lung microenvironment are able to imprint a core developmental program and identity of IMs that precedes their subsequent specification into distinct subsets (*9*, *10*, *12*–*14*).

Functionally, IMs have been attributed distinct roles upon exposure to allergens (*12*, *15*–*18*), bleomycin (*9*), influenza virus (*14*), or bacteria (*12*) and are thought to exert immunoregulatory functions in the context of allergic asthma (*15*–*18*), to dampen inflammatory responses (*9*, *12*, *14*), and to organize tertiary lymphoid tissues (*12*). However, in these nonhomeostatic contexts, monocytes can also be recruited to the lung and contribute to a pool of recruited macrophages that often overlap phenotypically with IMs (*1*, *3*, *19*). Such a convoluted landscape can complicate conclusions regarding the precise contributions of resident IMs versus recruited macrophages in various lung disorders. Hence, the potential tissue-supportive and homeostatic functions of IMs at steady state are still unclear.

Here, we found that Tgfβ1, produced by lung vWF^+ (von Willebrand factor–positive) blood vessel endothelial cells (Endos), shapes IM differentiation and imprints a core IM identity in the lung. In the absence of Tgfβ receptor in myeloid cells and of Tgfβ1 in Endos, monocytes accumulating in lung tissue could not fully differentiate into functional IMs. Moreover, disruption of IM-intrinsic Tgfβ receptor signaling triggered development of age-related mechanical abnormalities, hyperinflation, and collagen deposition. Our findings identify an endothelial-IM axis that contributes to IM development and can prevent the premature development of age-related defects, demonstrating a Tgfβ receptor–dependent homeostatic function of resident IMs.

[1]Laboratory of Immunophysiology, GIGA Institute, University of Liège, Liège, Belgium. [2]Faculty of Veterinary Medicine, University of Liège, Liège, Belgium. [3]Quantitative Systems Biology, Life and Medical Sciences (LIMES) Institute, University of Bonn, Bonn, Germany. [4]Laboratory of Tumor and Development Biology, GIGA Institute, University of Liège, Liège, Belgium. [5]Laboratory of Cellular and Molecular Immunology, GIGA Institute, University of Liège, Liège, Belgium. [6]PhyMedExp INSERM 1046, University of Montpellier, Montpellier, France. [7]Walloon Excellence in Life Sciences and Biotechnology (WELBIO) Department, WEL Research Institute, Wavre, Belgium.
†These authors contributed equally to this work.
*Corresponding author. Email: t.marichal@uliege.be (T.M.); qiang.bai@inserm.fr (Q.B.)

RESULTS

Lung endothelial Tgfβ1–IM Tgfβ receptor interactions are inferred from single-cell transcriptomics

IM development and function are thought to be shaped by microenvironmental cues, yet the ligand-receptor interactions involved remain poorly defined. To address this, we aimed to predict putative ligand-receptor interactions originating from lung structural cells and acting on IMs. Using NicheNet analyses (*20*), we analyzed single-cell RNA-sequencing (scRNA-seq) data of lung IMs, Ly6C$^+$ cMos, and nonhematopoietic lung niche cells, including Endos, epithelial cells (Epis), and stromal cells (Stros) captured at steady state (fig. S1) (*10*). The top interactions between ligands expressed by niche cells and the corresponding receptors on IMs were visualized using a Circos plot (Fig. 1A) (*21*). *Csf1*, coding for Csf1 or macrophage colony-stimulating factor, was expressed by the three niche cell populations and was predicted to be involved in IM development via Csf1r signaling, consistent with previous findings (*11*, *14*). An interaction between Endo-derived *Tgfb1* and IMs was also predicted (Fig. 1A). Analysis of predicted target genes triggered by Tgfβ1 signaling within receiver IMs revealed a high regulatory potential for the receptors *Tgfbr1* and *Tgfbr2*, as well as for various migration-related genes associated with integrin binding (i.e., *Itgb1*, *Itga4*, *Itgb5*, *Icam2*, *Itgax*, *Fn1*, *Igf1*, *Itga5*, *Calr*, *Thbs1*, and *Icam1*) (Fig. 1B). Moreover, *Tgfb1* expression was higher in Endos as compared with Epis or Stros (Fig. 1C).

Tgfβ1 can bind to the membrane Tgfβ receptor II (TgfβRII) subunit, allowing cooperative binding to TgfβRI and downstream signaling (*22*). We assessed *Tgfbr1* and *Tgfbr2* expression in lung cMos, AMs, CD206$^-$ IMs, and CD206$^+$ IMs in previously published bulk RNA-sequencing (RNA-seq) data (*11*). AMs and IMs expressed higher levels of *Tgfbr1* and *Tgfbr2* as compared with cMos (Fig. 1D). We next evaluated the protein expression of TgfβRI and TgfβRII on lung myeloid cells from wild-type (WT) mice by flow cytometry (fig. S2A). Lung monocytes, AMs, and IMs expressed TgfβRI, whose levels were lower in both IM subsets as compared with AMs or cMos (fig. S2, B and C). Whereas lung cMos and Ly6C$^-$ patrolling

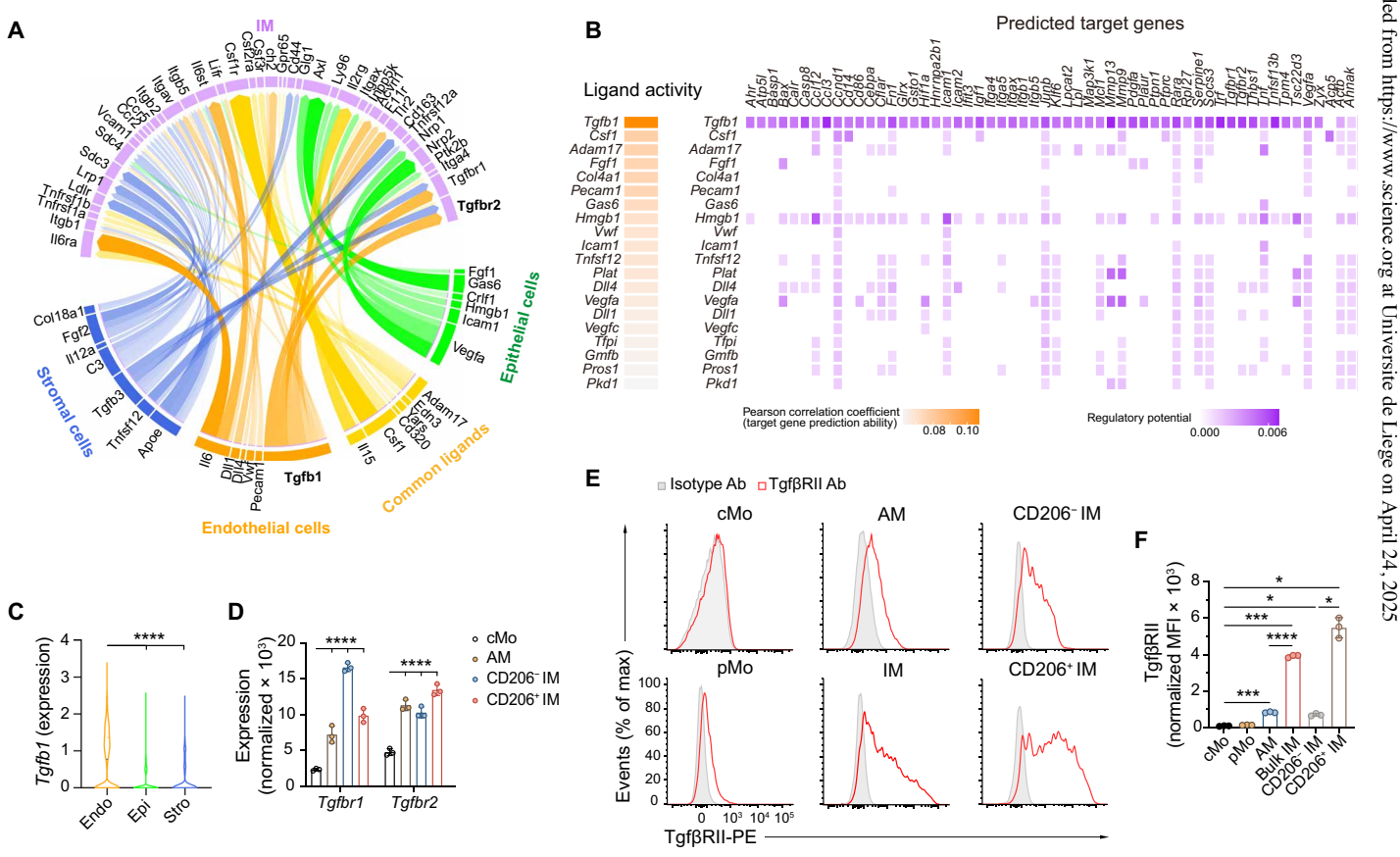

Fig. 1. Endothelial Tgfβ1–IM Tgfβ receptor interactions are predicted during IM development. (**A**) Circos plot depicting the putative interactions between structural cell–derived ligands (bottom) and IM-intrinsic receptors (top), evaluated by NicheNet analysis of scRNA-seq data of lung monocytes, IMs, and structural cells from naïve C57BL/6 WT mice (*10*). Opacity of the arrows correlates with the interaction score. (**B**) Heatmap depicting predicted ligand activity within lung Endos and IM-intrinsic target gene activation during IM development on the basis of NicheNet analyses as in (A). (**C**) Expression of *Tgfb1* within lung primary Endos, Epis, and Stros, extracted from the scRNA-seq data, as in (A), and depicted by violin plots (height, expression; width, abundance of cells). (**D**) Expression of *Tgfbr1* and *Tgfbr2* within lung cMos, AMs, CD206$^-$ IMs, and CD206$^+$ IMs of naïve C57BL/6 WT mice, extracted by bulk RNA-seq data analyses (*11*). (**E**) Representative histograms and (**F**) bar graph showing normalized MFI of TgfβRII expression in lung cMos, pMos, AMs, and IMs from naïve C57BL/6 WT mice. PE, phycoerythrin. [(D) and (F)] Data show means ± SEM and (D) $n = 3$ biological replicates of FACS-sorted cells; (F) data are representative of three independent experiments ($n = 3$ mice). *P* values were calculated using (C) a one-way analysis of variance (ANOVA) with Games-Howell's post hoc tests, (D) a two-way ANOVA with Dunnett's post hoc tests, or (F) a one-way ANOVA with Dunnett's post hoc tests. *$P < 0.05$; ***$P < 0.001$; ****$P < 0.0001$. Ab, antibody; MFI, mean fluorescence intensity.

monocytes (pMos) expressed low levels of TgfβRII, its expression was elevated in AMs and in IMs, especially in the CD206$^+$ IM subset (Fig. 1, E and F). Lung neutrophils, conventional dendritic cells, and blood myeloid cells also expressed lower levels of TgfβRII as compared with lung IMs (fig. S2, D and E). Together, our results indicate that IMs could be effective responders to Tgfβ through TgfβRII signaling and that Endos may represent an important source of Tgfβ1.

Lung endothelial Tgfβ1 triggers a core lung IM identity on Csf1-grown monocytes and macrophages ex vivo

We sought to investigate the potential impact of soluble factors, including Tgfβ, released from primary lung Endos, Epis, and Stros on monocyte differentiation and the acquisition of a distinct lung IM profile. To this end, BM-derived monocytes (BM Mos) were isolated from the BM of WT mice; cultured for 48 hours in basal medium (Ctrl) or conditioned medium (CM) from fluorescence-activated cell sorting (FACS)–sorted Endos (CM-Endo), Epis (CM-Epi), or Stros (CM-Stro) (fig. S2F); and subjected to bulk RNA-seq (Fig. 2A). Principal components analysis (PCA) showed distinct clustering patterns for BM Mos exposed to distinct CM, indicating unique gene expression profiles induced by each CM (Fig. 2B). We generated gene set signatures of lung CD206$^+$ IMs, CD206$^-$ IMs, and AMs on the basis of our previously published scRNA-seq data (*10*) and mapped these signatures to CM-stimulated BM Mos using gene set enrichment analysis (GSEA) (*23*). CM-Endo and CM-Stro triggered an enrichment in an IM signature regardless of the IM subset, but CM-Endo was the only treatment that stimulated a specific IM signature while not inducing an AM signature (Fig. 2C). These data suggest that lung Endos release soluble signals that can imprint a specific IM signature.

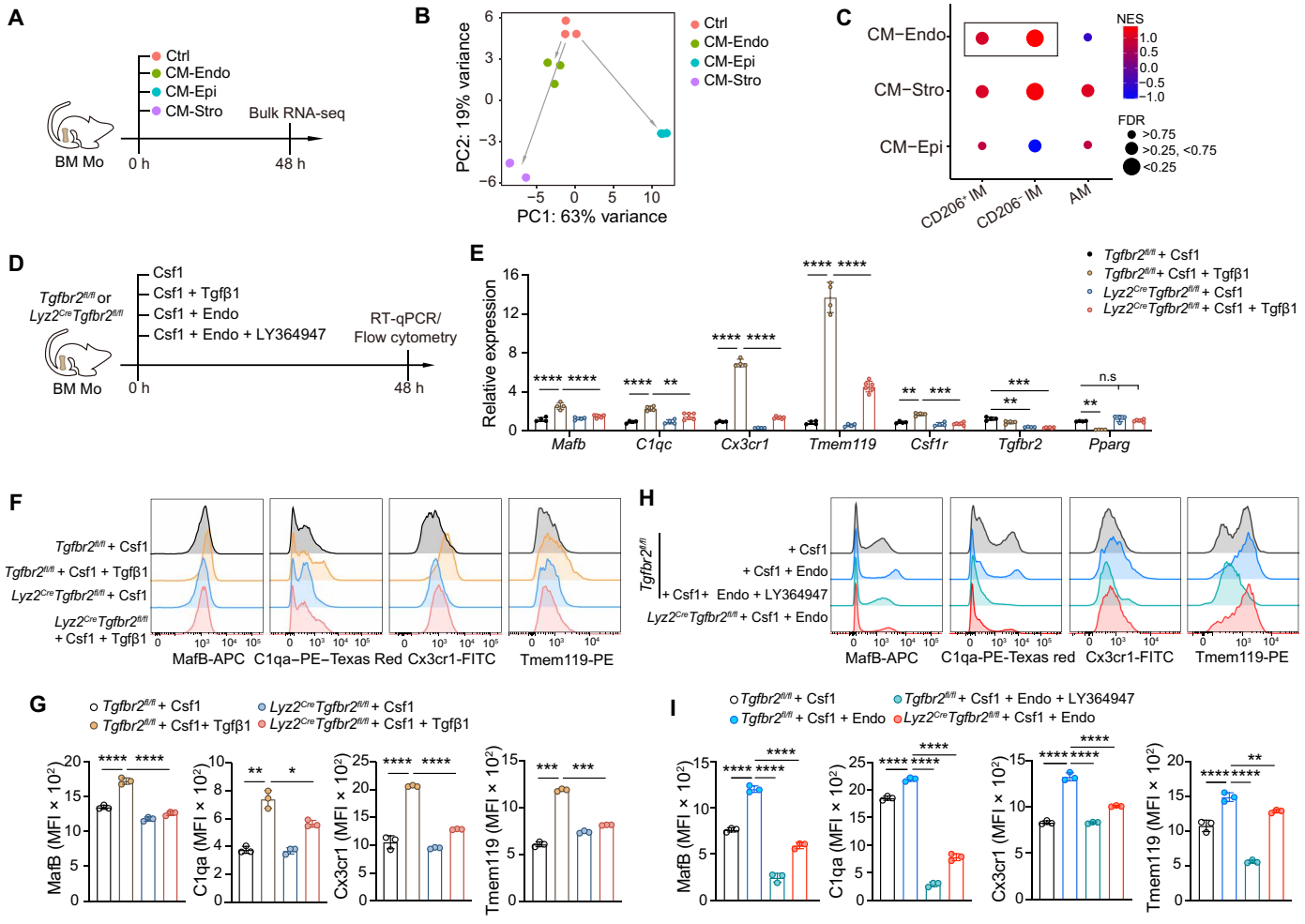

Fig. 2. Lung endothelial Tgfβ1 triggers a core IM signature on Csf1-grown BM Mos and BMDMs. (**A**) Experimental outline for (B) and (C). BM Mos from WT mice were cultured in basal medium (Ctrl) or lung primary CM-Endo, CM-Epi, or CM-Stro and subjected to bulk RNA-seq analyses 48 hours (h) later. (**B**) PCA plot of the BM Mo bulk RNA-seq data, as in (A). (**C**) GSEA comparing the transcriptomes of CM-stimulated BM Mos, as in (A), with signature gene sets characteristic of CD206$^+$ IMs, CD206$^-$ IMs, and AMs. (**D**) Experimental outline for (E) to (I). BM Mos from *Tgfbr2*$^{fl/fl}$ or *Lyz2*^{Cre} *Tgfbr2*$^{fl/fl}$ mice were [(E) to (G)] stimulated with Csf1 or Csf1 plus Tgfβ1 or [(H) and (I)] cocultured with or without lung primary Endos in the presence or absence of the TgfβR inhibitor LY364947 and analyzed 48 hours later. (**E**) Relative mRNA expression of the indicated genes in BM Mos, as in (D). (**F**) Representative histograms and (**G**) bar graph showing MFI of MafB, C1qa, Cx3cr1, and Tmem119 expression in BM Mos, as in (D). (**H**) Representative histograms and (**I**) bar graph showing MFI of MafB, C1qa, Cx3cr1, and Tmem119 expression in BM Mos, as in (D). [(E), (G), and (I)] Data show means ± SEM and are representative of three independent experiments ($n = 3$ to 6 mice). *P* values were calculated using (E) a two-way ANOVA with Tukey's post hoc tests and [(G) and (I)] a one-way ANOVA with Dunnett's post hoc tests. *$P < 0.05$; **$P < 0.01$; ***$P < 0.001$; ****$P < 0.0001$. n.s., not significant; FDR, false discovery rate; NES, normalized enrichment score.

Next, we investigated whether recombinant Tgfβ1 was sufficient to shift Csf1-grown BM Mos toward a lung IM gene expression profile. As opposed to AMs, bulk IMs can be specifically defined by elevated expression of Cx3cr1, Tmem119, MafB, and C1q (*10*–*12*). Hence, BM Mos from WT (i.e., *Tgfbr2*$^{fl/fl}$) mice were cultured with Csf1 in the presence or absence of Tgfβ1 for 48 hours and assessed for expression of IM identity genes and proteins (Fig. 2D). Tgfβ1 significantly up-regulated the transcript levels of *Mafb*, *C1qc*, *Cx3cr1*, *Tmem119*, and *Csf1r* in Csf1-treated BM Mos, whereas it had no effect on *Tgfbr2* expression and down-regulated the expression of the AM-specific transcription factor *Pparg* (Fig. 2E). At the protein level, MafB, C1qa, Cx3cr1, and Tmem119 were also significantly increased in Tgfβ1-treated Csf1-grown WT BM Mos as compared with those in untreated controls (Fig. 2, F and G).

To evaluate the impact of Tgfβ signaling through TgfβRII in this model, we used myeloid-specific *Tgfbr2*-deficient mice (*Lyz2*^{Cre} *Tgfbr2*$^{fl/fl}$ mice). A decrease in *Tgfbr2* expression and partial excision of the floxed allele were observed in BM Mos from *Lyz2*^{Cre} *Tgfbr2*$^{fl/fl}$ mice as compared with those from *Tgfbr2*$^{fl/fl}$ littermate controls (fig. S3). Induction of IM identity marker genes and proteins was decreased in Tgfβ1-treated *Tgfbr2*-deficient Csf1-grown BM Mos as compared with those in the WT counterparts, whereas Tgfβ1-triggered down-regulation of *Pparg* was no longer observed in the absence of *Tgfbr2* (Fig. 2, E to G). We also generated WT or *Tgfbr2*-deficient BM-derived macrophages (BMDMs) and treated them from day 7 to day 9 of culture with Tgfβ1 (fig. S4, A to C). Tgfβ1-triggered and TgfβRII-mediated increases in the expression of IM-specific markers on differentiated BMDMs were also observed, as seen in BM Mos (fig. S4, D and E). Treatment of BM Mos with Csf2 and Tgfβ1, two cytokines required for AM development and identity (*5*–*7*), triggered an AM-associated signature independently of the concomitant presence of Csf1 (fig. S5, A and B) and did not induce expression of IM signature genes. The addition of Csf2 to Csf1- or Tgfβ1- and Csf1-grown BM Mos exerted an inhibitory effect on the expression of IM signature genes and *Tgfbr2* (fig. S5, C and D). Together, these results show that, in the presence of Csf1, Tgfβ1 can signal through TgfβRII to imprint a core IM signature in BM Mos or in BMDMs.

Last, we asked whether coculture of Csf1-grown BM Mos with lung primary Endos would trigger a similar TgfβRII-dependent IM signature (Fig. 2D). Coculture of BM Mos with Endos induced an increase in the expression of the IM markers Cx3cr1, Tmem119, MafB, and C1qa (Fig. 2, H and I). Such induction of IM identity was abolished in the presence of LY364947, a TGFβ receptor inhibitor, and was decreased in BM Mos from *Lyz2*^{Cre} *Tgfbr2*$^{fl/fl}$ mice as compared with BM Mos from *Tgfbr2*$^{fl/fl}$ controls (Fig. 2, H and I). Our ex vivo results demonstrate that, in the presence of Tgfβ1 and Csf1 or lung primary Endos, BM Mos can acquire a Tgfβ receptor–dependent lung IM-specific phenotypic profile during macrophage differentiation.

Myeloid Tgfβ receptor signaling mediates lung IM development and identity in vivo

Next, we used *Tmem119*^{Cre} *Cx3cr1*$^{LSL\text{-}DTR}$ mice (i.e., IM^{DTR} mice) (*11*), in which diphteria toxin (DT) treatment causes a bolus depletion of the IM niche that is rapidly refilled by cMo-derived de novo IMs. To evaluate the contribution of Tgfβ receptor signaling to IM development, we combined IM depletion in IM^{DTR} mice with intraperitoneal injections of the Tgfβ receptor inhibitor LY363947 at days 2, 4, and 6 post-DT (Fig. 3A). At day 7 post-DT, the numbers of lung cMos and IMs were lower in LY363947-treated IM^{DTR} mice as compared with those in phosphate-buffered saline (PBS)–treated controls, whereas the numbers of pMos and AMs remained unchanged (Fig. 3B). Tgfβ receptor inhibition was associated with a decrease in the numbers of both CD206^{-} IMs and CD206^{+} IMs (fig. S6A). This was associated with an increase in the proportion of apoptotic annexin V^{+} lung cMos and IMs in LY364947-treated mice as compared with those in vehicle-treated counterparts (fig. S6B), whereas the proportion of blood Ly6C^{+} cMos was higher in LY363947-treated IM^{DTR} mice as compared with that in PBS-treated counterparts (fig. S6C), and the viability of BM and blood cMos was not affected by LY363947 (fig. S6D). These results suggested that Tgfβ receptor signaling affected lung cMo and IM survival capacity and was important for lung cMo recruitment or lung IM differentiation.

To assess whether myeloid-intrinsic Tgfβ receptor signaling played a role in either lung cMo recruitment or IM differentiation from cMos in vivo, we generated BM competitive chimeras in thorax-protected CD45.1/CD45.2 IM^{DTR} mice engrafted with a 1:1 BM cell mix from CD45.1 WT and CD45.2 *Lyz2*^{Cre} *Tgfbr2*$^{fl/fl}$ mice (Fig. 3C). At week 4 posttransfer, donor chimerism of blood cMos exceeded 80%, whereas AM donor chimerism was below 5%, indicating efficient BM donor reconstitution and thorax protection, respectively (Fig. 3, D and E). Seven days post-DT, we found that more than 85% of IMs were of donor origin, confirming efficient depletion and BM reconstitution (Fig. 3, D and E). Lung cMos of donor origin arose equally from CD45.1 WT and CD45.2 *Lyz2*^{Cre} *Tgfbr2*$^{fl/fl}$ cells, indicating that lung cMo recruitment was independent of Tgfβ receptor (Fig. 3, D to F). However, CD45.1 WT BM cells had a competitive advantage over CD45.2 *Lyz2*^{Cre} *Tgfbr2*$^{fl/fl}$ cells to become IMs, regardless of the IM subset, suggesting that TgfβRII-deficient monocytes, once in the lung, failed to fully differentiate into IMs and reconstitute the IM pool (Fig. 3, D to F).

To further characterize lung monocytes and macrophages in the absence of myeloid-intrinsic TgfβRII, we compared their numbers, localization, and identity by flow cytometry between myeloid-restricted *Tgfbr2*-deficient mice and littermate controls. First, IMs from *Lyz2*^{Cre} *Tgfbr2*$^{fl/fl}$ mice exhibited a 60% reduction in *Tgfbr2* expression as compared with those from littermate controls (fig. S7A). Second, no abnormalities were found in the blood leukocyte composition of such transgenic mice (fig. S7B). As expected (*7*), AM numbers exhibited a twofold reduction in *Lyz2*^{Cre} *Tgfbr2*$^{fl/fl}$ mice as compared with those in controls (Fig. 3G). IM numbers were also lower in *Lyz2*^{Cre} *Tgfbr2*$^{fl/fl}$ mice as compared with those in controls (Fig. 3G), and the remaining IMs in *Lyz2*^{Cre} *Tgfbr2*$^{fl/fl}$ mice exhibited a higher percentage of annexin V^{+} cells as compared with control IMs, supporting that IMs are more sensitive to apoptosis in the absence of TgfβRII signaling (fig. S7C). The percentage of Ki-67^{+} cells was also higher in IMs from *Lyz2*^{Cre} *Tgfbr2*$^{fl/fl}$ mice as compared with control IMs, suggesting that reduced cell proliferation does not account for the lower IM numbers in these mice (fig. S7D).

Flow cytometry–based uniform manifold approximation and projection (UMAP) plot representation of monocytes and macrophages highlighted the appearance of a distinct cell population in *Lyz2*^{Cre} *Tgfbr2*$^{fl/fl}$ mice (Fig. 3H). Back-gating analysis identified this population as Ly6C^{+}CD64^{+} monocytes (called CD64^{+} Mos) (Fig.

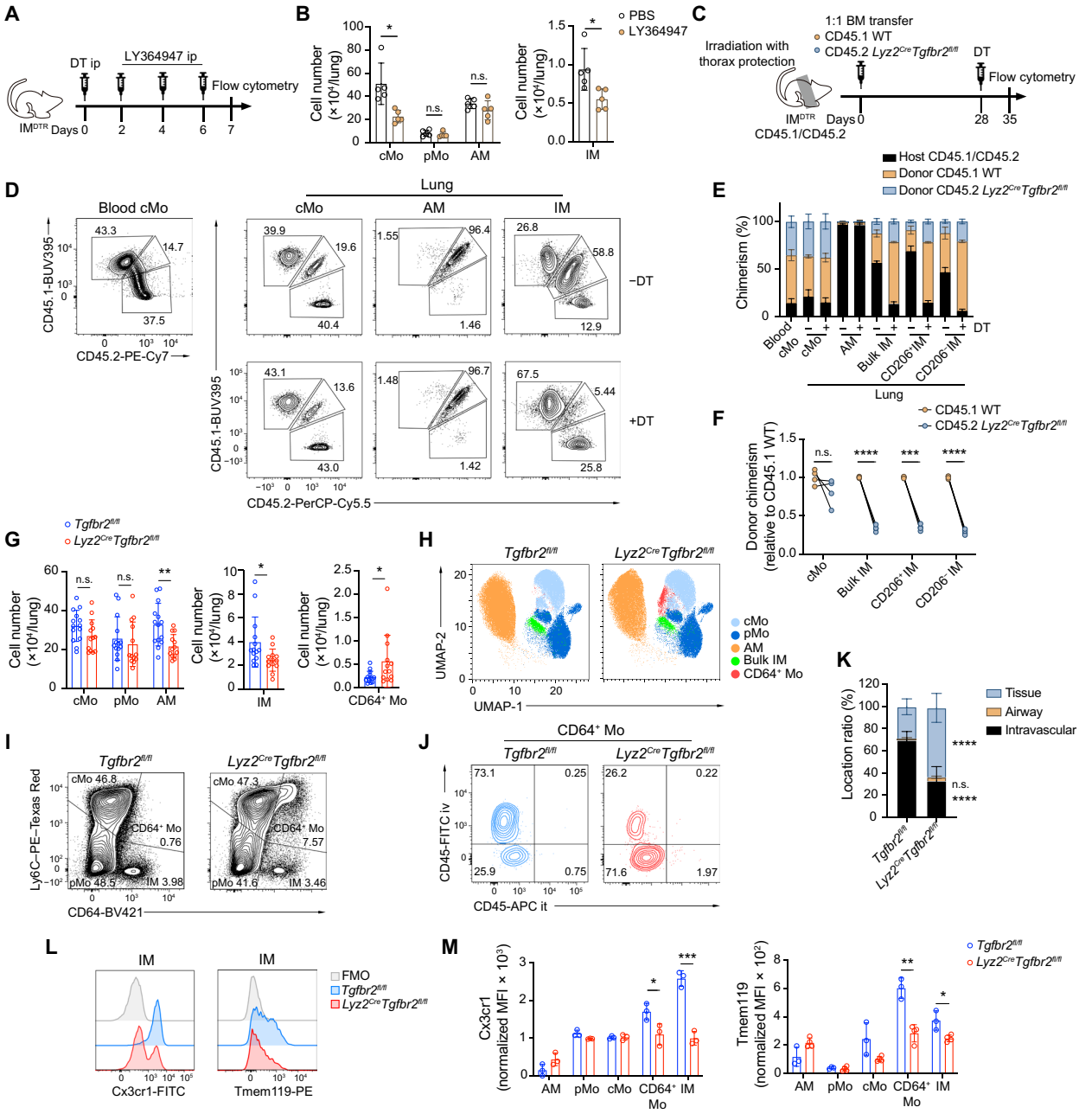

Fig. 3. Loss of Tgfβ receptor signaling impedes monocyte-to-IM development and IM identity in vivo. (**A**) Experimental outline for (B) and (C). (**B**) Absolute numbers of lung cMos, pMos, AMs, and IMs in PBS- or LY364947-treated IM^{DTR} mice at day 7 post-DT, as in (A). ip, intraperitoneal. (**C**) Experimental outline for (D) to (F). (**D**) Representative CD45.1 and CD45.2 contour plots and (**E**) bar graph showing % of host CD45.1/CD45.2, donor CD45.1 WT, and donor CD45.2 *Lyz2*^{Cre} *Tgfbr2*$^{fl/fl}$ chimerism in the indicated cell populations, assessed 7 days post–DT treatment in chimeric IM^{DTR} mice, as in (C). (**F**) Quantification of donor CD45.2 *Lyz2*^{Cre} *Tgfbr2*$^{fl/fl}$ chimerism relative to donor CD45.1 WT chimerism in the indicated cell populations, as in (D). (**G**) Absolute numbers of the indicated lung myeloid cell populations evaluated by flow cytometry in *Lyz2*^{Cre} *Tgfbr2*$^{fl/fl}$ mice and in *Tgfbr2*$^{fl/fl}$ littermate controls. (**H**) Representative UMAP plots of lung CD45^{+}CD11b^{+} and/or CD11c^{+} cells analyzed by flow cytometry in *Lyz2*^{Cre} *Tgfbr2*$^{fl/fl}$ mice and in *Tgfbr2*$^{fl/fl}$ littermate controls (merged data from two mice per group). (**I**) Representative Ly6C and CD64 plots of lung CD45^{+}SSC^{lo}CD11b^{+}F4/80^{+} cells from *Lyz2*^{Cre} *Tgfbr2*$^{fl/fl}$ mice and *Tgfbr2*$^{fl/fl}$ littermate controls. (**J**) Representative CD45-iv and CD45-it plots of lung CD64^{+} Mos from *Lyz2*^{Cre} *Tgfbr2*$^{fl/fl}$ mice and *Tgfbr2*$^{fl/fl}$ littermate controls injected with anti–CD45-FITC Ab intravenously and anti-CD45-APC Ab intratracheally before euthanasia. (**K**) Percentages of tissue (CD45-iv^{-}/CD45-it^{-}), airway (CD45-iv^{-}/CD45-it^{+}) and intravascular (CD45-iv^{+}/CD45-it^{-}) CD64^{+} Mos, as in (K). iv, intravenous; it, intratracheal. (**L**) Representative histograms and (**M**) bar graph showing MFI of Cx3cr1 and Tmem119 expression in IMs and the indicated lung myeloid cell populations of *Lyz2*^{Cre} *Tgfbr2*$^{fl/fl}$ mice and *Tgfbr2*$^{fl/fl}$ littermate controls. [(B), (E) to (G), (K), and (M)] Data show [(B), (E), and (M)] means ± SEM and are representative of two or three independent experiments (n = 3 to 6 mice), and (F) individual mice are representative of three independent experiments (n = 4 mice); [(G) and (K)] means ± SEM are pooled from three or four independent experiments (n = 8 to 14 mice). P values were calculated using [(B) and (M)] an unpaired Student's t test, (F) a paired multiple t test, (G) a Wilcoxon rank sum test, or (K) a two-way ANOVA with Šidák's post hoc tests. *P < 0.05; **P < 0.01; ***P < 0.001; ****P < 0.0001. Ab, antibody.

3I), whose numbers were significantly increased in *Lyz2*^{Cre} *Tgfbr2*$^{fl/fl}$ mice as compared with those in littermate controls (Fig. 3G). The phenotype of CD64$^+$ Mos was reminiscent of that of transitioning CD64$^+$ Mos that appear during IM development in IM^{DTR} mice (*11*) but could also correspond to inflammatory monocytes or macrophages recruited when inflammation is present (*10*, *15*). Hence, we evaluated the expression of proinflammatory genes on lung extracts of *Lyz2*^{Cre} *Tgfbr2*$^{fl/fl}$ and littermate control mice and found no evidence of inflammation in the absence of myeloid *Tgfbr2* in 8- to 12-week-old mice (fig. S7E). Next, we assessed the localization of CD64$^+$ Mos. To this end, we labeled intravascular cells by intravenous injection of anti–CD45–fluorescein isothiocyanate (FITC) antibodies 10 min before euthanasia and airway cells by intratracheal injection of anti–CD45-allophycocyanin (APC) antibodies 5 min before euthanasia. As expected, most cMos and pMos were intravascular, most AMs were in the airway lumen, and most IMs were parenchymal, regardless of the mouse genotype (fig. S7, F and G). Whereas the few lung CD64$^+$ Mos present in control mice were mostly intravascular, 70% of lung CD64$^+$ Mos from *Lyz2*^{Cre} *Tgfbr2*$^{fl/fl}$ mice were parenchymal (Fig. 3, J and K). These data further support the idea that, whereas monocyte entry in the tissue is not affected in the absence of intrinsic *Tgfbr2*, monocyte-to-IM differentiation is impaired and blocked at an early differentiation stage in the tissue. Last, we found that both CD64$^+$ Mos and IMs from *Lyz2*^{Cre} *Tgfbr2*$^{fl/fl}$ mice exhibited a decrease in the expression of Cx3cr1 and Tmem119 as compared with CD64$^+$ Mos and IMs from littermate control mice (Fig. 3, L and M), supporting a loss of IM identity in the absence of myeloid *Tgfbr2*. Numbers of heart and skin macrophages were, however, similar between *Lyz2*^{Cre}*Tgfbr2*$^{fl/fl}$ and control mice (fig. S7, H to J), suggesting that myeloid-intrinsic Tgfβ receptor signaling may play a more dominant role in the lung compared with that in other organs. Together, these results demonstrate that intrinsic TgfβR signaling plays an important role in imprinting a core IM identity during lung IM development in vivo.

Tgfβ1 acts in synergy with Csf1 to trigger a MafB-dependent IM identity

Next, we asked whether Tgfβ1 could trigger expression of MafB, a transcription factor involved in IM development (*11*), in BM Mos (Fig. 4A). We observed that, whereas Tgfβ1 or Csf1 alone could trigger *Mafb*, the combination of both treatments was the most potent in up-regulating *Mafb* expression, which correlated with the strongest induction in the IM identity genes *C1qc*, *Cx3cr1*, *Tmem119*, and *Csf1r* (Fig. 4B). Csf1 treatment increased *Tgfbr2* expression, whereas Tgfβ1 treatment alone did not trigger expression of *Csf1r* or *Tgfbr2* (Fig. 4B), suggesting that engagement of Csf1 signaling primes IM responsiveness to Tgfβ1. Supporting this hypothesis, Csf1 target gene activation preceded that of Tgfβ1 along a monocyte-to-IM trajectory (Fig. 4C) (*11*).

Next, we asked whether Tgfβ1-mediated induction of IM identity on BM Mos was dependent on MafB by analyzing BM Mos from *Lyz2*^{Cre} *Mafb*$^{fl/fl}$ mice (Fig. 4D) (*11*), which did not express *Mafb* (Fig. 4E). In the absence of MafB, Tgfβ1 treatment was no longer able to trigger an IM identity gene expression profile in BM Mos (Fig. 4E). Moreover, *Tgfbr2* expression itself was decreased in the absence of MafB, suggesting that MafB could also directly or indirectly regulate *Tgfbr2* expression (Fig. 4E). This was further evidenced by the differential expression (DE) of *Mafb*, *Tgfbr2*, and TgfβRII target genes along a monocyte-to-IM trajectory (*11*). *Mafb* and *Tgfbr2* showed similar up-regulation patterns, and Tgfβ1 target gene activation progressively increased in both CD206$^-$ IM and CD206$^+$ IM differentiation pathways, supporting Tgfβ signaling engagement in both subsets (Fig. 4F). Moreover, many predicted target genes downstream of TgfβRII signaling with the highest regulatory potential (Fig. 1B) were up-regulated during monocyte-to-IM development (Fig. 4G) but showed reduced expression in *Mafb*-deficient IMs from *Lyz2*^{Cre} *Mafb*$^{fl/fl}$ mice (*11*) as compared with those from WT counterparts (Fig. 4H).

Last, we quantified TgfβRII expression on IMs from *Lyz2*^{Cre} *Mafb*$^{fl/fl}$ and control mice and, whereas IMs from *Lyz2*^{Cre} *Mafb*$^{fl/fl}$ mice expressed detectable levels of TgfβRII, TgfβRII expression was lower on IMs from *Lyz2*^{Cre} *Mafb*$^{fl/fl}$ mice as compared with those from the WT counterparts (Fig. 4, I and J), indicating that MafB could regulate TgfβRII expression in IMs. Together, these data support that Tgfβ1-Tgfβ receptor interactions can activate MafB-dependent pathways, which then regulates IM-intrinsic TgfβRII expression and TgfβRII-dependent signaling events to mediate full development of mature IMs, in concert with Csf1.

vWF$^+$ blood vessel Endos release Tgfβ1 to shape IM development and identity

Next, we sought to identify the cellular source of Tgfβ1 necessary for IM development in vivo. We assessed intracellular expression of latent Tgfβ1 in lung structural cells at steady state by flow cytometry (fig. S2F). No Tgfβ1$^+$ cells were found in CD45$^-$EpCam$^+$CD31$^-$ Epis or in CD45$^-$EpCam$^-$CD31$^-$ Stros (Fig. 5, A and B). However, we found a substantial proportion of Tgfβ1$^+$ cells within CD45$^-$EpCam$^-$CD31$^+$ Endos, which was restricted to the vWF$^+$ blood vessel compartment but not the CD90.2$^+$ lymphatic or the vWF$^-$CD90.2$^-$ capillary compartment (Fig. 5, A and B) (*24*). We reasoned that latent Tgfβ1 would be released more readily in the lung microenvironment during replenishment of the IM niche. Thus, we depleted IMs by DT treatment in IM^{DTR} mice and tracked Tgfβ1$^+$ vWF$^+$ Endos during IM niche replenishment. We found a decrease in the percentage of Tgfβ1$^+$ cells among vWF$^+$ Endos at days 3, 5, and 7 post-DT, whereas levels had returned to baseline at day 14 post-DT (Fig. 5, C and D), consistent with the idea that vWF$^+$ Endos release more latent Tgfβ1 when IM development from monocytes is accelerated. Accordingly, the levels of latent Tgfβ1 found in the lungs of DT-treated IM^{DTR} mice at day 4 post-DT were higher as compared with those found in the lungs of PBS-treated IM^{DTR} mice (Fig. 5E). We also found that CD68$^+$ myeloid cells were present in the vicinity of Erg1$^+$Tgfβ1$^+$ Endos in lungs from IM^{DTR} mice that were treated with DT 4 days before (Fig. 5F), and we observed an increase in pairs of CD68$^+$ myeloid cells and Erg1$^+$Tgfβ1$^+$ Endos that were less than 10 μm apart in such lungs as compared with those of PBS-treated controls (Fig. 5G). These data suggest that vWF$^+$ blood vessel Endos could release Tgfβ1 and interact with tissue monocytes differentiating into IMs.

Last, we sought to formally address the contribution of endothelial Tgfβ1–to–IM development and identity. We generated *Cdh5*^{CreERT2} *Tgfb1*$^{fl/fl}$ mice that would be conditionally deficient in *Tgfb1* in Endos upon tamoxifen treatment. After weaning, *Cdh5*^{CreERT2} *Tgfb1*$^{fl/fl}$ and *Tgfb1*$^{fl/fl}$ littermate controls were fed tamoxifen for 28 days, followed by a normal diet. At day 49 postweaning, we confirmed a decrease in *Tgfb1* mRNA levels within lung CD45$^-$EpCam$^-$CD31$^+$ Endos from tamoxifen-fed *Cdh5*^{CreERT2} *Tgfb1*$^{fl/fl}$ compared with those from controls (Fig. 5, H and I). Similarly, the percentage of

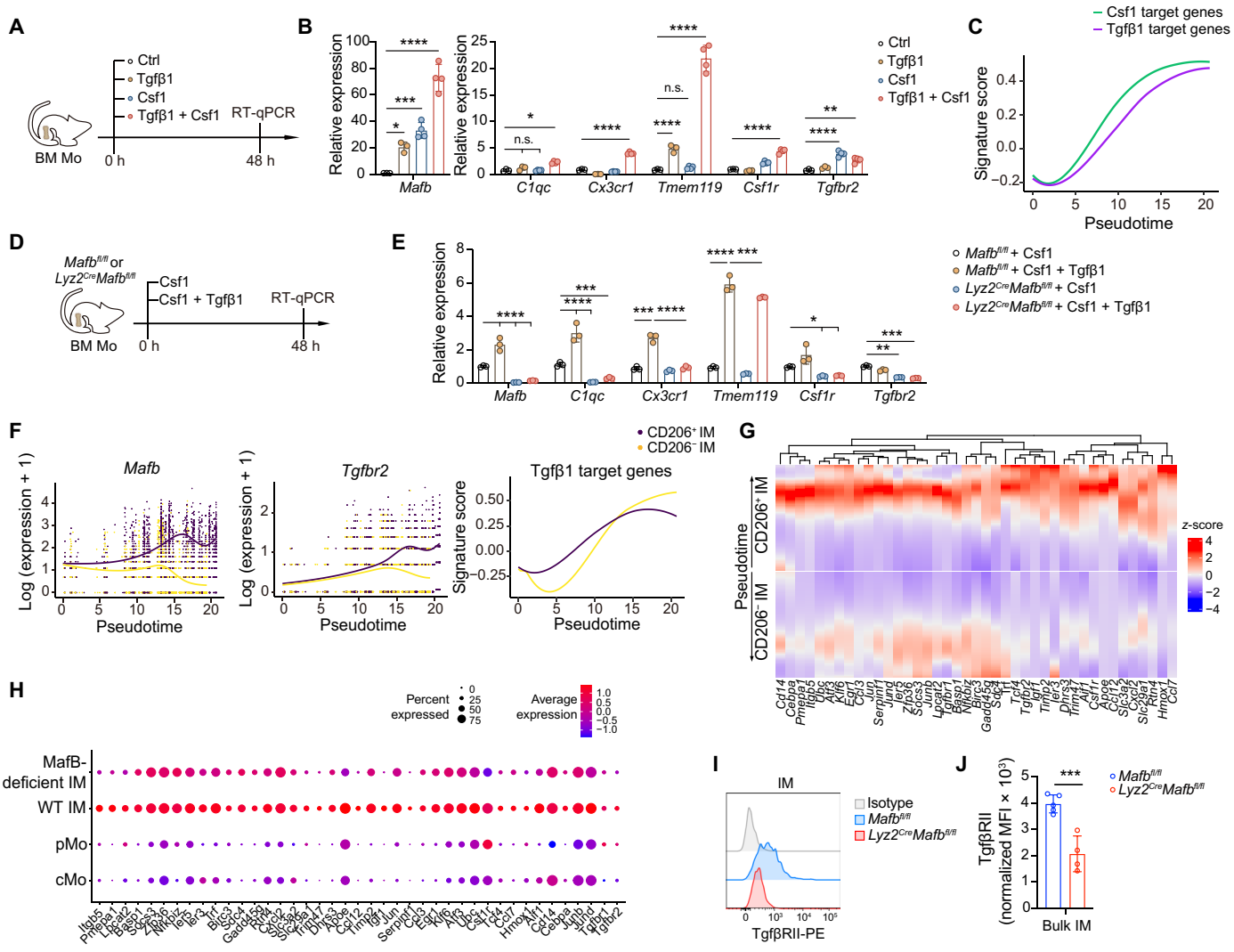

Fig. 4. Reciprocal regulation of MafB- and Tgfβ receptor–dependent pathways in IMs. (**A**) Experimental outline for (B). BM Mos from WT C57BL/6 mice were stimulated with Tgfβ1, Csf1, or Csf1 plus Tgfβ1 for 48 hours (h) and were analyzed by RT-qPCR. Freshly isolated BM Mos were used as controls. (**B**) Relative mRNA expression of the indicated genes in BM Mos, as in (A). (**C**) Signature scores of Csf1 and Tgfβ1 target genes along pseudotime during monocyte-to-IM development on the basis of the scRNA-seq mapping of monocyte-to-IM trajectory (*11*). (**D**) BM Mos from *Mafb*$^{fl/fl}$ or *Lyz2*^{Cre} *Mafb*$^{fl/fl}$ mice were stimulated with Csf1 or Csf1 plus Tgfβ1 for 48 hours and were analyzed by RT-qPCR. (**E**) Relative mRNA expression of the indicated genes in BM Mos, as in (D). (**F**) Expression of *Mafb* (left), *Tgfbr2* (middle), and signature scores of Tgfβ1 target genes (right) along pseudotime evaluated by TradeSeq in monocyte-to-IM trajectories (both CD206$^-$ and CD206$^+$ IM trajectories) (*11*). (**G**) Heatmap showing expression of the indicated genes along pseudotime during monocyte-to-IM trajectories, as in (F). (**H**) Dot plot showing average expression and % of cells expressing the indicated genes in clusters of cMos, pMos, WT IMs, and MafB-deficient IMs on the basis of previously published scRNA-seq data (*11*). (**I**) Representative histograms and (**J**) bar graph showing normalized MFI of TgfβRII expression in lungs from *Lyz2*^{Cre} *Mafb*$^{fl/fl}$ mice or *Mafb*$^{fl/fl}$ littermate controls. [(B), (E), and (J)] Data show means ± SEM and are representative of three independent experiments [*n* = 3 replicates from different mice in (B) and (E); *n* = 4 or 5 mice in (J)]. *P* values were calculated using (B) a two-way ANOVA with Dunnett's post hoc tests, (E) a two-way ANOVA with Tukey's post hoc tests, or (J) a two-tailed unpaired Student's *t* test. **P* < 0.05; ***P* < 0.01; ****P* < 0.001; *****P* < 0.0001.

Tgfβ1$^+$ cells within vWF$^+$ Endos and the levels of latent Tgfβ1 were lower in lungs from tamoxifen-fed *Cdh5*^{CreERT2} *Tgfb1*$^{fl/fl}$ mice as compared with those from controls (Fig. 5, H and I). After coculture of BM Mos with Csf1 and FACS-sorted Endos from tamoxifen-fed *Cdh5*^{CreERT2} *Tgfb1*$^{fl/fl}$ mice or control counterparts, we found that Endo-triggered induction of the IM markers Cx3cr1, Tmem119, MafB, and C1qa was lower when Tgfβ1 was knocked down (Fig. 5, J to L). In a separate cohort of mice, we lethally irradiated mice at day 35 postweaning to deplete hematopoietic cells and IMs and reconstituted them with donor CD45.1/CD45.2 BM cells (Fig. 5H). At day 14 postreconstitution, most blood cells and 50% of CD45$^+$ lung cells were of donor origin, regardless of the host genotype (fig. S8). In vivo, both the number and the percentage of donor IMs within CD45$^+$ cells were decreased in *Cdh5*^{CreERT2} *Tgfb1*$^{fl/fl}$ mice as compared with those in littermate controls (Fig. 5M), demonstrating that IM development was impaired when endothelial Tgfβ1 expression was decreased. In addition, expression levels of Cx3cr1 and Tmem119 were decreased in IMs from *Cdh5*^{CreERT2} *Tgfb1*$^{fl/fl}$ mice as compared with those from control mice (Fig. 5, N and O), indicating that endothelial Tgfβ1 can shape IM identity. Together,

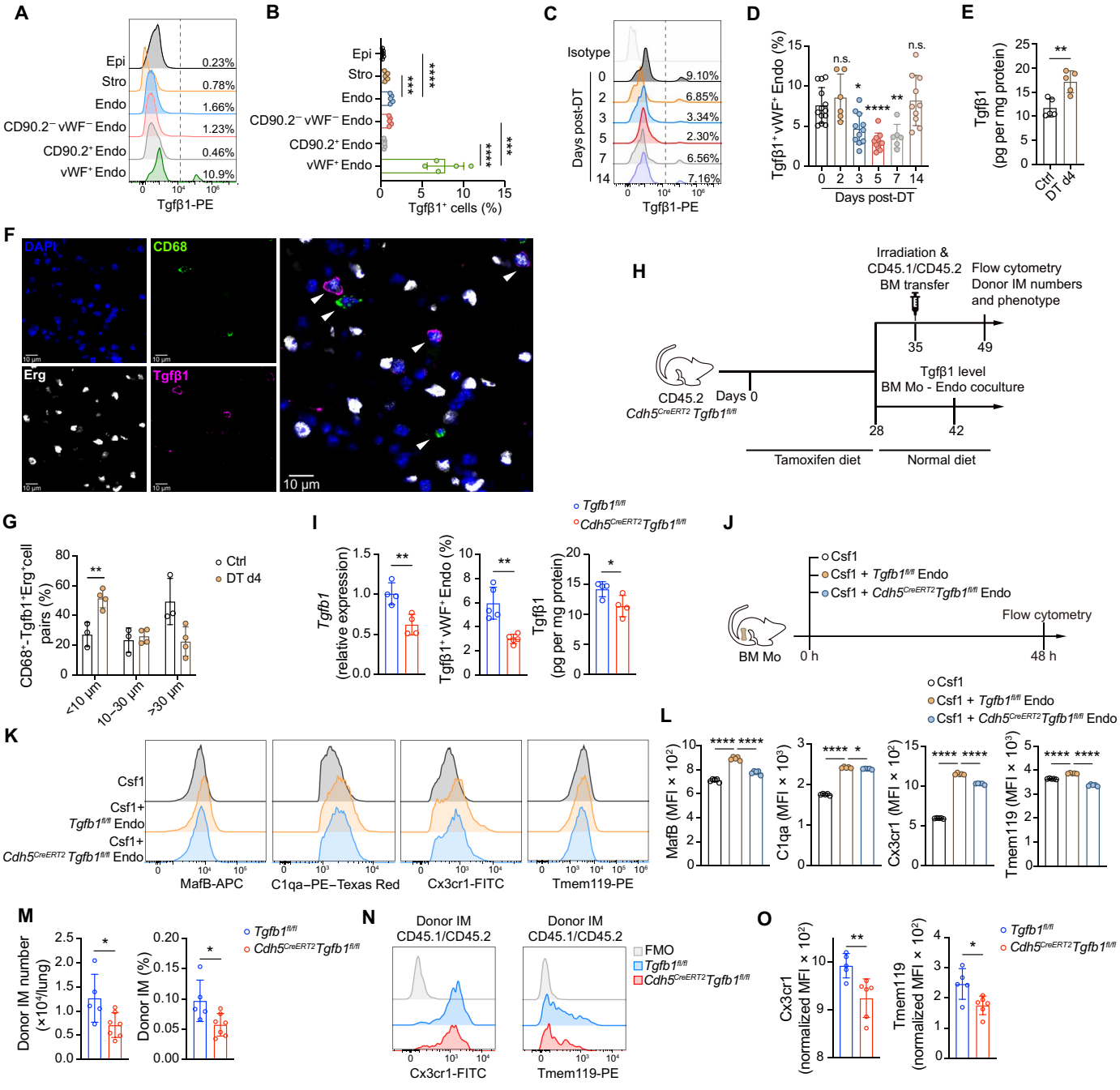

Fig. 5. Lung vWF$^+$ endothelial–derived Tgfβ1 contributes to IM development and identity. (**A**) Representative histogram of latent Tgfβ1 expression in lung Epis, Stros, and Endos from C57BL/6 WT mice. Endos were further divided into CD90.2$^-$vWF$^-$ capillary, CD90.2$^+$ lymphatic, and vWF$^+$ blood vessel Endos. (**B**) Percentage of Tgfβ1$^+$ cells in the indicated cell populations, as in (A). (**C**) Representative histogram of latent Tgfβ1 expression in lung vWF$^+$ blood vessel Endos from DT-treated IM^{DTR} mice at the indicated time points post-DT. (**D**) Percentage of Tgfβ1$^+$ cells within lung vWF$^+$ blood vessel Endos, as in (C). (**E**) Levels of latent Tgfβ1, assessed by enzyme-linked immunosorbent assay on lung extracts from PBS-treated (Ctrl) and DT-treated IM^{DTR} mice at day 4 posttreatment. (**F**) Representative confocal microscopy images of CD68$^+$ mononuclear phagocytes and Tgfβ1$^+$Erg$^+$ Endos in the lungs of DT-treated IM^{DTR} mice at day 4 post-DT. (**G**) Percentages of CD68$^+$ mononuclear phagocyte–Tgfβ1$^+$Erg$^+$ Endo pairs according to the distance separating the two cell types in lungs from PBS-treated (control) or DT-treated IM^{DTR} mice at day 4 post-DT. (**H**) Experimental outline for (I) to (O). (**I**) *Tgfb1* expression (left) and percentage of Tgfβ1$^+$ cells (middle) in Endos, and levels of latent Tgfβ1 in lung extracts from chimeric *Cdh5^{CreERT2} Tgfb1$^{fl/fl}$* mice or *Tgfb1$^{fl/fl}$* controls, as in (H). (**J**) Experimental outline for (K) and (L). (**K**) Representative histograms and (**L**) bar graph showing MFI of MafB, C1qa, Cx3cr1, and Tmem119 expression in BM Mos, as in (J). (**M**) Numbers (left) and percentages (right) of CD45.1 donor IMs from chimeric *Cdh5^{CreERT2} Tgfb1$^{fl/fl}$* mice or *Tgfb1$^{fl/fl}$* controls. (**N**) Representative histograms and (**O**) bar graph showing MFI of Cx3cr1 and Tmem119 expression in IMs from chimeric *Cdh5^{CreERT2} Tgfb1$^{fl/fl}$* mice or *Tgfb1$^{fl/fl}$* controls. Data show [(B), (E), (G), (I), (L), (M), and (O)] means ± SEM and are representative of three independent experiments ($n = 3$ to 7 mice); data show (D) means ± SEM and are pooled from four independent experiments ($n = 6$ to 13 mice). *P* values were calculated using [(B), (D), and (L)] a one-way ANOVA with Dunnett's post hoc tests, [(E), (I), (M), and (O)] a two-tailed unpaired Student's *t* test, or (G) a two-way ANOVA with Šidák's post hoc tests. *$P < 0.05$; **$P < 0.01$; ****$P < 0.0001$.

these data provide evidence that vWF$^+$ blood vessel Endos represent an important source of Tgfβ1 to support IM development.

Myeloid *Tgfbr2* deficiency is associated with a proliferative and dysfunctional IM profile

Next, we explored the potential functional consequences of IM-specific *Tgfbr2* deficiency. To this end, we generated a mouse strain in which AMs would retain TgfβRII expression, whereas IMs would be deficient. CD45.1/CD45.2 IM^{DTR} mice were lethally irradiated with thorax protection and were fully reconstituted with BM cells either from CD45.2 *Tgfbr2*$^{fl/fl}$ mice or CD45.2 *Lyz2*^{Cre} *Tgfbr2*$^{fl/fl}$ mice (Fig. 6A). Four weeks later, chimeric IM^{DTR} mice were treated with DT to specifically empty the IM niche and trigger IM niche refilling from either control or *Tgfbr2*-deficient monocytes. We confirmed that AMs and IMs were of host and donor origin, respectively (Fig. 6B). Bulk RNA-seq was performed on donor CD64$^+$ cells encompassing CD64$^+$ Mos and IMs at day 10 post-DT (fig. S9A), and knockdown of *Tgfbr2* exon 2 was confirmed (fig. S9B). PCA and unsupervised hierarchical clustering showed that control IMs clustered separately from *Tgfbr2*-deficient IMs (Fig. 6, C and D). Differential expression analyses showed 79 up-regulated genes in WT IMs and 152 up-regulated genes in *Tgfbr2*-deficient IMs (adjusted $P < 0.05$ and $\log_2$ fold change > or < 1, respectively) (Fig. 6E). We confirmed the down-regulation of the IM identity genes *Cx3cr1* and *Tmem119* in the absence of *Tgfbr2* (Fig. 6F). Further, using GSEAs, genes known to be up-regulated or down-regulated upon Tgfβ1 stimulation were enriched in *Tgfbr2*-sufficient or -deficient IMs, respectively, validating the model (Fig. 6G). *Tgfbr2*-deficient IMs were enriched in responses related to cell cycling and proliferation, further supporting that, in the absence of *Tgfbr2*, IMs are blocked in a premature proliferative stage that precedes IM differentiation (*11*). Moreover, responses related to cell-cell adhesion were enriched in *Tgfbr2*-deficient IMs. Conversely, a range of responses associated with homeostatic and immunoregulatory functions of macrophages were enriched in *Tgfbr2*-sufficient IMs, such as activation of mTORC1 signaling (*25*), antigen processing and presentation (*18*), and a signature of tolerogenic macrophages (Fig. 6G).

scRNA-seq analysis of lung CD45.1$^-$CD45.2$^+$Ly6G$^-$SiglecF$^-$CD11b$^+$SSC^{lo}CD64$^+$ cells isolated at day 90 post-DT from myeloid-intrinsic *Tgfbr2*-deficient chimeric IM^{DTR} mice indicated an accumulation of monocytes (*Ly6c2*, *Ccr2*, and *Irf8*) expressing *Fcgr4*, reminiscent of tissue monocytes (*10*), at the expense of CD206$^-$ IMs (*Cd72*, *Cd74*, and *H2-Eb1*) and CD206$^+$ IMs (*Mrc1* and *Folr2*), compared with controls (Fig. 6, H to J). DE and Gene Ontology (GO) analyses highlighted an enrichment in monocytes from *Tgfbr2*-deficient chimeric IM^{DTR} mice in the response to type II interferons (*Irf1*, *Cxcl9*, and *Stat1*), cell-cell adhesion (*Vasp*, *Sdc4*, and *Ccl5*), cell proliferation (*Mif* and *Cd38*), and apoptotic signaling as compared with those from *Tgfbr2*-sufficient controls (Fig. 6, K and L), supporting that tissue monocytes substantially contribute to the transcriptional changes observed by bulk RNA-seq. Our data thus support that TGFβ receptor signaling is essential for the differentiation and homeostatic functions of IMs, preventing their accumulation in an immature, proliferative state.

Myeloid Tgfβ receptor signaling drives monocyte and IM spatial organization in the lung microenvironment

Next, we used codetection by indexing (CODEX)–enabled multiplex imaging to investigate how monocyte and IM spatial niche occupancies were affected by the loss of Tgfβ receptor signaling (*26*, *27*). Using a 28-parameter staining panel, we identified donor monocytes and IMs (fig. S10) as well as other lung immune and structural cell types using established markers (table S2). Within the donor CD45.1$^-$CD45.2$^+$ population, we observed a higher proportion of monocytes in lungs from myeloid-intrinsic *Tgfbr2*-deficient chimeric IM^{DTR} mice compared with those from *Tgfbr2*-sufficient controls (Fig. 7A), confirming our flow cytometry and scRNA-seq data. Monocytes in myeloid-intrinsic *Tgfbr2*-deficient chimeric IM^{DTR} mice predominantly accumulated in the adventitial cuffs surrounding larger blood vessels (Fig. 7, B and C), which are composed of vWF$^+$ Endos (*24*). We next examined how cell interactions between monocytes, IMs, and their microenvironment were influenced by the loss of IM-intrinsic TGFβ receptor signaling. Interaction scores of monocytes with Endos and fibroblasts and, to a lesser extent, with Epis were reduced in lungs from myeloid-intrinsic *Tgfbr2*-deficient chimeric IM^{DTR} mice as compared with those from the *Tgfbr2*-sufficient controls (Fig. 7D). A similar reduction in interaction score with Endos was observed for *Tgfbr2*-deficient IMs (Fig. 7D), consistent with a role for Tgfβ receptor signaling in the positioning of monocytes and IMs in dedicated niches. We also found that the interaction score of monocytes with IMs was higher in the absence of myeloid TgfβRII (Fig. 7D), suggesting that IMs were retained in close proximity to monocytes and failed to migrate properly toward their specific niches. Whereas in control lungs, monocytes were closer to Tgfβ$^+$ Endos than to Tgfβ$^-$ Endos, supporting a preferential interaction, the distance between monocytes and Tgfβ$^+$ Endos was markedly increased in the absence of myeloid TgfbRII (Fig. 7, E and F). These data suggested that TGFβ receptor signaling is crucial for guiding monocytes and IMs to their dedicated niches and facilitating interactions with lung structural cells.

Loss of myeloid Tgfβ receptor signaling leads to premature development of age-associated lung abnormalities

To assess the consequences of IM-intrinsic *Tgfbr2* deficiency on lung homeostasis, we performed lung function measurements, histopathological analyses, and protein quantification in chimeric IM^{DTR} mice whose IMs were sufficient or deficient in *Tgfbr2*, at 4 months post-DT (Fig. 6A). Blood myeloid cells, lung neutrophils, and lung dendritic cells expressed lower levels of TgfβRII as compared with IMs (fig. S2, D and E), indicating that they are unlikely to represent major confounding factors in the model. We noticed a substantial death of chimeric IM^{DTR} mice in the absence of myeloid *Tgfbr2* from 2 months post-DT (fig. S11A), in line with previous reports, suggesting that myeloid *Tgfbr2* deficiency can trigger stroke (*28*). We only analyzed mice that were healthy without weight loss or other signs of morbidity. Lungs from myeloid-intrinsic *Tgfbr2*-deficient mice displayed higher inspiratory capacity, higher compliance, and lower elastance as compared to control lungs (Fig. 8A and fig. S11B), a phenotype that was similarly observed in 18-month-old WT mice as compared to that in 2-month-old WT mice (Fig. 8A and fig. S11B). These data are consistent with the hypothesis that, in the absence of *Tgfbr2* on IMs, lungs develop age-related functional abnormalities. A higher degree of alveolar dilatation was observed in the lungs of donor *Lyz2*^{Cre} *Tgfbr2*$^{fl/fl}$ mice as compared with those of donor *Tgfbr2*$^{fl/fl}$ mice (Fig. 8, B and C), a phenotype similar to senile hyperinflation (*29*). Perivascular accumulation of leukocytes, among which were CD68$^+$ monocytic cells close to vWF$^+$ Endos, was observed in the lungs of donor *Lyz2*^{Cre} *Tgfbr2*$^{fl/fl}$ mice

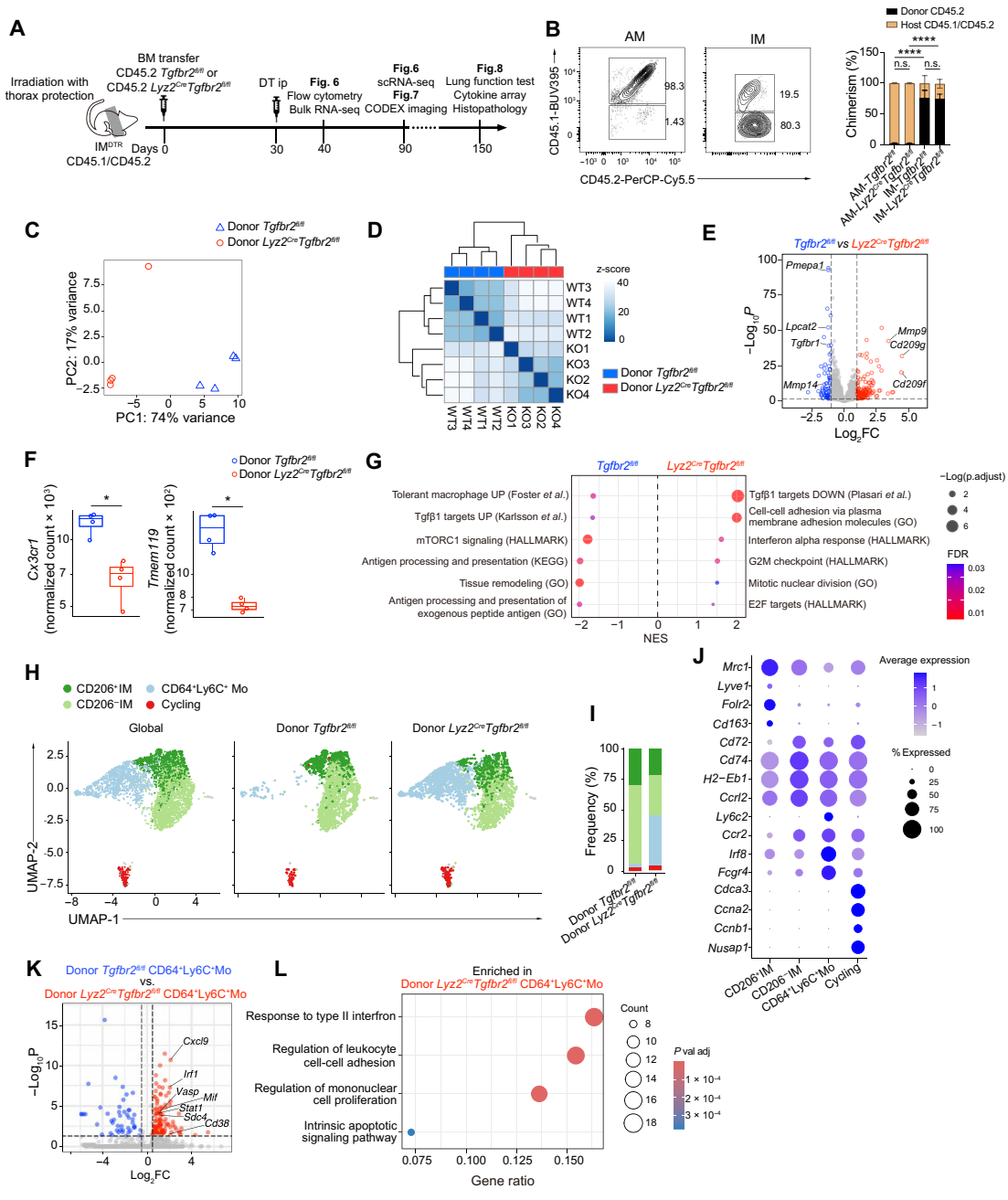

Fig. 6. Disruption of IM-intrinsic TgfβRII signaling is associated with an immature and dysfunctional IM profile. (**A**) Experimental outline. Thorax-protected CD45.1/CD45.2 IM^{DTR} mice were lethally irradiated and reconstituted with BM cells from either CD45.2 *Tgfbr2*$^{fl/fl}$ mice (group Donor *Tgfbr2*$^{fl/fl}$) or *Lyz2*^{Cre} *Tgfbr2*$^{fl/fl}$ mice (group Donor *Lyz2*^{Cre} *Tgfbr2*$^{fl/fl}$). Chimeric mice injected 4 weeks later with DT intraperitoneally and analyzed at days 10, 60, and 120 after DT. (**B**) Representative CD45.1 and CD45.2 plots (left) and chimerism (right) of AMs and IMs, assessed at day 10 post-DT, as in (A). (**C**) PCA plot showing the transcriptional identity of IMs, evaluated by bulk RNA-seq at day 10 post-DT, as in (A). $n = 4$ replicates per group, with each replicate representing a pool of IMs sorted from three mice in two independent sorting experiments. (**D**) Unsupervised hierarchical clustering of IMs, as in (C). (**E**) Volcano plot of the DE genes between *Tgfbr2*-sufficient and *Tgfbr2*-deficient IMs, as in (C). (**F**) Bar graphs showing expression of genes between *Tgfbr2*-sufficient and *Tgfbr2*-deficient IMs, as in (C). (**G**) GSEAs of *Tgfbr2*-sufficient and *Tgfbr2*-deficient IMs, as in (C). The NES and FDR are shown. (**H**) Global and genotype-specific UMAP plots depicting the transcriptional identity of lung CD64$^+$ Mos and IMs isolated from donor *Tgfbr2*$^{fl/fl}$ and donor *Lyz2*^{Cre} *Tgfbr2*$^{fl/fl}$ chimeric IM^{DTR} mice at day 60 post-DT, as in (A) ($n = 5$ pooled mice per group). (**I**) Frequency of each cell cluster from donor *Tgfbr2*$^{fl/fl}$ and donor *Lyz2*^{Cre} *Tgfbr2*$^{fl/fl}$ chimeric IM^{DTR} mice. (**J**) Dot plots showing average expression of the indicated genes and the percentages of cells expressing the genes within each cluster. (**K**) Volcano plot depicting DE genes between the monocyte cluster from donor *Tgfbr2*$^{fl/fl}$ and donor *Lyz2*^{Cre} *Tgfbr2*$^{fl/fl}$ chimeric IM^{DTR} mice. (**L**) Dot plot showing GO enrichment results comparing CD64$^+$Ly6C$^+$ monocytes coming from donor *Tgfbr2*$^{fl/fl}$ and donor *Lyz2*^{Cre} *Tgfbr2*$^{fl/fl}$ chimeric IM^{DTR} mice. [(B) and (F)] Data show means ± SEM and (B) are representative of two independent experiments ($n = 5$ mice) and (F) four biological replicates of FACS-sorted cells. *P* values were calculated using (B) a two-way ANOVA with Tukey's post hoc tests or [(E), (F), and (K)] a Wilcoxon rank sum test. [(E) and (K)] Significantly expressed genes were defined by $\log_2$ fold change ($\log_2$FC) > 0.5 and adjusted $P < 0.05$. *$P < 0.05$; ****$P < 0.0001$. DOWN, down-regulated genes; KEGG, Kyoto Encyclopedia of Genes and Genomes; mTORC1, mammalian target of rapamycin complex 1; UP, up-regulated genes.

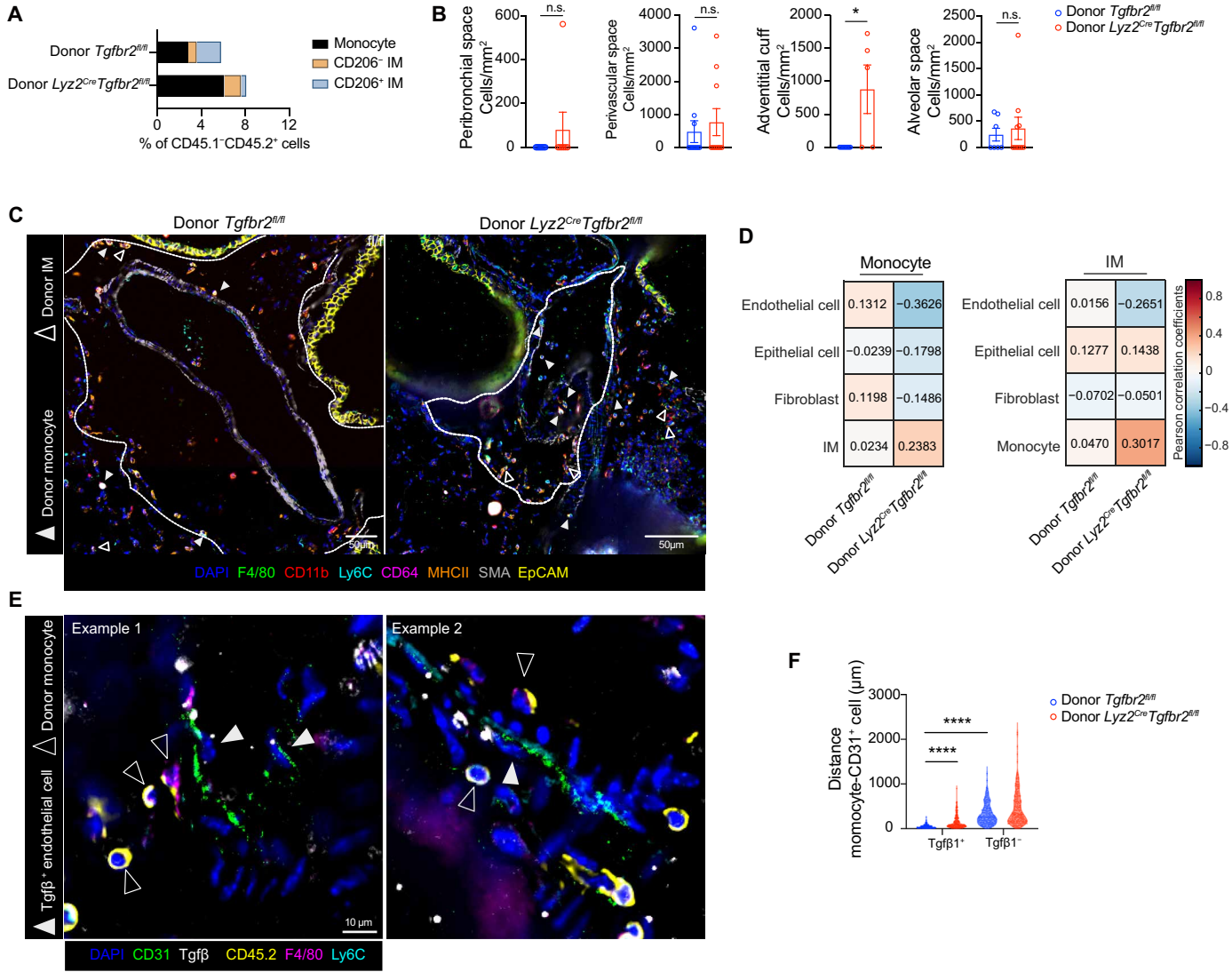

Fig. 7. Tgfβ receptor signaling in monocytes and IMs regulates niche occupancy and interactions with lung structural cells. (**A**) Bar graphs showing the proportion of monocytes and IM subsets within donor CD45.1$^-$CD45.2$^+$ cells, as in Fig. 6A. (**B**) Bar graphs showing the cell numbers of CD45.1$^-$CD45.2$^+$ monocytes in the four anatomical areas, peribronchial space, perivascular space, adventitial cuff, and alveolar space, as in Fig. 6A. (**C**) Representative imaging showing adventitial cuffs in donor *Tgfbr2*$^{fl/fl}$ and donor *Lyz2*^{Cre} *Tgfbr2*$^{fl/fl}$ chimeric IM^{DTR} mouse lungs with presence of CD45.1$^-$CD45.2$^+$ monocytes and IMs, as in Fig. 6A. (**D**) The interaction score of CD45.1$^-$CD45.2$^+$ monocytes or IMs with indicated cells in donor *Tgfbr2*$^{fl/fl}$ and donor *Lyz2*^{Cre} *Tgfbr2*$^{fl/fl}$ chimeric IM^{DTR} mouse lungs, as in Fig. 6A. (**E**) The proximity between CD45.1$^-$CD45.2$^+$ monocytes and Tgfβ$^+$ CD31$^+$cells in donor *Lyz2*^{Cre} *Tgfbr2*$^{fl/fl}$ chimeric IM^{DTR} mouse lungs, as in Fig. 6A. (**F**) Violin plots showing the shortest distance between CD45.1$^-$CD45.2$^+$ monocytes with Tgfβ$^+$ CD31$^+$cells or Tgfβ$^-$ CD31$^+$cells in donor *Tgfbr2*$^{fl/fl}$ and donor *Lyz2*^{Cre} *Tgfbr2*$^{fl/fl}$ chimeric IM^{DTR} mouse lungs, as in Fig. 6A. [(B) and (F)] Data show means ± SEM. *P* values were calculated using a Wilcoxon rank sum test. *$P < 0.05$; ****$P < 0.0001$. Scale bars, (C) 50 μm and (E) 10 μm. DAPI, 4′,6-diamidino-2-phenylindole; EpCAM, epithelial cell adhesion molecule; MHCII, major histocompatibility complex class II; SMA, smooth muscle actin.

(Fig. 8, B, D, and E). At the protein level, the lungs of donor *Lyz2*^{Cre} *Tgfbr2*$^{fl/fl}$ mice contained lower levels of many cytokines, chemokines, and growth factors as compared with those of donor *Tgfbr2*$^{fl/fl}$ mice (Fig. 8E), supporting an impairment of lung immune surveillance when IMs cannot engage Tgfβ receptor pathways. Moreover, the lungs of donor *Lyz2*^{Cre} *Tgfbr2*$^{fl/fl}$ chimeric mice displayed lower levels of interleukin-10 (IL-10), an immunosuppressive cytokine produced by IMs (Fig. 8F) (*9*, *10*, *15*, *16*), lower levels of elastin (Fig. 8G), and higher levels of soluble collagen (Fig. 8H) as compared with those of donor *Tgfbr2*$^{fl/fl}$ mice. Together, these data supported that disruption of IM-specific TgfβRII signaling has a profound impact on the lung immunoregulatory environment and triggers age-related changes.

DISCUSSION

Here, we found that blood vessel–associated vWF$^+$ Endos provide Tgfβ1 to monocytes entering the lung tissue to allow their transition toward functional lung IMs. Disruption of myeloid-intrinsic Tgfβ receptor signaling resulted in the accumulation of monocytes and immature IMs in adventitial cuffs and an impairment of IM development, identity, and niche occupancy, which was associated with

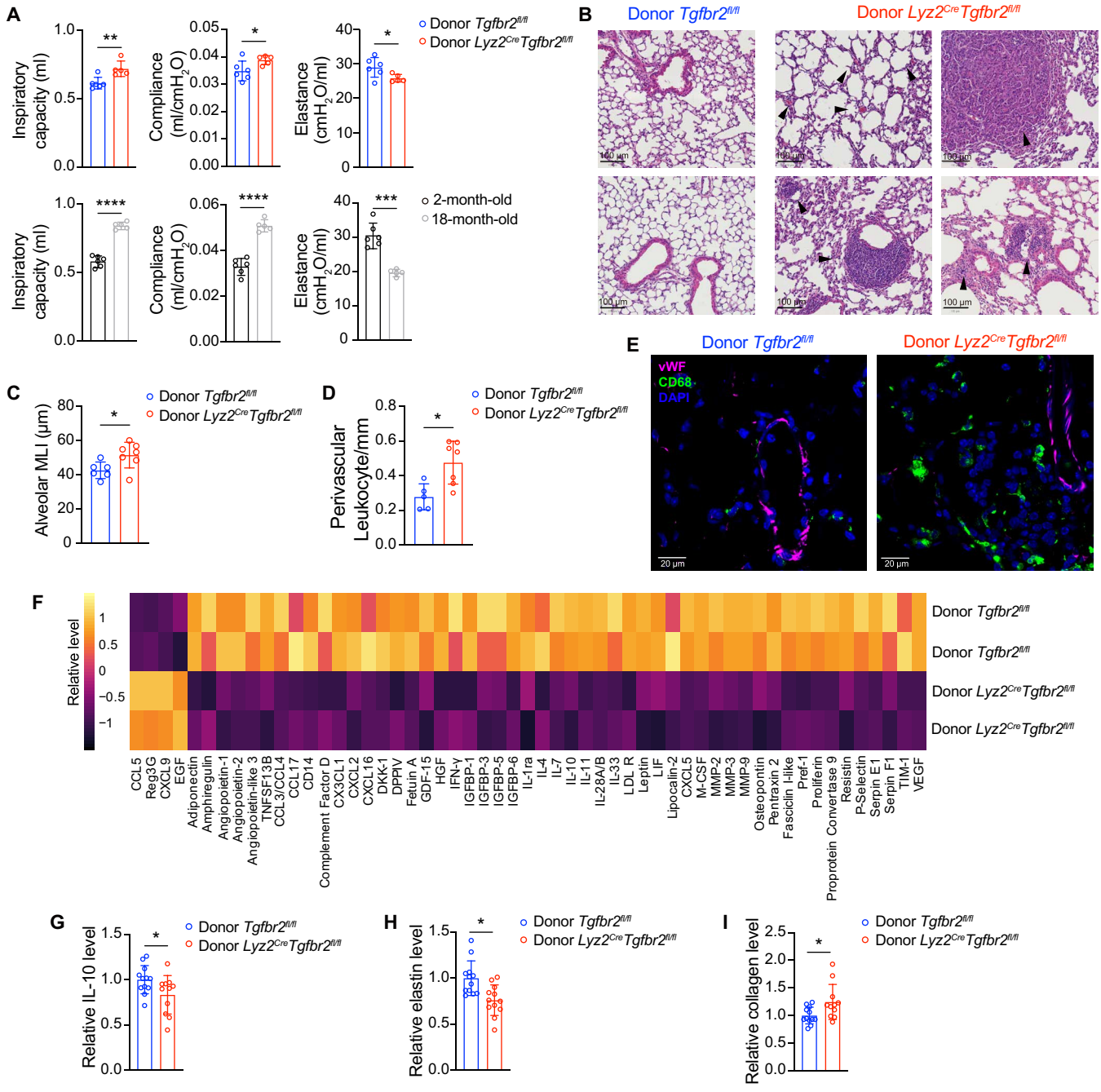

Fig. 8. IM-intrinsic *Tgfbr2* deficiency triggers age-related lung functional, structural, and immune abnormalities. (**A**) Invasive measurements of inspiratory capacity, lung compliance, and lung elastance in donor *Tgfbr2*$^{fl/fl}$ or donor *Lyz2*^{Cre} *Tgfbr2*$^{fl/fl}$ chimeric IM^{DTR} mice at day 120 after DT, as in Fig. 6A, and in 2-month-old or 18-month-old C57BL/6 WT mice. (**B**) Representative hematoxylin and eosin stainings of lung sections of chimeric IM^{DTR}, as in (A). (**C**) Alveolar dilatation assessed through measurements of alveolar MLI in the lungs of chimeric IM^{DTR}, as in (B). (**D**) Quantification of perivascular leukocyte infiltration in the lungs of chimeric IM^{DTR}, as in (B). (**E**) Representative confocal microscopy pictures of lung sections of chimeric IM^{DTR}, as in (B). Pictures are representative of one of the six mice, each giving similar results. (**F**) Heatmap depicting the relative abundance of the indicated proteins in lung extracts from chimeric IM^{DTR} mice at day 120 post-DT, as in (A). (**G** to **I**) Levels of (G) IL-10, (H) elastin, and (I) soluble collagen in lung extracts from chimeric IM^{DTR} mice, as in (A). Data show means ± SEM [(A), (C), and (D)] and are representative of two independent experiments ($n = 5$ to 7 mice per group) or [(G) to (I)] are pooled from two independent experiments ($n = 11$ or 12 mice per group). (F) Data represent biological replicates of cells sorted by FACS. [(A), (C), (D), and (G) to (I)] *P* values were calculated using a two-tailed unpaired Student's *t* test. *$P < 0.05$; **$P < 0.01$; ***$P < 0.001$; ****$P < 0.0001$. CCL, C-C motif chemokine ligand; DDPIV, dipeptidyl peptidase 4; DKK-1, dickkopf WNT signaling pathway inhibitor 1; EGF, epidermal growth factor; GDF-15, growth differentiation factor 15; IGFBP-1, insulin like growth factor binding protein 1; LDL R, low-density lipoprotein receptor; LIF, leukemia inhibitory factor; M-CSF, macrophage colony-stimulating factor; MLI, mean linear intercept; MMP, matrix metalloproteinase; TIM-1, T-cell immunoglobulin and mucin domain 1; TNFSF13B, tumor necrosis factor superfamily member 13b; VEGF, vascular endothelial growth factor.

changes in the lung immunoregulatory environment and age-related abnormalities. These observations highlight a previously undescribed endothelial-IM axis involved in lung homeostasis and the preservation of lung integrity at steady state.

Tgfβ signaling plays an important role in RTM biology and tissue adaptation. In the gut, neuron-associated muscularis macrophages are instructed by Tgfβ from the enteric nervous system (*30*), and colonic macrophage differentiation also requires Tgfβ receptor signaling (*31*). In the lung, AMs rely on both Csf2 and autocrine Tgfβ for their development, maintenance, and homeostatic functions (*7*). Csf2-cultured fetal monocytes can differentiate into AM-like cells when treated with Tgfβ (*7*). Similarly, BM Mos cultured with Csf2 and Tgfβ1 up-regulated AM signature genes. However, in Csf1-treated BM Mos, Tgfβ1 induced MafB expression, thus promoting IM-like differentiation while repressing PPAR-γ. Adding Csf2 to Csf1- and Tgfβ1-containing cultures suppressed IM-specific genes and *Tgfbr2*, suggesting that Csf2 dominates over Csf1 by favoring AM fate. Thus, Tgfβ1 appears to act as a context-dependent cofactor, synergizing with Csf1 to drive MafB-dependent IM-associated pathways but enhancing AM-specific programs in the presence of Csf2. The substantial down-regulation of *Tgfbr2* in Csf2-treated cultures might limit the ability of Tgfβ1 to drive IM-like differentiation, although it could also paradoxically constrain its ability to promote full AM development. In vivo, these dynamics are likely influenced by the spatial and temporal availabilities of Csf1, Csf2, and Tgfβ1. In the brain, microglia rely on Tgfβ1 for their development and identity, and disruption of Tgfβ receptor signaling in adult microglia results in an aberrant activation phenotype and neurological disorders (*32*–*35*). Although lung IMs and microglia differ in origin and other aspects, they share a common gene signature characterized by elevated *Cx3cr1*, *Tmem119*, *MafB*, and *C1q* expression (*11*, *32*, *36*), a signature that is induced by Tgfβ1. The source of Tgfβ1 is, however, different, given that microglia produce Tgfβ1 autonomously (*37*, *38*), whereas lung IMs receive it from Endos. Our observations suggest that a combination of signals can act in concert to imprint a functional specification of RTMs in tissues. In the lung, besides Csf1 and Tgfβ1 contributing to global IM development (*11*, *14*, *39*, *40*), the identification of IM subset-specific microenvironmental signals that act within tissular niches to functionally imprint distinct IM subpopulations will require further investigation.

In the IM^{DTR} mouse model, previously developed to investigate monocyte-to-IM differentiation (*11*), we observed a decrease in intracellular Tgfβ1 within vWF^+ blood vessel Endos during IM differentiation and niche refilling. This was accompanied by a concomitant increase in lung Tgfβ1 level and decreased distance between $Tgfβ1^+$ Endos and $CD68^+$ monocytes, suggesting a direct interaction during IM development. Furthermore, inhibiting Tgfβ receptor signaling during IM niche refilling led to a reduction in both $CD206^+$ and $CD206^-$ IM subsets, supporting a role for Tgfβ1-Tgfβ receptor interactions in IM development before subset-specific differentiation occurs. BM-mixed chimera experiments in thorax-protected, DT-treated IM^{DTR} mice further supported that myeloid-intrinsic *Tgfbr2* expression conferred a competitive advantage to differentiate into both IM subsets. We found that Tgfβ1 could synergistically act with Csf1 to trigger MafB, a regulator of IM development (*11*); the expression of IM signature genes (i.e., *Cx3cr1*, *Tmem119*, and *C1q*); and the up-regulation of TgfβRII expression. In microglia, Tgfβ1 has been shown to promote *Cx3cr1* (*41*) and *Tmem119* (*42*) expression, possibly via Smad activation downstream of Tgfβ receptor signaling and the presence of Smad binding elements in their promoter sequences (*41*, *42*). Although $CD206^-$ IMs express lower levels of TGFβRII compared with $CD206^+$ IMs, our findings suggest that TGFβ signaling plays a role in the differentiation of both IM subsets from monocytes, likely at an early stage of monocyte-to-IM transition. This is consistent with the early requirement for MafB in IM differentiation, despite its higher expression in $CD206^+$ IMs (*11*). Hence, our data are consistent with the idea that monocytes, once extravasated in the tissue, first require activation of Csf1 signaling to up-regulate TgfβRII. Such a process primes IM precursors for Tgfβ responsiveness and allows sensing of endothelial Tgfβ1 and Tgfβ signaling engagement to trigger MafB, induce expression of migration-associated genes downstream of TgfβRII, and pursue their migration and differentiation trajectory in the lung. Further supporting this idea, myeloid *Tgfbr2* deficiency was associated with the accumulation of parenchymal $CD64^+$ Mos held in a proliferative state, i.e., the precursors of IMs (*11*), and a reduction in IM numbers, as well as a loss of their identity markers Cx3cr1 and Tmem119. Although the decrease in IM numbers in $Lyz2^{Cre}$ $Tgfbr2^{fl/fl}$ mice was modest, we speculate that some remaining IMs may still express TgfβRII, given that LysM-Cre–driven *Tgfbr2* depletion is not complete in myeloid cells.

In the last part of the study, we uncovered a role for endothelial Tgfβ1-IM TgfβRII interactions in the prevention of age-related lung abnormalities. To this end, we generated a chimeric mouse strain in which IMs, but not AMs, did not express *Tgfbr2*, overcoming previous limitations because of the lack of tools specifically targeting IMs. Bulk and scRNA-seq analyses of monocytes and IMs in these chimeric mice revealed an immature, proliferative, and dysfunctional IM profile in the absence of *Tgfbr2*. Multiplex imaging further supported that Tgfβ signaling–mediated endothelial-IM interactions guide IM precursors toward specific niches in the lung. Without TgfβRII signaling, monocytes and immature IMs accumulated in adventitial cuffs, suggesting that they failed to activate intrinsic migration programs or sense extrinsic positional cues, such as chemokines from lung structural niche cells. Such reduced interaction with their microenvironment likely impaired IM imprinting, survival, and functional specification. Consequently, niche cells might lack the necessary IM support to sustain their homeostatic functions. Additionally, the perivascular accumulation of immature monocytes could itself contribute to the development of age-related abnormalities developing when IM-intrinsic TgfβRII is disrupted. By 6 months of age, the lungs of those mice exhibited increased compliance and decreased elastance, resembling the phenotype of 18-month-old WT mice. Alveolar enlargements, increased collagen, and decreased elastin contents were also observed as compared with control lungs, processes known to occur with age and predispose to lung diseases (*29*, *43*). Moreover, the levels of many cytokines and growth factors, including IL-10, were reduced in the absence of IM-intrinsic *Tgfbr2*, potentially compromising immune surveillance and tissue integrity. IMs may directly or indirectly regulate the extracellular matrix (ECM) by modulating ECM-degrading enzymes such as matrix metalloproteinases, which were decreased in lungs containing *Tgfbr2*-deficient IMs, or by producing IL-10, known to regulate ECM deposition (*44*, *45*). Whereas their cellular source remains to be identified, other factors found to be decreased in lungs with *Tgfbr2*-deficient IMs are potential suppressors of fibroblast-driven collagen deposition, such as adiponectin (*46*), hepatocyte growth factor (HGF) (*47*), or pentraxin-2 (*48*). Excessive collagen

deposition and elastin degradation could then contribute to lung stiffening and alveolar enlargements, both hallmarks of aging lungs (*49*–*51*). Last, IMs may also play a role in preserving the integrity of the alveolar-capillary barrier by interacting with Epis and Endos. Loss of TGFβRII signaling in IMs may disrupt their ability to occupy dedicated niches and to promote the production of growth factors and cytokines that maintain endothelial and epithelial integrity and functions, including adiponectin (*52*), angiopoietin-1 (*53*), amphiregulin (*54*), and lipocalin-2 (*55*). Identifying the precise IM-driven mechanisms involved and whether specific IM subsets preferentially carry out such homeostatic functions represent interesting avenues for future research.

In conclusion, our work identifies an endothelial-myeloid crosstalk involving Tgfβ1-Tgfβ receptor interactions, which constantly takes place during IM transition from monocytes in adult mice. Disruption of such a pathway critically affects lung homeostasis and triggers the premature development of age-related changes, highlighting an essential role for lung IMs in supporting tissue integrity and immune homeostasis at steady state via Tgfβ receptor–dependent mechanisms.

MATERIALS AND METHODS

Study design

In this study, we investigated the niche-derived signals instructing lung IM development and identity and the functional consequences for lung homeostasis. To this end, we used ex vivo and in vivo approaches combined with transcriptional profiling, flow cytometry, multiplex imaging, BM chimeras, IM^{DTR} mice, gene targeting, and lung functional and histopathological analyses. For most mouse experiments, group sizes ranged from three to six mice to ensure sufficient statistical power (≥80%) with a significance threshold of 5%. In some experiments, sample sizes were not predetermined using statistical methods; however, they were consistent with those reported in previous studies (*10*, *11*, *56*, *57*). Unless specified otherwise, data from independent experiments were pooled for analysis with each panel. No data were excluded, and all replication attempts were successful, yielding comparable results. Lung histopathological analyses were assessed in a blinded manner. Detailed information on sample sizes, experimental replicates, and the statistical analyses can be found in the corresponding figure legends.

Mice

All experiments, unless otherwise specified, were performed on age-matched 8- to 12-week-old male and female mice on the C57BL/6 background. In this study, the following mice were used on the C57BL/6 background: CD45.2 WT (the Jackson Laboratory); CD45.1 WT (the Jackson Laboratory, 002014); $Lyz2^{Cre}$ (the Jackson Laboratory, 004781); $Mafb^{fl/fl}$ (*11*); $Tgfbr2^{fl/fl}$ (the Jackson Laboratory, 012603); $Cdh5^{CreERT2}$ (Taconic Biosciences, 13073); $Tgfb1^{fl/fl}$ (the Jackson Laboratory, 065809); and $Tmem119^{Cre}$ $Cx3cr1^{LSL\text{-}DTR/+}$ mice, called IM^{DTR} mice (*11*). Myeloid-restricted *Tgfbr2* or *Mafb* depletion was achieved by crossing $Tgfbr2^{fl/fl}$ or $Mafb^{fl/fl}$ mice with $Lyz2^{Cre}$ mice. *CD45.1/CD45.2* IM^{DTR} mice were generated by crossing CD45.1 $Tmem119^{Cre}$ with *CD45.2* $Cx3cr1^{LSL\text{-}DTR}$ mice. $Cdh5^{CreERT2}$ and $Tgfb1^{fl/fl}$ mice were crossed to produce $Cdh5^{CreERT2}$ $Tgfb1^{fl/fl}$ mice.

Mice were housed under specific pathogen–free conditions and maintained in a 12-hour light-dark cycle with food and water ad libitum. Experiments were reviewed and approved by the Institutional Animal Care and Use Committee of the University of Liège (ethical approval no. 1956). The *Guide for the Care and Use of Laboratory Animals* prepared by the Institute of Laboratory Animal Resources, National Research Council, and published by the National Academy Press, as well as European and local legislations, were followed carefully. Accordingly, the temperature and relative humidity were 21°C and 45 to 60%, respectively.

In vivo treatments with chemicals and antibodies

For DT-induced depletion of IMs, IM^{DTR} mice were administered a single intraperitoneal injection of 50 ng of DT (List Biological Labs, 150), whereas control mice were injected with PBS. In TgfβR inhibitor experiments, IM^{DTR} mice received three intraperitoneal injection of LY364947 at 1 mg/kg of body weight (Selleckchem, S2805) in 200 μl of PBS at days 2, 4, and 6 post-DT. Control mice were injected with 200 μl of PBS intraperitoneally.

For assessment of cell localization in the lung, 1 μg of FITC-conjugated anti-mouse CD45.2 (clone 104; BD Biosciences, 564616) was injected intravenously 10 min before and 1 μg of APC-conjugated anti-mouse CD45.2 (clone 104; BD Biosciences, 558702) was injected intratracheally 5 min before euthanasia to distinguish intravascular ($CD45\text{-}FITC^{+}$ $CD45\text{-}APC^{-}$), parenchymal ($CD45\text{-}FITC^{-}$ $CD45\text{-}APC^{-}$), and airway ($CD45\text{-}FITC^{-}$ $CD45\text{-}APC^{+}$) cells. To achieve endothelial-specific *Tgfb1* deletion, 4-week-old $Cdh5^{CreERT2}$ $Tgfb1^{fl/fl}$ mice or $Tgfb1^{fl/fl}$ controls were fed a tamoxifen diet (0.25 g/kg; SAFE, E8404A01R 00008) for 4 weeks and then were fed with normal diet afterward.

Reagents and antibodies

A complete list of the reagents and antibodies used in this manuscript can be found in table S1.

Flow cytometry

Cells (0.5×10^6 to 5×10^6) were preincubated with mouse Fc block (BD Biosciences, 553142) to avoid nonspecific binding to Fc receptors and then stained with appropriate antibodies at 4°C in the dark for 10 min. Unless otherwise instructed, all antibodies were diluted 1:100 for staining at 4°C for 30 min. Cell viability was assessed using LIVE/DEAD fixable near-IR (775) stain (Thermo Fisher Scientific, L34976), and cell apoptosis was detected by annexin V after surface staining, according to the manufacturer's instructions. TgfβRII (R&D Systems, FAB532P), Cx3cr1 (R&D Systems, FAB5825G), and Tmem119 (Thermo Fisher Scientific, 12-6119-82) stainings were performed at 37°C for 30 min with a 1:50 dilution. Intracellular cytokine staining was performed using an intracellular staining set (Thermo Fisher Scientific, 00-5523-00). For Ki-67 staining, cells were permeabilized and stained extracellularly using a FITC mouse anti-Ki67 set (BD Biosciences, 556026). Annexin V/propidium iodide (PI) stainings were performed at room temperature for 15 min. The cell suspensions were analyzed with an LSRFortessa (BD Biosciences). FlowJo software (BD Biosciences) was used for data analysis. For the bulk and scRNA-seq experiments, lung $CD45.1^{-}$ $CD45.2^{+}Ly6G^{-}SiglecF^{-}CD11b^{+}SSC^{lo}CD64^{+}$ Macs ($CD64^{+}$ Mos and IMs) were sorted using a Sony MA900. To generate CM, Endos ($CD45^{-}CD31^{+}Epcam^{-}$), Epis ($CD45^{-}CD31^{-}Epcam^{+}$), and Stros ($CD45^{-}CD31^{-}Epcam^{-}$) were sorted using a FACSAria III (BD Biosciences). The list of antibodies used can be found in table S1.

Generation of BM (competitive) chimeras

Eight-week-old CD45.1/CD45.2 IM^{DTR} mice were anesthetized via intraperitoneal injection of xylazine (10 mg/kg; Bayer, 0076901) and ketamine (75 mg/kg; Dechra, 804132) in 200 μl of PBS. A 0.6-cm-thick lead shield was used to protect the thoracic cavity, and the mice underwent lethal irradiation in two 6–gray (Gy) doses, spaced 15 min apart. After regaining consciousness, they were intravenously administrated with 10^7 BM cells from either CD45.2 *Tgfbr2*$^{fl/fl}$ or CD45.2 *Lyz2*^{Cre}*Tgfbr2*$^{fl/fl}$ donors. For generating mixed BM chimeras, mice received 10^7 BM cells comprising an equal mixture of CD45.1$^+$ WT cells and CD45.2 *Lyz2*^{Cre}*Tgfbr2*$^{fl/fl}$ cells via intravenous injection. Nine-week-old *Cdh5*^{CreERT2} *Tgfb1*$^{fl/fl}$ mice were lethally irradiated with two doses of 4 Gy, 15 min apart. The mice were injected intravenously with 10^7 BM cells from CD45.1.2 WT mice after 2 hours of irradiation and were treated with enrofloxacin (0.05 mg/ml; Baytril, Bayer) in drinking water for 4 weeks from the day of irradiation.

Ex vivo BM Mo and BMDM experiments

To generate CM, FACS-sorted lung Endos, Epis, and Stros were cultured in RPMI medium (Thermo Fisher Scientific, 21875-034) containing 10% v/v FBS, penicillin-streptomycin (50 U/ml; Thermo Fisher Scientific, 15070-063), 1 mM sodium pyruvate (Thermo Fisher Scientific, 11360-070), 1× minimum essential medium nonessential amino acids (MEM NEAA) solution (Thermo Fisher Scientific, 11140-035), and 50 μM 2-mercaptoethanol (Thermo Fisher Scientific, 31350-010) at 37°C. After 12 hours, the CM was collected by centrifugation to obtain the supernatant. BM Ly6C$^+$ monocytes were isolated from mice using a monocyte isolation kit (Miltenyi Biotec, 130-100-629). These monocytes were then treated with CM, whereas the control monocytes were cultured in the medium at 37°C for 48 hours. BM Mos were then collected, and RNA was extracted by TRIzol.

BM Ly6C$^+$ monocytes were isolated from *Tgfbr2*$^{fl/fl}$, *Lyz2*^{Cre} *Tgfbr2*$^{fl/fl}$, *Mafb*$^{fl/fl}$, and *Lyz2*^{Cre} *Mafb*$^{fl/fl}$ mice and treated with or without Tgfβ1 (20 ng/ml) together with Csf1 or Csf2 (40 ng/ml) at 37°C for 48 hours. All samples were analyzed by flow cytometry or reverse transcription quantitative polymerase chain reaction (RT-qPCR).

For coculture experiments, Endos were isolated from mouse lung single-cell suspensions using the CD31 MicroBeads kit (Miltenyi Biotec, 130-097-418) and cocultured with BM Mos from *Tgfbr2*$^{fl/fl}$ or *Lyz2*^{Cre} *Tgfbr2*$^{fl/fl}$ mice with Csf1 (40 ng/ml) at 37°C for 48 hours. One coculture group from *Tgfbr2*$^{fl/fl}$ mice was treated with 5 μM of the TgfβR inhibitor LY-364947 (Selleckchem, S2805). The ratios of Endos to BM Mos were 2:1 in Fig. 2 (H and I) and 1:2 in Fig. 5 (J to L).

For the generation of BMDMs, BM Mos were treated with Csf1 (40 ng/ml) on the first day, and the medium containing Csf1 (40 ng/ml) was changed twice at days 3 and 5. At day 7, 95% of cells were F4/80$^+$CD11b$^+$ as confirmed by flow cytometry.

CODEX stainings, imaging, processing, and analysis

Frozen lung sections from chimeric IM^{DTR} mice were prepared for CODEX staining using a 28-plex antibody panel. After fixation, photobleaching, and blocking, samples were stained overnight and processed for imaging. CODEX imaging was performed using a wide-field fluorescence microscope, capturing multiple channels with *z*-spacing of 1.5 μm. Raw files were processed for background subtraction, stitching, and cell segmentation.

Cell populations were identified and classified using fluorescence markers and a strategy akin to flow cytometry (table S2), and downstream analyses were performed. Additional details can be found in the Supplementary Materials.

Statistical analysis

Graphs were generated using GraphPad Prism 10 (GraphPad software) or R Bioconductor (version 3.5.1). As indicated in the figure legends, parametric tests were conducted under the assumption of normal data distribution. No data were excluded from the analyses. Statistical tests were conducted using Prism 9 (GraphPad Software) and R Bioconductor (3.5.1) with the Seurat package used for scRNA-seq data analysis. The specific statistical methods used for each experiment are detailed in the corresponding figure legends. Statistical significance was defined as $P < 0.05$, with significance levels indicated as follows: $*P < 0.05$; $**P < 0.01$; $***P < 0.001$; $****P < 0.0001$; n.s., not significant. Additional sections and details about Materials and Methods can be found in the Supplementary Materials.

Supplementary Materials

The PDF file includes:
Materials and Methods
Figs. S1 to S11
Tables S1 and S2
References (*58*–*63*)

Other Supplementary Material for this manuscript includes the following:
Data file S1
MDAR Reproducibility Checklist

REFERENCES AND NOTES

1. H. Aegerter, B. N. Lambrecht, C. V. Jakubzick, Biology of lung macrophages in health and disease. *Immunity* **55**, 1564–1580 (2022).
2. J. Schyns, F. Bureau, T. Marichal, Lung interstitial macrophages: Past, present, and future. *J. Immunol. Res.* **2018**, 5160794 (2018).
3. M. Guilliams, F. R. Svedberg, Does tissue imprinting restrict macrophage plasticity? *Nat. Immunol.* **22**, 118–127 (2021).
4. C. Schneider, S. P. Nobs, M. Kurrer, H. Rehrauer, C. Thiele, M. Kopf, Induction of the nuclear receptor PPAR-γ by the cytokine GM-CSF is critical for the differentiation of fetal monocytes into alveolar macrophages. *Nat. Immunol.* **15**, 1026–1037 (2014).
5. J. Gschwend, S. P. M. Sherman, F. Ridder, X. Feng, H.-E. Liang, R. M. Locksley, B. Becher, C. Schneider, Alveolar macrophages rely on GM-CSF from alveolar epithelial type 2 cells before and after birth. *J. Exp. Med.* **218**, e20210745 (2021).
6. M. Guilliams, I. De Kleer, S. Henri, S. Post, L. Vanhoutte, S. De Prijck, K. Deswarte, B. Malissen, H. Hammad, B. N. Lambrecht, Alveolar macrophages develop from fetal monocytes that differentiate into long-lived cells in the first week of life via GM-CSF. *J. Exp. Med.* **210**, 1977–1992 (2013).
7. X. Yu, A. Buttgereit, I. Lelios, S. G. Utz, D. Cansever, B. Becher, M. Greter, The cytokine TGF-β promotes the development and homeostasis of alveolar macrophages. *Immunity* **47**, 903–912.e4 (2017).
8. M. Liegeois, C. Legrand, C. J. Desmet, T. Marichal, F. Bureau, The interstitial macrophage: A long-neglected piece in the puzzle of lung immunity. *Cell. Immunol.* **330**, 91–96 (2018).
9. S. Chakarov, H. Y. Lim, L. Tan, S. Y. Lim, P. See, J. Lum, X.-M. Zhang, S. Foo, S. Nakamizo, K. Duan, W. T. Kong, R. Gentek, A. Balachander, D. Carbajo, C. Bleriot, B. Malleret, J. K. C. Tam, S. Baig, M. Shabeer, S.-A. E. S. Toh, A. Schlitzer, A. Larbi, T. Marichal, B. Malissen, J. Chen, M. Poidinger, K. Kabashima, M. Bajenoff, L. G. Ng, V. Angeli, F. Ginhoux, Two distinct interstitial macrophage populations coexist across tissues in specific subtissular niches. *Science* **363**, eaau0964 (2019).
10. J. Schyns, Q. Bai, C. Ruscitti, C. Radermecker, S. De Schepper, S. Chakarov, F. Farnir, D. Pirottin, F. Ginhoux, G. Boeckxstaens, F. Bureau, T. Marichal, Non-classical tissue monocytes and two functionally distinct populations of interstitial macrophages populate the mouse lung. *Nat. Commun.* **10**, 3964 (2019).
11. D. Vanneste, Q. Bai, S. Hasan, W. Peng, D. Pirottin, J. Schyns, P. Maréchal, C. Ruscitti, M. Meunier, Z. Liu, C. Legrand, L. Fievez, F. Ginhoux, C. Radermecker, F. Bureau, T. Marichal, MafB-restricted local monocyte proliferation precedes lung interstitial macrophage differentiation. *Nat. Immunol.* **24**, 827–840 (2023).

12. X. Li, A. B. Mara, S. C. Musial, F. W. Kolling, S. L. Gibbings, N. Gerebtsov, C. V. Jakubzick, Coordinated chemokine expression defines macrophage subsets across tissues. *Nat. Immunol.* **25**, 1110–1122 (2024).
13. S. A. Dick, A. Wong, H. Hamidzada, S. Nejat, R. Nechanitzky, S. Vohra, B. Mueller, R. Zaman, C. Kantores, L. Aronoff, A. Momen, D. Nechanitzky, W. Y. Li, P. Ramachandran, S. Q. Crome, B. Becher, M. I. Cybulsky, F. Billia, S. Keshavjee, S. Mital, C. S. Robbins, T. W. Mak, S. Epelman, Three tissue resident macrophage subsets coexist across organs with conserved origins and life cycles. *Sci. Immunol.* **7**, eabf7777 (2022).
14. B. B. Ural, S. T. Yeung, P. Damani-Yokota, J. C. Devlin, M. de Vries, P. Vera-Licona, T. Samji, C. M. Sawai, G. Jang, O. A. Perez, Q. Pham, L. Maher, P. Loke, M. Dittmann, B. Reizis, K. M. Khanna, Identification of a nerve-associated, lung-resident interstitial macrophage subset with distinct localization and immunoregulatory properties. *Sci. Immunol.* **5**, eaax8756 (2020).
15. C. Sabatel, C. Radermecker, L. Fievez, G. Paulissen, S. Chakarov, C. Fernandes, S. Olivier, M. Toussaint, D. Pirottin, X. Xiao, P. Quatresooz, J. C. Sirard, D. Cataldo, L. Gillet, H. Bouabe, C. J. Desmet, F. Ginhoux, T. Marichal, F. Bureau, Exposure to bacterial CpG DNA protects from airway allergic inflammation by expanding regulatory lung interstitial macrophages. *Immunity* **46**, 457–473 (2017).
16. D. Bedoret, H. Wallemacq, T. Marichal, C. Desmet, F. Quesada Calvo, E. Henry, R. Closset, B. Dewals, C. Thielen, P. Gustin, L. de Leval, N. Van Rooijen, A. Le Moine, A. Vanderplasschen, D. Cataldo, P. V. Drion, M. Moser, P. Lekeux, F. Bureau, Lung interstitial macrophages alter dendritic cell functions to prevent airway allergy in mice. *J. Clin. Invest.* **119**, 3723–3738 (2009).
17. X.-Z. Tang, L. S. M. Kreuk, C. Cho, R. J. Metzger, C. D. C. Allen, Bronchus-associated macrophages efficiently capture and present soluble inhaled antigens and are capable of local Th2 cell activation. *eLife* **11**, e63296 (2022).
18. C. Legrand, D. Vanneste, A. Hego, C. Sabatel, K. Mollers, J. Schyns, P. Maréchal, J. Abinet, A. Tytgat, M. Liégeois, B. Polese, M. Meunier, C. Radermecker, L. Fiévez, F. Bureau, T. Marichal, Lung interstitial macrophages can present soluble antigens and induce Foxp3+ regulatory T cells. *Am. J. Respir. Cell Mol. Biol.* **70**, 446–456 (2024).
19. C. Ruscitti, C. Radermecker, T. Marichal, Journey of monocytes and macrophages upon influenza A virus infection. *Curr. Opin. Virol.* **66**, 101409 (2024).
20. R. Browaeys, W. Saelens, Y. Saeys, NicheNet: Modeling intercellular communication by linking ligands to target genes. *Nat. Methods* **17**, 159–162 (2020).
21. M. Krzywinski, J. Schein, İ. Birol, J. Connors, R. Gascoyne, D. Horsman, S. J. Jones, M. A. Marra, Circos: An information aesthetic for comparative genomics. *Genome Res.* **19**, 1639–1645 (2009).
22. J. L. Wrana, L. Attisano, R. Wieser, F. Ventura, J. Massagué, Mechanism of activation of the TGF-β receptor. *Nature* **370**, 341–347 (1994).
23. A. Subramanian, P. Tamayo, V. K. Mootha, S. Mukherjee, B. L. Ebert, M. A. Gillette, A. Paulovich, S. L. Pomeroy, T. R. Golub, E. S. Lander, J. P. Mesirov, Gene set enrichment analysis: A knowledge-based approach for interpreting genome-wide expression profiles. *Proc. Natl. Acad. Sci. U.S.A.* **102**, 15545–15550 (2005).
24. D. Grant, N. Wanner, M. Frimel, S. Erzurum, K. Asosingh, Comprehensive phenotyping of endothelial cells using flow cytometry 1: Murine. *Cytometry A* **99**, 251–256 (2021).
25. Q. Li, H. Cheng, Y. Liu, X. Wang, F. He, L. Tang, Activation of mTORC1 by LSECtin in macrophages directs intestinal repair in inflammatory bowel disease. *Cell Death Dis.* **11**, 918 (2020).
26. S. Black, D. Phillips, J. W. Hickey, J. Kennedy-Darling, V. G. Venkataraaman, N. Samusik, Y. Goltsev, C. M. Schürch, G. P. Nolan, CODEX multiplexed tissue imaging with DNA-conjugated antibodies. *Nat. Protoc.* **16**, 3802–3835 (2021).
27. Y. Goltsev, N. Samusik, J. Kennedy-Darling, S. Bhate, M. Hale, G. Vazquez, S. Black, G. P. Nolan, Deep profiling of mouse splenic architecture with CODEX multiplexed imaging. *Cell* **174**, 968–981.e15 (2018).
28. M. C. Hollander, L. L. Latour, D. Yang, H. Ishii, Z. Xiao, Y. Min, A. Ray-Choudhury, J. Munasinghe, A. S. Merchant, P. C. Lin, J. Hallenbeck, M. Boehm, L. Yang, Attenuation of myeloid-specific TGFβ signaling induces inflammatory cerebrovascular disease and stroke. *Circ. Res.* **121**, 1360–1369 (2017).
29. G. Sharma, J. Goodwin, Effect of aging on respiratory system physiology and immunology. *Clin. Interv. Aging* **1**, 253–260 (2006).
30. M. F. Viola, M. Chavero-Pieres, E. Modave, M. Delfini, N. Stakenborg, M. C. Estévez, N. Fabre, I. Appeltans, T. Martens, K. Vandereyken, H. Theobald, J. Van Herck, P. Petry, S. Verheijden, S. De Schepper, A. Sifrim, Z. Liu, F. Ginhoux, M. Azhar, A. Schlitzer, G. Matteoli, K. Kierdorf, M. Prinz, P. Vanden Berghe, T. Voet, G. Boeckxstaens, Dedicated macrophages organize and maintain the enteric nervous system. *Nature* **618**, 818–826 (2023).
31. A. Schridde, C. C. Bain, J. U. Mayer, J. Montgomery, E. Pollet, B. Denecke, S. W. F. Milling, S. J. Jenkins, M. Dalod, S. Henri, B. Malissen, O. Pabst, A. Mcl Mowat, Tissue-specific differentiation of colonic macrophages requires TGFβ receptor-mediated signaling. *Mucosal Immunol.* **10**, 1387–1399 (2017).
32. O. Butovsky, M. P. Jedrychowski, C. S. Moore, R. Cialic, A. J. Lanser, G. Gabriely, T. Koeglsperger, B. Dake, P. M. Wu, C. E. Doykan, Z. Fanek, L. Liu, Z. Chen, J. D. Rothstein, R. M. Ransohoff, S. P. Gygi, J. P. Antel, H. L. Weiner, Identification of a unique TGF-β-dependent molecular and functional signature in microglia. *Nat. Neurosci.* **17**, 131–143 (2014).
33. H. Lund, M. Pieber, R. Parsa, D. Grommisch, E. Ewing, L. Kular, J. Han, K. Zhu, J. Nijssen, E. Hedlund, M. Needhamsen, S. Ruhrmann, A. O. Guerreiro-Cacais, R. Berglund, M. J. Forteza, D. F. J. Ketelhuth, O. Butovsky, M. Jagodic, X.-M. Zhang, R. A. Harris, Fatal demyelinating disease is induced by monocyte-derived macrophages in the absence of TGF-β signaling. *Nat. Immunol.* **19**, 1–7 (2018).
34. T. Zöller, A. Schneider, C. Kleimeyer, T. Masuda, P. S. Potru, D. Pfeifer, T. Blank, M. Prinz, B. Spittau, Silencing of TGFβ signalling in microglia results in impaired homeostasis. *Nat. Commun.* **9**, 4011 (2018).
35. S. G. Utz, P. See, W. Mildenberger, M. S. Thion, A. Silvin, M. Lutz, F. Ingelfinger, N. A. Rayan, I. Lelios, A. Buttgereit, K. Asano, S. Prabhakar, S. Garel, B. Becher, F. Ginhoux, M. Greter, Early fate defines microglia and non-parenchymal brain macrophage development. *Cell* **181**, 557–573.e18 (2020).
36. O. Matcovitch-Natan, D. R. Winter, A. Giladi, S. Vargas Aguilar, A. Spinrad, S. Sarrazin, H. Ben-Yehuda, E. David, F. Zelada González, P. Perrin, H. Keren-Shaul, M. Gury, D. Lara-Astaiso, C. A. Thaiss, M. Cohen, K. Bahar Halpern, K. Baruch, A. Deczkowska, E. Lorenzo-Vivas, S. Itzkovitz, E. Elinav, M. H. Sieweke, M. Schwartz, I. Amit, Microglia development follows a stepwise program to regulate brain homeostasis. *Science* **353**, aad8670 (2016).
37. A. Bedolla, E. Wegman, M. Weed, M. K. Stevens, K. Ware, A. Paranjpe, A. Alkhimovitch, I. Ifergan, A. Taranov, J. D. Peter, R. M. S. Gonzalez, J. E. Robinson, L. McClain, K. M. Roskin, N. H. Greig, Y. Luo, Adult microglial TGFβ1 is required for microglia homeostasis via an autocrine mechanism to maintain cognitive function in mice. *Nat. Commun.* **15**, 5306 (2024).
38. G. L. McKinsey, N. Santander, X. Zhang, K. Kleemann, L. Tran, A. Katewa, K. Conant, M. Barraza, K. Waddell, C. Lizama, M. La Russa, H. J. Koo, H. Lee, D. Mukherjee, H. Paidassi, E. S. Anton, K. Atabai, D. Sheppard, O. Butovsky, T. D. Arnold, Radial glia promote microglial development through integrin αVβ8 -TGFβ1 signaling. *bioRxiv* 548459 [Preprint] (2023). https://doi.org/10.1101/2023.07.13.548459.
39. M. Greter, I. Lelios, P. Pelczar, G. Hoeffel, J. Price, M. Leboeuf, T. M. Kündig, K. Frei, F. Ginhoux, M. Merad, B. Becher, Stroma-derived interleukin-34 controls the development and maintenance of langerhans cells and the maintenance of microglia. *Immunity* **37**, 1050–1060 (2012).
40. Y. Wang, K. J. Szretter, W. Vermi, S. Gilfillan, C. Rossini, M. Cella, A. D. Barrow, M. S. Diamond, M. Colonna, IL-34 is a tissue-restricted ligand of CSF1R required for the development of Langerhans cells and microglia. *Nat. Immunol.* **13**, 753–760 (2012).
41. S. Chen, D. Luo, W. J. Streit, J. K. Harrison, TGF-β1 upregulates CX_3CR1 expression and inhibits fractalkine-stimulated signaling in rat microglia. *J. Neuroimmunol.* **133**, 46–55 (2002).
42. A. Attaai, N. Neidert, A. von Ehr, P. S. Potru, T. Zöller, B. Spittau, Postnatal maturation of microglia is associated with alternative activation and activated TGFβ signaling. *Glia* **66**, 1695–1708 (2018).
43. S. J. Cho, H. W. Stout-Delgado, Aging and lung disease. *Annu. Rev. Physiol.* **82**, 433–459 (2020).
44. A. Moroguchi, K. Ishimura, K. Okano, H. Wakabayashi, T. Maeba, H. Maeta, Interleukin-10 suppresses proliferation and remodeling of extracellular matrix of cultured human skin fibroblasts. *Eur. Surg. Res.* **36**, 39–44 (2004).
45. S. Reitamo, A. Remitz, K. Tamai, J. Uitto, Interleukin-10 modulates type I collagen and matrix metalloprotease gene expression in cultured human skin fibroblasts. *J. Clin. Invest.* **94**, 2489–2492 (1994).
46. R. G. Marangoni, Y. Masui, F. Fang, B. Korman, G. Lord, J. Lee, K. Lakota, J. Wei, P. E. Scherer, L. Otvos, T. Yamauchi, N. Kubota, T. Kadowaki, Y. Asano, S. Sato, W. G. Tourtellotte, J. Varga, Adiponectin is an endogenous anti-fibrotic mediator and therapeutic target. *Sci. Rep.* **7**, 4397 (2017).
47. B. Crestani, S. Marchand-Adam, C. Quesnel, L. Plantier, K. Borensztajn, J. Marchal, A. Mailleux, P. Soler, M. Dehoux, Hepatocyte growth factor and lung fibrosis. *Proc. Am. Thorac. Soc.* **9**, 158–163 (2012).
48. D. Pilling, R. H. Gomer, Persistent lung inflammation and fibrosis in serum amyloid P component ($Apcs^{-/-}$) knockout mice. *PLOS ONE* **9**, e93730 (2014).
49. D. Sicard, A. J. Haak, K. M. Choi, A. R. Craig, L. E. Fredenburgh, D. J. Tschumperlin, Aging and anatomical variations in lung tissue stiffness. *Am. J. Physiol. Lung Cell. Mol. Physiol.* **314**, L946–L955 (2018).
50. S. Kononov, K. Brewer, H. Sakai, F. S. A. Cavalcante, C. R. Sabayanagam, E. P. Ingenito, B. Suki, Roles of mechanical forces and collagen failure in the development of elastase-induced emphysema. *Am. J. Respir. Crit. Care Med.* **164**, 1920–1926 (2001).
51. S. Meiners, O. Eickelberg, M. Königshoff, Hallmarks of the ageing lung. *Eur. Respir. J.* **45**, 807–827 (2015).
52. K. Nakanishi, Y. Takeda, S. Tetsumoto, T. Iwasaki, K. Tsujino, H. Kuhara, Y. Jin, I. Nagatomo, H. Kida, S. Goya, T. Kijima, N. Maeda, T. Funahashi, I. Shimomura, I. Tachibana, I. Kawase, Involvement of endothelial apoptosis underlying chronic obstructive pulmonary

disease–like phenotype in adiponectin-null mice: Implications for therapy. *Am. J. Respir. Crit. Care Med.* **183**, 1164–1175 (2011).
53. M. Jeansson, A. Gawlik, G. Anderson, C. Li, D. Kerjaschki, M. Henkelman, S. E. Quaggin, Angiopoietin-1 is essential in mouse vasculature during development and in response to injury. *J. Clin. Invest.* **121**, 2278–2289 (2011).
54. L. A. Monticelli, G. F. Sonnenberg, M. C. Abt, T. Alenghat, C. G. K. Ziegler, T. A. Doering, J. M. Angelosanto, B. J. Laidlaw, C. Y. Yang, T. Sathaliyawala, M. Kubota, D. Turner, J. M. Diamond, A. W. Goldrath, D. L. Farber, R. G. Collman, E. J. Wherry, D. Artis, Innate lymphoid cells promote lung-tissue homeostasis after infection with influenza virus. *Nat. Immunol.* **12**, 1045–1054 (2011).
55. H. Saiga, J. Nishimura, H. Kuwata, M. Okuyama, S. Matsumoto, S. Sato, M. Matsumoto, S. Akira, Y. Yoshikai, K. Honda, M. Yamamoto, K. Takeda, Lipocalin 2-dependent inhibition of mycobacterial growth in alveolar epithelium. *J. Immunol.* **181**, 8521–8527 (2008).
56. C. Radermecker, C. Sabatel, C. Vanwinge, C. Ruscitti, P. Maréchal, F. Perin, J. Schyns, N. Rocks, M. Toussaint, D. Cataldo, S. L. Johnston, F. Bureau, T. Marichal, Locally instructed $CXCR_4^{hi}$ neutrophils trigger environment-driven allergic asthma through the release of neutrophil extracellular traps. *Nat. Immunol.* **20**, 1444–1455 (2019).
57. C. Ruscitti, J. Abinet, P. Maréchal, M. Meunier, C. de Meeûs, D. Vanneste, P. Janssen, M. Dourcy, M. Thiry, F. Bureau, C. Schneider, B. Machiels, A. Hidalgo, F. Ginhoux, B. G. Dewals, J. Guiot, F. Schleich, M.-M. Garigliany, A. Bellahcène, C. Radermecker, T. Marichal, Recruited atypical $Ly6G^+$ macrophages license alveolar regeneration after lung injury. *Sci. Immunol.* **9**, eado1227 (2024).
58. F. Bayerl, D. A. Bejarano, G. Bertacchi, A.-C. Doffin, E. Gobbini, M. Hubert, L. Li, P. Meiser, A.-M. Pedde, W. Posch, L. Rupp, A. Schlitzer, M. Schmitz, B. U. Schraml, S. Uderhardt, J. Valladeau-Guilemond, D. Wilflingseder, V. Zaderer, J. P. Böttcher, Guidelines for visualization and analysis of DC in tissues using multiparameter fluorescence microscopy imaging methods. *Eur. J. Immunol.* **53**, e2249923 (2023).
59. C. R. Stoltzfus, J. Filipek, B. H. Gern, B. E. Olin, J. M. Leal, Y. Wu, M. R. Lyons-Cohen, J. Y. Huang, C. L. Paz-Stoltzfus, C. R. Plumlee, T. Pöschinger, K. B. Urdahl, M. Perro, M. Y. Gerner, CytoMAP: A spatial analysis toolbox reveals features of myeloid cell organization in lymphoid tissues. *Cell Rep.* **31**, 107523 (2020).
60. G. Crowley, S. Kwon, E. J. Caraher, S. H. Haider, R. Lam, P. Batra, D. Melles, M. Liu, A. Nolan, Quantitative lung morphology: Semi-automated measurement of mean linear intercept. *BMC Pulm. Med.* **19**, 206 (2019).
61. P.-E. Grillet, E. Desplanche, Q. Wynands, F. Gouzi, P. Bideaux, A. Fort, V. Scheuermann, A. Lacampagne, A. Virsolvy, J. Thireau, P. De Tombe, A. Bourdin, O. Cazorla, Diastolic cardiomyopathy secondary to experimentally induced exacerbated emphysema. *Am. J. Respir. Cell Mol. Biol.* **69**, 230–241 (2023).
62. B. Singh, K. Shinagawa, C. Taube, E. W. Gelfand, R. Pabst, Strain-specific differences in perivascular inflammation in lungs in two murine models of allergic airway inflammation. *Clin. Exp. Immunol.* **141**, 223–229 (2005).
63. P. M. Wang, D. L. Kachel, M. F. Cesta, W. J. Martin, Direct leukocyte migration across pulmonary arterioles and venules into the perivascular interstitium of murine lungs during bleomycin injury and repair. *Am. J. Pathol.* **178**, 2560–2572 (2011).

Acknowledgments: We thank all members of the Immunophysiology laboratory (GIGA Institute, Liège, Belgium) for discussions: S. Ormenese, R. Stefan, A. Hego, G. Lefevre, C. Vanwinge, and J.-M. Collard from the GIGA In Vitro Imaging Platform; P. Drion, G. Lambert, L. B. Remy, and all staff members from the GIGA Mouse facility and Transgenics Platform; W. Coppieters, L. Karim, M. Deckers, A. Mayer, A. Lavergne, and members from the GIGA Genomics Platform; and P. Maréchal, M. Di Cesare, M. Sarlet, R. Fares, I. Sbai, and A. Lio for excellent technical and administrative support. **Funding:** This work was supported by FRFS-Welbio Advanced Grant WELBIO-CR-2022A-10 (T.M.); ERC Starting Grant ERC StG 2018 IM-ID: 801823 (T.M.); ERC Consolidator Grant ERC CoG 2023 MoMacTrajectALI: 101124390 (T.M.); Baillet Latour Biomedical Fund (T.M.); Research Project of the F.R.S.-FNRS T015021F (T.M.); Research Concerted Action of the Fédération Wallonie-Bruxelles (T.M.); Deutsche Forschungsgemeinschaft (DFG; German Research Foundation) under Germany's Excellence Strategy – EXC2151 – 390873048 (A.S.); and SFB 1454-P05-432325352 (A.S.). **Author contributions:** T.M. conceived, supervised, and secured funding for the project. Q.B. supervised the project and performed bioinformatic analyses. W.P., D.V., Q.B., and T.M. designed the experiments. W.P. did most of the experiments, compiled the data, and prepared the figures. D.V., M.M., and C.R. were involved in experiments related to the analysis of myeloid-restricted *Tgfbr2*- and endothelial-restricted *Tgfb1*-deficient mice. J.A. performed bioinformatic analyses. D.B. and A.S. performed the CODEX multiplex imaging experiment and analyses. F.B. was involved in experiments involving myeloid-restricted *Mafb*-deficient mice. F.P. and D.C. performed the invasive measurements of lung function. T.M., Q.B., and W.P. wrote the manuscript. All authors provided feedback on the manuscript. **Competing interests:** The authors declare that they have no competing interests. **Data and materials availability:** Bulk and scRNA-seq data have been deposited at the Gene Expression Omnibus (GEO) and are available under GEO accession GSE271467 and GSE285104. Previously published scRNA-seq data (*10*, *11*) were deposited at EMBL-EBI under accession number E-MTAB-7678 (*10*) and at GEO under GEO accession GSE194021 (*11*). The bulk RNA-seq data of cMos, AMs, and IM subsets in the lungs of adult C57BL/6 WT mice used in Fig. 1D were previously published and deposited at GEO under GEO accession GSE194021 (*11*). Original codes have been deposited at Zenodo and are available at https://zenodo.org/records/14974309. Tabulated data underlying the figures are provided in data file S1. All other data needed to evaluate the conclusions in the paper are present in the paper or the Supplementary Materials.

Submitted 5 July 2024
Accepted 25 March 2025
Published 18 April 2025
10.1126/sciimmunol.adr4977